CONDUCTIVE BIOIMPRINT FOR REGENERATIVE MEDICINE: SYNTHESIS AND CHARACTERISATION

NOR AZILA BINTI ABD. WAHID

A thesis submitted in partial fulfilment of the requirements for the

Degree of Doctor of Philosophy in

Biomedical Engineering

Department of Electrical and Computer Engineering,

University of Canterbury, Christchurch, New Zealand

Summer, December 2018

ABSTRACT

The ability to manufacture the cell culture platforms that guide biological cells to differentiate in controlled manners and in situ monitoring their viability and response to stimulate is important in a number of applications such as lab-on-chip, tissue engineering and biosensing.

This research presents the development of conductive bioimprinting based on conducting polymer poly(3,4–ethylenedioxythiophene):polystyrene sulfonate (PEDOT:PSS) for cell features replication and monitoring platform. Conductive bioimprinting is a new technology that integrates hydrogel and glycerol into PEDOT: PSS to imitate cell-like features using a soft lithography method. Adding functionality to the bioimprint process by enabling not only high resolution replica but also monitoring cell growth/viability through changes in their conductivity, an approach that has not been investigated before. Moreover, the use of hydrogel, glycerol and crosslinker demonstrates enhancement in biocompatibility, low degradation/water solubility and mechanical properties of the conductive substrate.

Six different concentrations of PEDOT:PSS (0%, 2%, 3%, 4% and 6% w/w) were studied in the synthesis of the conductive hydrogel via chemical method. The success in the synthesis and optimisation of the conductive hydrogel resulted in a very high replication fidelity with more than 90% accuracy when used for replicating myoblast C2C12 cellular features down to micro- and nano-sized details. The high-resolution conductive bioimprint replicas were utilised as a secondary cell culture substrate to investigate the cells response to cell–like topography as compared to featureless flat surfaces.

The synthesised conductive hydrogel underwent chemical and surface modifications to optimise the electrical conductivity, swelling behaviour, mechanical properties, biocompatibility and cell response on different topography. Conductive hydrogel films that were chemically crosslinked with microbial Transglutaminase (mTg) showed significant increase in the electrical conductivity from 10^{-6} to 1 Scm^{-1}, in addition to improve water solubility. Moreover, cultured myoblast C2C12 cells on the crosslinked

conductive substrates showed that they attached, grew and proliferated on all surfaces after 24 hours of cell seeding. In addition, conventional patterning of the conductive hydrogel substrates were employed *in vitro* to culture myoblast C2C12 cells and observe the cell–material interactions. Crystal violet stained cells revealed that cells are very responsive to their micro environment and they prefer to attach on a patterned surface as compared to a flat surface under the same cell culture media conditions.

In investigating the physicochemical properties of crosslinked conductive hydrogel films with different concentrations, several techniques have been employed for the analysis and testing of the synthesised material. Wettability, biocompatibility, biodegradability, mechanical analysis and some chemical analysis were performed. Results showed that the conductive hydrogel films have a good wettability and excellent hydrophilic properties. These material features acted favourably for the myoblast cell adhesion onto the conductive hydrogel substrate as compared to glass, gold and PDMS substrates. *In vitro* biodegradation tests when conducted in a culture medium at temperature of 37 ℃ for 15 days revealed that the degradation of the conductive hydrogel films was slowed down with increasing PEDOT: PSS concentrations. The tensile testing showed that the conductive hydrogel exhibited excellent stretchability properties: the elasticity modulus was decreased from 77.87 ± 1.12 MPa for the 2% films to 1.11 ± 0.10 MPa for the 6% films. Furthermore, from the chemical analysis: ultraviolet visible spectroscopy (UV-Vis), X-ray photoelectron spectroscopy (XPS), Fourier transform infrared spectroscopy (FTIR) and Thermogravimetric analysis (TGA) confirmed that the appropriate and expected chemical elements were present in the synthesised conductive hydrogel polymer films.

The electrical cell-substrate impedance spectroscopy (ECIS) measurements were performed on myoblasts C2C12 cells. The myoblast cell's impedance changed during adhesion, growth, proliferation and toxin addition. The sensitivity of the conductive hydrogel biochip during cell culture experiments were measured and analysed. These results demonstrate a new method of using cell impedance spectroscopy on conductive hydrogel to study the cell behaviour and would help researchers' better understanding on cellular responses/ events in real–time.

The developed conductive bioimprint shows high replication resolution, good conductivity, biocompatibility, stretchability and water resistance. The results of the synthesis and characterisation of the conductive hydrogel substrate with patterned surfaces demonstrated by this research work have a great potential to be used for monitoring acceptance of medical implants in the human body and manipulating implant–tissue reactions for medical devices.

Keywords: conductive bioimprint, PEDOT: PSS, soft lithography, electrical properties, biocompatibility, biodegradability, stretchability and ECIS.

ACKNOWLEDGEMENT

First and foremost, I would like to express my sincere appreciation to my supervisor, Professor Maan M. Alkaisi, for his immense support and faith in me. He gave me a chance to prove my abilities in research and was always a door knock away for discussions and help. Though I might have bored him at many times with my weekly reports, his kind words and appreciation always helped my motivation and dedication to my research.

Secondly, I would like to express my deepest gratitude to my co-supervisor Professor John J. Evans for providing an excellent support at the University of Otago, Christchurch and for his supervision during preparation of my thesis. Also, I would like to acknowledge Dr Kenny Chitcholton for his immense support and advice whenever I needed it. His ideas were unique and he was always happy to answer my questions in the most eloquent manner.

I would like to thank to my husband, Rahimi bin Ahmad, for his love, being my best friend, help and never ending support. Special appreciation is due to my son, Ahmad Razif and my daughter Nur Faiqah for enduring so patiently the division of my attention during this research.

I'm very grateful to all of my lab mates, Giang, Tiffany, Azadeh, Louise, Yiling, Linda, Amalraj, Wafaa, Alex, Dhiraj and Mak. You guys were a great help for discussions and suggestions along the way. There is no way I can forget the important person in the Nano Laboratory. Thank you to Helen and Garry, the first two people from our group that I met, who helped with advice and guidance on equipment in my research.

Finally, I am deeply indebted to my mums, sister and brothers for their support throughout the years I lived far from them and I apologise for not taking care of them as much as I should have.

PUBLICATION AND PRESENTATIONS

Conference presentations

A. Wahid, N. A., Hashemi, A., Evans, J, J., Alkaisi, M. M. (2017). Development of Water Stable Conductive Bioimprint. 8th International Conference on Advanced Materials and Nanotechnology (AMN 8). Queenstown, New Zealand. 12-16 February 2017.

A. Wahid, N. A., Evans, J, J., Alkaisi, M. M. (2017). Conductive Bioimprint for Cell Culture Sensing. 11th IEEE International Conference on Nano/Molecular Medicine and Engineering. Shenzhen Virtual University Park, Shenzhen, China. 1-4 December 2017.

A. Wahid, N. A., Evans, J, J., Alkaisi, M. M. (2018). Conductive Bioimprint: A Novel Cell Culture Platform. International Conference on Nanoscience and Nanotechnology (ICONN 2018), University of Wollongong, Sydney, Australia. 29 January-2 February 2018.

Poster presentations

A. Wahid, N. A., Hashemi, A., Evans, J, J., Alkaisi, M. M. (2017). Conductive Bioimprint Surface Patterning based on PEDOT: PSS for use as cell culture substrate. University of Canterbury, Christchurch, New Zealand: Health Research Poster Event. 10 August 2017.

Alkaisi, M. M., Evans, J, J., A. Wahid, N. A. (2018). Conductive Bioimprint for Cell Culture Applications. 44th International Conference on Micro and Nanoengineering (MNE) 2018, Copenhagen, Denmark. 22 September 2018.

No matter where you are, your dreams are valid….So don't stop believing

With L.O.V.E

Nor Azila Abd Wahid

LIST OF ABBREVIATIONS

PEDOT:PSS	Poly(3,4-ethylenedioxythiophene): polystyrene sulfonate
mTg	microbial Transglutaminase
ECIS	Electrical Cell-substrate Impedance Spectroscopy
UV-VIS	Ultraviolet visible spectroscopy
XPS	X-ray photoelectron spectroscopy
FTIR	Fourier transform infrared spectroscopy
TGA	Thermogravimetric analysis
3D	Three dimensional
CP	Conducting polymer
AFM	Atomic force microscopy
PDMS	Polydimethylsiloxane
ECM	Extracellular matrix
PBS	Phosphate buffer saline
HMDS	Hexamethyldisilazane
DMEM	Dulbecco's Modified Eagle's medium
FBS	Fetal bovine serum
IDE	Interdigitated electrode
DOX	Doxorubicin
LOC	Lab-on -chip
CH	Conductive hydrogel
PVP	Polyvinylpyrrolidone

LIST OF CONTENTS

LIST OF FIGURES

LIST OF TABLE

CHAPTER 1

Motivation and Outline

1.1 Motivation

Over the past decade, the development of new topographically modified substrate as platforms for monitoring cell growth has been extensively researched to gain real–time insights the working of complex living units (tissues, organs and organisms) in the body. During *in vitro* studies, the substrate surface not only change the cell–surface interactions but can also contain catalysts, mediators and cofactors that induce an internal reorganisation of cellular architecture. This development has inspired the field of implantable biosensors, tissue engineering and drug delivery applications. For instance, in bone-implant research, the design of the devices has a major effect on the ability to induce, control and guide cell growth, and produce rapid healing [1]. However , in certain applications such as cardiovascular prosthesis, catheters and contact lenses, the biomaterial design must not stimulate cell adhesion, which can lead to thrombus formation and high risk of infection [2], [3]. In the early 1900s, Harrison was the first scientist researching tissue culture to observe the changes of cell response to surface structure [4]. Since then scientists have realised that topography plays an important role in guiding cell attachment, growth, migration and differentiation [4]–[11].

In recent years the advance development of conducting polymer (CP) film has created enormous potential interest in many biological applications, including tissue engineering, diagnostics, actuation (micro catheters, artificial muscles, electric/artificial organs etc.), and drug delivery systems [12]–[18]. This is due to their flexible properties, excellent compatibility with biological systems, mixed electrical and iconic conductivity and ability to from a 3D pattern (bioimprint). Numerous studies have shown that the choice of conducting polymer materials can influence interactions with living tissue, neurons and protein [13], [19]. Moreover, the integration of a solid surface with the electro-

physical properties could stimulus cell behaviours such as adhesion, migration, and secretion.

In this work, we present for the first time the development of a CP film with bioimprinted surface features based on poly (3,4-ethylenedioxythiophene): polystyrene sulfonate (PEDOT:PSS) by using a soft lithography technique. The conductive bioimprint has been used for studying cell adhesion, morphology and cell–surface interactions. This conductive substrate also could be used for monitoring the differentiation of biological cells with respect to the electrical conductivity properties.

CPs such as polyacetylene (PA), polypyrrole (PPy), polythiophene (PT) and polyaniline (PANI) have great potential in the development of electroactive biomaterial for biosensing and bioengineering applications [20]–[26]. The discovery of CP hydrogel was first reported by Gilmore *et al*. in 1997 [27]. A polythiophene derivative, PEDOT:PSS has attracted the attention of many scientists during the last decade for applications in supercapacitors [28], transistors [29], solar cells [30], [31], batteries and bio-electronics [31]–[33] owing to its good conductivity, high stability at room temperature, flexibility with an aqueous solution and it is relatively inexpensive [20], [25], [26], [28]–[32], [34]. PEDOT:PSS based CP is becoming an attractive material for interfacing with biological systems, it has good forming properties and is chemically stable. This material is also well characterised with biocompatible properties *in vitro/vivo*, which opens up a range of opportunities for soft tissue augmentation and regeneration [35]–[37]. However, PEDOT: PSS is a water-based conducting polymer and has limited applications in imprinting processes. By mixing a CP with gelatin, a conductive hydrogel (CH) has been developed that is suitable for sensing applications employed in this project. Despite this conductive material having good biocompatibility properties, work on CH optimisation and investigation the qualities of cell adhesion and growth under various topographies as a function of electrical signals were described in this thesis. Motivated by the goal of conductive biomaterial as an electrode coating, a variety of conducting polymer hydrogels have been explored based on PPy [38]–[40], PEDOT [35]–[37], [41]–[43] and PANI [44], [45] for implantable devices, tissue engineering and drug delivery. In addition, the performance of CH is dependent on a number of factors such as conductivity, degree of crosslinking and swelling behaviour of hydrogel [46], [47].

Gelatin is a colourless natural biopolymer hydrogel derived from collagen. This unique polymer has biocompatible and biodegradable characteristics, given the well-documented has non toxicity, low antigenicity and promotes cellular adhesion as well as proliferation [35]–[37], [48]. It has been reported to be effective used for skin and bone repair, cartilage and tissue engineering [27], [34]–[37].

1.2 Bioimprint

Implant failure incidence and escalated risk of cancer are both problematic which have to be minimised. There is a continued and growing demand for innovative alternatives to reduce the rate of medical device failure and to diagnose potential of infection or inflammation in real–time. With these problems in mind, the bioimprinting technique is a promising new approach that mimics biological cell topography and replicates them permanently onto polymer matrices. Since the surface topography is strongly influence cell phenotype in many ways such as (adhesion, differentiation, morphology, etc.) and offers opportunities to manipulate cells and tissues. Therefore, bioimprint was developed to enhance imaging of cells using atomic force microscopy (AFM) and to create the cell culture platform for guidance role of micro-nano environment on cell development [49], [50].

The term “bioimprint” was first developed in 2006 by Dr. James Muys and patented in the Department of Electrical and Computer Engineering at the University of Canterbury, New Zealand [51]. In this thesis, a novel approach is presented to enable non-destructive AFM imaging and analysis of cells by replicating a cell’s delicate features onto a hard polymer. In earlier studies, liquid polydimethylsiloxane (PDMS) was used as a bioimprinting polymer medium. Unfortunately, due to curing requirements, the baking process caused cell dehydration and deformation effects before the PDMS was completely polymerised. It also experiences a very long curing time with ultraviolet light exposure, which was not practical under certain conditions without causing artefacts. Ideally, the polymer utilised for the bioimprint process will be able to meet several criteria: firstly, the polymer must be completely transformed into solid form after the curing process and easy to peel in order to avoid any artefacts or denaturation effect. It must also be able to replicate cell features

at high resolution and be biocompatible as a cell-culture platform. To overcome the curing time problem, photo-initiated methacrylate elastomer was used for cell replication and the polymer solidified in less than one minute [52], [53].

Further development and investigation of methacrylate elastomer bioimprinting using a soft lithography technique was continued in the doctoral dissertation of Dr. Fahmi Samsuri [54]. In his research a simple fabrication method for cell replication that involved biocompatible polymer, fast curing and low temperature was developed. By using a soft lithography technique, the bioimprinting process provides an easy fabrication method to permanently capture the cellular footprint at high resolution down to nanometre scale. Interestingly, the soft lithography technique is a dominant technology that has been adopted successfully in materials science, microfluidics and flexible displays with unlimited feature-size resolution [10], [11], [55].

Numerous studies have been reported on the response of biological cells cultured on various surface topography patterns and on different non-CPs such as PDMS [8], [9], glass[9], Permanox [9], methacrylate [8], [54], [56], [57], polystyrene [6]–[9], poly (ethylene glycol) terephthalate–poly (butylene terephthalate), (PEGT–PBT) [58] and casein [59]. These studies have been used to demonstrate cell–surface interactions, growth, adhesion, spreading, morphology, and the differentiation of biological cells. Interestingly, these studies showed that cells behave differently on different topographies [8], [9], [60] and substrate material in addition to changes in expression of signalling proteins and sensitivity to cancer drugs [6]. In addition, the cells grow randomly on a flat surface, but align themselves with and move along the pattern [4], [5], [7]–[9], [60], [61]. However, all of these studies mostly focused on improved understanding of cell behaviour under different physical conditions with respect to the chemical and mechanical properties but not the electrical properties.

In this thesis presents the development of a new bioimprint that utilises conducting polymer PEDOT:PSS called “conductive bioimprint” employs soft lithography technique. The conductive bioimprint materials and approach investigated for this work will be described in detail, together with the modifications, optimisation, and improvements on the previous technique and materials employed. The conductive substrate with patterned

surface that was developed also offers good stimuli responsive as secondary cell culture substrate, high resolution replication fidelity, excellent electrical conductivity and is also biocompatible, stretchable and biodegradable, which suitable for various applications.

The conductive bioimprint substrate is a very desirable as an implant coating in help to promote cells growth and monitor the healing process of tissues or possible infections in the injury sites in real-time after surgeries. Then, the information will be transmitted to the doctor, researchers and patient via wireless communication technologies such as bluetooh, radio frequency identification (RFID) and WI-FI. These outcomes would allow not only faster recovery for the patient, but also decreased patient morbidity, improved patient psychology, and decreased health care costs. Furthermore**,** the stretchable and biodegradable characteristics of conductive bioimprint are very envisage to develop future implantable devices. This substrate supports the electronic component, flexing, and moulding to rough and smooth surface alike. As a coating substrate that conform to the medical implant it need to be stretchable and flexible which to allow for implant topography moulding. Once the conductive bioimprint completed guiding and improving cells implant interface and the coating is no longer needed have to be degradable into nontoxic components and leaving the resulted tissues behind. Therefore patient does not need secondary surgery for implant removal. Figure 1.1 summarises the synthesis of conducting polymer hydrogels, presents their properties and further opportunities in biomedical applications.

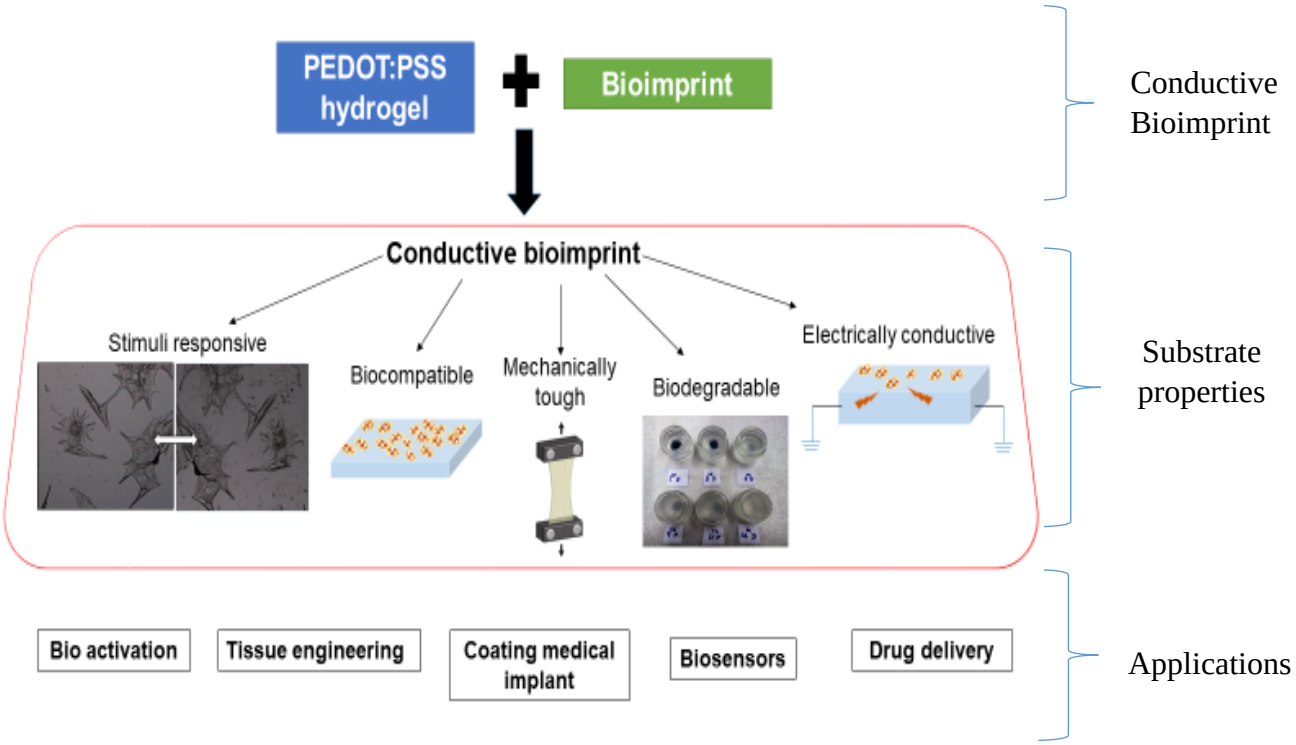

Figure 1.1: The synthesis, properties and applications of conductive bioimprint.

1.3 Cell adhesion

Cell adhesion is one of the main processes that influence cellular communication and regulation between cell–substrate material interactions. This is also an important biological phenomenon for the development and maintenance of multicellular tissue structures [62]–[64]. *In vitro*, the majority of mammalian cells are anchorage-dependent and adhere tightly on appropriate substrate material [65]. An understanding of the cell–substrate adhesion mechanism is essential for better insight into cell adhesion properties in developing methods for disease diagnostics, lab-on-chip, artificial bone, inflammation, biomaterial studies for biosensor, implantable devices, cancer progression analysis, immunity testing, drug delivery and tissue engineering [63], [64], [66].

The process of cell adhesion *in vitro* occurs in three phases: attachment, spreading and differentiation events, as shown in Figure 1.2. The early phase of this mechanism involves the interaction between receptor transmembrane glycoproteins called integrin and the extracellular matrix (ECM). As the cell receptor–ECM interactions increase, the ECM–

substrate surface contact area increases through formation of actin microfilaments and cell spreading. Integrin can regulate many cellular functions such as adhesion, motility, shape, growth and differentiation during cell receptor-ECM interactions. Failure of cells to interact with the appropriate biological surface or molecule can be detrimental to the fate of the cells, which contribute to cancer cell metastases, arthritis and osteoporosis [67]–[70]. With an appropriate signal from the matrix, cells then proceed to arrange their cytoskeleton protein as characterised by the formation of focal adhesions and actin-containing stress fibres. Focal adhesions consist of ECM proteins, scaffolding molecules and signalling components that link the actin cytoskeleton [71], [72].

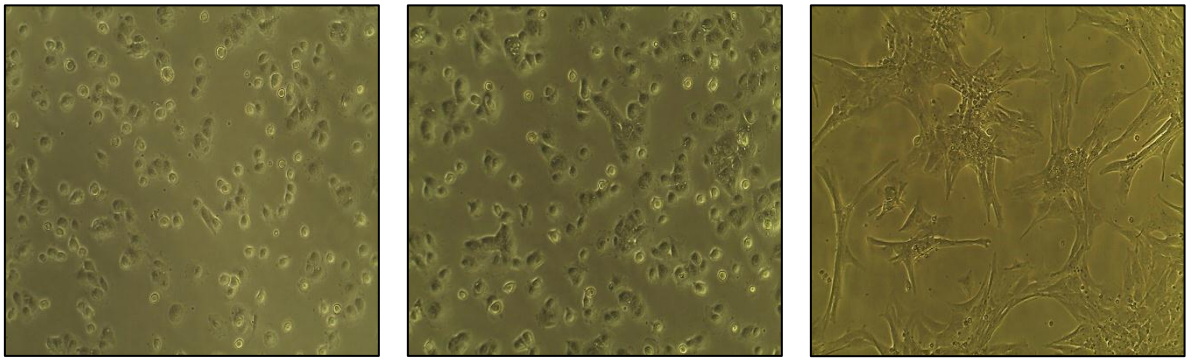

(a) Adhesion (b) Spreading (c) Differentiation

Figure 1.2: Schematic diagram of cell adhesion event for (a) attachment, (b) spreading and (c) differentiation of cell in culture flask. Once cells adhere on the local extracellular matrix as well as on the substrate surface, the beginning of an extensive proliferation in order to differentiate themselves and build up a tissue or a fibre in case of muscle cells.

Today, there are many studies that have evolved, such as Micro Patterning, 3-D Traction Force Quantification, Microfluidics, Polyacrylamide-Traction Force Microscopy, and Resonance Frequency to analyse single or population of cell adhesion mechanism to a substrate. This include how fast do cells attach to a surface? Do they change their morphology or adhesion area because of a substance or physical stress and how good is their attachment?

1.4 The effect of surface roughness, surface topography and surface chemistry on cell adhesion

When fabricating artificial biomaterials for the purpose of medical implants into the body, it is essential to create materials that encourage or stimulate the cell adhesion process such as attachment, migration, proliferation and differentiation of biological cells. The interaction of the cells with the artificial substrates is normally mediated by proteins such as fibronectin, laminin, and collagen, which form part of the ECM. These proteins bind to the substrate surface and express specific sequences that are recognised by the cell–surface receptors or integrin's. The main factors that have been recognised as strongly influencing cell response with the biomaterial are surface roughness, surface topography, surface chemistry of substrate materials [62], [63]. Various studies have shown the interaction between biomaterial surface characteristics and cells can be manipulated in order to control those situations [1], [4], [63], [66], [73], [5], [6], [8], [12], [21], [32], [35], [36].

Roughness is a component of surface morphology of the substrates that can be used to describe and quantify the degree of surface topography, which can be classified as hydrophobic or hydrophilic. Surface measurement is important parameter for determining a surface's suitability for various applications. In biomedical applications, surface roughness has been shown to affect cellular behaviour *in vitro* and tissue response *in vivo*. *In vitro* studies on roughness have shown that cells adhered well on the rougher surfaces, whereas the smooth surfaces are known to promote inflammation due to a reduction of interfacial motion at a cellular level, which leads to destruction of cells and the extracellular matrix [74]. On the other hand, research group from AO Research Institute found that culturing cells on rough titanium and steel does not significantly affect fibroblast cell adhesion or subsequent growth when compared with smooth surfaces [75].

Furthermore, cell behaviour such as adhesion, proliferation, morphology, gene expression and motility is also influenced by the topographical features. Topography can be described as the variation in amplitude, pattern of features such as a cell's footprint bioimprint, microfluidics, pillars, pits, wells and pyramids. Modification in surface topography strongly impact the surface energy and wetting behaviour that leads to

enhancement in protein adsorption, cell adhesion and growth. In addition, topography modification that attempts to mimic the extracellular environment is an effective technique to determine the sensitivity and cell response to the certain micro-environmental cues, for example during wound healing.

The role of topography on cellular outgrowth *in vitro* was developed by Harrison in 1911 [76]. They found that cultured embryonic frog on a meshwork pattern showed cells preferentially extended along the solid support of the filaments. Since then numerous approaches have been used in topography modification in order to study the cell behaviour for drug delivery, tissue engineering and biomedical applications [4], [5], [61], [62], [66]. Bioimprinting is a new approach developed in our lab that mimics biological cell-like topography replicated into polymer matrices that can be used to investigate cell behaviour in response to changes in surface morphology. It is worth mentioning that Murray *et al*. demonstrated that cancer cells cultured on bioimprinted polymethacrylate substrate exhibited different behaviour and can distinguish between cell-like topographies and flat areas on the culture platforms [8]. It has also been reported that surface topography can modify endometrial cancer cell responses of signalling proteins, and sensitivity to anti-cancer drugs [6].

Since we know that surface roughness and topography influence cell behaviour, surface chemistry also has an important factor on cell response, protein adsorption and cell adhesion. The first work demonstrating the importance of surface chemistry was begun in 1984 by Baier *et al*. [62]. They found that hydrophilic surfaces trigger the adhesion and proliferation of cells on the substrate. Initially, wettability of the solid substrate is affected by three aspects: the surface tension of the solid, the surface tension of the liquid and the interfacial tension [77]. The surface wettability of biomaterials is usually evaluated by the water contact angles at the material surface. Research on determining and investigating the contact angle with various biomaterials found that reduction in contact angle will enhance wettability which leads to improving biocompatibility properties of the substrate [77]. This happens when the polymeric surfaces are exposed to polar liquids: the orientation of the molecules changes and point towards the polar phase. On the other hand, if the materials are exposed to air or other hydrophobic environments, the

hydrophobic groups within the polymers will migrate towards the surface of the material, making the surface water resistance [77].

1.5 Research objectives

This research focuses on developing a novel device that utilises cell-like footprints made of CH for many applications in medical implant biosensors. The developed technology is called a "conductive bioimprint". The required properties of the conductive bioimprint include high replication resolution, biocompatibility, suitable mechanical (stretchable) and electrical (highly conductive) properties, and being biodegradable. This study will show how the conductivity of living biological cells is related to the cell functions, growth, spread and apoptosis. Other cell activities such as cell–surface interactions, growth, adhesion, spreading and morphology will also be examined. The conductive bioimprint have an important potential for monitoring medical implant success in real–time. Moreover, this work addresses a significant challenge of the synthesisation and polymerisation process of CH by integrating glycerol and gelatin into PEDOT:PSS via chemical methods. This successful approach was achieved by combining the biocompatibility and biodegradability properties of hydrogel and flexibility properties of glycerol into conductive properties of PEDOT:PSS.

To achieve these objectives, the specific aims and plans were as follows:

1) To synthesise CH composites that incorporate the biomaterial hydrogel and glycerol into PEDOT:PSS. Then, replicate the cell surface features into CH composite and compare the conductive bioimprint replica with PDMS master mould and the actual features of C2C12 cell.

2) To investigate the effects of chemical and surface modification on the electrical properties, swelling behaviour and cell behaviour under different conditions, such as the influence of cross-linkages and topography.

3) To determine the physicochemical properties of CH films with different concentrations of PEDOT:PSS, such as wettability, biocompatibility, biodegradation and physical/mechanical properties. To characterise the chemical component of the conductive composite by using: ultraviolet visible spectroscopy (UV-Vis), X-ray photoelectron spectroscopy (XPS), Fourier transform infrared spectroscopy (FTIR) and Thermogravimetric analysis (TGA).

4) To monitor the cell's impedance change in real-time as a function of adhesion, growth, proliferation and apoptosis on gold and CH biochips.

1.6 Thesis outlines

Chapter 1 introduces the motivation behind this study and the evolution of the "bioimprint" technology for use as a cell-culture platform. In addition, the cell adhesion process and the influence of surface roughness, surface topography and surface chemistry on cell adhesion is highlighted. The objectives and outline of this research work are also presented in this chapter.

Chapter 2 provides literature reviews; the first is a theoretical introduction regarding the basic concepts of biosensors. It discusses their advantages in biomedical applications, explains the different types of detection methods, and defines the selection of electrode materials, which play an important role in the biosensor's performance. The next review describes the conducting polymer hydrogel and the major driving forces for the development of these materials-based biosensors. The principle of electric cell–substrate impedance sensing system (ECIS) such as the use of microelectrodes, for monitoring and measuring cell adherence, are also discussed in detail.

Chapter 3 describes various materials and methods that were used in performing the conductive bioimprint fabrication employed in this thesis. Cell culture protocol, cell counting, cryopreservation procedure, fixation and staining method are included in this chapter. The various analytical methods used for physicochemical characterisations of CH substrate are described in the next section. The fabrication methods of gold

interdigitated electrodes through photolithography and PDMS bioimprint master mould by using soft lithography techniques are presented. Finally, the electrical properties measurements by using four-probe Hall effect and ECIS are also discussed in the last section.

Chapter 4 demonstrates the template synthesis process and optimisation of a novel fabrication method to develop a conductive bioimprint based on PEDOT:PSS films by using a soft lithography technique. The following section discusses the resolution replication fidelity from the analysis of AFM imagery of myoblast C2C12 cells imprinted on different substrates: fixed cells on glass, negative/positive PDMS bioimprint and positive/negative conductive bioimprint.

Chapter 5 describes the influence of chemical and surface film modification on electrical the properties, swelling behaviour and cell behaviour, and the resulting conclusions regarding cell adhesion onto different patterned substrate surfaces.

Chapter 6 investigates the physicochemical properties of CH as a soft electrode material. Wettability, biocompatibility, biodegradation and physical/mechanical analysis were examined. In addition, the chemical properties of synthesised CH polymers were characterised by using UV–Vis, XPS, FTIR and TGA.

Chapter 7 is devoted to impedance measurements of myoblast C2C12 activity on CH microelectrodes. This chapter describes the investigation of ECIS in studying myoblast C2C12 adhesion, spreading and drug effects in real time, on CH and gold biochips.

Chapter 8 concludes the thesis by summarising the methods, findings and conclusions in the previous chapters. This chapter covers research contributions and suggestions for future work required to further advance these techniques.

CHAPTER 2

Literature Review

2.1 Biosensors

The rapid research in the field of biomedical engineering is geared towards the development of analytical platforms for more effective monitoring, testing, non-invasive analysis and portable elements for disease diagnosis. Implantable biosensors permit the internal biologically controlled by the central nervous system to communicate with an external body sensor using a wireless communication technology. Moreover, biosensors using polymeric biomaterials result in intelligent diagnostics, biocompatibility, low limit of detection, high sensitivity, lower applied potential, adjustable and good mechanical properties [78], [79]. The polymeric materials such as CP, redox polymer (RP), hydrogel and chitosan are of interest in that they offer most of the above characteristics.

In general, a sensor can be described as a device used to detect or measure the changes in its physical environment (heat, light, pressure, position, temperature, acceleration, sound, etc.) and respond with feedback. Sensors are widely used as a core element in many applications ranging from daily use appliances, laboratory and scientific research, engineering and military equipment, whereas a biosensor is a combination of two components connected in series (*bioreceptor* and *transducer*) that converts and amplifies a biological response to an analytical signal via a detector circuit using the appropriate reference and sends it for processing, for example by computer software [80]–[82]. It can also be defined as a compact, integrated bioanalytical, self-contained unit that has a biological sensitive component connected to a compatible physicochemical transducer [83], [84]. The two components work together to transpose the concentration of an analyte or a similar group of analytes; they are measurable responses that transform the signal. A biosensor provides a high degree of selectivity and sensitivity for the analyte to be measured. Selectivity gives a measure of the ability of the system to detect the analyte in

the presence of other interfering molecules, while sensitivity refers to the lowest detectable analyte concentration.

The general structure of biosensors is illustrated in Figure 2.1. A bioreceptors element detects the analyte of interest to the physicochemical transducer (detector) and converts the spot target into a measurable electrical signal. This element detects bioanalytes including enzymes, protein, antibodies, microorganisms, biological tissue and deoxyribonucleic acids (DNA) from the biological organisms [82], [85]–[88]. After interacting with the target analytes in the system, the physicochemical properties of the sensitive layer change and can be detected through the optical properties, weight or resistance of the sensing element. The transducer then takes the changed parameter and converts it to an equivalent, measurable electrical signal, which is amplified. In order to achieve the required detection, numerous interface materials have been used for transducer coatings such as metallic electrodes, carbon nanotubes, nanowires, graphene, quantum dot, and conducting polymer. The amplified signal is proportional to the concentration of the substance processed by the signal processor then analysed in appropriate hardware or software. The transducer can be electrochemical, calorimetric, piezometric, optical, magnetic or micro chemical or a combination of these [80].

The term “biosensor” was proposed by Clark and Lyons in 1962 to measure glucose in biological samples using an immobilised glucose oxidase electrode. Since then, progress has increased exponentially both in technology and application of biosensors with novel approaches integrating nanotechnology to bioelectronics [89]. Furthermore, better understanding the concept of immobilised bioreceptors have significantly toward the development of practical biosensors both by academic and commercial sectors.

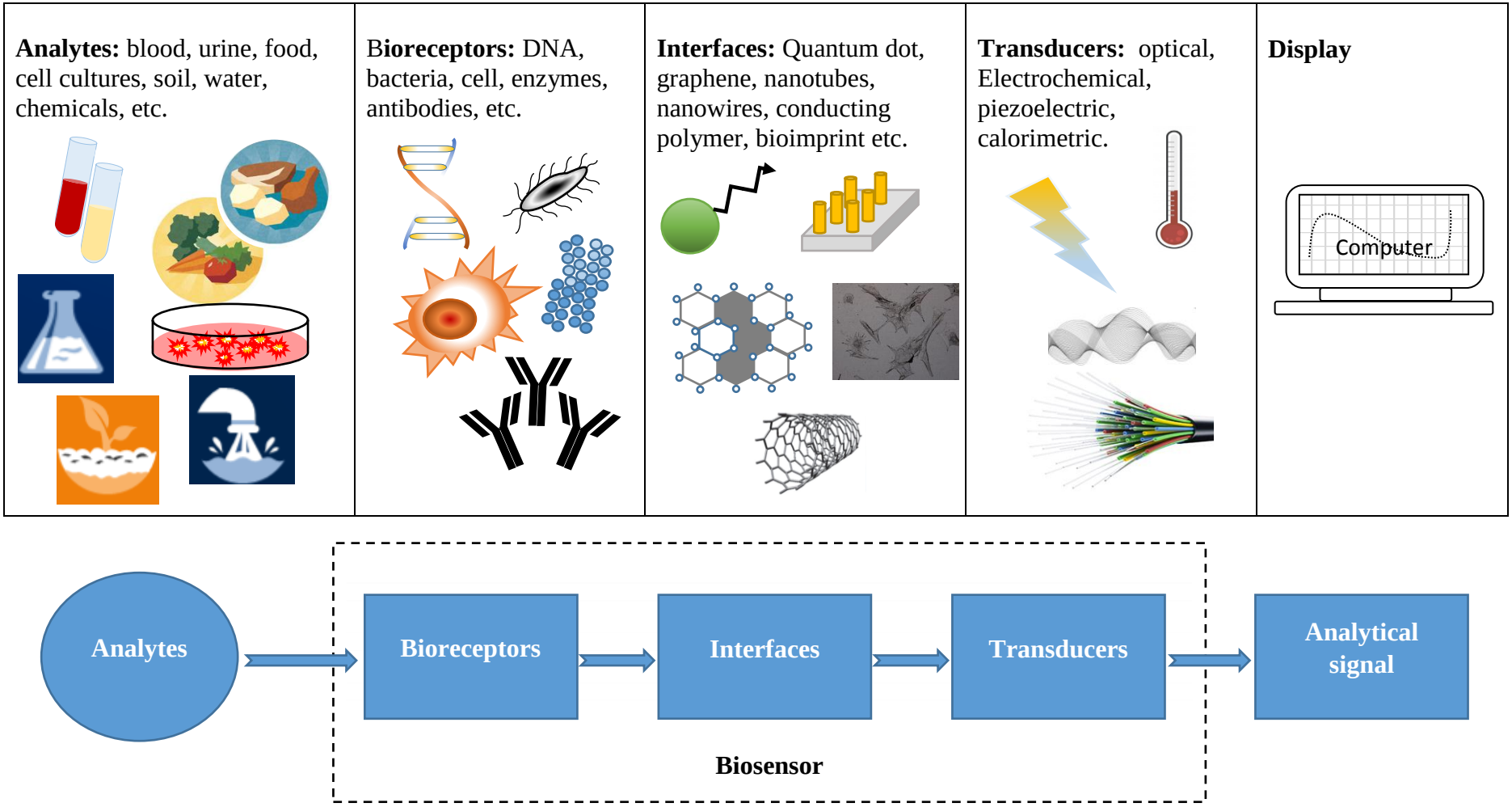

Figure 2.1: Schematic of the generalised biosensor.

One of the major driving forces for the development of these devices is in biomedical diagnosis. The main advantages of biosensors include:

- low cost and light weight
- small size requiring only small volume of materials for testing
- fast analysis on multiple samples
- easy to use, portable and can be used by non-specialist
- the sensitivity and selectivity greater than the current sensor technology.

The superiority of cheap, user-friendly biosensors has the potential to revolutionise the practice of healthcare monitoring and point-of-care diagnostics. Biosensors have also been used in specialised applications including agriculture, food technology, environmental monitoring, industry and in the biomedical field [85], [86], [88]. Furthermore, growth in the field of biosensors has been phenomenal and according to the global biosensors market survey it is expected that significant growth from 15.4 billion USD in 2014 to 31.0 billion USD in 2024 is expected through myriads of applications [90].

2.1.1 Transducers and their applications

Biosensors are typically categorised according to the transduction method they employ. There are four types of the transducers commonly used in biosensors, based on the principle involved [91]; these are electrochemical, optical, piezoelectric, and calorimetric transducers. This classification is illustrated in Figure 2.2.

2.1.1.1 Electrochemical biosensors

Electrochemical biosensors were introduced by Clark and Lyons more than five decades ago based on the principle of the enzyme electrode with immobilised glucose oxidase [89], [91], [92]. The development of electrochemical biosensors have received great attention to date because it offers a great selectivity and sensitivity over other types of biosensors [92], [93]. In this configuration, the changes of electrical potential between immobilised biomolecules and target analytes are induced as a result of consumption of either ions or electrons. There

are four different types of electrochemical biosensors: amperometric, potentiometric, conductometric and impedimetric operating transducers.

2.1.1.2 Optical biosensors

Optical biosensors are based on the changes of analytes on the basis of surface plasma resonance (SPR), Raman, FTIR, and light scattering [93], [94]. The reaction causes a change in fluorescence or absorbance due to change in the refractive index of the surface between two media that differ in density. For instance, if antibodies bind on a metal layer, the refractive index of the medium in contact with this layer will change. Since they are non-electrical, optical biosensors have the advantages of lending themselves to *in vivo* applications and allowing multiple analytes to be detected by using different monitoring wavelengths. Fibre-optic probes add to the versatility of the biosensors due to their capacity to transmit signals that report on changes in wavelength, wave propagation, time, intensity, distribution of the spectrum, or polarity of the light.

2.1.1.3 Piezoelectric biosensors

Piezoelectric biosensors are considered to be mass-sensitive detectors, also known as acoustic biosensors. The use of piezoelectric crystals is based on the principle of surface acoustic waves (sound vibrations) at resonant frequency. The common piezoelectric sensors are based on surface acoustic waves (SAW) devices and quartz crystal microbalance (QCM). The advantages of these mass-sensitive transducers are their ability to react to minimal changes of analyte weight attached on the piezoelectric surface and their low cost. In this condition, the interaction between analyte and the detector sets up mechanical vibration, which is converted to an electrical signal. Unfortunately, the drawback of this type of biosensors is lack of sensitivity and specificity when used in solution because the crystal may stop vibrating in a liquid phase [94].

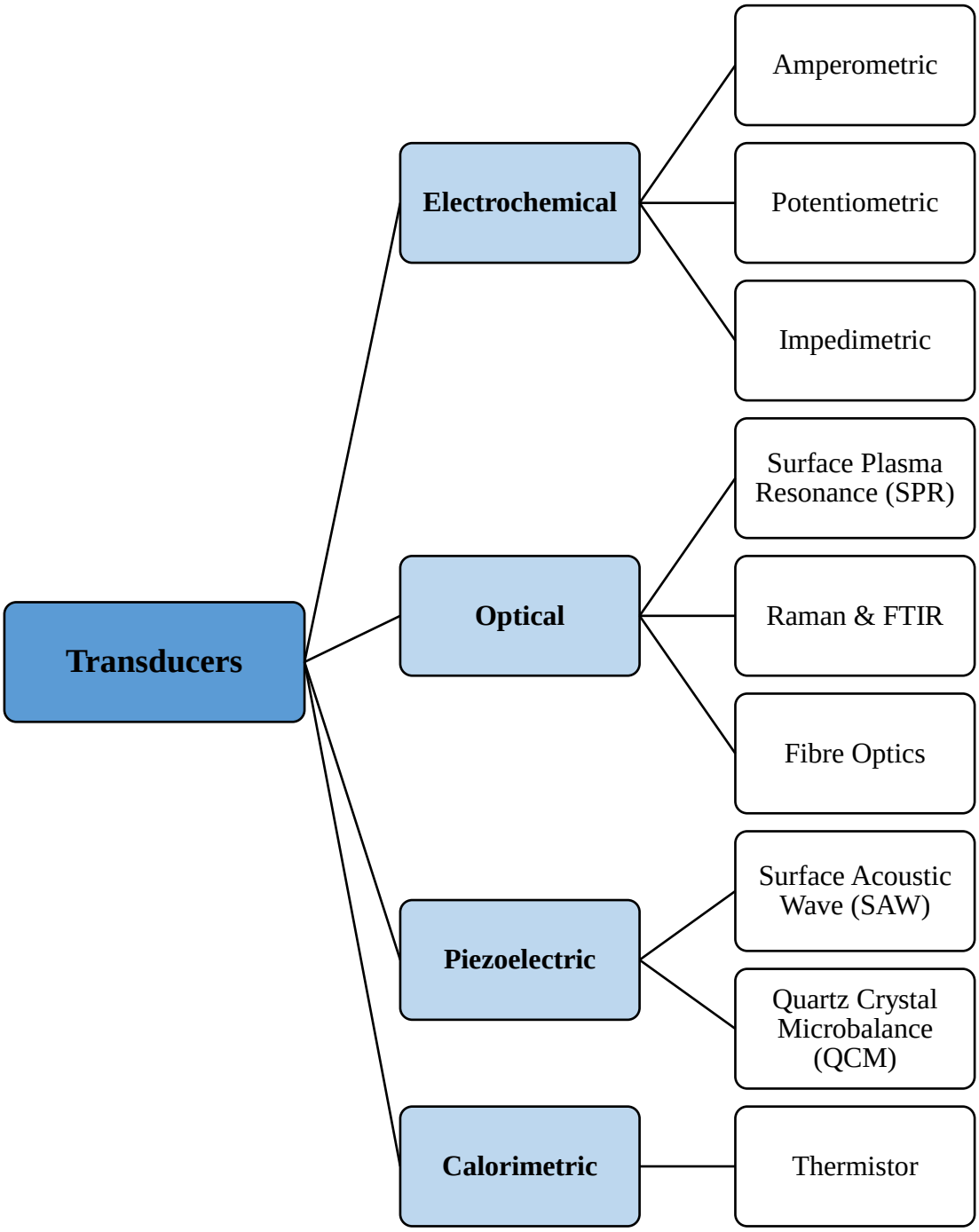

Figure 2.2: Classifications of transducers employed in biosensor construction. The method of transduction depends on the type of the physicochemical changes resulting from the sensing event.

2.1.1.4 Calorimetric biosensors

Most enzyme-catalysed reactors are sufficiently exothermic to make calorimetric detection a practical proposition. There are two thermistors used to measure the temperature changes of circulating solution during biochemical reaction. Usually the immobilised enzymes are used as a suitable biorecognition element. Thermic reactions catalysed by enzymes are measured with a thermistor, which consists of metal oxide beads or discs.

2.1.2 Materials-based transducers

The history of the development biosensors dates back to 1956 when Clark and Lyons demonstrated an enzyme electrodes for oxygen. Later, in 1962 they expand the range of analytes to glucose detection using dialysis membrane. This was followed by Guilbault and Montalvo's discovery of a urea biosensor [95], and finally the first commercial biosensor was successfully launched in 1975 by the Yellow Springs Instrument Company. Ever since the development of the electrode-based biosensor, remarkable progress has been achieved in the field of biosensors. This is evident in the publication records, where there are more than ten thousand research articles on the biosensors topic.

Advances in nanotechnology have led to the development of biosensor fabrication especially on bioanalytical applications. Moreover, the selection of electrode material plays a key role in ensuring high sensitivity and selectivity properties of the biosensors. There are various nanomaterials that have been considered to replace the electrode-based sensors, such as nanoparticles, quantum dots, nanowires (NWs), carbon nanotubes (CNTs), graphene and CPs, which have had a profound influence on biosensor performance.

Amongst the metal nanoparticles, mainly gold nanoparticles (AuNPs) are used for biosensor application due to their high electrical conductivity, small size, biocompatibility, chemical inertness, fast electron transfers and high surface-to-volume ratio. This helps in providing a stable immobilisation activity [96]–[98]. Furthermore, the use of nanoparticles has improved electron microscopy scanning but is also a good candidate for optoelectronic applications for DNA diagnosis [98]. Fayazfar *et al*. have developed a novel DNA impedance biosensor with excellent sensitivity properties for the detection of the TP53 gene mutation. In their research,

they succeeded in growing AuNPs on multi-wall carbon nanotubes(MWCNTs) through an electrochemical process [99].

Whereas, quantum dots are inorganic nanoparticles with approximately less than 10 nm size that has unique properties such as broad excitation energy, narrow emission spectra, high photochemical stability and negligible photo bleaching. Alternatively, quantum dots have been used to fluorophores for optical biosensors in ions detection, organic compound, pharmaceutical analytes, and biomolecules. In fact, quantum dot have been widely used for multiplexed optical bioanalysis owing to ultra-high sensitivity, high specificity, cost effectiveness, and rapid analyte detection [82], [100].

Since 2000, nanotubes (NTs) have revolutionised the electronic detection devices because of its ability to provide label-free and real-time, yet sensitive and selective detection of a wide range of chemical and biological analyte [100]–[102]. Carbon nanotubes (CNTs) were first discovered in 1991 during fullerenes preparation [103]. There are two types of CNTs: multi-walled carbon nanotubes (MWCNTs) [103] described earlier and single-walled carbon nanotubes (SWCNTs) [104]. Most notably, CNTs offers several advantages over conventional carbon-based electrodes, such as high electrical conductivity, minimum surface fouling, chemical stability, and mechanical strength [101], [105]–[107]. Initially, electrodes based on carbon were widely used owing to inexpensive, possess good electron transfer kinetics and are biocompatible criteria. The CNT was successfully used in diagnostic devices, tissue engineering, biosensors and drug delivery [101], [105], [108]. On the other hand, graphene is a three dimensional (3D) form of carbon atoms arranged in a hexagonal lattice with potential applications in sensing devices [109], [110]. Graphene have been used in various biosensors-based concept depending on the sensing mechanisms owing to its high sensitivity, inexpensive, fast response and easy operation [109], [111].

CPs are organic materials that are very stable, flexible, easy to synthesise, versatile, and inexpensive, with good conductivity, and they can be fabricated with various polymer matrices; this makes them a great electroactive material for sensing applications [20], [112]. Due to these unique features, most CPs are also being extensively used in biomedical applications such as drug delivery, neural probes, tissue engineering biosensors and bio actuators [20]. The physical, electrical and chemical properties can be tuned to create

substrates with high surface area in order to decrease their impedance in neural probe applications [20], [113], [114], timed release of drugs, anti-inflammatory drugs [115], tissue engineering [115], entrapment of molecules [23], biosensors [20], [23], [113]–[116] and DNA sensors [116] .

In summary, it has been shown that the numerous developments in biosensors mostly rely on their specificity, material, sensitivity, fast response, non-toxicity, small size and low cost for specific applications. Innovation in the design of biosensors for the clinical diagnostics industry by the integration of biosensing device configuration and material selection is key for the successful development of specific, purpose-made biosensors suitable for the modern era.

2.2 Conducting polymer–based biosensors

Polymers are made up of many molecules bound together to form long and repeating chains. The term polymer comes from the Greek word poly meaning “many” and -mer meaning “segment or parts”. Polymers are often referred to plastics, such as nylon, and rubbers, as they can be shaped or moulded for household, electronics and packing industries.

CPs, on the other hand, also known as “synthetic metals” are organic polymers that conduct electricity. The attractiveness of CPs relies on their ability to act as an effective material for immobilisation of biomolecules and to improve the biosensor performance in terms of sensitivity and specificity [26]. CPs have received significant interest for their physical, mechanical, chemical and electrical properties and find many practical applications such as thin film transistors, antistatic coatings, light emitting diodes, fuel cells, computer monitors, batteries, corrosion-resistant coatings, supercapacitors, sensors, biosensors and most recently in biomedical applications [20], [23], [26], [39], [45], [117], [118]. Research on CPs for biomedical and tissue engineering expanded greatly after the 1980s because the properties of these materials can be tailored and made compatible with many biological molecules.

The very first reporting on organic conducting polymers [poly (acetylene)] behaving as semiconductors was in 1977, by Shirakawa, Heegar and MacDiarmid [119]. Shirakawa and

his co-workers wrote on the synthesis and characterisation of a poly (acetylene) doped with halogen producing remarkably high conductivity [119], [120]. For this discovery, they were awarded the Nobel Prize in Chemistry in 2000. Following this discovery, a new class of organic CP materials were developed, such as polypyrrole, polyaniline and polythiophene (Table 2.1) [26]. Nowadays, many articles, reviews and books have been published covering the use of CPs in wide areas of device research and material sciences for better understanding.

Polymer	**Discovered**	**Chemical structure**	**Conductivity (Scm^{-1})**	**Ref.**
Polyacetylene, PA	1977	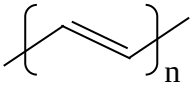	10^3–10^5	[119]
Polypyrrole, PPy	1979	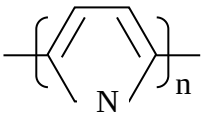	10^2–10^3	[121]
Polyaniline, PANI	1980	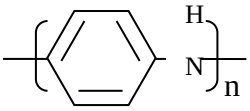	10^2	[122]
Polythiophene, PT	1981	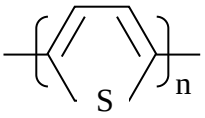	10–10^3	[123]

Table 2.1: Chemical structures of representative CPs and those most commonly explored for biomedical applications.

2.2.1 Doping

It has been reported that the electrical properties of CPs can be tuned either by chemical or electrochemical modification or by atomic– or molecular–scale doping [30], [47], [124]. Doping has been widely used for various conjugated polymers. It was found that dopants play a crucial role in changing the properties of a CP, comparable to those of conventional semiconductor.

CPs are usually chemically synthesised by blending the monomer solution with an oxidising agent. This process produces a very thick film or powder of the polymer and suitable for commercial production [20]. The advantages of this synthesis method is that it can be applied to all types of CPs including the polymers that cannot be synthesised by the electrochemical method. Inappropriately, this method will generate lower electrical conductivities than those CPs produced via electrochemical synthesis. There are numbers of factors that affect the conductivity of the CPs such as type of solvent, stirring rate, reagent concentration, time and temperature.

Alternatively, the CPs can be synthesised using electrochemical method by applying an electrical current through electrodes in the solution containing diluted polymeric monomer and solvent [26]. The advantage of this technique that it can produce a very thin film as thin as 20 nm and well–controlled morphology [20]. The electrical current leads to film deposition and oxidisation on the working electrode that produce insoluble polymer chains. Normally, the deposited film is affected by several of factors such as temperature, deposition time, electrode system, doping and solvent agents [26].

In general, materials can be categorised into three classes depending on the electrical conductivity: insulators, semiconductors and conductors. An overview of the broad conductivity ranges of CPs, metals, semiconductors and insulators is given in Figure 2.3. The most essential property that distinguishes polymers from metals is their electrical conductivities. The electrical conductivity for metals is very high and is generally in the range of 10^{3}–10^{8} Scm^{-1} while a good insulator's conductivity is as low as 10^{-18} Scm^{-1}, and semiconductors have conductivities ranging between conductors and insulator. In contrast, the electrical and optical properties of CPs can be modified from insulator–to–metal transition by changing the doping concentration [125]. The progress in doping method offers wide range opportunity for switching semiconducting properties in many optoelectronics applications such as light-emitting diodes (LED), photoresistors organic-polymer–based transistors and polymer-based organic solar cells.

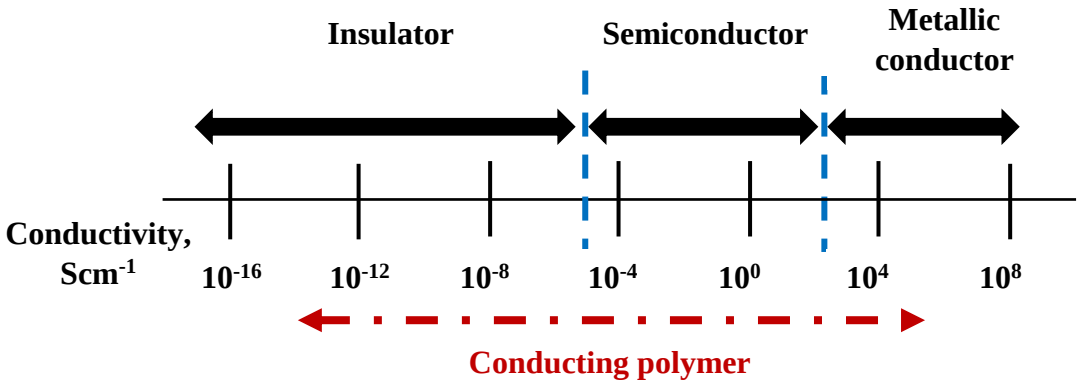

Figure 2.3: Conductivity of CPs can cover the whole insulator–semiconductor–metal region by changing the degree of doping [125].

2.2.2 Poly (3,4-ethylenedioxythiophene): polystyrene sulfonate, PEDOT:PSS

PEDOT:PSS is a CP made from a mixture of two ionomers, namely poly (3,4-ethylenedioxythiophene) and polystyrene sodium sulfonate. The combination of PEDOT and PSS macromolecules formed a very stable water-soluble CP. The chemically polymerised PEDOT: PSS was first discovered by Jonas and Schrader at Bayer AG research laboratories in Germany in 1988 [126]. PEDOT:PSS has been applied in light-emitting diodes [31], [126], [127], solid electrolyte capacitors [128], antistatic coatings [129], transistors [29], [31], [130], photovoltaic cells [31], [127], [131] and conductive textile [132]. Moreover, PEDOT: PSS is a potential candidate to replace indium tin oxide (ITO) due to its flexibility, ease of processing, inexpensive and good optical properties, and is a widely used material as a transparent electrode [133], [134]. Nevertheless, more novel ideas must be found to further improve the electrical conductivity of PEDOT: PSS with additives such as dimethyl sulfoxide, glycerol and ethylene glycol. Kim *et al*. reported that the electrical property of PEDOT: PSS can be enhanced by about two orders of magnitude due to the effect of organic solvents on the conduction band of the polymer chain [135]. Meanwhile, Xue *et al.* reported that the performance of poly(3-hexylthiophene) (P3HT) thin-film transistors (TFTs) modified with PEDOT-PSS as source and drain electrodes has similar characteristics to those devices with gold contact material [130].

2.3 Hydrogel-based biosensors

Hydrogel-based biosensing has attracted significant attention due to its unique characteristics over to the conventional biosensors. Currently, hydrogels are widely utilised in contact lenses manufacturing, hygiene products, tissue engineering scaffolds, drug delivery systems, and in wound healing. Hydrogels are hydrophilic three-dimensional (3D) polymeric networks. Initially, hydrogels are normally protein based and come from natural origins such as collagen, fibrin, chitosan, dextran, hyaluronic acid (HA) and alginate. These polymers are inherently biocompatible, biodegradable and bioactive [136], [137]. However, their use are limited owing to water solubility and poor mechanical properties. These limitations can be overcome through either chemical or physical crosslinkers [138]–[140].

A great number of research paper and review studies have shown that hydrogel-incorporated biomolecular biosensors can be an excellent alternative system to detect a wide range of biomolecules [141], [142], pathogens [143], enzymes, [137], [144] proteins [145], neurons [140], [146] and genes [146]. This hydrogel polymer can be produced into a number of device sizes and shapes that potentially for integration into a sensing device [144], [147]. The technique of surface patterning of hydrogel not only produces excellent non-fouling properties but is also effectively used to control and promote cell attachment [148], [149].

2.4 Conducting Polymer hydrogel based biosensor

Recently, conducting hydrogels have drawn considerable attention in the field of biosensors and biomedical devices [25], [26], [34]. The biosensors used for the biological research are prepared using the conducting hydrogel polymers based on polyaniline (PANI), poly(3, 4-ethylenedioxythiophene) (PEDOT) and polypyrrole (PPy), due to their unique properties such as high stability, good conductivity, facile polymerisation and biocompatibility [25], [26], [34], [150]. Moreover, the combination of conducting polymer and hydrogel could potentially be used as electro-sensitive biomaterials in tissue engineering as their ability to mimic tissue components and at the same time provide electrical stimuli in the system.

In this work, we used PEDOT:PSS as a conducting element to create a conductive substrate with cell-like features, known as a conductive bioimprint. This material has been examined

to sense the cell reactivity as a function of cell electrical conductivity. PEDOT:PSS is one of the most successful polymers owing to its biocompatibility with biological systems, excellent environment stability and high electrical conductivity properties. In addition, this unique CP features enable the fabrication of flexible electronic devices in low-cost methods such as soft lithography, drop casting, dipping, spin coating, spray coating, inkjet printing, and screen printing [29].

Physically, PEDOT:PSS exhibits fragility, has poor mechanical properties and is not suitable for tissue engineering when used on its own. By blending PEDOT:PSS with chitosan, elastomer and gelatin, results in a more CH with improved imprinting quality, chemically stability, enhanced mechanical properties, good electrical conductivity, in addition to biocompatibility and biodegradability [34], [35], [37], [42], [151], [152]. From the previous studies, the electrical properties of PEDOT:PSS can tune cellular behaviour such as adhesion, migration, proliferation, and differentiation through electrical stimulation [32]. Thus, the integration of hydrogel into PEDOT:PSS helps to trigger the cells' desorption [153]. Conducting biomaterials are excellent candidates in tissue engineering for the development of inexpensive, biodegradable, bioimplantable devices, portable, miniaturisation and non-invasive biosensors.

2.5 Electric Cell–substrate Impedance Sensing (ECIS)

Electric cell–substrate impedance sensing is a real–time, label–free, and non–invasive method to investigate cellular behaviour such as adhesion, growth, proliferation and motility on the electrode surface [154]. The concept of using the ECIS measurement of a cell monolayer was first documented in 1991 by Giaever and Keese [155]. They have monitored the micromotion of fibroblast cells on gold electrodes with an applied electric field in the impedance system.

Alternatively, the standard methods that widely used for cell-based assay monitoring includes using trypan blue exclusion test, fluorescent staining, crystal violet, coomassie brilliant blue, MTT assays and atomic force microscopy [156], [157]. Trypan blue tests is a simplest method to determine live and dead cell in culture sample. Unfortunately this procedure impair the cell membrane integrity by involving the addition of a blue dye to penetrate the membranes of

dead cells. It also incapable to be used for large number of sample and require time consuming after the staining process. Fluorescent labels are different because they are used to stain components of living cells. The use of fluorescent labels can provide highly accurate results about cellular viability and require sophisticated equipment. Crystal violet and coomassie blue is the most common, easier and cheaper method to stain protein. However, the protocol requires time to remove unwanted stain form the sample. In a MTT assay, a dye is added to the cells, which changes colours upon reduction by enzymes present in live cells. The colour change can then be used to show changes in cell viability. The disadvantages of this method that the labels will alter the natural state of the cells and need post analysis with specific tool for the analysis. In comparison from the dyes method, atomic force microscopy (AFM) is a very powerful and expensive instrument to measure cell behaviour such as viability, adhesion and topography [157]. The major disadvantage of AFM is that it can only obtain the surface of the sample information and has scanning speed limitation, requiring several minutes for typical scan. Furthermore, there is possibility of image artefacts due to sharp tips cantilever and poor operating environment.

Staining Method	**Advantages**	**Disadvantages**
Trypan blue	-Easy procedure -inexpensive	-Invasive and change cell environment -need post-test analysis
Fluorescent staining	-High accuracy	-Invasive and change cell environment -need post-test analysis -Need sophisticated and expensive equipment
Crystal violet	-Easy procedure -inexpensive	-Invasive and change cell environment -need post-test analysis
Coomassie blue	-Easy procedure -inexpensive	-Invasive and change cell environment -need post-test analysis
MTT assay kit	-Inexpensive	-Invasive and change cell environment -need post-test analysis

AFM	-High accuracy	-Invasive and change cell environment -Need sophisticated and expensive equipment

Table 2.2: The summary of cell-based assay techniques for medical diagnosis and monitoring.

The sharp contrast use of ECIS that is allows for the monitoring the changes of cellular adherence and viability as a function of electrical properties from the beginning of the experiment and continuously throughout the experiment. To date, the conventional and commercial ECIS system has been successfully demonstrated for wound healing with several cell lines such as myoblasts, fibroblasts, osteoblasts and endothelial on gold electrode [158]–[161]. The conventional ECIS system consists of gold electrodes in the bottom of the cell culture dishes, connected to the impedance analyser machine that controls, measures and stores the data. Figure 2.4 and 2.5 illustration a schematic diagram and the equivalent circuit of ECIS system without/with cell within a sweep frequency range. The electrical impedance |Z| of ECIS system is calculated by the ratio of voltage, V(t) and current I(t) according to Ohm's law:

$$Z = \frac{V(t)}{I(t)} \qquad (2.1)$$

Figure 2.4 (a) shows the without cell system immersed in culture medium. The solid blue arrows indicate that the current flows unrestrained from the surface of the gold electrodes. The equivalent circuit can be described as: R_1 is an electrode resistance in parallel with the dielectric capacitance (C_{Elec}) of the electrode are connected in series with the resistance of medium-electrode interface (R_{MED}) as shown in Figure 2.4 (b).

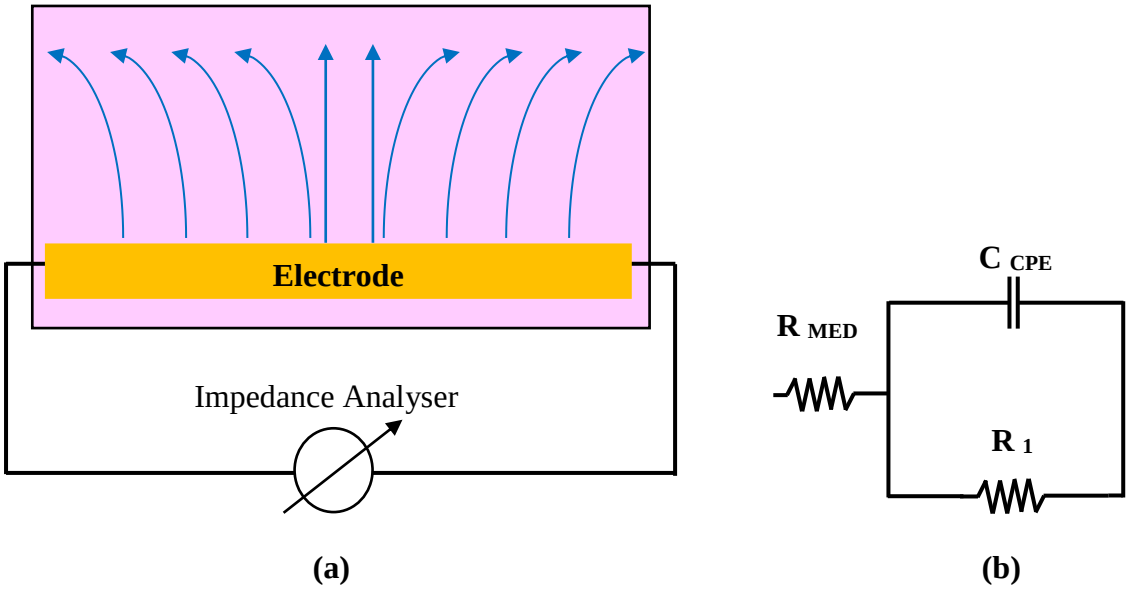

Figure 2.4: ECIS system without cell in culture medium (a) a schematic diagram of unrestricted electric current path from gold electrode surface and (b) equivalent circuit of cell-free medium system.

When cells are seeded and attach to the ECIS electrodes arrays, the increases in the impedance due to the cells response because they act like insulator/dielectric elements to the system. As cells grow and covering the electrodes, the current flow was affected to the number of cells covering between the electrodes and the changes in impedance fluctuated with cultivation time. In addition, the degree of the impedance change is determined by number of cells seeded on the electrode, cell–cell interaction, cell morphology and motility. As in Figure 2.5 (a), the solid blue arrows indicate the current path through the cell membranes at low frequency [160], [162]. While high frequencies, a current path (red dashed straight arrows) moving in the solution spaces between the electrode and the plasma membrane, then moving through between the cellular [160], [162].

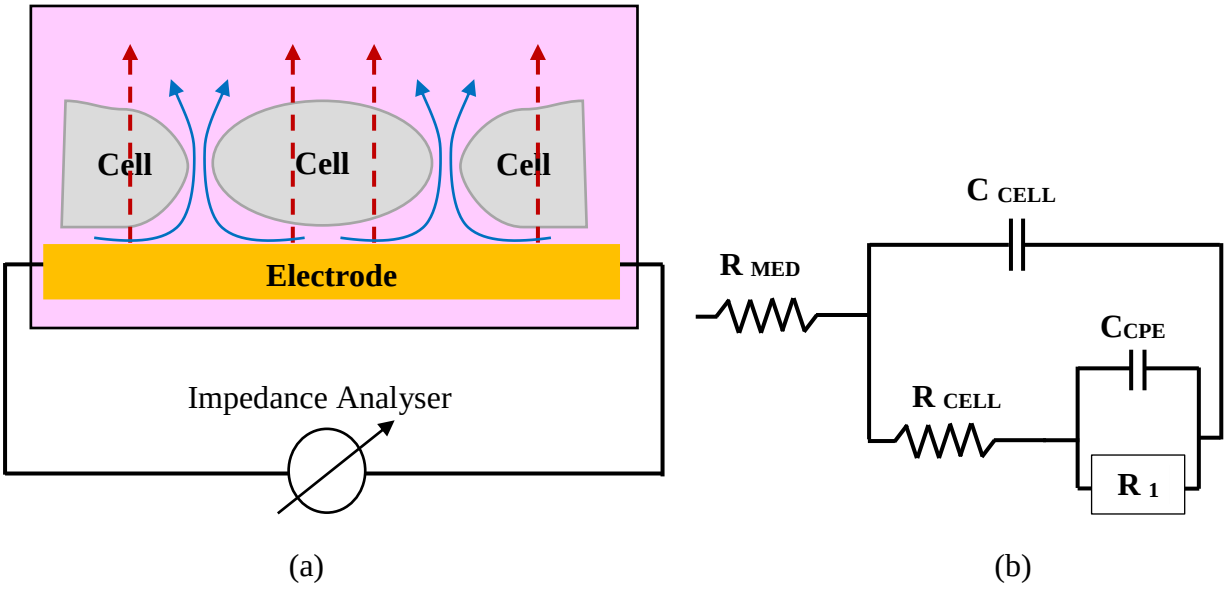

Figure 2.5: ECIS system with cell in culture medium (a) a schematic diagram of an electric current path flow passing from the electrode through/between the cells at low and high frequency (b) equivalent circuit after cell seeding.

As can be seen in Figure 2.5 (b), the equivalent circuit of ECIS measurements on intact cells. The best fitting of the cell-culture medium system can be presented to C_{CELL} the capacitance of the biomolecule adsorption layer and cells on the electrode surface is connected in parallel with a cell resistance (R_{CELL}).

Recently, impedance-based sensing technology has gained a great deal of attention for medical diagnosis, monitoring drug-induced cytotoxicity and cellular events at implant sites [163], [164]. There are many commercial ECIS systems available in the market with various designs and electrode sizes, such as BioPhysics (http://www.biophysics.com), ibidi (https://ibidi.com) and ACEA Biosciences, Inc (https://www.aceabio.com. These companies provide ECIS systems to researchers for drug research, clinical diagnostics and laboratory facilities. These products provide excellent ECIS platforms systems to researchers for demonstrating the ability to measure large changes in impedance in cellular studies. However, the disadvantage of these systems is that both are require dedicated laboratory space for operation and large size of electrodes. The devices are not portable and cannot be integrated with other cell culturing equipment. In order to maintain control over the cell culture

environment, special accessories such as incubators must be purchased specifically for the systems.

CHAPTER 3

Materials and Methods

This chapter describes the various materials and methods that were utilised in performing the research presented in this thesis. It begins with an overview of the major materials used, followed by a description of the main methods and equipment employed for cell-culture protocols, fabrication processes and characterisation tools of the new conductive bioimprint technique.

3.1 Materials

Phosphate buffered saline (PBS) tablets (Sigma Aldrich), polydimethylsiloxane, PDMS (Sylgard 184, Dow Corning Corp.), 0.1% w/w hydroxypropylmethylcellulose, HPMC (H8384, from Sigma Aldrich), 0.05% trypsin-EDTA, 10% sodium dodecyl sulphate, 25% glutaraldehyde (G5882-50ML, Sigma-Aldrich) diluted to 2.5% in deionised water, 0.4% trypan blue solution (T8154, Sigma Aldrich), hexamethyldisilazane, HMDS (reagent grade ≥99%, Sigma Aldrich), 0.2% crystal violet with 20% ethanol in deionised water, GlutaMAX (11995-065, Sigma Aldrich), ethanol (analytical grade, from LabServ), penicillin/streptomycin 100x (Gibco (via Invitrogen)),negative photoresist AZ 1518 and developer MIF 326 (MicroChemicals GmbH).

3.2 Cell culture protocol

Tissue culture technology has found wide applications in the field of biochemistry, biomedicine and biotechnology since it was invented at the beginning of the twentieth century [4]. Cell culture is a procedure for growing or maintaining cells *in vitro* under controlled or aseptic conditions. In this research, the cell culture protocols were performed according to the institutional guidelines of the Christchurch School of Medicine and Health Sciences, University of Otago, New Zealand as shown in Figure 3.0 (a) to (h). Mouse myoblast, C2C12

cell line was used and obtained from the University of Otago. Myoblast cell line was selected for this research because they offer higher proliferation rates and robust baseline viability [165]. Before the cell cultures were realised, all solutions and equipment had to be sterilised and stored at an appropriate temperature.

In the physical containment level 2 (PC2) laboratory, the frozen cells cryovial was thawed by gentle agitation in a water bath at temperature 37 ℃ (Fig. 3.1 (a)). After defrosting for about two minutes, the cryovial was removed and sprayed with 70% ethanol for decontamination. It was then placed in a laminar flow tissue culture hood and all aseptic conditions were strictly followed. The cryovial lid was unscrewed and the contents were transferred into a 25 cm^3 tissue culture flask containing Dulbecco's modified Eagle's medium (DMEM, Life Technologies) supplemented with 10% fetal bovine serum (FBS, Life Technologies), 1% Fungizone (Life Technologies) and 1% penicillin-streptomycin (P/S, Life Technologies) (Fig. 3.1 (b)). In fact, the cell culture medium was an important factor that influenced the cell growth. It was then incubated at temperature 37 ℃ with a concentration of 5% CO_2 until it reached 80–90% confluency (Fig. 3.1 (c)). Cells were checked microscopically daily to ensure they were healthy and growing as expected. The working medium was replenished every two days during the culture period for maximum cell growth. Attached cells should have been mainly attached to the bottom of the flask, round and plump or elongated in shape and refracting light around their membrane.

As cells reached confluency, they were sub-cultured or passaged to decreased mitotic index and cell death. The culture medium was discarded from the culture flask and rinsed twice with PBS (pH 7.4) solution to remove any unattached cells. A 5mL of 0.5% trypsin-EDTA solution was pipetted until it covered the flask surface and this was left in the incubator for 10 to 15 minutes for the detaching process (Fig. 3.1 (d)). The detached cells were transferred into the centrifuge tube and spun down at 1500 rpm for 5 minutes (Fig. 3.1 (e) & (f)). The supernatant was aspirated from the cell pellet, then the pellet was re-suspended in an appropriate volume of growth medium in order to deactivate the trypsinisation process and to prevent cells from dehydrating (Fig. 3.1 (g) & (h)). A volume of 10 µL of cell suspension was pipetted into a hemocytometer to determine the cell number and concentration in the cell medium.

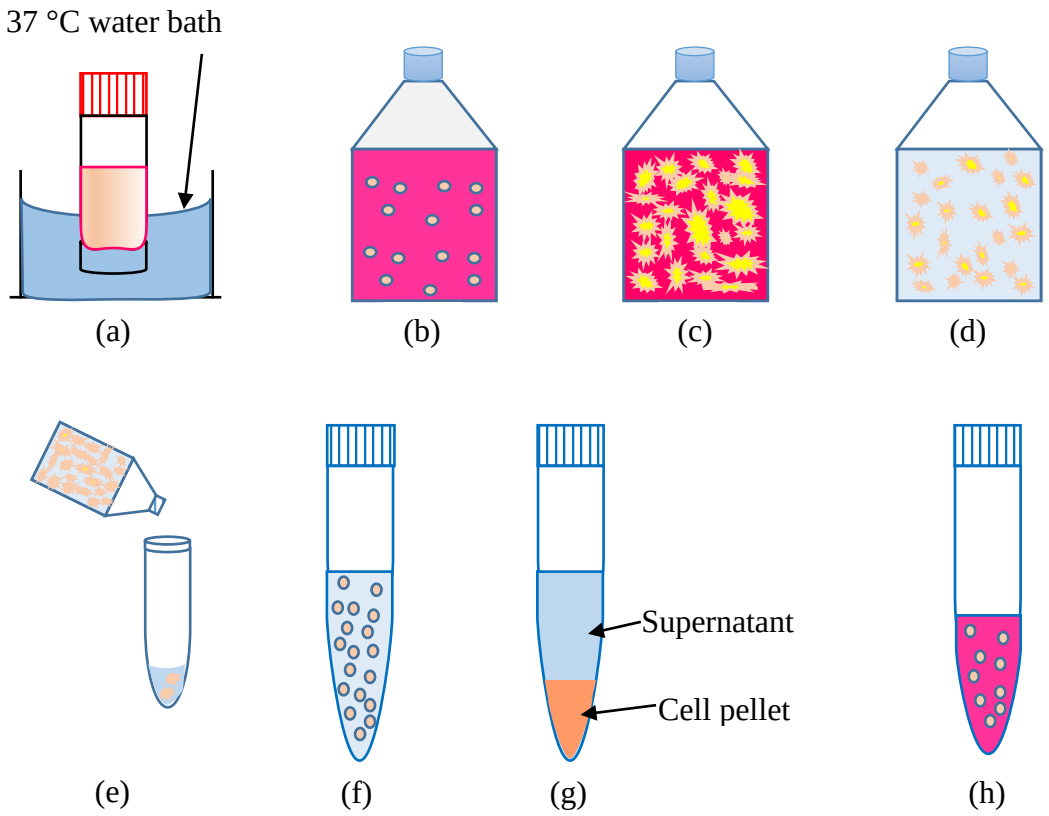

Figure 3.1: Schematic diagram of cell culture protocol: (a) thaw the frozen cell in a 37 ℃ water bath, (b) transfer vial contents into 25cm^3 tissue culture flask, (c) incubate at 37 ℃, 5% CO_2 until 80–90% confluency (d) remove culture medium, rinse with PBS solution and add 5mL of 0.5% trypsin EDTA (e) incubate for 10 to 15 minutes to detach process and dispense disassociated cells into centrifuge tube, (f) spin at 1500 rpm for 5 minutes, (g) aspirate off supernatant, and (h) add an appropriate expansion growth medium in a cell pellet.

3.2.1 Cell counting

Cell viability can be tested by using the trypan blue exclusion method. Initially, 0.4% trypan blue was used to distinguish between live and dead cells. Trypsinised cells were stained with 100 µL of 0.4% trypan blue in 100 µL of PBS (pH7.4). After three minutes, 10 µL of cell suspension was pipetted into the V-shaped well of the hemocytometer. The cell counting chamber was then placed on the inverted light microscope stage with a 10x objective. The live cells have intact cell membranes that exclude trypan blue dyes causes viable cells appeared clear and shiny. While, the dead cells will absorb these dyes and they were stained blue. The number of live or dead cells were only counted within a four-red-square boundary straight line as shown in Figure 3.2. The number of cells /mL was calculated by the average of cell number per square x dilution factor × 10^4 /mL.

Example of calculation:

$$= \left(\frac{\text{Total number of cells in square (A+B+C+D)}}{4} \right) \times \text{Dilution factor x } 10^4 \text{ /mL}$$

= Number of cell /mL in original suspension.

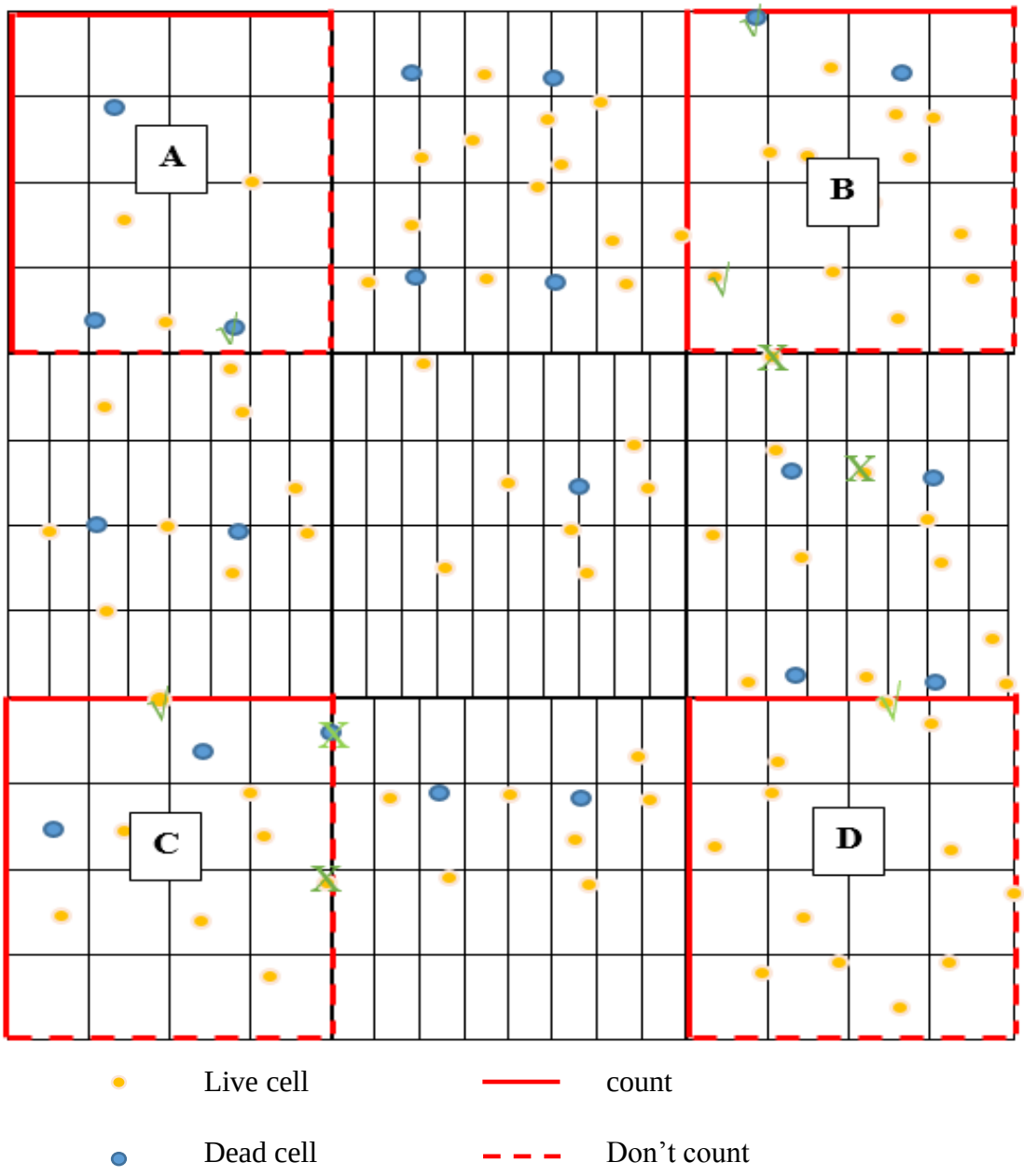

Figure 3.2: Hemocytometer diagram indicating four set of 16 squares that should be used for cell counting.

3.2.2 Cryopreservation protocol

A freezing procedure is the best way to preserve or generate sufficient cell stock for use at later date. As usual, the culture medium was aspirated from the 25 cm^3 culture flask when the cell confluency reached 80–90%. It was then rinsed twice with PBS solution and pipetted with 0.5% trypsin solution on the cells until all cells began to detach. The disassociated cells were removed in a 15 mL tube and centrifuged at 1500 rpm for five minutes. The supernatant was aspirated and the cell pellet resuspended in the freezing medium of 10% DMSO/ 80% FBS/ 10% cell medium DMEM. This cell suspension was dispensed into a 1.5 mL cryovial, placed in a Nunc freezing container and quickly stored at a temperature of –80 ℃ in a freezer. After 24 hours at –80 ℃, the frozen cryovial was removed and stored in a liquid nitrogen tank until required.

3.3 Fixation methods

There are several reagents that can be used to fix the cells. In this research there are four types of fixative solution used for replication and imaging purposes, namely paraformaldehyde, glutaraldehyde, crystal violet and fluorescence staining. The idea behind these methods is to halt cell decomposition, freeze cellular proteins and subcellular structures.

3.3.1 Paraformaldehyde

In this method, paraformaldehyde is used to form a crosslink between protein in tissues and the surroundings. Formaldehyde is by far the most popular agent used for histopathology due to its simple and fast method, which usually provides the best preservation for cellular proteins and have made it useful as a general purpose fixative. Cell cultured substrates were washed twice with PBS (pH7.4) solution and covered with 4% paraformaldehyde solution for 30 minutes at room temperature. Following fixation, cells were washed with sterile water at least three times to remove the PBS salt. Then, fixed cells were kept at 4 ℃ overnight for the drying process before the bioimprinting processes or imaging.

3.3.2 Glutaraldehyde

As an alternative to paraformaldehyde, cells can be fixed by using glutaraldehyde. Glutaraldehyde is widely used for ultrastructural studies requiring electron microscopy and requiring a long time protocol. When cells were ready for the fixation process, they were washed twice with PBS (pH 7.4) solution to remove unwanted debris. Then, cells were fixed with 2.5% of glutaraldehyde in 0.1 M PBS (pH 7.4) solution for two hours at room temperature. The fixative was removed and cultures were replaced in 70%, 85%, 95%, 100% ethanol for five minutes and finally in HMDS for five minutes.

3.3.3 Crystal violet assay

Crystal violet is one of the simple and versatile methods that stains adherence cells on the substrate and make them visible to the eye. Crystal violet is a purple dye – the mixture of 0.2% crystal violet solution in 2.0% ethanol acts as a fixative and keeps cellular structures intact. The protocol used provided a quick screening method for the examination of cell survival and growth inhibition.

When cells were ready for staining, the cell culture medium was aspirated from the culture flask. Then, samples were washed twice with PBS (pH 7.4) solution and stained with crystal violet dye for 30 minutes at room temperature. After that, the purple dye was discarded and the excess stain removed by washing repeatedly with tap water until the colour of the water changed from blue into clear blue.

3.3.4 Fluorescent staining

When using the fluorescence microscope technique to study cells, it is essential that the cell structure and content are preserved before imaging. The cells were fixed with 4% paraformaldehyde for 45 minutes at room temperature, followed by a wash with PBS (pH 7.4) solution four times. Then, the cells were covered with plasma membrane dye and placed in a 4 °C room overnight. This staining was essential to observe cellular functions such as mobility and contraction of cells during proliferation. After primary antibody incubation, the cell's

nucleus was labelled with Hoechst 33258 DNA dye for 30 minutes and washed three times with PBS (pH 7.4) solution. Fluorescence microscopy and confocal fluorescence imaging was performed using Leica DMI4000B and Zeiss Axio Imager epifluorescence microscope (Carl Zeiss Meditec AG, Jena, Germany) and image analysis was performed using Image J software.

3.4 Contact angle

Contact angle analysis was used to measure the property of a solid surface known as wettability. Contact angle indicates the degree at which a liquid, usually deionised water interacts with a solid surface. This measurement plays an important role in a wide range of applications including the coating industry [166], textiles [167], printing [168], biological cell study [77] and in the renewable energy solar cell industry [169]. There has been an increasing interest in the study of wettability of surfaces and their influence on cell adhesion and spread, due to their potential in tissue engineering and biomedical applications [77].

Wettability, hydrophilicity and hydrophobicity are closely related phenomena, and wettability gives information about the hydrophilic or hydrophobic properties of the solid surface. The definitions of "hydro" in Greek word means water, so "philicity" means bonding, and "phobicity" means lack of bonding [170].

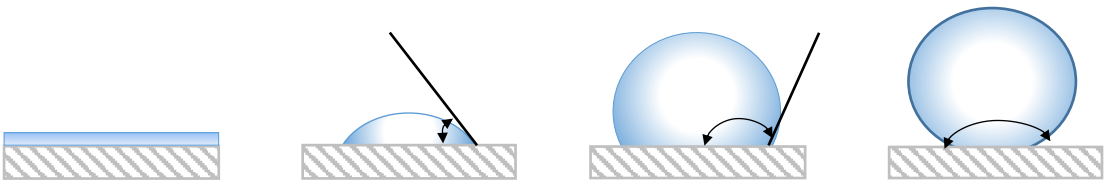

Figure 3.3: Illustration of various contact angles: (a) the condition $\theta = 0^{\circ}$ indicates that solid surface is superhydrophilic, (b) $0^{\circ} \leq \theta \leq 90^{\circ}$ indicates hydrophilicity, (c) $90^{\circ} \leq \theta \leq 150^{\circ}$ is hydrophobicity and $\theta \geq 150^{\circ}$ is superhydrophobic [170], [171]

Figure 3.3 shows the illustration of various possibilities for contact angles when water spreads on a solid surface. It can be seen that if the water contact angle is 0˚, this indicates that the

solid surface is superhydrophilic and wetting well, while for contact angles less than 90˚ it shows that the surface is hydrophilic and favourable for water. If the angle is between 90˚ and 150˚ the surface is said to be a hydrophobic surface or low wetting. If it is greater than 150˚ the solid surface is superhydrophobic or non-wetting [168], [170].

In this research, the water contact angle measurement was carried out with a high speed contact angle measurement device telescope goniometer–CAMP 2008 KSV system at Nanofabrication Laboratory, University of Canterbury (Figure 3.4). Deionised water was used in measuring the water contact angle to deduce the hydrophobicity or hydrophilicity of the surface. A 5µL sample of deionised water was dropped on the substrate surface and the image was captured by the system. Then, the water contact angle images were analysed by Image J software.

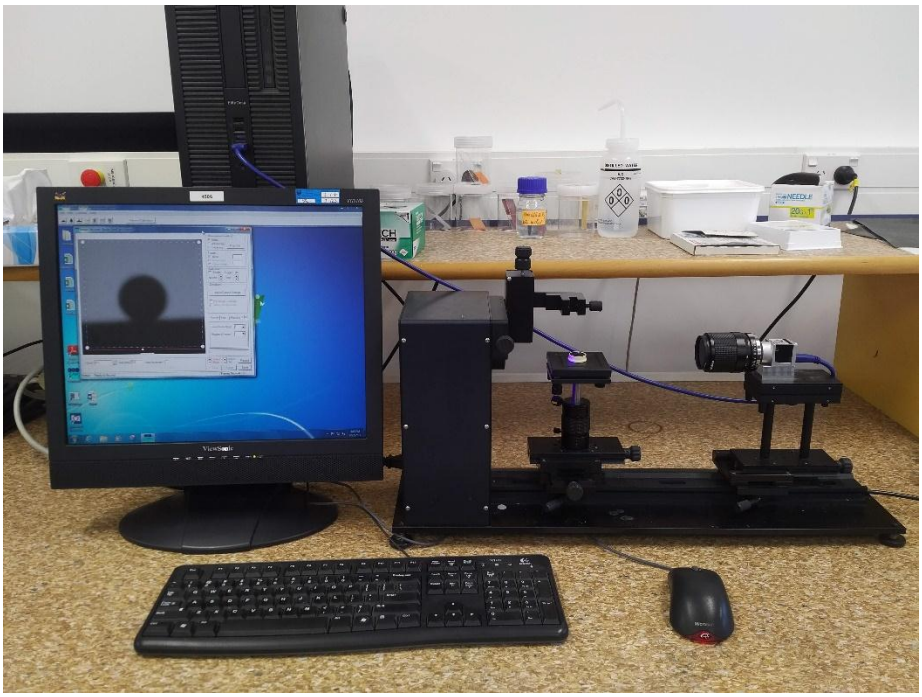

Figure 3.4: Telescope goniometer–CAMP 2008 KSV system for water contact measurement.

3.5 State of the art of monitoring technologies

In this research, all fabricated and experimental samples were visualised by using various microscopy technologies: atomic force microscopy, fluorescence microscopy, and optical

microscopy methods. These imaging analysis microscopies were used for characterizing surface topography and cell morphology.

3.5.1 Atomic Force Microscopy

Atomic force microscopy (AFM) is a powerful imaging technique to study the surface topography and cell morphological structures at sub-nanometre resolution without the use of potentially interfering fluorescent labels. This technique was discovered in 1985 by Nobel Prize winners Gerd Binnig, Christoph Gerber and Calvin Quate in Zurich. Figure 3.5 show the schematic diagram of an AFM system. The main elements comprise a cantilever with a sharp tip that raster scans across the sample surface using a piezoelectric tube controlled by computer. The cantilever tip taper is made of silicon nitride, typically with less than 10 nm radius of curvature. The deflection of the cantilever is monitored using an optical detection system in the form of a laser that reflects off the back of the cantilever and onto a photodiode detector. A feedback loop maintains a constant tip-sample force.

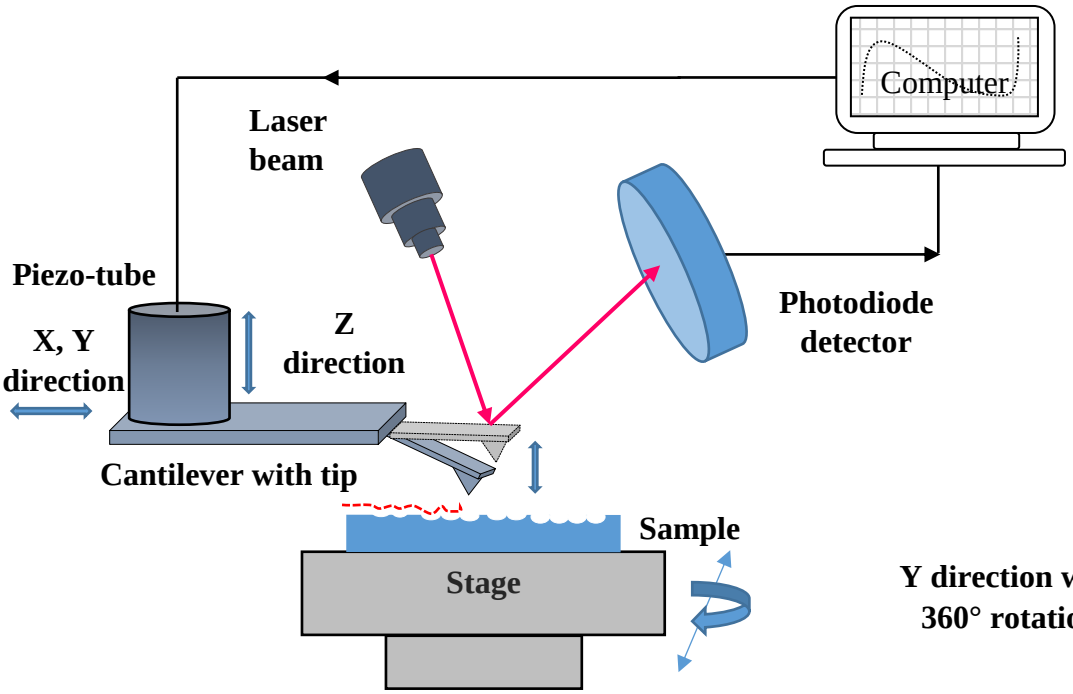

Figure 3.5: Schematic diagram of AFM system. A cantilever with sharp tip at the end is rigidly connected to the piezoelectric tube. The optical shaft consists of a laser beam focused on the top of the cantilever-tip assembly which is reflected to the quad photodiode detector array.

There are three different types of operating mode: contact mode, dynamic mode and non-contact mode. In contact mode operation, the tip scans in close contact with the sample surface as shown in Figure 3.6. The movement of the tip is strongly influenced by frictional and adhesive forces, which can cause tip and sample damage.

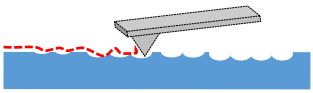

Figure 3.6: Schematic illustration of contact mode. The force between the tip and surface is constant, which can damage the sample surfaces.

Figure 3.7 illustrates the dynamic or tapping mode, which is the most common mode for imaging surface topography at high resolution. This mode of operation is less destructive than contact mode because it eliminates the frictional and adhesion force by intermittently contacting the sample surface. The other advantage is that it is very useful for imaging very soft and fragile samples, such as membrane.

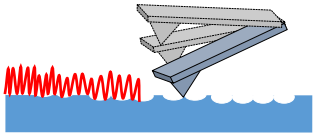

Figure 3.7: Schematic illustration of dynamic or tapping mode. The tip basically touches the sample surface of each swing and results in a surface topography being scanned.

In non-contact mode, the tip does not touch the sample surface as shown in Figure 3.8. This operation mode detects the Van der Waals forces acting between the sample surface and tip during scanning. However the forces from the sample are substantially weaker than the forces used in contact mode.

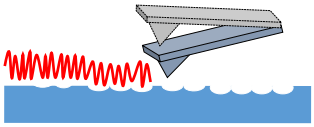

Figure 3.8: Schematic illustration of non-contact mode. The tip would hover above the surface of the sample.

In this work, the Digital Instruments (DI) 3100 Nanoscope III AFM from Vecco Instruments Inc. as shown in Figure 3.9 was used for imaging. Fixed cells and imprint samples were imaged in tapping mode, which provides a resolution on the nanoscale. X, Y and Z axial limits of 100 µm × 100 µm and 6 µm, respectively with a resolution of 256 × 256 pixels. All images were taken at multiple sample positions and presented in an amber colour contrast scheme, and were then processed using the Gwyddion software.

Figure 3.9: Digital Instruments (DI) 3100 Nanoscope III AFM from Vecco Instruments Inc. in the Nanofabrication Laboratory, University of Canterbury, used for imaging surface topography and cell morphology.

3.5.2 Light microscopy

There are two types of light microscopes used in this research to visualise images. These are brightfield microscopes and fluorescence microscopes. The light microscopes can be used in combination for diagnostic and research.

3.5.2.1 Brightfield microscope

An optical microscope, also known as brightfield microscope was mainly used in this research to visualise the sample, cell culture progress and substrates. The optical microscope uses visible light and a system of lenses to magnify images of small objects with a range from 4× to 100×. The majority of images taken in this work used the Nikon 80i microscope, as shown in Figure 3.10, which is located in the Nanofabrication Laboratory at the University of Canterbury.

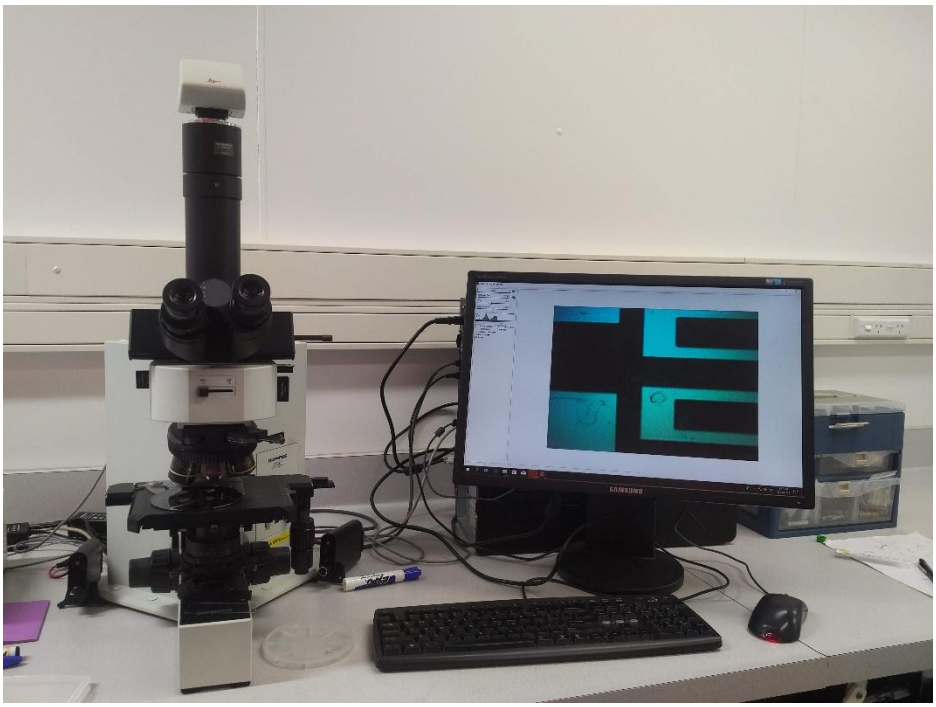

Figure 3.10: Nikon 80i microscope in Nanofabrication Laboratory, University of Canterbury for visualizing the sample, cell culture progress and substrates at the microscale.

Figure 3.11 shows schematic illustrations of the optical microscopy systems. As shown on the schematic diagram, the sample is placed on the glass slide and clipped to the microscope stage. Then the sample is positioned under the light source using X-Y-Z mechanical stage knobs. There are five different objective lens to lower or increase magnifications, these are: 4×, 10×, 20×, 50× and 100×.

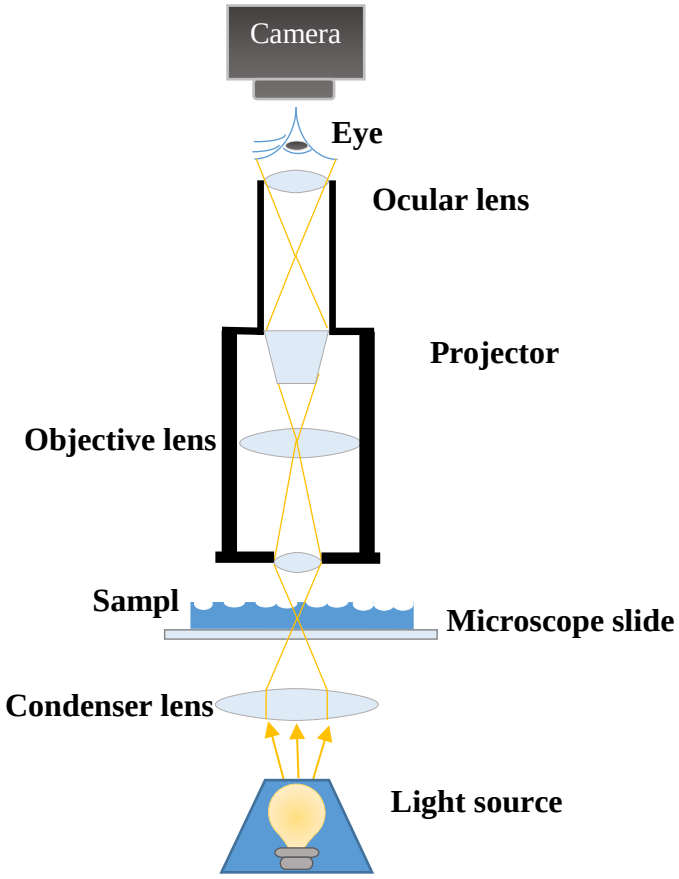

Figure 3.11: Schematic illustration of optical microscope system.

3.5.2.2 Fluorescence microscopy

The fluorescence microscope is also an optical microscopy technique but it uses fluorophores to image, as opposed to absorption, scattering or reflection. Fluorescence uses a type of dye such as nucleic acid dyes 4′, 6′-diamidino-2-phenylindole (DAPI), FITC and acridine orange. These dyes are used to mark plasma membrane, nucleus and cells with a fluorescent label for examination by fluorescence microscopy. These fluorophores are capable absorbing the

energy from a light source (often ultraviolet) and re-emitting that energy as visible light of shorter wavelength. Fluorescence microscope is a very useful in clinical microbiology research and they range from very simple systems such as an epifluorescent microscope, to extremely complex such as confocal systems. Figure 3.12 shows the schematic illustration of a fluorescence microscope system. In this research, the fluorescent stained samples were visualised with Zeiss Axio Imager epifluorescence microscope (Carl Zeiss AG, Germany) as shown in Figure 3.13, and the image analysis was performed using Image J software.

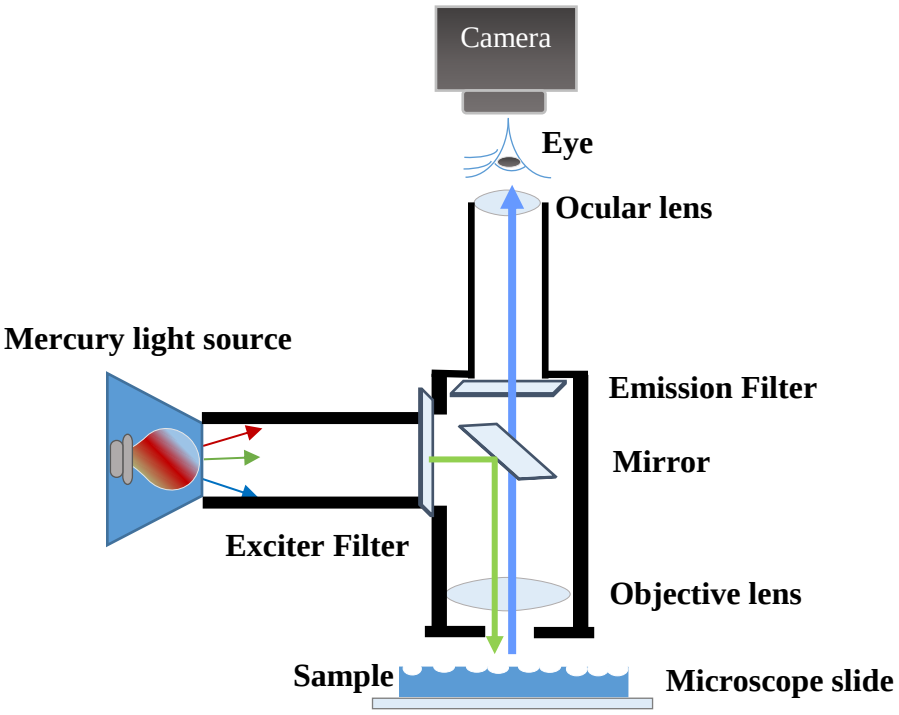

Figure 3.12: Schematic illustration of fluorescence microscope system.

Figure 3.13: Zeiss Axio Imager epifluorescence microscope used to visualise fluorescent stained samples.

3.6 Film characterisations

The physicochemical properties of the synthesised CH films were characterised by using ultraviolet–visible spectroscopy (UV-Vis) to determine the optical properties of the samples, Fourier transform infrared spectroscopy (FTIR) to analyse the chemical structure, thermal gravimetric analysis (TGA) to evaluate the physical changes of the films as a function of temperature and X-ray photoelectron spectroscopy (XPS) to examine the electronic elements of the material.

3.6.1 Ultraviolet–Visible (UV-Vis) Spectroscopy

Ultraviolet–visible spectroscopy (UV-Vis) is used to measure the absorption or transmittance of light across a sample in the ultraviolet and visible light wavelengths. UV-Vis analysis is also commonly used for various applications such as solar cells, sensors, integrated circuits and batteries. In general, the total absorbance results from light transmittance losses due to reflection, scattering, and absorption of the incident light. Hence, the absorption measurement obeys the Beer–Lambert law, as given in Equation 3.1 [172]:

$$A=\log_{10}(I_0/I) = \varepsilon lc \qquad (3.1)$$

Where,

A = the absorbance,

I_0 = the intensity of the incident light at a given wavelength

I = the transmitted intensity

ε = the molar absorptivity coefficient,

l = the path length (cm),

c = the concentration of the absorbing species.

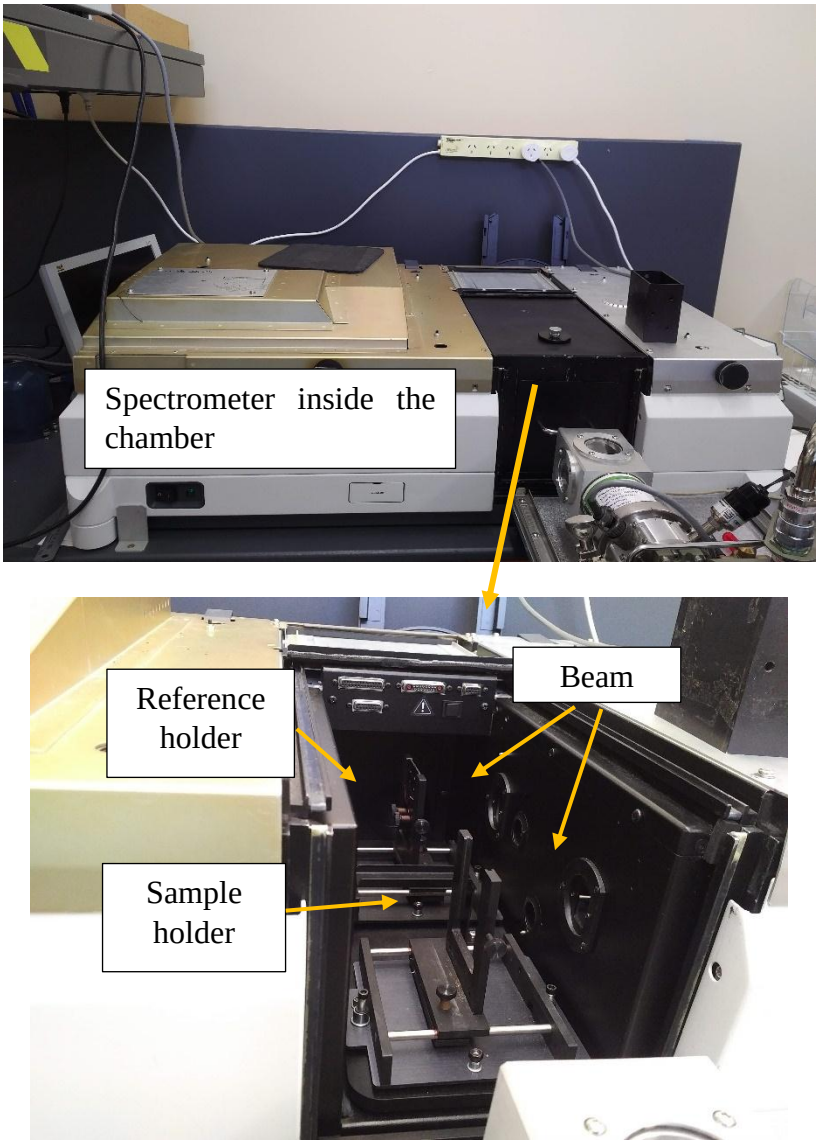

Figure 3.14: UV-Vis spectrophotometer (Agilent Cary 6000i) used for absorption or transmittance measurements.

For the purpose of this study, UV–Vis absorbance spectra of the CH films were confirmed by a UV–Vis spectrophotometer (Agilent Cary 6000i), as illustrated in Figure 3.14. After creating baseline data, the prepared films were inserted into the sample holder. The absorbance spectra were recorded using UV–Vis in the wavelength range between 300 nm and 800 nm. This machine was located at the College Sciences, University of Canterbury, New Zealand.

3.6.2 Fourier Transform Infrared (FTIR) Spectroscopy

Fourier transform infrared (FTIR) spectroscopy was used to analyse the chemical bonding and functional groups of the film in a dry state. In this research, the existence of PEDOT:PSS in a CH matrix was verified by an FTIR spectrometer ALPHA from Bruker Optics equipped with single reflection diamond attenuated total reflectance (ATR) from Graseby Specac (Kent, U.K) and supported by OPUS Mentor software as shown in Figure 3.15. To perform FTIR, the films were cut into (0.5 × 0.5) cm samples and placed on the ATR platform. Then the film was pressed with a compression tip to ensure it was in contact with the ATR diamond. This machine was located at the College of Sciences, University of Canterbury, New Zealand. Each spectrum was recorded as the average of 16 scans at a resolution of 4 cm^{-1} in the range between 4000 and 500 cm^{-1}.

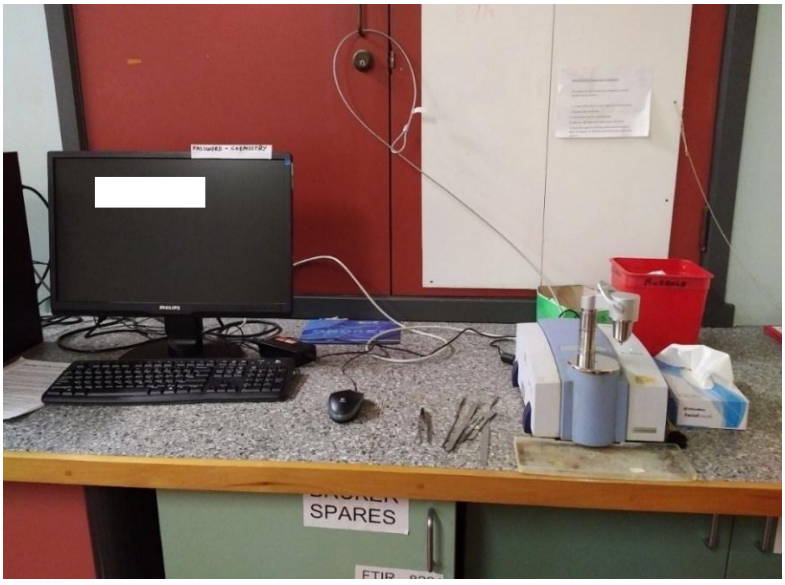

Figure 3.15: FTIR spectrometer ALPHA equipped with diamond attenuated total reflectance (ATR) for analysing chemical component in material.

3.6.3 Thermal Gravimetric Analysis (TGA)

Thermal stability of the prepared CH was analysed by TGA in order to measure any changes in mass as a function of temperature. This technique can analyse thermal events like decomposition and residual weight of the material. Approximately 10 mg of the dried sample was heated in a platinum crucible under nitrogen, N_2 atmosphere at a heating rate of −5 ℃/ minute from 25 ℃ to 600 ℃. Figure 3.16 shows the STA 449F1 Jupiter® (NETZSCH-Geratebau GmbH, Selb, Germany) located at the College of Sciences, University of Canterbury, New Zealand.

Figure 3.16: STA 449F1 Jupiter® used to measure the film weight changes within the range from 25 ℃ to 600 ℃.

Figure 3.17 shows the schematic diagram of thermogravimetric analysis. It consists of a furnace, and electronic microbalance, temperature programmer and a computer. Initially, about 10 mg of sample is loaded in a small sample crucible and analysis was carried out by increasing the temperature slowly in a specific inert gas such as nitrogen, argon or helium at certain heating rate. The thermogravimetric apparatus analyses the changes in mass of the films as a function of temperature with a specified gas environment and heating rate.

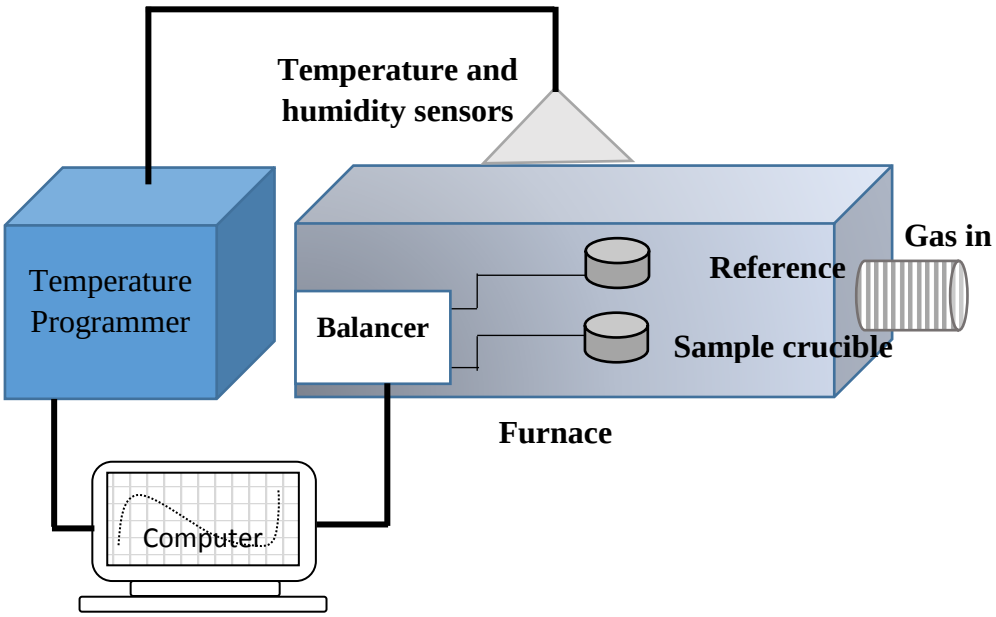

Figure 3.17: Schematic diagram of thermogravimetric analysis consisting of furnace, temperature programmer, computer, and temperature and humidity sensors.

3.6.4 X-ray Photoelectron Spectroscopy (XPS)

X-ray Photoelectron Spectroscopy (XPS), also known as electron spectroscopy for chemical analysis (ESCA) is a powerful tool used for analysing the surface chemistry composition of a material. In this research, the surface analyses were conducted using a Kratos Axis Ultra DLD XPS equipped with a hemispherical electron energy analyser as shown in Figure 3.18.

The XPS analysis was performed by Dr Colin Doyle at the University of Auckland. The spectra were recorded by using monochromatic Al Kα X-rays (1486.69 eV) with the X-ray source operating at 100 W [173]. The measurements were carried out in a normal emission geometry. The analysis chamber was at pressures in the 10^{-9} torr range throughout the data collection. XPS peaks were analysed to determine the presence of conductive and hydrogel particles such as carbon, nitrogen, oxygen, and sulphur using the XPS survey scan, CasaXPS (www.casaXPS.com).

Figure 3.18: Kratos Axis Ultra DLD instrument at University of Auckland use for XPS analysis.

3.7 Electrode fabrication

The electrode fabrication process starts with designing a photomask then the pattern is transferred through a photolithography process and finally a gold layer is deposited using an electron beam evaporation system.

3.7.1 Mask design

The first step in electrode fabrication is designing an optical mask or photo mask for the electrode patterns. These patterns are drawn by using a CAD software package, L-Edit Pro v14.3 (Tanner Inc.). Then, the layout patterns are uploaded into a Heidelberg μPG 101 Laser Writer, as shown in Figure 3.19. The mask writer machine uses a 405 nm wavelength laser beam to define patterns onto the mask's substrate (mask plate). Once exposed to the laser beam, the 4-inch (12-cm) or 3-inch (7.5 cm) glass substrate pre-coated with AZ1518 resist, were written with the required patterns. Next, the mask pattern was developed by gently agitating in MIF AZ326 developer for one minute followed by etching in chrome etchant for

one minute, and finally the remaining resists were removed with acetone solution for one minute.

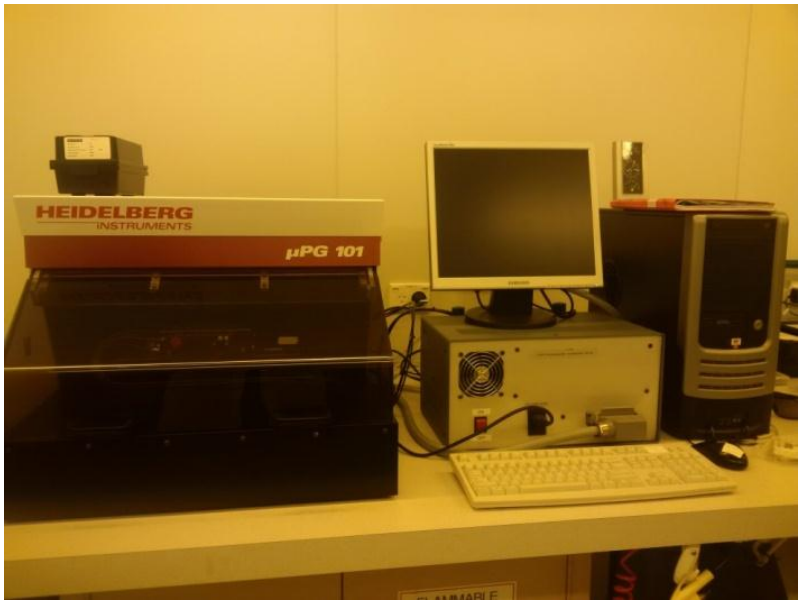

Figure 3.19: Heidelberg µPG 101 Mask Writer for making photo mask.

In this research, the microelectrode masks were designed with different electrode widths and gap dimensions. Different parameter (width and gap size) combinations were analysed to evaluate the effect of electrode specifications on the sensitivity of the sensor, as shown in Figure 3.20.

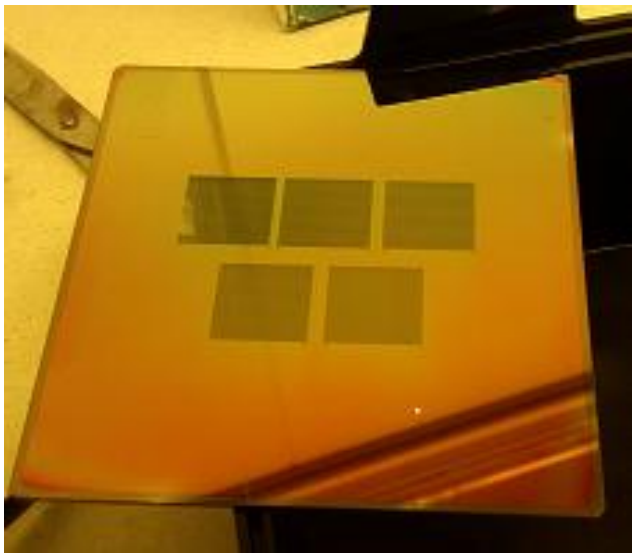

Figure 3.20: Sample of the fabricated chrome mask with the different electrode width and gap sizes.

3.7.2 Photolithography technique

Photolithography technique is a process of transferring the design of a pattern from a photomask to a photoresist-layer coated substrate. This technique uses five process steps: wafer cleaning, photoresist coating, UV exposure, pattern development and hard bake.

In Figure 3.21 shows a schematic diagram of the photolithography technique. In Figure 3.21 (a) the wafer surface is chemically cleaned with three types of solvent: acetone, methanol and isopropanol in an ultrasonic machine, followed by a dehydration process in the Heratherm OGH60 hot oven (Figure 3.22) at temperature 180 ℃overnight. This step is important in order to remove any particulate matter on the surface as well as any traces of water, fingerprint, organic, ionic, and metallic impurities. In addition, it also modifies the surface condition of the substrate, which improves the adhesion of the photoresist layer. Then, the wafer was removed from the oven and allowed to cool. Next, the wafer surface was spun coated with HMDS solution and spin coat positive photoresist AZ1518 at 2000 rpm for 60 seconds with Headway PWM32-PS-R790 spinner machine (Figure 3.23) to form a uniform layer of photoresist as shown in Figure 3.21 (b). HMDS is often used as a source of saline, which offers good adhesion to photoresist.

After the coating process, the film undergo soft bake at temperature 95 ℃ for 2 minutes on a hotplate in order to dry the photoresist by removing the excess solvent (Figure 3.21 (c)). The main reason for removing the solvent is to stabilise the resist film. Then, the photo mask is aligned with the substrate for pattern definition using Karl Suss MA-6 mask aligner (Figure 3.24). The patterns were transferred onto the photoresist layer under a 350 Watt of UV light source with wavelength 365 nm in vacuum contact modes (Figure 3.21 (d)). Then, the photoresist is developed using MIF 326 developer for 10 seconds to produce the photoresist pattern on the substrate (Figure 3.21 (e)). Then, post-bake, the patterned wafer at is treated at temperature 120 ℃ for 2 minutes on a hot plate to harden the final resist layer so that it will withstand the harsh environments of wet etching. The hard-baking process shown in Figure 3.21 (f) is the final process to crosslink the resin polymer in the photoresist and to make it thermally stable.

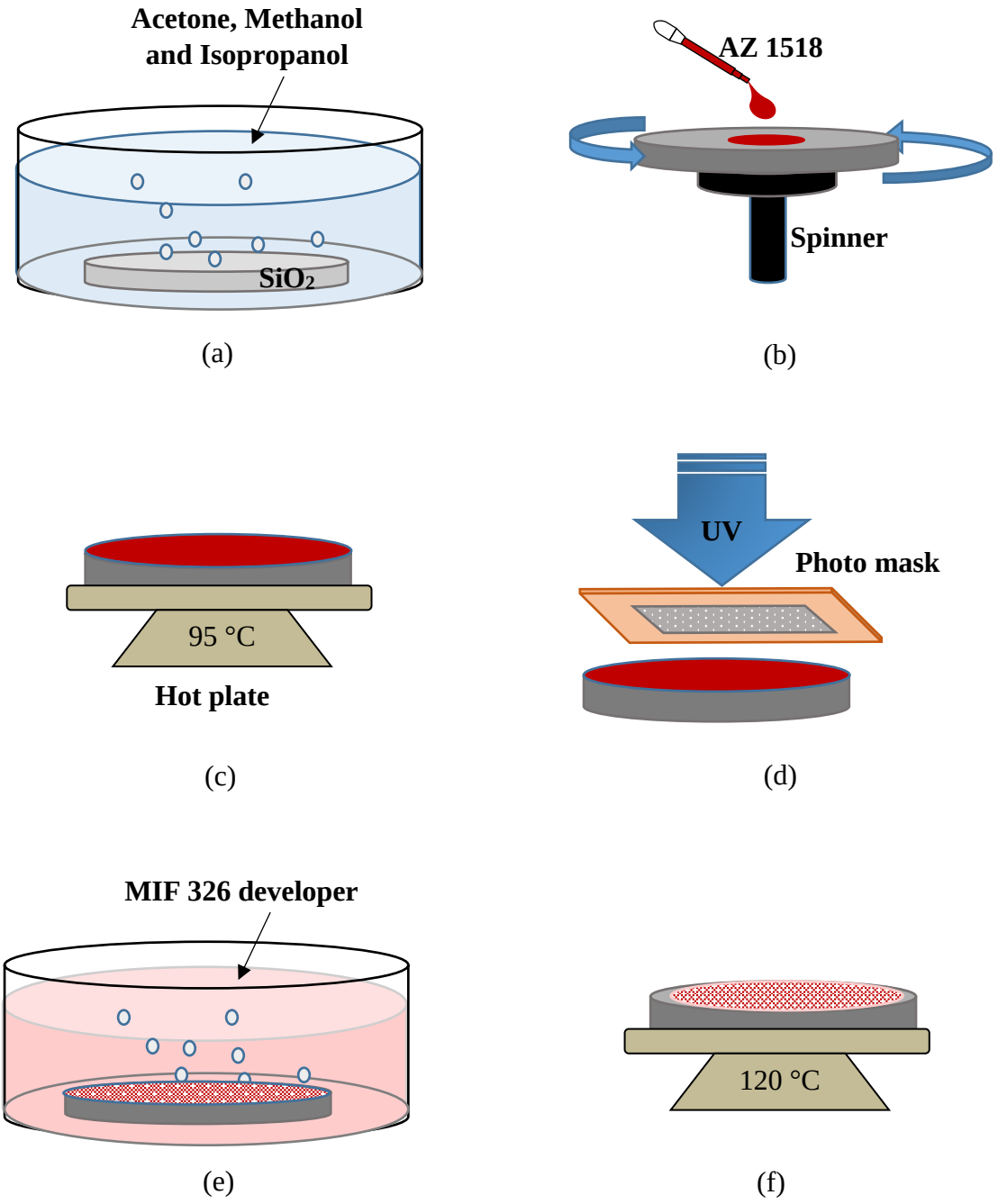

Figure 3.21: A typical sequence of photolithography processing steps: (a) cleaning the wafer surface with acetone, methanol and isopropanol, (b) spin coating with positive photoresist AZ1518 at 2000 rpm for 60 seconds, (c) soft baking at temperature 95 ℃ for 2 minutes on hot plate, (d) transferring the patterns onto the photoresist layer with UV light source, (e) developing the exposed photoresist with the MIF 326 developer, and (f) hard bake or post bake at temperature 120 ℃ for 2 minutes.

Figure 3.22: Heratherm OGH60 hot oven for dehydrating process.

Figure 3.23: Headway PWM32-PS-R790 spinner machine.

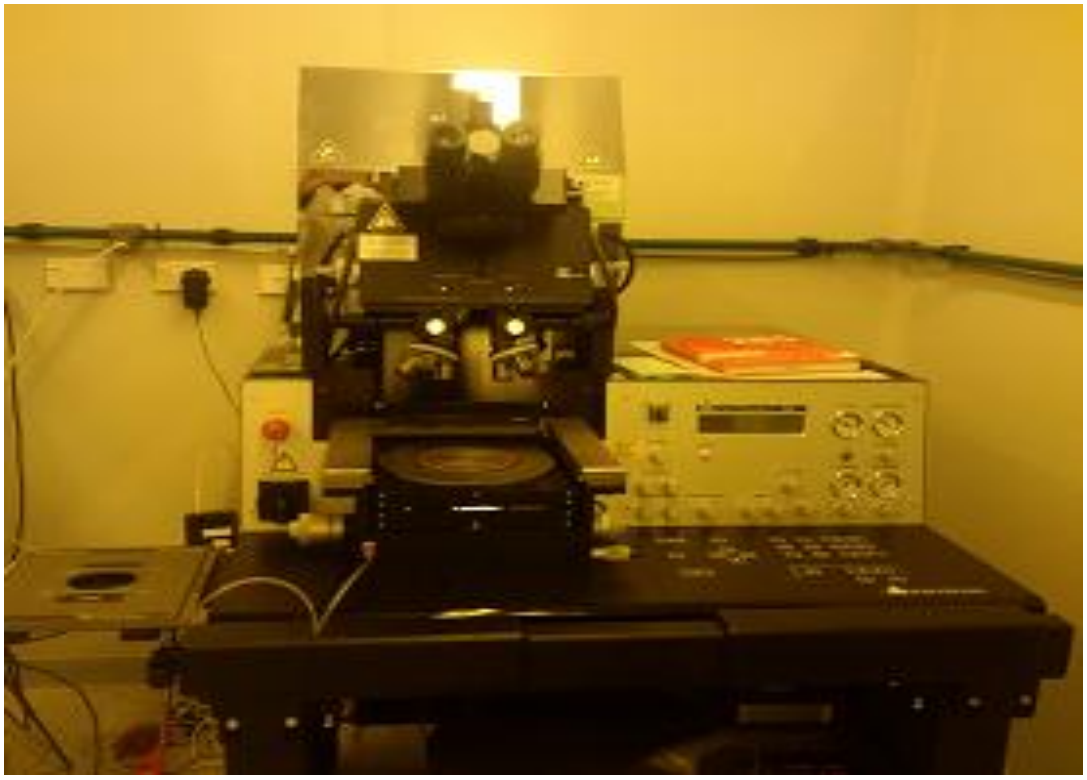

Figure 3.24: The Karl Suss MA-6 mask aligner for photolithography and UV-NIL.

3.7.3 Electron-Beam evaporation

Figure 3.25 shows the diagram of the electron beam gun evaporation system or E-Beam. This technique is based on a vapour deposition technique in which the target material such as molybdenum (Mo), titanium (Ti), aluminium (Al) and nickel-chromium (Ni-Cr) is bombarded by high energy electron beam resulting in evaporation of the pure material and coating of the substrate under high vacuum environment. In this process the source materials were placed in the crucible and heated by the electron bombardment. By applying a large voltage, electrons are drawn from the filament and focused as a beam on the source material.

In this work, gold and titanium layers were deposited by using the electron beam evaporation technique. Figure 3.26 shows the Edward Auto500 Magnetron Sputtering system embedded with a 5 keV electron beam evaporator unit available at the Nanofabrication Laboratory, UC.

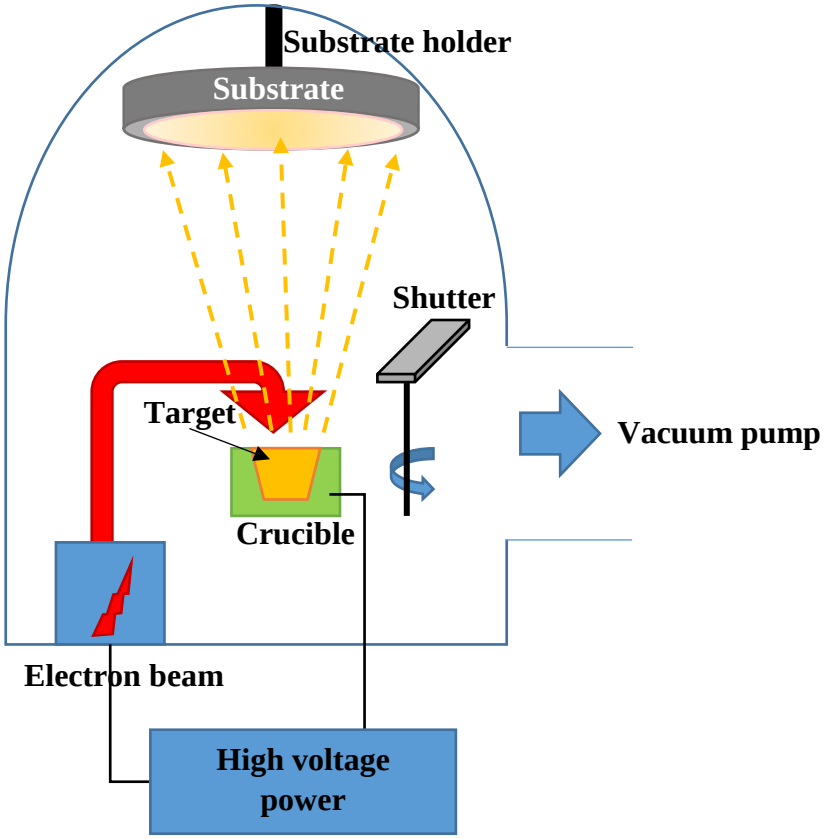

Figure 3.25: The diagram of the electron beam gun evaporation system.

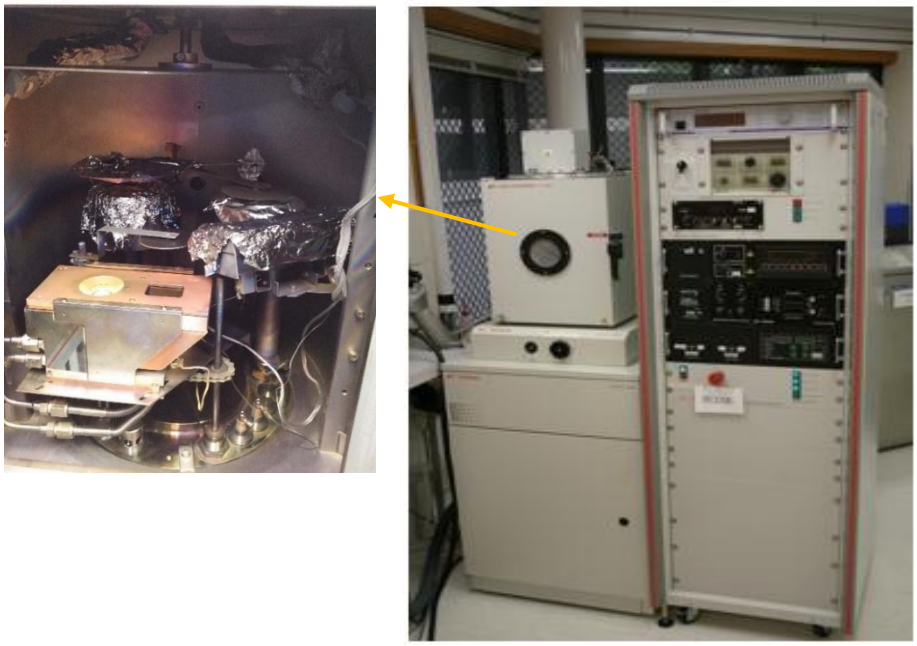

Figure 3.26: Edward Auto500 Magnetron Sputtering system use for electron titanium and gold deposition.

3.8 PDMS bioimprint as a master mould

As mentioned in Chapter 1, bioimprinting is a soft lithography technique designed to capture cellular morphology permanently at high resolution into a polymer matrix. In this work, a novel development in the fabrication of conductive bioimprint was started by learning the fabrication of polydimethylsiloxane (PDMS) bioimprint used as a master mould.

Positive and negative PDMS bioimprint master moulds were prepared according to a similar method reported by our group [58]. In brief, PDMS elastomer liquid and curing agent were mixed at 10:1 w/w ratio and stirred thoroughly by hand for 30 seconds. Figure 3.27 (a) shows that the PDMS mixture was placed in a desiccator for 30 minutes to remove the bubbles before pouring onto the fixed cells. The curing process is accomplished at temperature 37 °C for 12 hours to prevent any thermal damage to the cells, as shown in Figure 3.27 (b). The imprinting polymer was then peeled off and baked for another two hours at temperature 80 ℃ for further crosslinking, as in Figure 3.27 (c). Next, this negative PDMS bioimprint was washed in 10% w/v of sodium dodecyl sulphate (SDS, Sigma Aldrich) in 0.01 M hydrochloric acid and 0.05% trypsin-EDTA (Life Technologies) in PBS for 3 minutes to remove any biological debris on the polymer surface. Rinsing was done with deionised water for three minutes to remove any unwanted acidic monomer, as shown in Figure 3.27 (d).

One of the main elements for a successful reverse-imprinting depends on the surface energy between mould and the substrate. The mould surface energy must be lower than the substrate's surface energy, so that the polymer film will have excellent adhesion to the substrate and will easily peel off from the mould [11]. Here, the negative bioimprint surfaces were treated with anti-sticking layer 0.1% w/w hydroxypropylmethylcellulose solution in PBS for 10 minutes to lower the surface energy between the negative and the cured positive bioimprint. After it had dried, a liquid PDMS 10:1 w/w ratio was poured onto the negative PDMS mould and cured at temperature 37 °C for 12 hours as shown in Figure 3.27 (e). Then, it was peeled off the positive bioimprint and further baked at temperature 80 ℃ for two hours to complete the polymerisation, as shown in Figure 3.27 (f).

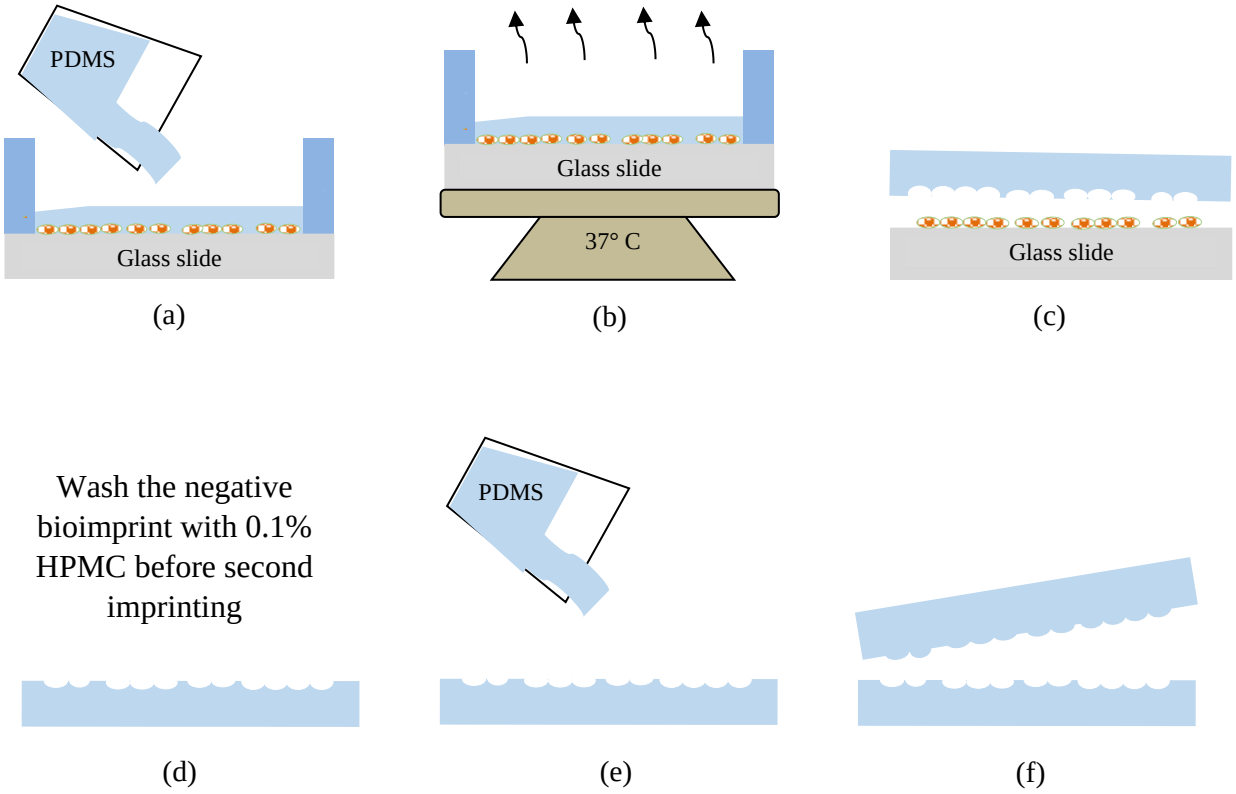

Figure 3.27: Schematic diagram of negative and positive PDMS bioimprint fabrication process: (a) fixed cells are coated with 10:1 w/w PDMS mixtures, (b) the polymer is cured at temperature 37 °C for 12 hours, (c) the negative bioimprint is carefully peeled off from fixed cells and post-baked at temperature 80 ℃ to complete polymerisation, (d) negative PDMS master mould is washed with 0.1% HPMC, (e) 10:1 w/w PDMS is poured on negative, then the curing process follows as in in step (b), and (f) the positive bioimprint PDMS is peeled off from negative PDMS bioimprint.

3.9 Mechanical testing

The elastic modulus and yield stress for the plastic material were measured with a simple tensile test. In this research, the tensile strength of the CH substrate was evaluated using a MTS858, tensile machine with MTS 25 kN load cell of pneumatic pressure-controlled grips, as shown in Figure 3.28. The MTS 858 system is capable of performing specialised mechanical testing for biomedical and biomechanical samples. The films were cut into rectangular shape with the dimensions 25 mm × 110 mm and tested at room temperature. The extension rate was 0.1 mm/min. Tests were done according to ASTM D638 which is the

standard test method for tensile properties of plastics [174] and D882 which is the test method for tensile properties of thin plastic sheeting [175].

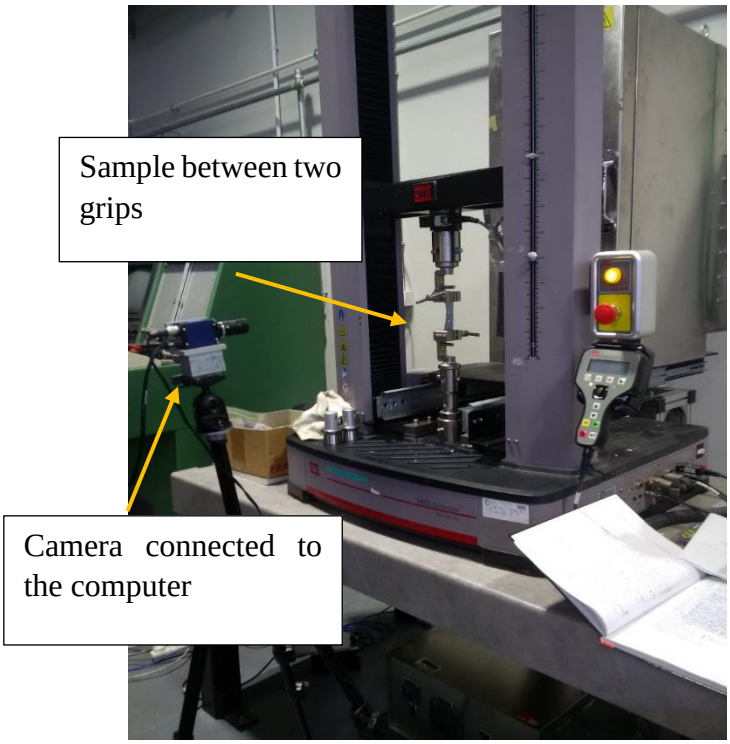

Figure 3.28: The tensile testing of CH films were perfomed on a MTS 858 machine.

The stress–strain values are calculated according to the following formula:

$$\partial = \frac{F}{A} \tag{3.2}$$

where the tensile stress, ∂ is the ratio of the axial load, F applied during the experiment to the cross-sectional area, A (mm^2) of the sample. Then strain, ε is defined as:

$$\varepsilon = \frac{\Delta L}{L_0} \tag{3.3}$$

where L_0 in mm is the original gauge length of the sample test and ΔL also in mm is the elongation. Therefore the elastic modulus, E (MPa) is the slope of the linear line in the stress–strain curve:

$$E = \frac{\Delta \partial}{\Delta \varepsilon} \tag{3.4}$$

3.10 Electrical properties analysis

The electrical characterisations of CH substrates were performed by using two techniques: (1) four-probe Hall effect and (2) electrical cell–substrate impedance sensing.

3.10.1 Four-probe Hall effect measurement

Hall effect measurement is a very useful tool to study the intrinsic and doped materials synthesised in this work. The conductivity and resistivity of conductive films were measured using a four-point probe technique. Figure 3.29 shows a Van der Pauw Hall effect Measurement System under a magnetic field strength of 0.51 T.

Figure 3.29: Van der Pauw Hall effect measurement method under a magnetic field of 0.51 T.

The different concentrations of conductive mixtures were spun coated on (5 × 5) mm glass slides and placed on the spring-loaded connection board. The board was then connected to a HP 4155A parameter analyser, and Agilent B1500A semiconductor device analyser or the Hall measuring system for electrical measurements. Current (I)–voltage (V) scans confirmed the Ohmic behaviour of the sample contacts. All measurements were conducted at room temperature.

3.10.2 Electric Cell–substrate Impedance Sensing analysis (ECIS)

Electric cell–substrate impedance sensing (ECIS) is a very useful method for investigating various cellular events such as adhesion, growth, proliferation and motility on the electrode surface in real time and label-free. In this work, the Keysight E4990A impedance analyser shown in Figure 3.30 was used to study cell morphology changes on the CH biochip. All connections were connected with coaxial cable to minimise any background noise and the impedance measurements were collected from 100 Hz to 1 MHz at the voltage of 40 mV_{pp} with a 0 V DC offset voltage.

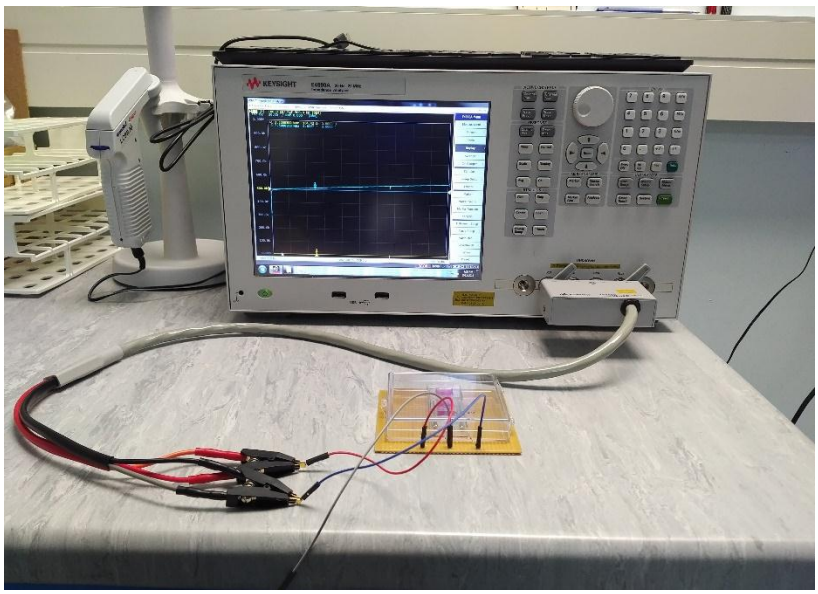

Figure 3.30: The impedance analysis of cells grown on CH films was measured by using a Keysight E4990A impedance analyser.

By culturing cancer cells on the control and CH surfaces, cell-induced impedance signal changes can reflect the characteristics of the cells when they adhere and spread on the electrodes. Figure 3.31 (a) shows a schematic diagram of ECIS system and Figure 3.31 (a) represent the photo of an experimental setup for electric cell–substrate sensing in the PC2 lab. All numerical data were recorded in an Excel spreadsheet for further analysis.

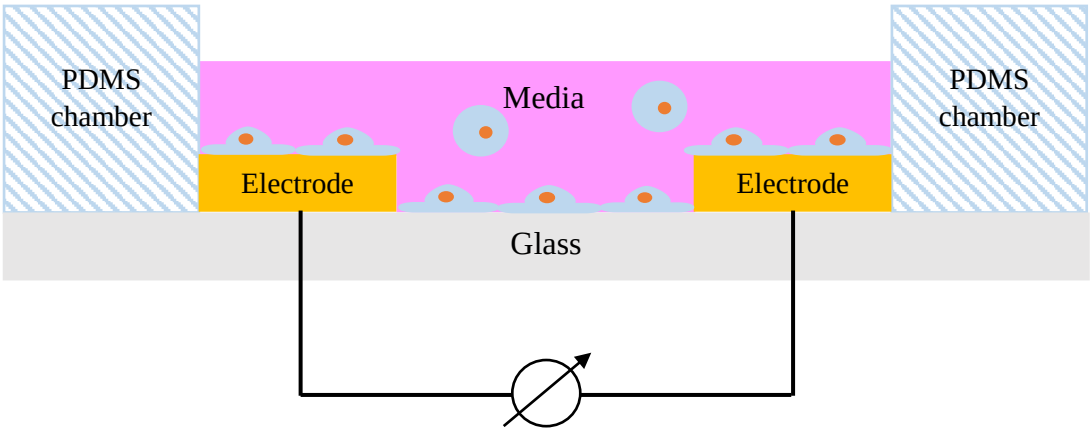

(a)

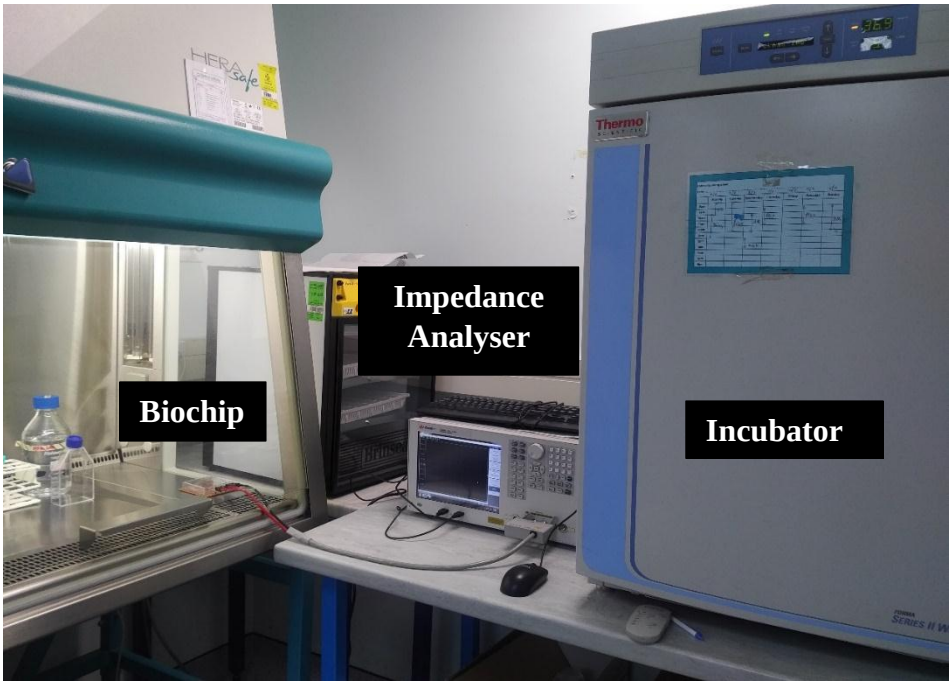

(b)

Figure 3.31: The experimental setup for impedimetric real-time monitoring of C2C12 cell interactions: (a) an illustration of ECIS system, and (b) the setup for impedance measurement in the PC2 Laboratory.

CHAPTER 4

Conductive Bioimprint Based On PEDOT: PSS

Conductive bioimprinting is a novel approach that combines replicating a 3D imprint of cellular morphology into a biocompatible CP, PEDOT:PSS. Using soft lithography, the bioimprinting technique provides an easy fabrication method to permanently capture the cellular footprint at high resolution down to the nanometre scale. In the preliminary research, a feasibility study was conducted to employ glycerol as a plasticiser in the CP to reduce the solubility and enhance the electrical properties of the PEDOT:PSS thin film. The results showed that glycerol significantly influences film transparency, water contact angle, electrical conductivity and surface morphology of doped PEDOT:PSS thin films. Due to problems with low viscosity and film thickness, the replication of cellular structures by using the plasticiser-assisted soft embossed (PASE) technique in conductive thin films showed a loss of the micron- and nano-sized cellular details. To achieve better results, a gelatin (A 300 Bloom porcine) was incorporated into plasticised PEDOT:PSS solution to overcome those challenges. The AFM cross-section profiles of the mouse myoblast replicas showed that the conductive bioimprint conformed to more than 90% of the original cellular features down to micro- and nano-sized details compared to the PDMS master mould. This material, with cell-like surface features, has exciting potential for monitoring acceptance of medical implants into the body and manipulation of implant-tissue reactions of medical devices.

4.1 Introduction

A new class of conductive biomaterial with engineered surface patterns are of great potential to serve as bioactive scaffolds with the ability to electrically stimulate cells and regulate their functions. The integration of the electroactive component of the conducting polymer and the biocompatible property of hydrogel matrix has emerged

as a promising development for the next generation of bioactive electrode coatings in many different fields, such as regenerative medicine, biorobotics, and biosensing.

Over the past decade, the application of micro fabrication in the field of biology has stimulated interest in and experiments on cell growth on topographically modified surfaces. The term "bioimprint" was first developed in 2006, and describes a soft lithography technique for replicating cell surface features into hard polymer for the purposes of improved cell imaging and formation of culture platforms [60], [176]. Numerous studies have been reported that culture platforms with topographical features influence cell orientation, migration, morphology and proliferation on defined patterns with different non-CPs such as PDMS [8], [9], glass[9], Permanox [9], methacrylate [8], [54], [56], [57], polystyrene [6]–[9], poly (ethylene glycol) terephthalate-poly (butylene terephthalate), (PEGT-PBT) [58] and casein [59]. However, the study of cell behaviour on conductive patterned surfaces is still challenging.

This chapter demonstrates a novel fabrication process called "conductive bioimprinting" using the soft lithography technique. Conductive bioimprinting is a new technology that employs a CH matrix based on PEDOT:PSS to create a 3D imprint of cell topography. This conductive bioimprint is suitable as a cell culture platform, enabling the monitoring of cell behaviour as a function of their conductivity. The features of the culture platform surface play an important role in the regulation of cell behaviour [4], [5], [9], [61]. An understanding of the mechanisms behind the interaction is central to many developments in lab-on-chip devices, medical implants and biosensors. In the preliminary work, we started by developing the fabrication process of the bioimprint based on PDMS (as described in Chapter 3.8) and then investigated the effects of the solvent and gel additives on the electrical properties of the conducting polymer PEDOT:PSS. The next step was to adopt the bioimprint technique and optimise it for the PEDOT:PSS process to fabricate a conductive substrate with cell-feature topography. This conductive substrate with surface patterns offers good conductivity in the cell culture platform, high resolution replication fidelity and is also biocompatible, stretchable and biodegradable and so is suitable for tissue engineering and implantable biosensor devices.

4.2 Materials

The following materials and chemicals were used in this part of the work:
PEDOT:PSS with 1.3 wt.% dispersion in deionised water (483095-250G, Sigma Aldrich), Type A porcine skin powder (G2500, Sigma Aldrich), phosphate-buffered saline (PBS) tablets (Sigma Aldrich), GlutaMAX (11995-065, Gibco via Invitrogen), fetal bovine serum (Gibco via Invitrogen), penicillin-streptomycin 100x (Gibco via Invitrogen), Fungizone (Gibco via Invitrogen), Polydimethylsiloxane, (Sylgard 184, Dow Corning Corp.), ethanol and glycerol (analytical grade, from LabServ). AZ 1518 photoresists (MicroChemicals GmbH), AZ 326 MIF developer (MicroChemicals GmbH,), microscope glass slide 25 mm × 75 mm (Corning, Amsterdam, Netherlands), acetone, methanol and isopropanol (Sigma Aldrich, Dorset, UK).

4.3 Synthesis of plasticised PEDOT: PSS films

To study the incorporation of glycerol into PEDOT:PSS, six different concentrations of glycerol (0%, 0.5%, 1%, 2%, 3% and 4%w/w) were used to synthesise plasticised PEDOT:PSS by following the method used by Meier *et al.* [31]. The use of glycerol was intended to aid the investigation into changes of transparency, water contact angle, electrical conductivity, surface morphology, and the performance of the bioimprint replication of a doped PEDOT:PSS thin film. Figure 4.1 shows a schematic diagram of the synthesis of plasticised PEDOT:PSS. The PEDOT:PSS solution was purchased from Sigma Aldrich and consists of 1.3 wt.% dispersed in deionised water.

The water based PEDOT:PSS solution was agitated in an ultrasonic bath for 15 minutes at room temperature and filtered using 5 µm PTFE filters in a further purification process, as illustrated in Figure 4.1 (a). Then, different concentrations of glycerol as a plasticiser agent were added to the purified PEDOT:PSS and stirred thoroughly using a magnetic flea until a homogeneous solution was formed (Figure 4.1 (b)). Note that the purification process and homogeneous condition are important to prevent aggregation of PEDOT:PSS in the mixture. Before the spin coating process, the glass substrate is chemically cleaned with three types of solvent: acetone, methanol and isopropanol in an ultrasonic bath for 5 minutes; this was followed by treatment with oxygen plasma at 100 Watt for 5 minutes to improve surface adhesion. Then, the

homogeneous mixture of PEDOT: PSS was spun coated on a microscope glass substrate at 1000 rpm for 60 seconds with a Headway PWM32-PS-R790 spinner machine (Figure 4.1 (c)). As in Figure 4.1 (d), the coated glass substrate is baked at temperature 80 ˚C on hotplate until fully dry (time depend on the glycerol content).

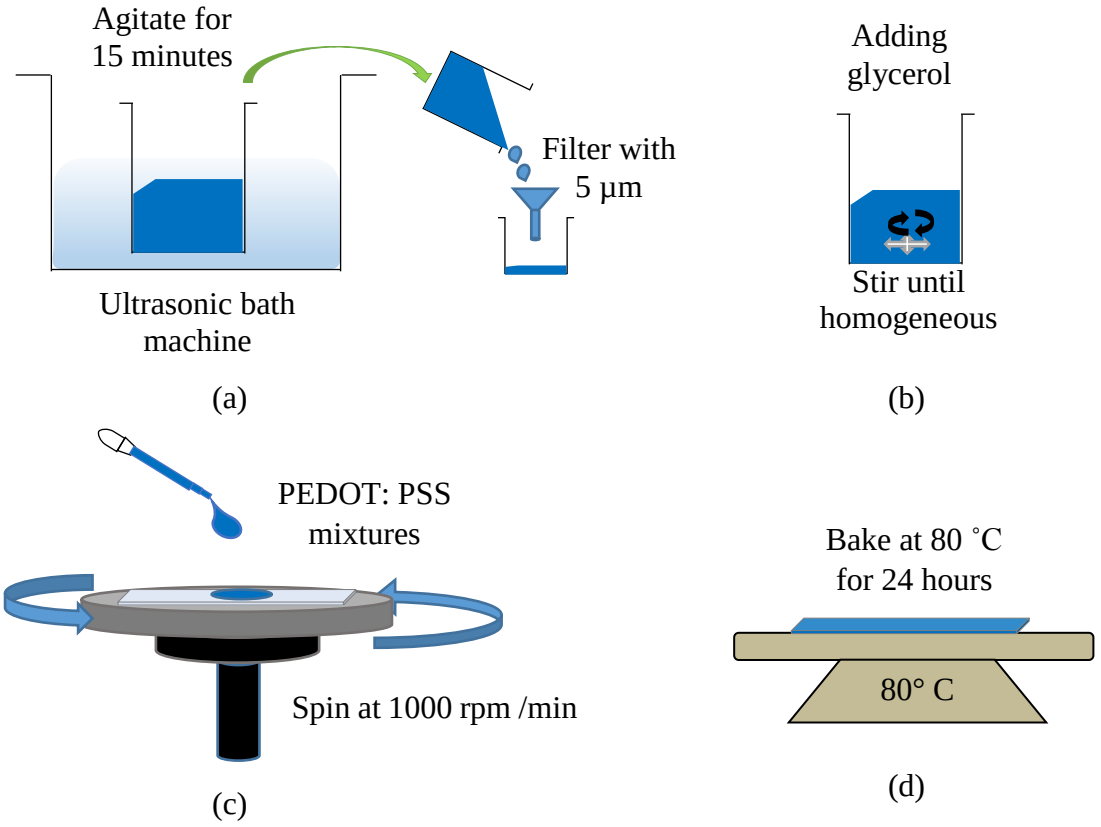

Figure 4.1: Schematic diagram illustrating the synthesis of plasticised PEDOT:PSS (a) purification process of PEDOT:PSS solution, (b) stirring the mixture until it is homogeneous, (c) spin coating a glass substrate with PEDOT:PSS mixtures and (d) soft baking the plasticised PEDOT:PSS thin film until dry.

4.3.1 Physical appearance of plasticised PEDOT: PSS thin films.

In this section, the electrical properties and the quality of the bioimprint replication of plasticised PEDOT:PSS thin films based on method introduced by Meier *et al* work are presented and discussed [31]. Their research showed that they imprinted high-resolution periodic microstructures by using a plasticiser-assisted soft embossing

PASE technique for organic solar cell (OSC) applications. PASE is a soft embossing technique using polymeric stamps instead of hard surfaces such as aluminium, glass and silicon [177]–[179]. This low-cost and simple method opens up a broad range of polymeric materials for use as a mould and reduces the problem of breaking the mould, increasing mould reusability [180].

PEDOT:PSS is a water-based CP that chemically blends with PSS. This conductive material has been widely used in electronics [29], [31], [126]–[128], [130], [131], [181], transparent coatings [129], conductive textiles [132] and bio-electronics [32], [33] due to its unique properties that combine good conductivity, stability, flexibility, processability, high transparency and low cost. A number of researchers have demonstrated that certain additives such as DMSO, ethylene glycol, glycerol and sorbitol [30], [133], [135], [182], [183] are effective mixtures to modify the properties of PEDOT:PSS. Figure 4.2 shows the physical appearance of the cured plasticised PEDOT:PSS thin films and Table 4.1 presents the water contact angle analysis and thickness of the thin films as a function of glycerol. According to the images shown in Figure 4.2, the colour of the plasticised PEDOT:PSS thin film did not change for any concentration.

Figure 4.2: Physical appearance of the plasticised PEDOT:PSS thin films on glass substrate with different concentrations of glycerol, showing no significant changes in film colour.

Percentage of glycerol in PEDOT:PSS	Contact angle	Thickness (nm)
0	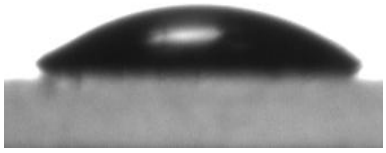 31.96°	90±1.7
0.5	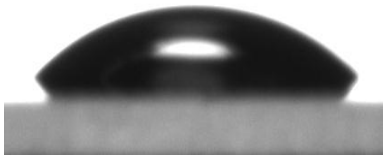 37.64°	105±1.0
1	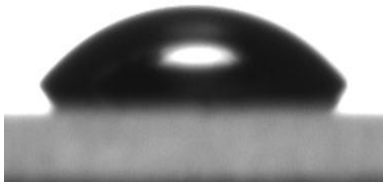 43.12°	114±1.3
2	 47.82°	119±1.3
3	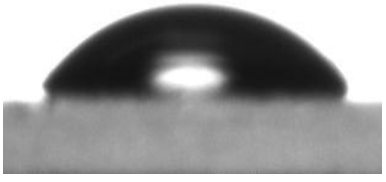 51.23°	122±1.2

Percentage of glycerol in PEDOT:PSS	Contact angle	Thickness (nm)
4	 52.94°	125±1.3

Table 4.1: Water contact angle analysis and the thickness of the plasticised PEDOT:PSS films after adding different concentrations of glycerol. There are significant changes in film water contact angle and thickness with the increase of glycerol additive.

Table 4.1 exhibit the water contact angle and film thickness measurement of plasticised PEDOT:PSS thin films using the telescope goniometer-CAMP 2008 KSV system and surface DEKTAK 150 profilometer, respectively. The measurement was carried out three times for each sample to calculate the standard deviation. The analysis of water contact angle shows an increase from 31.98° at 0% w/w to 52.94° at 4% w/w caused by the presence of glycerol. Despite the significant changes in film contact angles, the addition of glycerol in the mix increased the viscosity of the mixture which ultimately increased the thickness of the film from 90 nm for 0% w/w to 125 nm for 4% w/w of glycerol. This increment in film thickness agrees with previous reports in the literature [31].

4.3.2 Electrical and optical properties of plasticised PEDOT:PSS thin film.

The four-probe technique and AFM imaging were used to investigate the influence of glycerol concentrations in the CP on electrical conductivity, surface morphology and roughness. Figure 4.3 compares the conductivity measurements of the plasticised

PEDOT:PSS thin films together with the surface roughness measurements. It was found that the electrical conductivity of the pristine PEDOT:PSS thin film was 1.28 Scm^{-1}; this increased to 443 Scm^{-1} after the addition of 4% w/w of glycerol. It is possible that the presence of glycerol broke the ionic bond in the PEDOT:PSS chains so the PEDOT particles exhibited more aggregation and formed a stronger bond between the counter ions in the chains [30], [124]. Huang *et al.* [47] reported that the electrical conductivity of doped CP films increased two- to threefold owing to the uniform distribution of PEDOT molecules in the PEDOT:PSS films and produced better pathways for charge transport perpendicular to the film.

To further understand the conductivity enhancement due to the addition of additives, the surface roughness and morphology of the samples by AFM analysis were observed. Note that all the AFM images are set to the same scale on the vertical z-axis with an investigation area of (1 × 1) μm^2. In addition, the root-mean-square roughness (R_{rms}) is the most commonly evaluated parameter representing the surface roughness. The red line in the graph of Figure 4.3 showed that the addition of glycerol has a noticeable effect on the surface roughness values. Xiong and Liu described the addition of dopant stimulating the PEDOT grains, which results in the surface roughness of the film increasing [184].

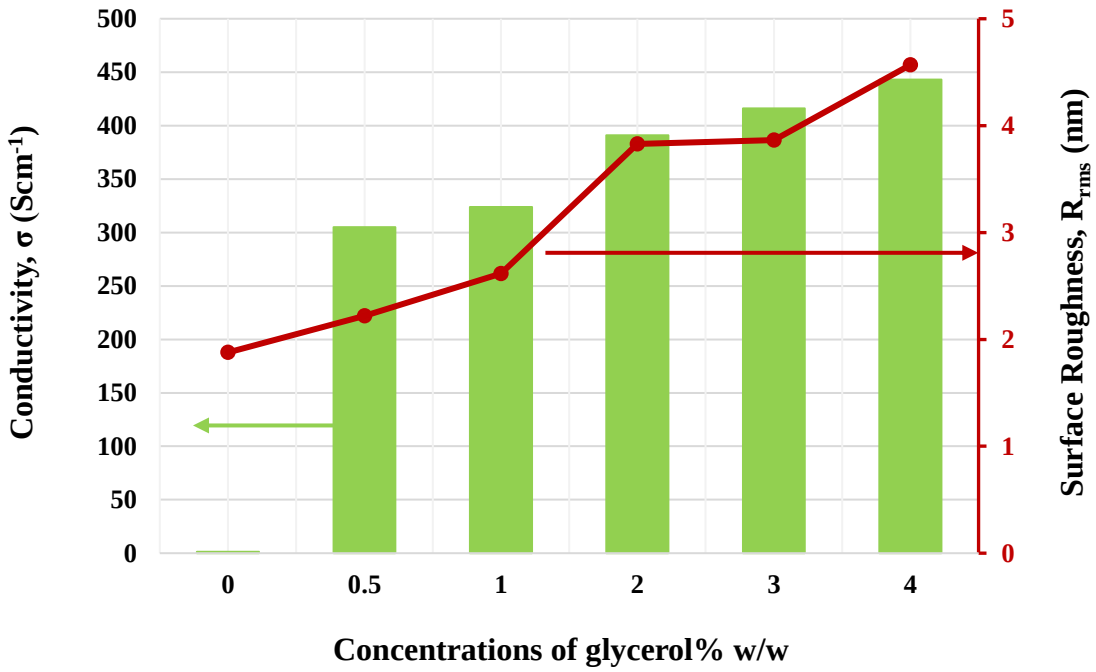

Figure 4.3: Showing the conductivity (σ) and surface roughness (R_{rms}) of the films as a function of glycerol concentration. Both of these properties have significantly increased with the addition of glycerol suggesting that the presence of glycerol has rearranged the PEDOT:PSS morphology and might improve the interconnections between the PEDOT chains.

Figure 4.4 clearly shows the three-dimensional (3D) AFM morphology images of plasticised PEDOT:PSS with different concentrations of glycerol. The surface of the 0% w/w thin film is shown with random trough and peak morphology. As the glycerol concentration increased, the 3D films exhibit valley-shaped surface morphology. In addition the film conductivity has a direct relation to the PEDOT particle size. These result also indicated that the PEDOT grains size (bright regions) increase while the PSS in the dark region decrease due to the reduction of energy barrier for electric charge transport on the PEDOT chain leading to a higher electrical conductivity. Hence this has led to the increase of PEDOT grain size and resulting in reduces PSS barriers will bring to conductivity enhancement [184].

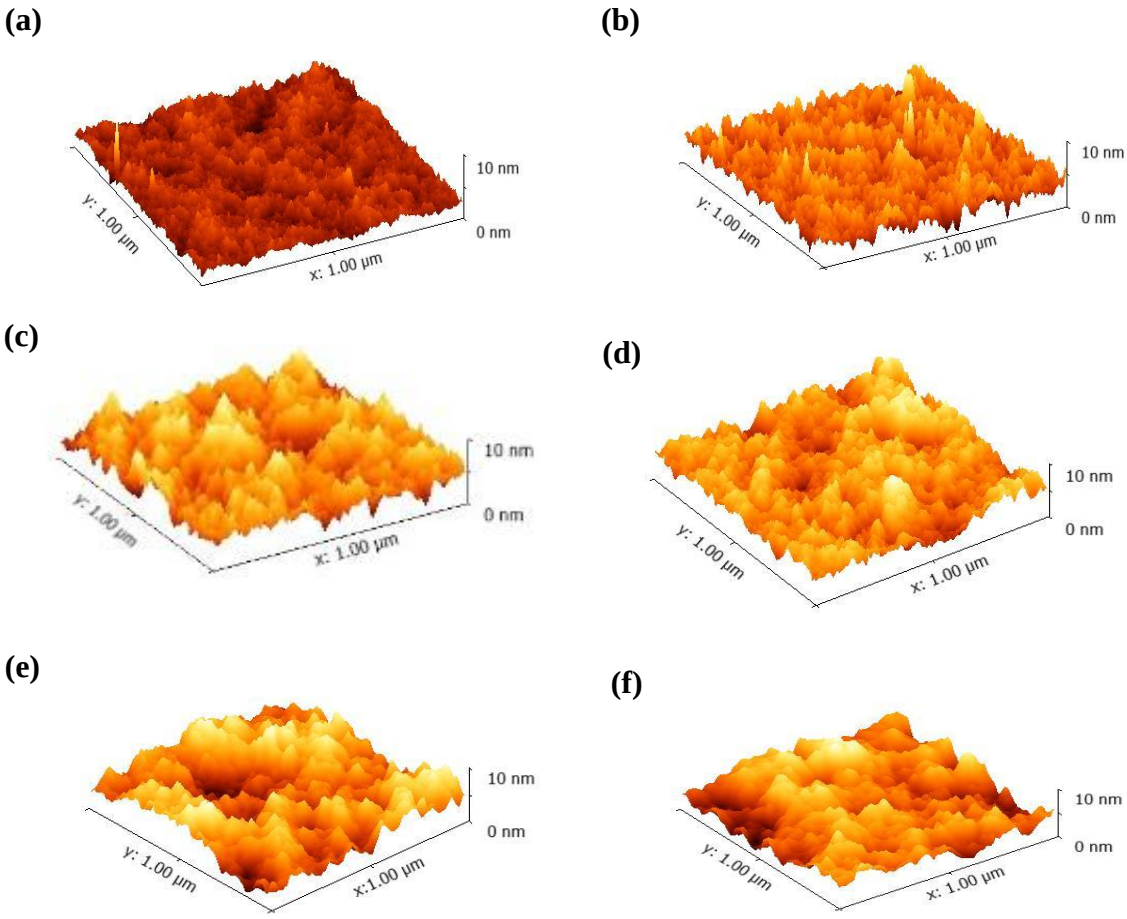

Figure 4.4: AFM images of plasticised PEDOT:PSS film surface topography with six different concentrations: (a) pristine (b) 0.5% glycerol, (c) 1% glycerol, (d) 2% glycerol, (e) 3% glycerol and (f) 4% w/w glycerol. The data shows a significant change in surface topography as the percentage of the glycerol was increased in the PEDOT:PSS matrix.

4.4 Fabrication of plasticised PEDOT: PSS bioimprint

As mentioned in section 4.3, the method used by Meier *et al*. was adopted for different purposes and applications in this work. This method was used to imprint the cellular features into conductive film. Figure 4.5 shows the fabrication process of plasticised PEDOT:PSS bioimprint using a soft embossing technique. The negative PDMS bioimprint mould was fabricated as described in section 3.8. The prepared homogeneous plasticised PEDOT:PSS mixtures were spun coated on microscope glass

substrates at 1000 rpm for 60 seconds with a Headway PWM32-PS-R790 spinner machine as illustrated in Figure 4.5 (a). Then, a negative PDMS mould was brought into contact with the coated substrates and a constant pressure of 40 kPa was applied for 48 hours at temperature 37 ℃ on a hot plate, as shown in Figure 4.5 (b). Note that before the imprinting process, it is necessary to treat the PDMS stamp with an oxygen plasma at 100 Watt for 30 seconds to establish a more hydrophilic surface.

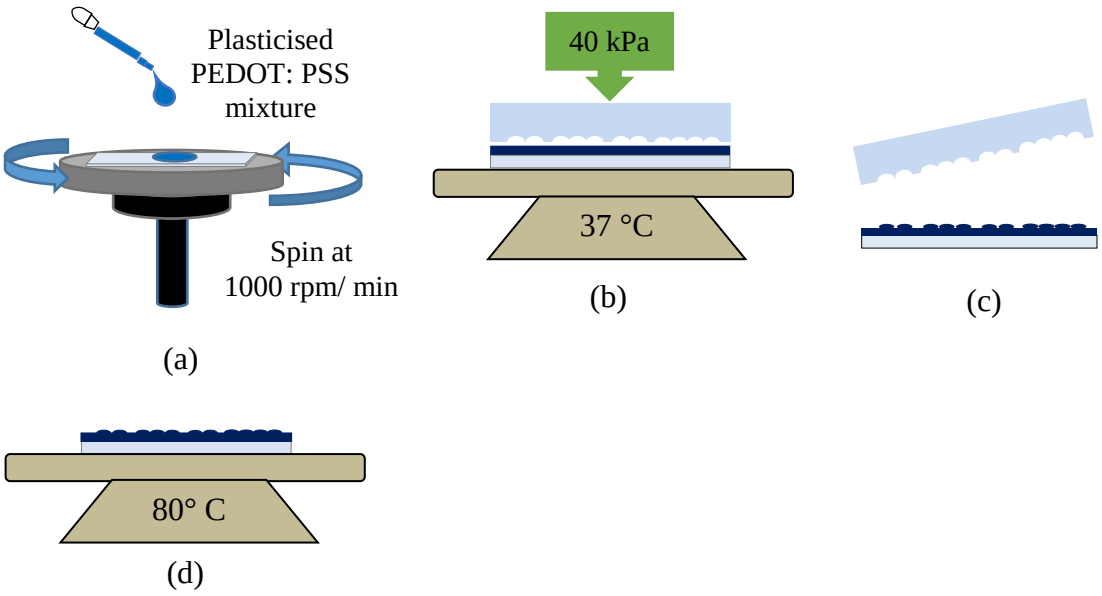

Figure 4.5: The fabrication process of plasticised a PEDOT:PSS bioimprint: (a) spin coat the substrate with plasticised PEDOT:PSS mixture, (b) bring PDMS mould into contact, (c) peel off the master mould from the substrate and (d) bake until completely dry.

When the conductive film was dried, the negative PDMS bioimprint mould was carefully peeled off the conductive substrate (without dragging) as shown in Figure 4.5 (c). Then, the positive bioimprint in plasticised PEDOT:PSS was baked again at temperature 80 ℃ for 30 minutes to remove the residual glycerol molecules (Figure 4.5 (d)).

4.4.1 Plasticised PEDOT: PSS bioimprint

In investigating the feasibility of replicating the cell-like features onto plasticised PEDOT:PSS film using PASE technique, three concentrations of glycerol (1%, 2% and 3% w/w) were used. Figure 4.6 shows the optical images of the plasticised PEDOT:PSS films presented after the bioimprinting process. The images clearly show that the cellular features have been successfully transferred only in the 3% w/w glycerol film, but with very low resolution.

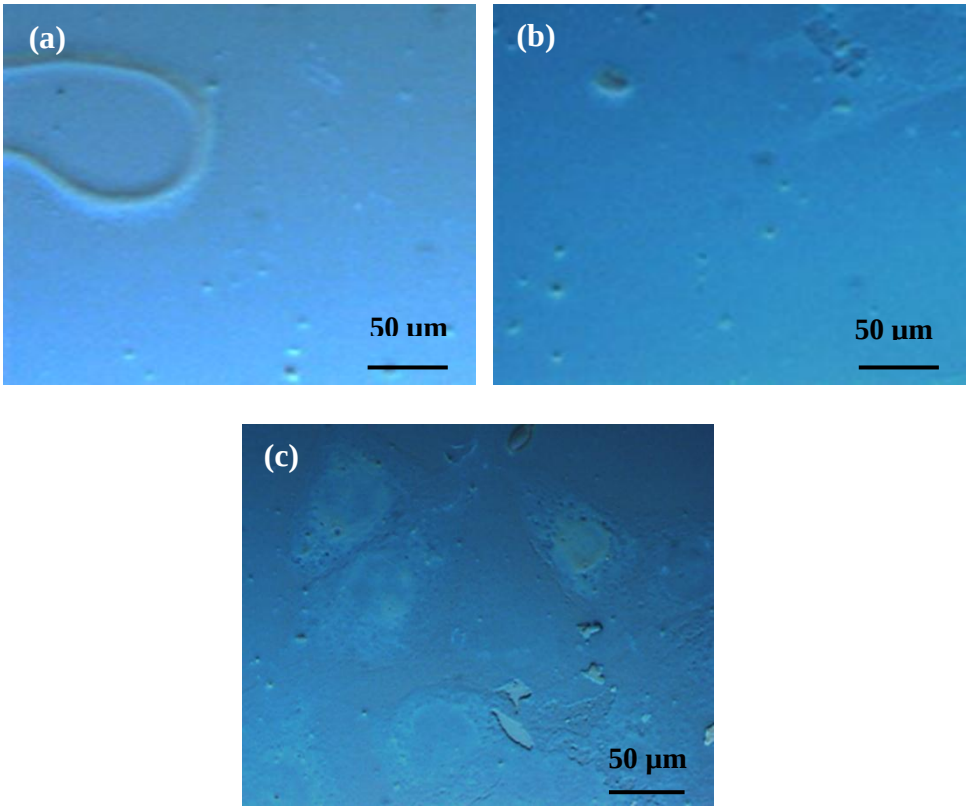

Figure 4.6: Optical images of plasticised PEDOT:PSS thin films after the bioimprint process (a) 1%, (b) 2% and (c) 3% glycerol. The cellular features can only be seen at 3% glycerol concentration.

To confirm the resolution of the replication, the cell topography of 3% (w/w) plasticised PEDOT:PSS was imaged using AFM. Images in Figures 4.7 shows the fixed C2C12 cells on the glass slide and the positive replica in plasticised PEDOT:PSS film respectively. Note that the images are not for the same cell but from the same sample. As can be seen in Figure 4.7 (a), the image shows that the fixed cell on glass contains cellular components including nucleus, filopodium, lamellipodium and cell membrane in micro- and nano-sized detail. However, Figure 4.7 (b) clearly shows that only the nucleus and cell membrane with artefacts were transferred onto plasticised PEDOT:PSS. Possibly this poor transfer was due to the very low viscosity and thickness (90 nm to 125 nm) of the plasticised PEDOT:PSS film, which made it harder for the PDMS mould pattern to press uniformly onto the target film. We conclude that with the PASE approach, the electrical properties of the thin film were increased, but it is not suitable for transfer of cell-like features, due to viscosity and thickness problems, which caused loss of the micron- and nano-sized cellular details.

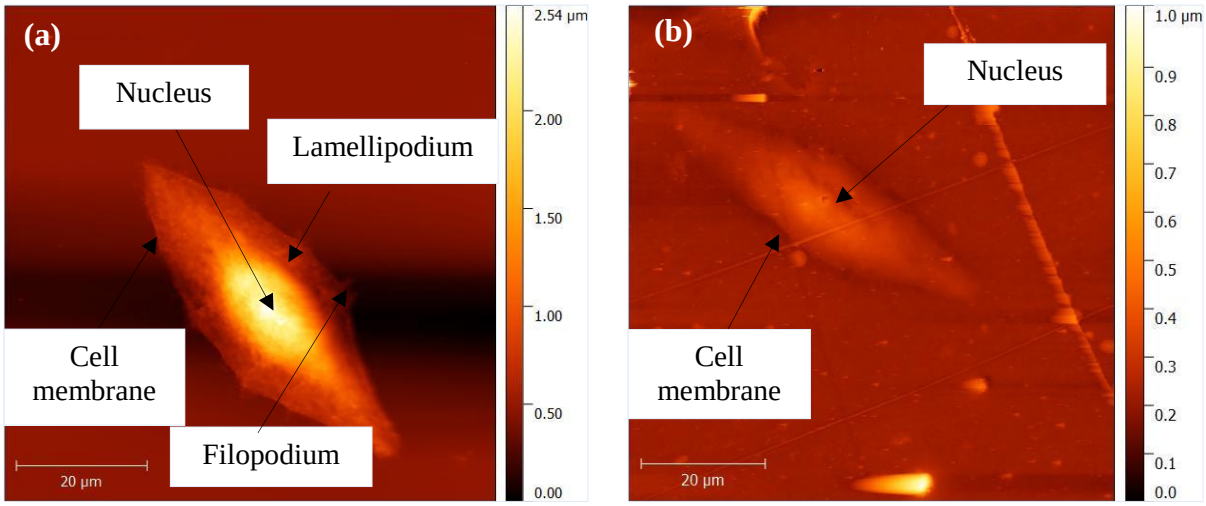

Figure 4.7: AFM images of (a) fixed cell on the glass prior to imprint and (b) positive cell replica with 3% (w/w) of plasticised PEDOT:PSS. Images are not of the same cell but from the same sample. The replica in plasticised PEDOT:PSS shows the loss of micro- and nanoscale cellular details.

4.5 Synthesis of conductive hydrogel

In order to overcome the low viscosity and thickness issues, an alternative method of introducing the hydrogel was developed in this work so as to achieve a biocompatible

CH for a cell culture substrate. Integrating colourless gelatin and glycerol into the PEDOT:PSS solution combined the advantages of both polymers while compensating for the limitations of each material. Hydrogel was chosen because of its hydrophilic, biocompatible and biodegradable properties. In addition, the tuneable properties of the developed CH polymer enables the formation of 3D patterning with a number of printing techniques. Various studies have reported that CHs are attractive as scaffolding materials for regenerative medicine applications due to their ability to mimic many physical properties of tissues [34], [36], [185]–[188].

CH was synthesised by mixing 12.5 wt.% of 300 Bloom gelatin powder in PBS (pH 7.4) solution and heated at temperature 60 ℃until the gelatin powder was dispersed in the solvent. The films were modified with six different equal concentration of glycerol and PEDOT:PSS 2%, 3%, 4% & 6% from 12.5gm of gelatin solution and continuously stirred at temperature 70 ℃ until the mixtures became homogeneous. The mixtures were poured directly onto a mould and dried at room temperature. Even though gelatin is a soft biopolymer but it will become more stiff and rigid when it is dried. The addition of the glycerol effectively improved/increases the flexibility of the conductive hydrogel film owing to the plasticiser able to interact with protein chains and bind with the molecules of water during the dehydration [189].

4.5.1 Physical appearance of conductive hydrogel

This section presents further results from the synthesis of the CH mixture. As can be seen in Figure 4.8 the polymerisation of CH films at six different concentrations of PEDOT:PSS produces polymers with different darkness. The CH film with 0% w/w PEDOT:PSS is transparent while as the concentrations of PEDOT:PSS solution increased, the resultant PEDOT:PSS hydrogel films change to a dark blue colour.

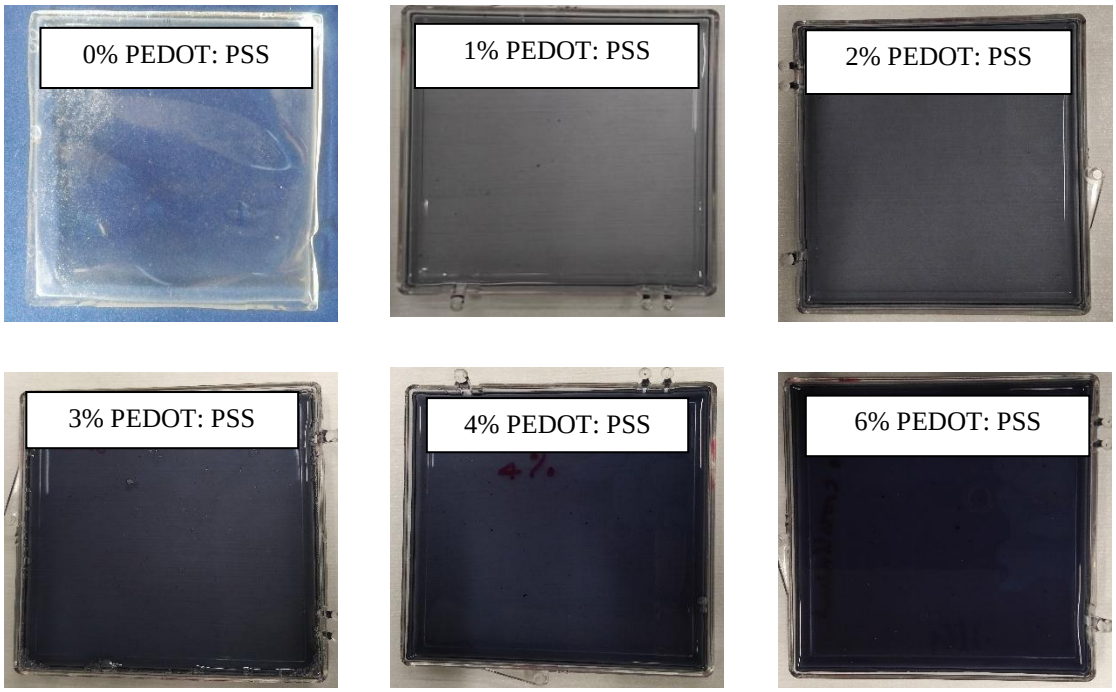

Figure 4.8: Physical appearance of 6 different concentrations of CH films. As the concentration of PEDOT:PSS increased in the mixtures the CH film changed in colour from transparent to dark blue.

4.5.2 Fabrication of conductive micropatterns

The fabrication processes of PDMS micropatterns master mould is presented in this section. The master mould substrate was prepared according to the method established by our research group [59] and is illustrated in Figure 4.9 (a–d). A positive photoresist AZ1518 was coated onto a silicon wafer at a spinning speed of 2000 rpm for 60 seconds, and the soft baking process was carried out on a hot plate at temperature 100 ℃ for 90 seconds (Figure 4.9 (a)). As shown in Figure 4.9 (b), the soft-baked photoresist layer was subsequently exposed to UV light through a prepared chrome mask to define the pattern. The silicon wafer was then developed with MIF 326 developer for 45 seconds and rinsed with deionised water. Then the resist pattern was post-baked on a hotplate at temperature 120 ℃ for 2 minutes in order to smooth the sidewalls (Figure 4.9 (c)). A PDMS pre-polymer and a curing agent in a 10:1 weight ratio were mixed and degassed under a vacuum until all bubbles disappeared. Then, the pre-polymer mixture was poured over the photoresist master mould and cured on a hotplate at temperature 80 ℃ for 2 hours, as shown in Figure 4.9 (d). Finally, the PDMS was

carefully peeled from the silicon wafer and was further crosslinked by being baked for an additional 2 hours at temperature 80 ℃.

Next, a soft lithography technique was used to fabricate a CP micropatterns as shown in Figure 4.9 (e-f). In Figure 4.9 (e), the prepared CH mixture was liquid cast immediately onto the treated PDMS mould and left in the incubator at temperature 37 ℃ for overnight. The cured CH film was then left at 4 ℃ for 48 hours to further polymerisation. Note the PDMS mould was oxygen plasma treated at 100 Watt for 30 seconds to establish a more hydrophilic surface to enhance cavities filling before the imprinting process. The conductive micropatterned films were carefully peeled off to avoid tearing effects (Figure 4.9 (f)). The patterns on the PDMS master mould and on the CH were then compared using optical microscopy inspection.

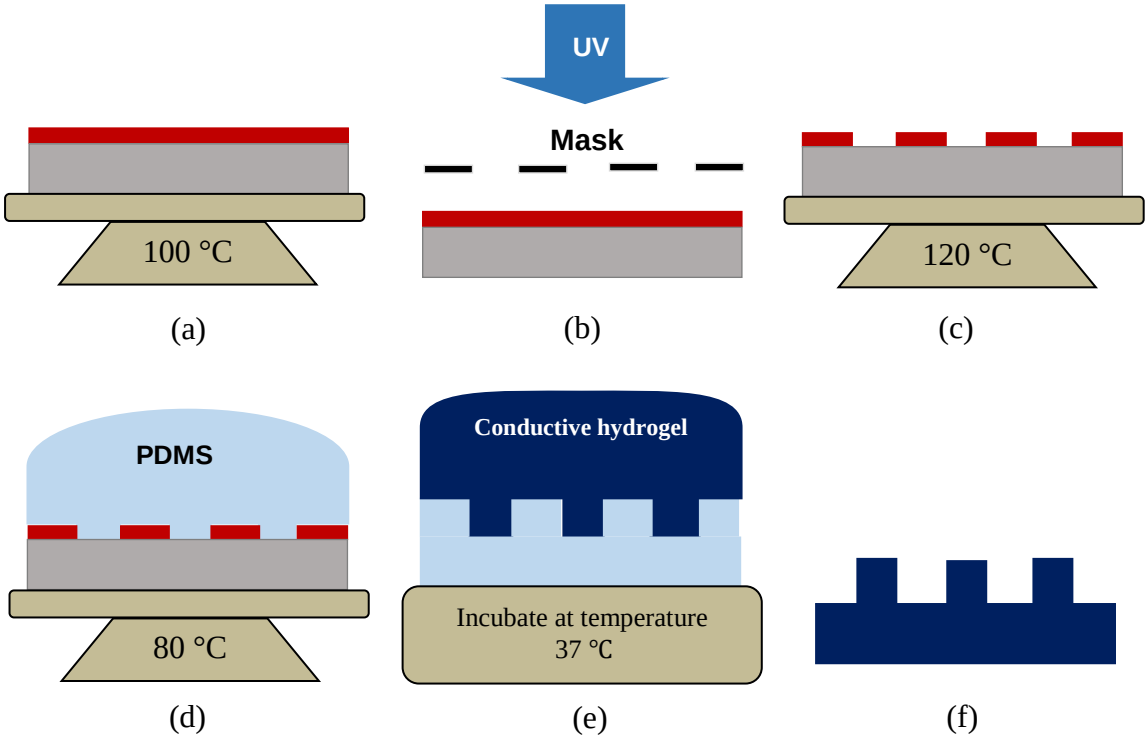

Figure 4.9: The schematic showing the fabrication of CP micropatterns: (a) spin coating AZ1518 on Si wafer and bake, (b) define patterns under UV light, (c) develop and post bake the developed resist layer, (d) pour pre-polymer PDMS over the micropatterns, cure and peel off, and (e) liquid cast the conductive mixture on PDMS micropatterns mould and cure, (f) peel off the cured film from PDMS mould.

4.5.3 Conductive micropatterns films

Figure 4.10 shows the optical images of the PDMS master mould and the conductive micro-imprints with different concentrations of plasticising agent and PEDOT:PSS. It must be emphasised that only the amount of glycerol and PEDOT:PSS were changed; the other experimental conditions were kept constant. As can be seen in Figure 4.10 (b) and (c), at low concentrations (1% and 2% w/w) of plasticised PEDOT:PSS the microstructures show poor replication with artefacts, while for dopant concentration above 3% w/w the patterns were faithfully replicated from the master mould. This improvement in integrity of replication has resulted from the use of the optimised concentration of plasticised PEDOT:PSS in the CH film.

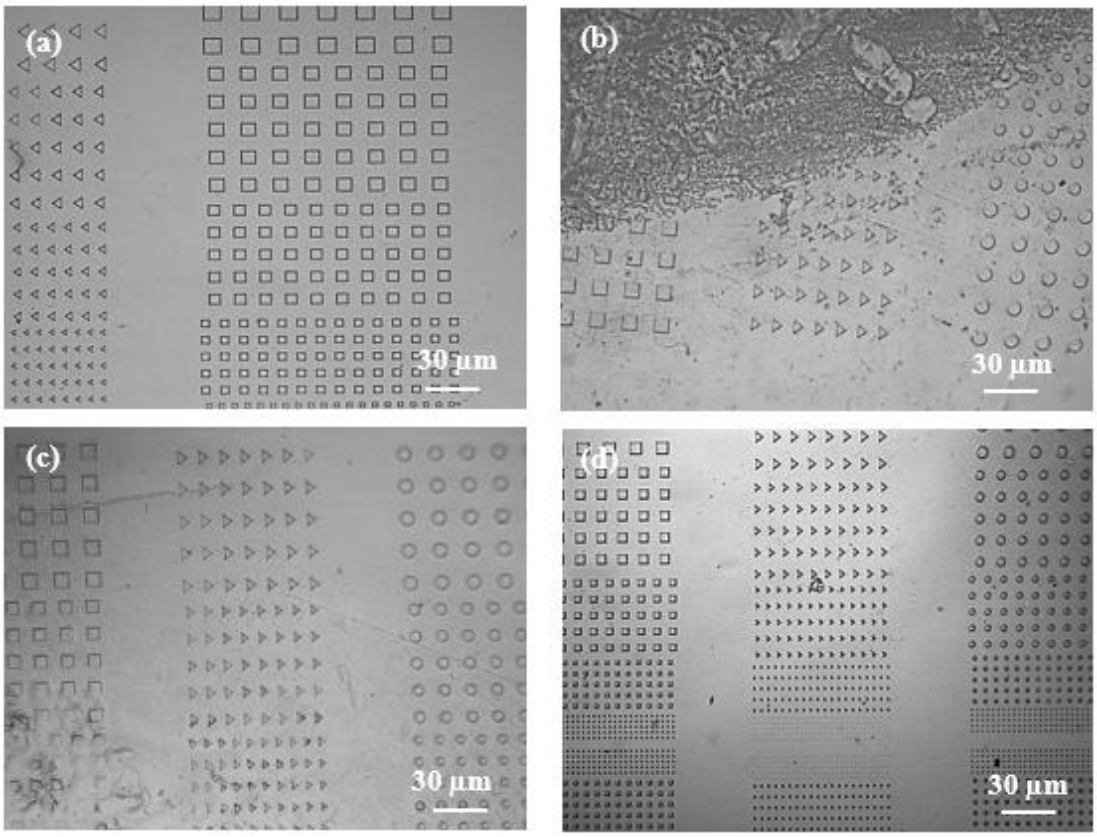

Figure 4.10: Optical images of micropatterns replication into: (a) PDMS master mould and CH micropatterns films with (b) 1% w/w, (c) 2% w/w and (c) 3% w/w. From the images of the conductive replicas it is evident that the replication fidelity is best at 3% (w/w) concentration of plasticised PEDOT: PSS.

4.5.4 Fabrication of conductive bioimprint films

After successful replication of the conductive micropatterns, the suitability of the CH was investigated to develop the conductive bioimprinting technique. As in the bioimprint protocols, where the negative and positive PDMS master moulds as described in section 3.8 were made first. In the conductive bioimprint process PDMS master mould were made in both positive and negative impressions.

Figure 4.11 shows the full fabrication process for the positive and negative conductive bioimprint. As described in Chapter 4.4, 12.5 wt.% of gelatin powder was dissolved in PBS (pH 7.4) solution and heated at temperature 60 ℃ for 15 minutes. In this bioimprint fabrication process, the mixture is modified with 3 concentrations of glycerol and PEDOT: PSS (2%, 3% and 4%) from the 12.5 wt.% gelatin solution and were thoroughly stirred at temperature 70 ℃ until homogeneous mixture was formed. In Figure 4.11 (a), each conductive mixture was immediately liquid cast onto the PDMS mould and left in the incubator at temperature 37 ℃ for overnight. Again, the PDMS moulds were oxygen plasma treated at 100 Watt for 30 seconds to establish a more hydrophilic surface before the imprinting process. Then, the conductive bioimprint material was then kept at temperature 4 ℃ for 48 hours to complete the polymerisation. The conductive bioimprinted film obtained was then carefully peeled off to avoid tearing effects (Figure 4.11(b)). The second replication from a negative mould results in a positive replica bioimprint and vice versa (Figure 4.11(c)). Both the imprints on the PDMS master moulds and on the CH were then compared using optical microscopy and AFM imaging.

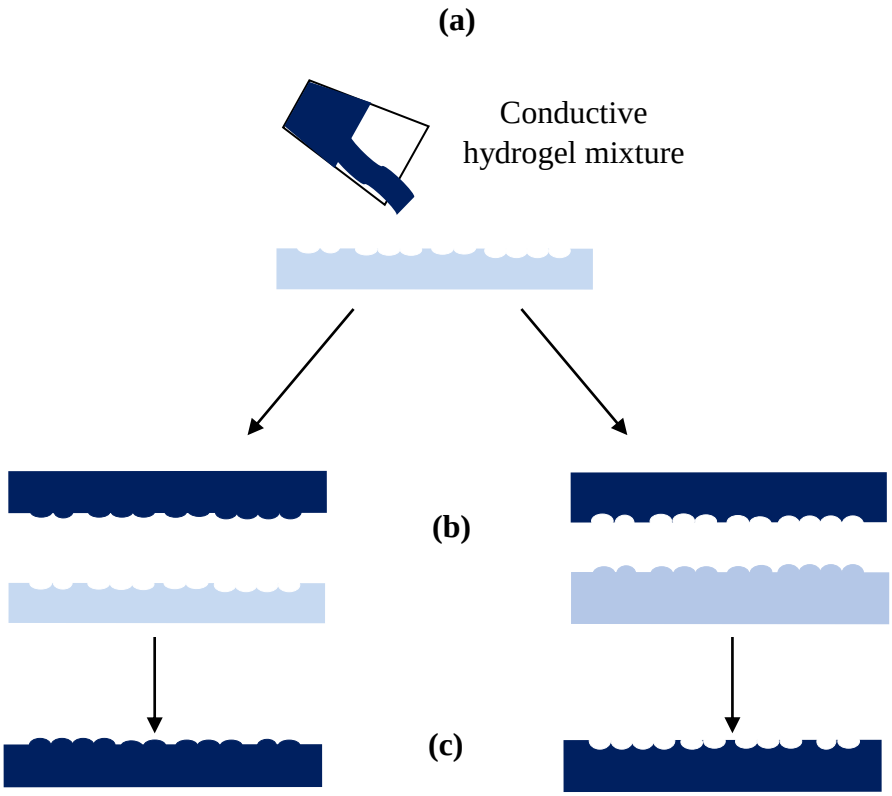

Figure 4.11: Schematic of positive/negative conductive bioimprint process: (a) Liquid cast the CH mixture onto the negative/positive PDMS mould (light blue) and leave it in incubator at temperature 37 ˚C overnight, then further cure at temperature 4 ℃ for 48 hours, (b) peel off the conductive bioimprint from the PDMS mould and (c) positive/negative bioimprinted onto CH layer (dark blue).

4.5.4.1 Analysis of cellular features replica on conductive bioimprint films

Figure 4.12 shows optical microscopy images of the conductive bioimprint with two different magnifications, 10x and 20x for 2%, 3% and 4% (w/w) of glycerol / PEDOT:PSS concentrations in a gelatin solution. We first culturing the C2C12 the cells by following the standard protocol and fixed the cells after they reach 80-90% confluency at certain period of time. Then, the PDMS bioimprint master mould was made out of the fixed cells. In the conductive bioimprint process, PDMS master mould were made in both positive and negative impressions. Image (a) in Figure 4.12 for a 2% w/w concentration shows low resolution, and the cell-like features although visible but poorly replicated. There are also formation of black dots on the PEDOT:PSS film. However, Figure 4.12 (b) for

the 3% w/w shows an improved replication compared to the image in Figure 4.12 (a). Whereas the optical image in Figure 4.12 (c) clearly shows a high replication fidelity and the nano-and micro-sized cell features have been faithfully replicated at 4.0% w/w.

Based on the investigation and analysis conducted on the resolution of the replication for the 4% w/w glycerol concentration and PEDOT:PSS, this mixture was selected for use as the conductive bioimprint substrate. In this work, positive and negative bioimprints were prepared and used to quantify the cell replica morphology compared to the original cell features. In order to facilitate direct comparison between the original and replica features, C2C12 cells were cultured on grid-patterned microscope glass. The fabrication process of the grid-patterned glass substrate followed the photolithography method, as in Azadeh *et al.* [59].

The fabrication process started with the glass substrates being cleaned using acetone, methanol and isopropanol for three minutes in an ultrasonic bath. It was then oxygen plasma treated for ten minutes at power of 100 W. The substrate was spin coated with AZ1518 negative photoresist at 1000 rpm for 60 seconds. The grid patterns were defined under UV light onto a glass substrate coated with positive resist using the Karl Suss MA-6 mask aligner for 15 seconds and was soft-baked for ten minutes at temperature 100 ℃ on a hotplate. The glass was then developed in the MIF 326 developer and washed with deionised water. The developed substrate was then soft-baked on a hotplate at temperature 100 °C for ten minutes. Finally, the glass substrate was etched with hydrofluoric acid for two to three minutes, then the resists were stripped using acetone and the slide sterilised under UV light before use as a cell-culture substrate.

Figure 4.13 shows the optical images of the cells and the 4% w/w conductive bioimprint, as well as the corresponding AFM images. These images reveal that the patterns are transferred with extremely low fidelity, resulting in a lack of resolution on the CH film for cellular features at the micro- and nano-sized level, compared with the original features. To measure the transfer image, the cross-section of the same cells is compared in Figure 4.14.

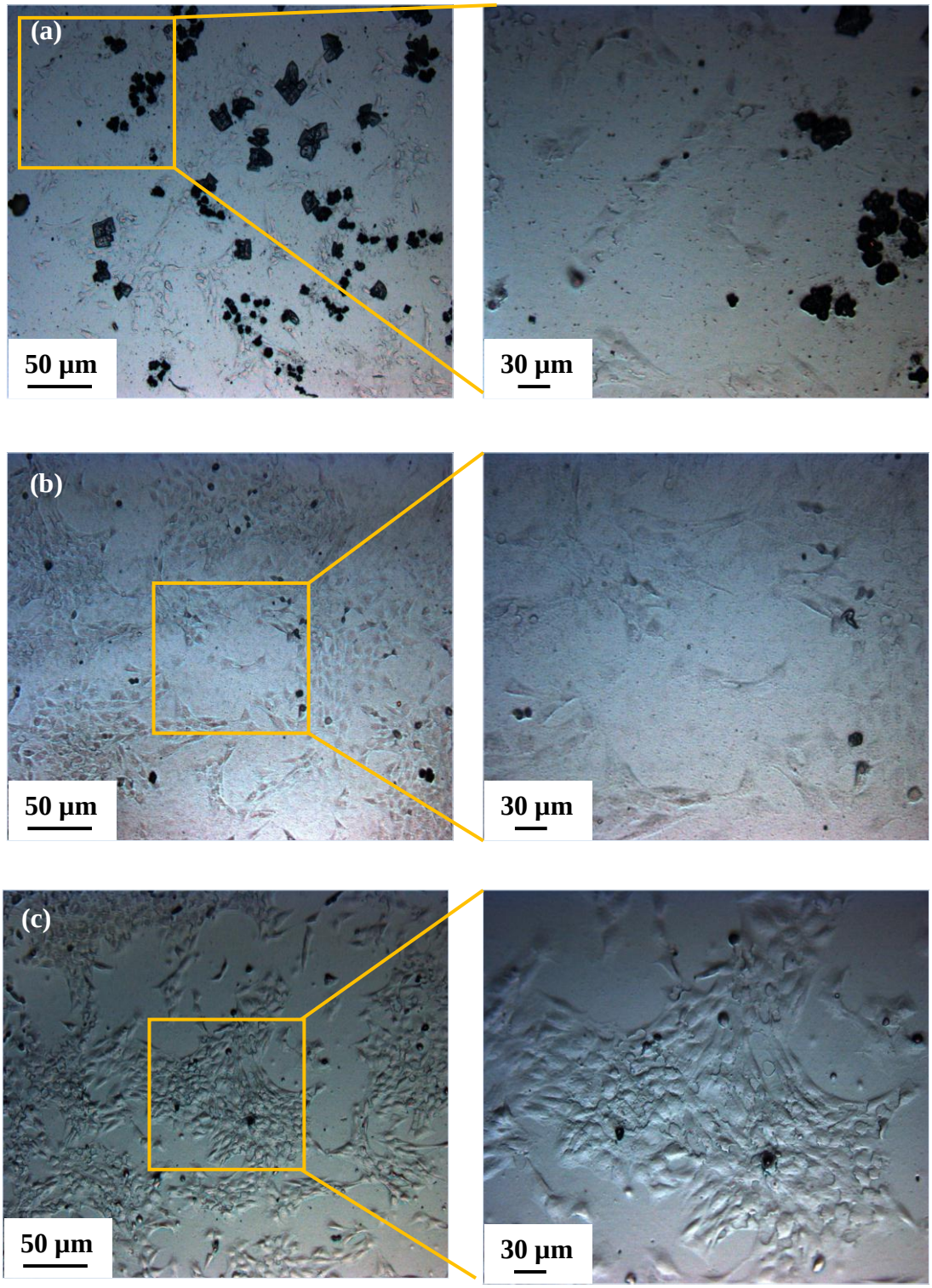

Figure 4.12: Optical images of replicated cells onto conductive gelatin with different magnifications for: (a) 2% w/w, (b) 3% w/w (c) 4% w/w. By increasing the percentage of glycerol and PEDOT: PSS in the mixture the replication resolution is improved. Note that the black spots in (a) are some debris from the PEDOT: PSS formation on the bioimprinted cellular features. Moreover, as the concentration increases to 4% w/w in (c) showing an improvent in replication as compared with the images in Figure 4.12 (a) and (b).

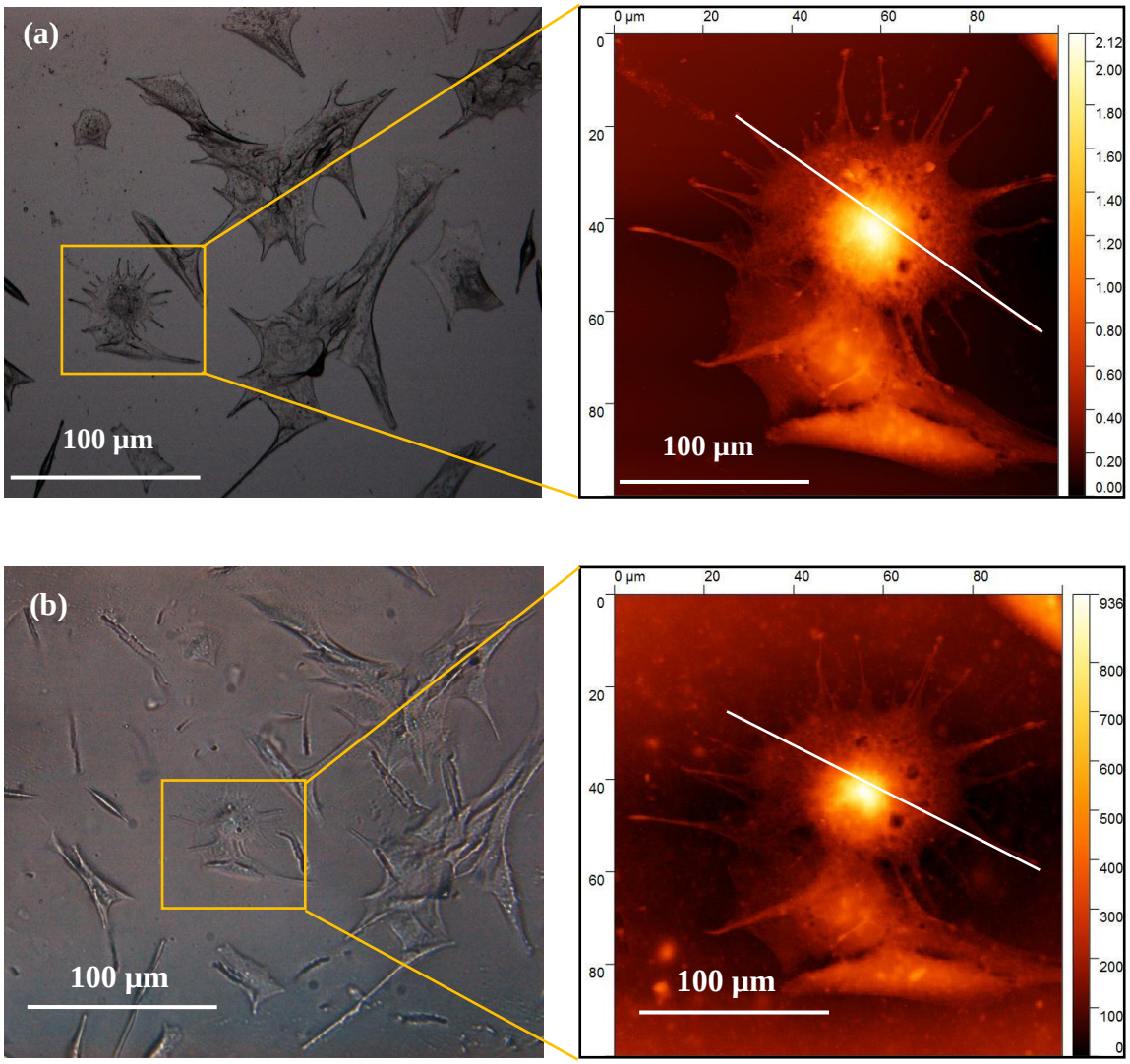

Figure 4.13: On the left, optical micrographs of (a) fixed C2C12 myoblast cells on glass before imprinting and (b) positive replication with 4% (w/w) of plasticised PEDOT: PSS in CH. On the right, AFM images of cells on different substrates that highlights a unique cell used in the cross-sectional profile images in Figure 4.14.

The 2D-profile of AFM trace shows that the replication details of the conductive bioimprint reached only 30% from peak to peak of the original features. This happens because the CH mixture did not penetrate thoroughly into all the fine details on the PDMS master mould. Note that, the replica essentially compare to the fixed cells on the glass from peak to peak on the AFM trace which assume the fixed cells to be 100%.

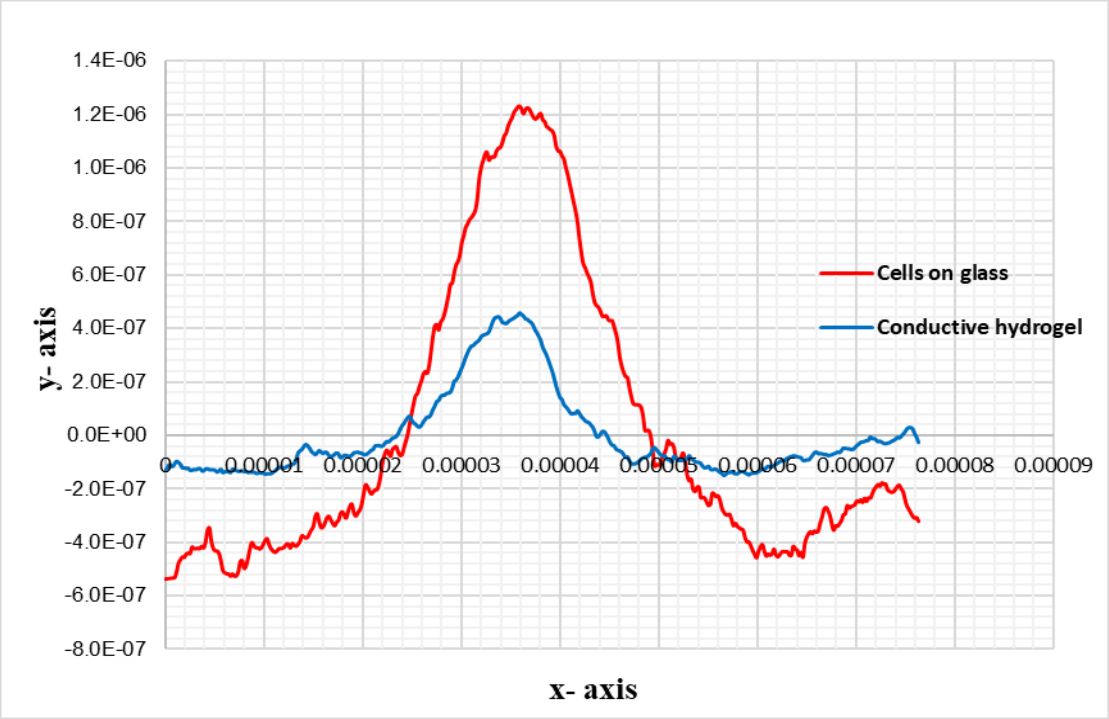

Figure 4.14: Topographic profiles extracted from comparison of AFM data between positive conductive bioimprint and fixed cell on glass substrate. Features details formed on conductive film indicate only 30% replication fidelity compared to the original fixed cell.

4.5.4.2 Enhancement conductive bioimprint resolution

To overcome the challenges, two process steps were taken to enhance the replication resolution of the conductive bioimprint. Firstly, the bioimprinted PDMS film was treated with oxygen plasma for 30 seconds at 100 Watt. The treated PDMS film was immersed in a 22.2% w/v solution of polyvinylpyrrolidone (PVP) in deionised water for one minute followed washed thoroughly with deionised water and dried. Then, the treated PDMS substrate was liquid cast with CH mixture and cured on a hot plate at temperature 50 ℃for one hour. The PVP and additional curing steps will helps to allow the CH to fill and penetrate into the micro- and nanoscale features. The PVP is water-based hydrophilic polymer, which help to turn PDMS surface substrate to be hydrophilic for a relatively long period of time. The conductive bioimprint was left in

the incubator at temperature 37 ℃ for overnight and then left at 4 ℃ for 48 hours to further film polymerisation.

Figures 4.15 (a) to (c) show the optical images of fixed cells, negative bioimprinted PDMS and positive bioimprinted on 4% w/w CH. The optical micrographs exhibit that the replication fidelity of the CH bioimprint in the red circle is increase significantly after compared with the results obtained in the previous process. AFM trace scanning was used to examine the resolution of the conductive bioimprint, negative PDMS bioimprint and the fixed cellular features on a glass substrate.

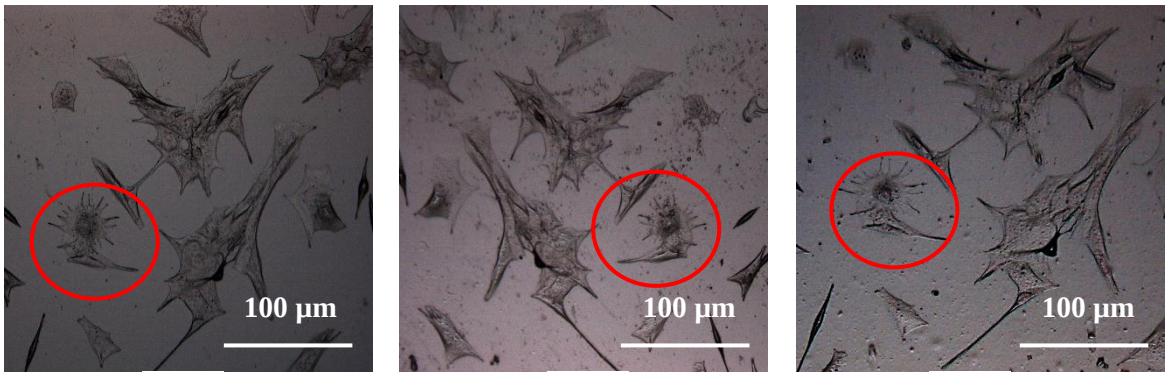

(a) **(b)** **(c)**

Figure 4.15: Optical images of (a) fixed C2C12 myoblast cells on glass before imprinting, (b) negative replication into PDMS, and (c) positive replication with 4% (w/w) of plasticised PEDOT: PSS in CH. The red circle highlights a unique cell that was used in the subsequent AFM images of Figure 4.16.

Figures 4.16 (a), (b) and (c) show the AFM images of the fixed cells, positive and negative PDMS bioimprints respectively, while Figures 4.16 (d) and (e) show the positive and negative cell replicas in CH polymer. These images clearly indicate that the detailed features of the CP replica have been replicated faithfully down to the micro- and nanoscale. To quantify the replication fidelity, comparisons between the two replicas' cross-sections were performed using the AFM trace scan.

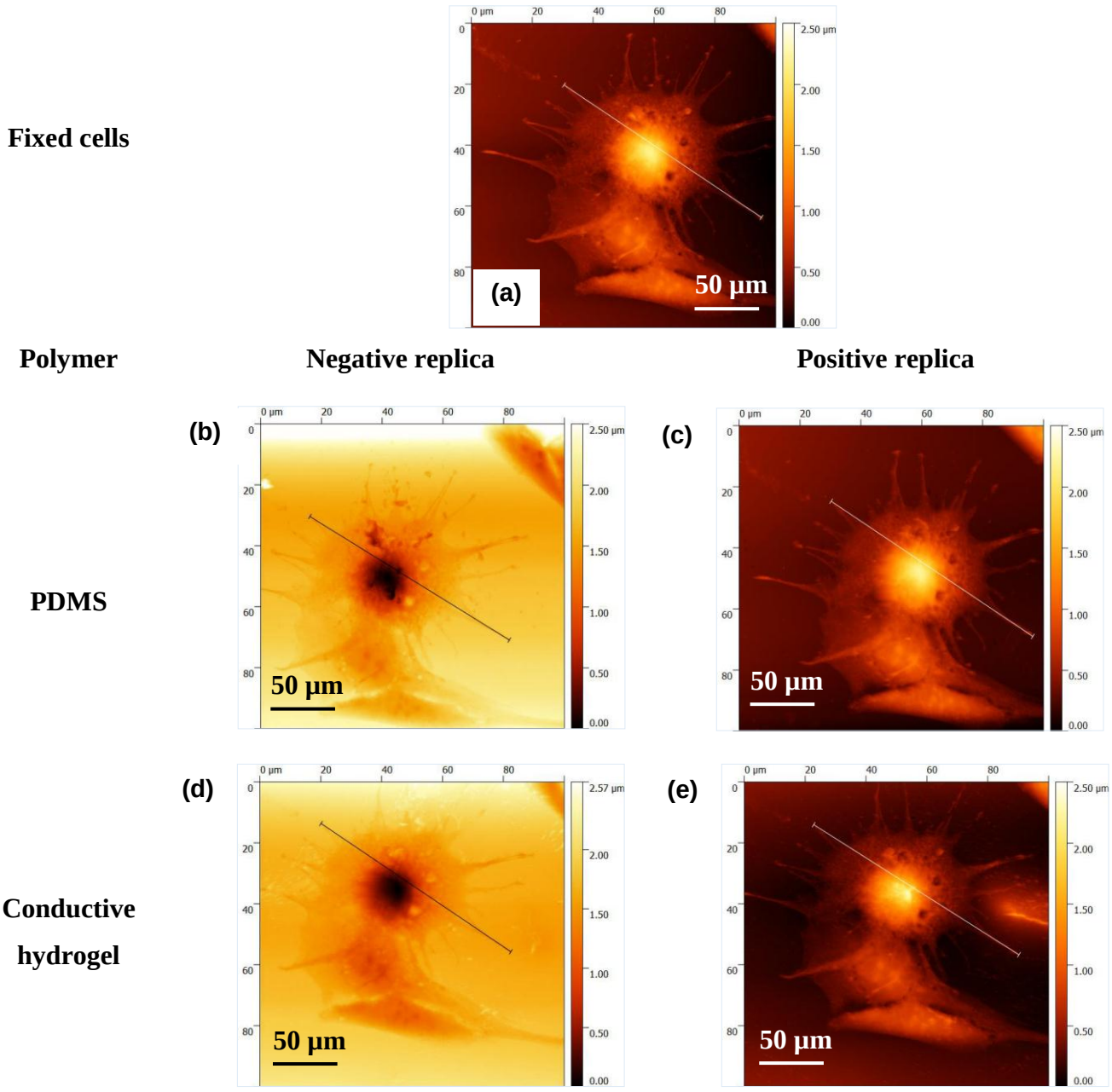

Figure 4.16: AFM images of (a) fixed rat muscle cells on glass, (b), (c) negative and positive PDMS bioimprint and (d), (e) negative and positive bioimprint CH. The conductive bioimprint successfully replicated cell features down to micro- and nanoscale.

Figure 4.17 and 4.18, illustrate a 2D trace scan of fixed cells, positive replica and negative replica of two different polymers (PDMS and CH substrates). This demonstrates the successful replication of the cellular features with an average

replication fidelity of about more than 90% as compared to the original features. In fact, this novel fabrication process is able to replicate the cellular features without any deformation and artefacts, while maintaining the cell morphologies in micro- and nano-sized details.

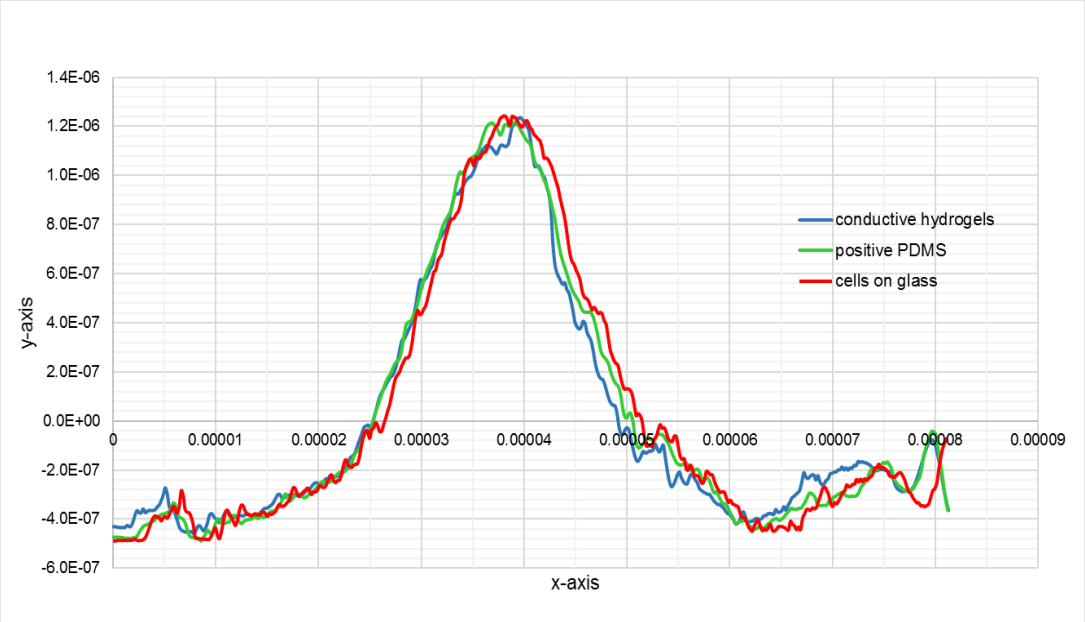

Figure 4.17: Topographic profiles extracted from AFM data between fixed cells and the pattern transferred onto conductive film with more than 90% replication fidelity.

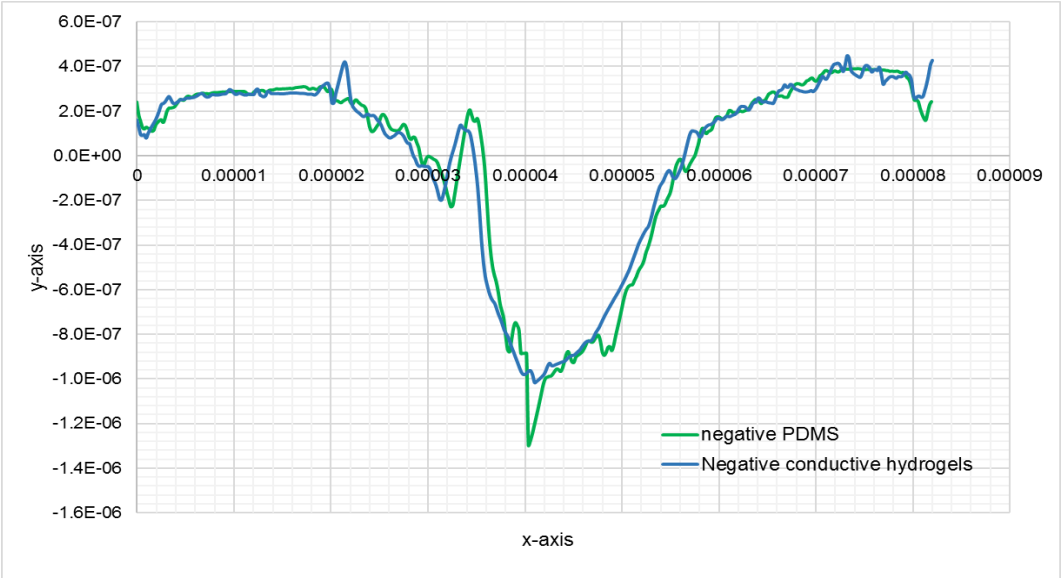

Figure 4.18: Comparison of the topographic profiles extracted from AFM data between negative PDMS master mould and negative pattern formed on conductive film, demonstrating more than 90% replication fidelity.

4.6 Conclusions

A soft lithography technique was used in fabricating a novel conductive bioimprint based on CP PEDOT:PSS. The fabrication process started by using different concentrations of glycerol to determine the influence of the additive on the changes of transparency, water contact angle, electrical conductivity, surface morphology and the replication fidelity of doped PEDOT:PSS thin films. It was found that the concentration of glycerol significantly affected the PEDOT:PSS thin films. Moreover, fabrication of the bioimprint with the PASE technique showed the loss of micron- and nano-sized cellular details due to the very low viscosity and thickness problems.

To overcome those challenges in fabricating a biocompatible for cell-culture platforms, gelatin was incorporated into the PEDOT:PSS along with glycerol. A soft lithography technique was used to replicate micropatterns and cell surface features into a CH film. The new 3D conductive bioimprint of mouse myoblast C2C12 showed very high replication fidelity with more than 90% of the fine details original cellular features. The summary of the comparison between the conductive micropatterns replication resolution and the bioimprint with different concentrations of glycerol and PEDOT:PSS is shown in Table 4.2.

Film	Gelatin (w/w),%	Plasticised PEDOT:PSS (w/w),%	Replication quality of micropatterns	Replication quality of cells
1	12.5	1.0	Poor	-
2	12.5	2.0	Good	Poor
3	12.5	3.0	Excellent	Good
4	12.5	4.0	-	Excellent with > 90% fidelity

Table 4.2: The quality of the replication for conductive micropatterns and bioimprint films with different concentrations of glycerol and PEDOT: PSS. It is clearly shows that at 3% w/w of glycerol and PEDOT: PSS solution gave the best replication for micropatterns while 4% (w/w) was excellent for replication of cells.

CHAPTER 5

Modifications to Improve the Substrate Culture Platform

In Chapter 5 will present the effects of chemical and surface modification of the CH films on electrical conductivity, swelling properties, biocompatibility and cell behaviour. The main challenge to the incorporation of a CP and hydrogel matrix is that both of these materials are highly soluble in most common solvents such as deionised water, culture mediums and PBS solution. Chemical modification was pursued to overcome this challenge. The synthesised CH was chemically crosslinked with Activa TI microbial transglutaminase (mTg). We determined the significant effects of the mTg crosslinker on the electrical conductivity properties and swelling behaviour of the films. It was found that the electrical conductivity of the crosslinked CH films increased from 10^{-6} to 10^{0} Scm^{-1} with a decrease in water absorption.

For the biocompatibility study, myoblast C2C12 cells were cultured on a conducting polymeric material in order to observe cell viability and adhesion activity. This revealed that none of the crosslinked conductive substrates showed any toxic effects on myoblasts after 24 hours of cell seeding. In addition, CH surfaces was modified with micropillars and bioimprint cell replicas were prepared using a soft lithography technique to study the influence of surface topography on cell adhesion and proliferation. Staining cells with crystal violet showed that substrate topography affects cell morphology and their migration behaviour. Cells cultured on a conductive micropillars substrate revealed that cells are preferentially more elongated and possess branched shapes compared to those cultured on areas of flat surfaces. Moreover, the analysis of cell growth on conductive bioimprinted surfaces and on flat surfaces showed that cells preferred to attach and grow on the platform with cell-like features and spread well as they grew. Hence, the CH obtained offers an attractive substrate for

applications in the area of soft tissue augmentation and regenerative medicine and implantable devices.

5.1 Introduction

A CH substrate represents a class of functional biomaterial that combines the electroactive component of a CP with the physical and mechanical components of a soft-wet hydrogel matrix. CHs have significant applications in many biological applications, including tissue engineering, bioactive electrode coating, micro catheters, artificial muscles, organs on chip, and drug delivery systems [12]–[18]. The conductive material based on PEDOT:PSS has been a subject of interest to several research programmes for regulating cell behaviour through electrical stimulation and helping to trigger cell desorption [32], [153]. Physically, conducting polymer PEDOT:PSS shows fragile and poor mechanical properties and is not suitable for tissue engineering when used by itself [42]; therefore, by blending PEDOT:PSS with, for example, chitosan, elastomer and gelatin, the resulting CH material exhibited improved imprinting quality, better chemical stability and enhanced mechanical properties, higher electrical conductivity and improved biocompatibility in addition to its biodegradable properties [34], [35], [37], [42], [151], [152].

Most of the hydrogels exhibits water swelling and poor mechanical properties that severely hinder and limit their potential applications in the biomaterials field. In addition, the swelling problem of the hydrogel matrix could lead to loss of electrical conductivity component due to the percolation circumstance [190]. Thus, by tuning their mechanical properties using the crosslinker, a CH system with improved mechanical properties will be obtained, which retains its electrical properties and lower its water absorption [42].

On the other hand, numerous studies have been done to investigate the cellular–substrate topographical interactions. These studies have provided new insights into cell behaviour in response to their microenvironments and how it has influenced cell functions and properties such as adhesion, proliferation, motility, and morphology [73],

[191]–[193]. In order to understand these issues, Ghibaudo *et al*. studied the responses of the fibroblasts on microsized pillars with different geometries. They found that the cell transmigration was influenced by the substrate topography, where cells showed elongation of the nucleus and membrane actin along the pattern lines on pillar-coated substrates compared with cells on flat surfaces which were normally random [194]. Moreover, Murray *et al*. demonstrated that cancer cells cultured on non-conductive bioimprinted substrates can distinguish the difference between cell-like topographies and those of flat areas [8]. The relative importance of surface topography is illustrated in the responses of endometrial cancer cells to anti-cancer drugs as reported by Tan *et al*. [6]. This study showed that despite the cancer cells behaving differently on convex and concave cell-like features, there were also changes in the expression of signalling proteins and different respond to cancer drugs.

In this study, we demonstrate the effects of the chemical and surface modification of CH based on conducting polymer PEDOT:PSS for use as a cell-culture platform. We found that by using an mTg crosslinker with the CH films, the electrical conductivity increased and the swelling decreased. To obtain a better cytocompatibility and cell viability outcome, C2C12 myoblast were cultured on the conductive substrates for 24 hours. The morphology, attachment and viability of the cells were studied on different well-defined surfaces *in vitro.* These studies clearly showed that cells are very sophisticated and can distinguish between surface patterns by following the surface footprint. The simplicity of the fabrication process enabled scaling down to micro- and nanoscale morphologies, which are useful for creating patterns for biomedical applications and implantable biomaterial devices.

5.2 Materials

All chemicals used in this work and their suppliers are listed below:
CP, PEDOT:PSS 1.3 wt.% dispersion in water (483095-250G, Sigma Aldrich) (PEDOT content 0.5 wt.% and PSS content 0.8 wt.%), type A 300 g Bloom porcine skin powder (G2500, Sigma Aldrich), phosphate-buffered saline (PBS) tablets (Sigma Aldrich), 1000U/g microbial transglutaminase (supplied from Ajinomoto, Japan),

Kimwipes tissues (Kimberly Clark), GlutaMAX (11995-065, Gibco^{R} via Invitrogen), fetal bovine serum (Gibco^{R} via Invitrogen), penicillin-streptomycin 100x (Gibco^{R} via Invitrogen), Fungizone (Gibco^{R} via Invitrogen), 0.5% trypsin-EDTA 10x (Gibco^{R} via Invitrogen), Hoechst 33342 (Life Technologies, Inc., Invitrogen), intracellular fixation buffer (Invitrogen), 10μm-thick negative resist (ADEX20, DJ MicroLaminates Inc., USA), propylene glycol monomethyl ether acetate (484431, Sigma Aldrich), polydimethylsiloxane, (Sylgard 184, Dow Corning Corp.), 0.2% crystal violet solution (C0775, Sigma Aldrich) in 2.0% ethanol, ethanol and glycerol (analytical grade, from LabServ).

5.3 Chemical modification

In this work, electrically conductive and mechanically stable CH were produced based on conducting polymer PEDOT:PSS containing glycerol and gelatin. In order to have conductive substrates with high water resistance suitable for a cell-culture platform, the CH was chemically polymerised with mTg crosslinker. The mTg was chosen because it showed the ability to chemically crosslink the hydrogel matrix while maintaining the biocompatibility properties and increasing cell attachment [195]. Transglutaminase is a purified natural enzyme found in living organisms and is widely used in many food manufacturing industries such as milk and meat to improve the texture for human consumption [195]–[197].

5.3.1 Preparation of crosslinked conductive hydrogel

CH mixtures based on PEDOT:PSS were chemically polymerised by crosslinking with mTg crosslinker. The hydrogel mixture was prepared by dissolving 12.5 wt.% of gelatin powder in PBS (pH 7.4) solution at temperature 60 ˚C. Next, different concentrations of PEDOT:PSS and glycerol were added into the gelatin mixture and stirred at temperature 70 ˚C until the mixtures became homogeneous.

To crosslink films, 0.5 g of mTg was dissolved with 20 mL of PBS solution and mixed with the CH mixture. Then, the crosslinked mixture was immediately poured directly

onto a mould containing the required features and dried in the incubator at temperature 37 ˚C for five hours to form the physical and chemical crosslinks. Note that the crosslinked mixture will solidify faster than non-crosslinked mixtures. After crosslinking the CH films were stored at temperature 4 ˚C for 48 hours before use to complete the polymerisation.

5.3.2 Conductivity measurement

The electrical resistivity of the conductive films was measured using a four-point probe technique with Hall effect measurement system. However the system automatically run the Hall measurement after the resistivity and conductivity measurement by the four-probe technique. In this technique, the spring loaded probes were placed directly on four-contact points of the surface sample (5 mm x 5mm) and then connected to EGK HEM-2000 Hall effect and four probe measuring system provided with the programmed semiconductor device analyser under 0.51 T of magnetic field. Film thickness, *t* was measured by using a Surface DEKTAK 150 Profilometer (Veeco, USA). Resistance measurement was carried out three times for each sample. The resistivity ρ and conductivity σ are calculated according to the following formula:

$$\text{Resistivity}, \rho = \frac{Rtw}{l} \tag{5.1}$$

in which

$$\text{Conductivity}, \sigma = \frac{1}{\rho} \tag{5.2}$$

and where R = resistance (Ω), ρ = resistivity of the material (Ωcm), l = length of the film (cm), w = width of the film (cm), and t = thickness of the film (cm).

5.3.3 Degree of swelling behaviour

In this study, the hydrated of non-crosslinked and crosslinked CH films were immersed in deionised water at room temperature for up to 14 days to determine weight change. Then, the swollen film was removed from the deionised water and weighed after gentle

surface wiping with a Kimwipes tissue. The swelling behaviour was measured by visual inspection and swelling analysis. The analysis was performed only on the 4% CH film due to the excellent replication fidelity of this mixture ratio. The swelling percentage was calculated using the following equation:

$$\text{Swelling ratio}\% = \frac{(W_s - W_d)}{W_d} \times 100\% \qquad (5.3)$$

where W_s and W_d are the weights of the film in its swollen and dry state, respectively.

5.3.4 Cell attachment on a conductive hydrogel chip

We have fabricated a conductive bioimprint for studying cell growth on CH, following the cell culture protocols described in the doctoral dissertation of Dr Lynn Murray [49]. The illustration of top view and cross-section for the platform design is shown in Figure 5.1. The chip fabrication beginning with the plasma-treated microscope glass slides, different crosslinked CH mixtures were liquid cast onto the slides, followed by the curing process in the incubator as described in section 5.3.1.

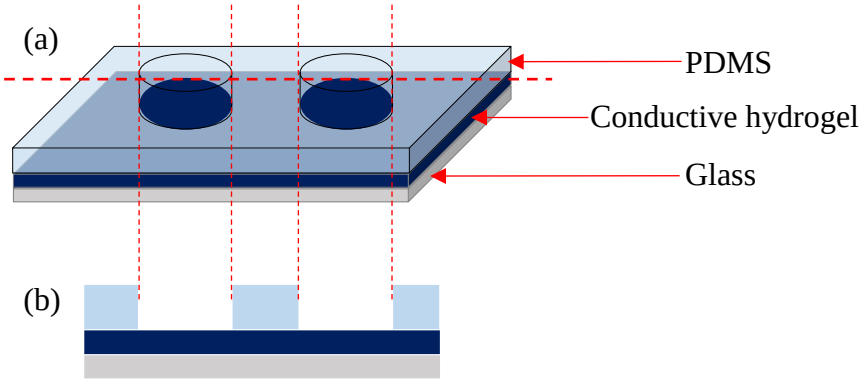

Figure 5.1: Illustration of PDMS chambers sealed on CH: (a) the top view and (b) the cross-sectional view.

To produce a flat surface of CH for the cell culture experiment, a cured CH film was sandwiched between a PDMS chamber sheet and a glass substrate. The PDMS circular chambers were punched into cured a PDMS sheet using a cork borer with diameter of 15 mm. The most common approach to bond hydrophobic PDMS with glass is to

expose the substrate surface with an oxygen plasma treatment. Then, the PDMS chamber was sealed on the glass or CH substrate immediately after oxygen treatment at 100 Watt for 30 seconds to form permanent bonding. Note that a glass substrate was chosen as a control flat substrate. Additionally, the open-top design permits easy cell seeding and culture media exchange.

All sealed substrates shown in Figure 5.2 (a-e) were sterilised by UV irradiation in a laminar flux cabinet for 60 minutes. After sterilisation, the CH films were incubated in a culture medium for four hours until they reached swelling equilibrium. Films were then washed with sterilised PBS solution followed by a cell medium to neutralise leaching of the CH film. Cells were seeded at 5×10^4 cells/mL and incubated as in mention in section 3.2. The culture medium was changed every day for optimum cell growth and adhered onto the CH film [198].

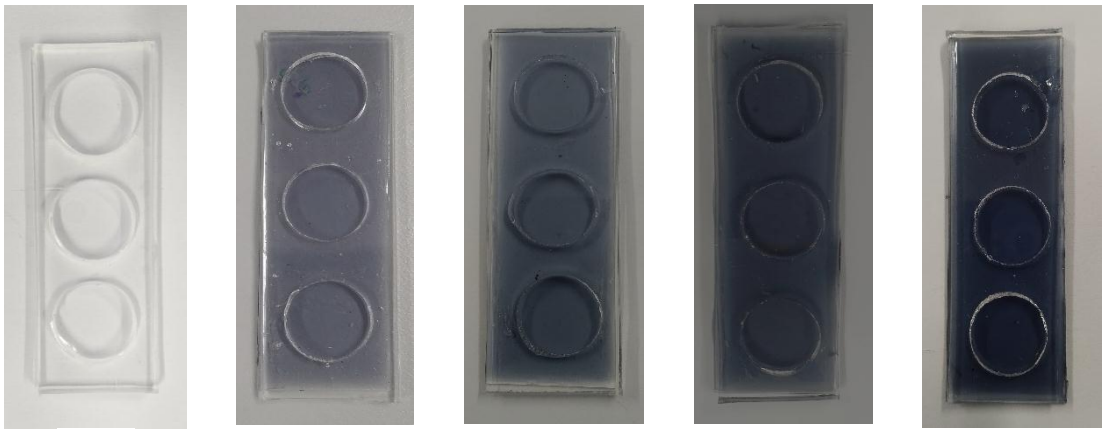

(a) (b) (c) (d) (e)

Figure 5.2: Photograph of PDMS circular chambers sealed on different substrates and used as cell culture platforms: (a) glass, (b) 2% CH, (c) 3% CH, (d) 4% CH and (e) 6% CH.

Cell viability was photographed and measured after 24 hours of incubation. To measure cell viability, the cultured films were trypsinised with 0.5% trypsin-EDTA solution until the film surface was covered and left in the incubator at 37 ℃ for 15 minutes. Meanwhile, the culture medium was decanted into the centrifuge tube and spun at 1500 rpm for 5 minutes. The supernatant was aspirated from the cell pellet, then the pellets

were resuspended in an appropriate volume of growth medium. 10 µL of trypsinised cells suspension were pipetted into a hemocytometer to determine the attached/unattached cells in each sample.

5.3.5 Fluorescent imaging of C2C12

To examine the feasibility of utilising the CH as a coating material on neural electrodes for promoting intimate cellular integration. Myoblasts C2C12 cells were seeded on CH substrate for 24 hours and stained with PKH26 Red Fluorescent linker kit. In brief, the C2C12 myoblasts were fixed with intracellular fixation buffer solution for 45 minutes and washed four times with PBS solution. Then, cells were stained with plasma membrane in red colour and placed in a 4 ℃ enclosure overnight. This staining was essential to observe the cellular morphology. Then, the cell nuclei were labelled with Hoechst 33342 DNA dye for 30 minutes and washed three times with PBS solution. Fluorescence microscopy with 10x of magnification imaging was performed using Carl Zeiss Axio Imager epifluorescence microscope (Carl Zeiss Meditec AG, Jena, Germany), and image analysis was performed using Image J.

5.4 Surface modifications

Previous studies on non-conductive materials with well- defined topographical features such as bioimprints [7], [60], microfluidic array [56], pillars [60], pits [199], wells [200] and pyramids [201] can mediate cellular behaviour (adhesion, migration and differentiation). To have a deeper insight of cell–substrate interactions, C2C12 cells were cultured C2C12 cells on conductive micropillars and bioimprint replica substrates to investigate cell morphology changes after four to 24 hours of cell seeding. It was remarkable to observe for the first time how cells reacted to the patterned conductive surface substrate. The results presented in this research show that the electro-biocompatible interaction between myoblast cells and CH provides evidence that the material is promising for applications in bioelectronics and orthopaedics. It should be emphasised that no previous report exists in the literature about a conductive bioimprint’s notable ability to support cell growth.

5.4.1 Fabrication of conductive micropillar substrate

A schematic diagram of the conductive micropillars fabrication is shown in Figure 5.3 (a–d). A standard soft lithography technique was used to generate the micropillar PDMS substrates.

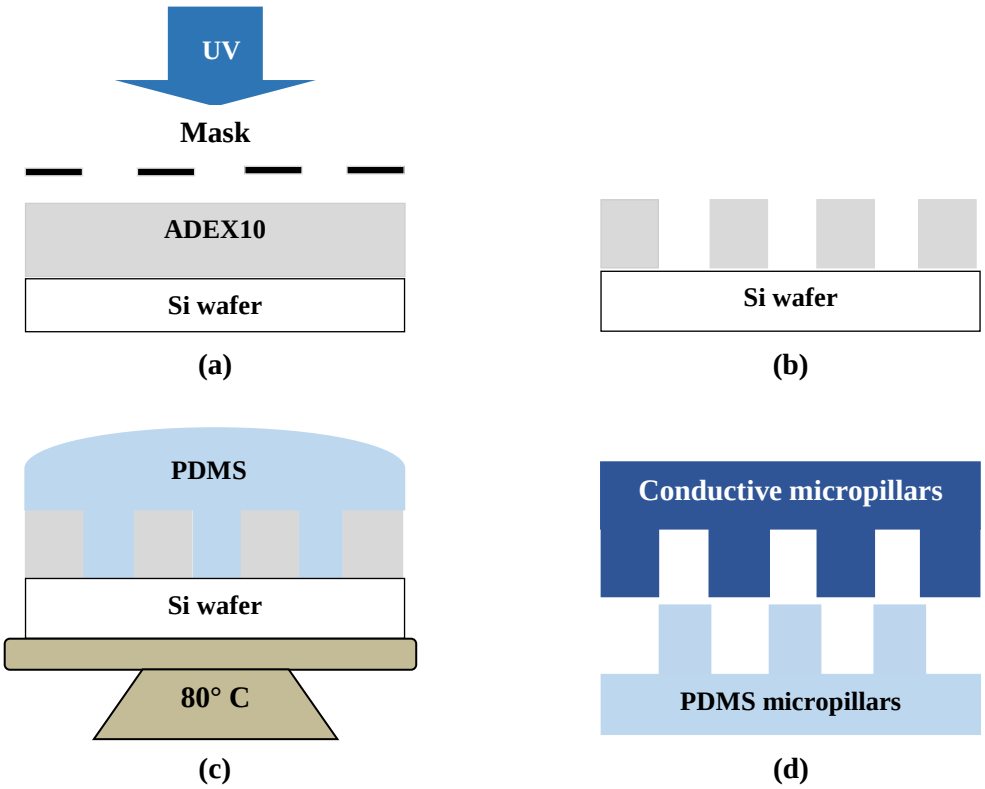

Figure 5.3: Schematic diagram showing the fabrication of conductive micropillars: (a) hot-roll laminating of ADEX 10µm on silicon wafer and ramping post-bake, (b) develop with PGMEA, (c) pre-polymer PDMS was poured over the silicon wafer embedded with an array of micropillars, cured and peeled off, (d) to obtain conductive micropillars, CH mixture was liquid cast over the PDMS mould, cured and carefully peeled off to avoid tearing effects.

A 4-inch silicon wafer was laminated with 10 µm-thick negative resist (ADEX20, DJ MicroLaminates Inc., USA) by using a hot-roll laminator at 65 ℃ with speed one setting. To create the micropillars pattern, the negative PR-coated silicon wafer was exposed to UV in vacuum contact mode at 125 $mJcm^{-2}$ for 30 seconds under a photomask using Karl Suss MA6 mask aligner (MA-6, Suss MicroTec) as shown in Figure 5.3 (a). Subsequently, the silicon wafer was post-exposure ramp-baked on a

HP30, Torrey Pines Scientific hot plate for five minutes at temperature 65 ℃ followed by ten minutes at temperature 95 ℃ and finished off for another 20 minutes at temperature 20 ℃. Figure 5.3 (b) shows that the transferred micropillar patterns were developed in propylene glycol monomethyl ether acetate, PGMEA and rinsed with isopropyl alcohol. Next, PDMS pre-polymer was mixed at a 10:1 w/w ratio, and degassed for approximately 30 minutes. Once all the bubbles had disappeared from the solution, it was then poured on the silicon wafer and baked at temperature 80 ℃ overnight as shown in Figure 5.3 (c). Once it was solid, the micropillars PDMS was peeled off from the silicon wafer. The micropillars PDMS was then treated with 22.2% w/v PVP solution and oxygen plasma as mentioned in section 4.5.4.2 to establish a more hydrophilic surface before the imprinting process. The treated PDMS micropillars substrate was ready for liquid casting with 4% w/w crosslinked CH mixture (Figure 5.3 (d)). Then, the film was cured in the incubator as described in section 5.3.1.

5.4.2 Fabrication of crosslinked conductive bioimprint substrate

The conductive bioimprint was made from PDMS master mould as described in section 3.8. Figure 5.4 presents the schematic diagram of crosslinked conductive bioimprint fabrication. The bioimprinting process started with the culture of C2C12 myoblast which were fixed on a glass microscope slide as in Figure 5.4 (a). Fixed cells were then washed with PBS and distilled water to remove unwanted cell debris. Then, PDMS pre-polymer was mixed at a ratio 10:1 w/w, degassed, dispensed onto fixed cells and cured at temperature 37 ℃ overnight, and further baked at temperature 80 ℃ to complete the PDMS polymerisation (Figure 5.4 (b)-(c)). Peel-off the negative PDMS master mould and treated with 22.2% w/v PVP solution and oxygen plasma treatment at 100 Watt for 30 seconds to improve surface energy contact before the imprinting process Figure 5.4 (d). The crosslinked CH mixture was then liquid cast onto the negative PDMS and cured as mentioned in the previous section (Figure 5.4 (e)). Finally, the conductive bioimprinted films obtained were then carefully peeled off to avoid tearing effects (Figure 5.4 (f)).

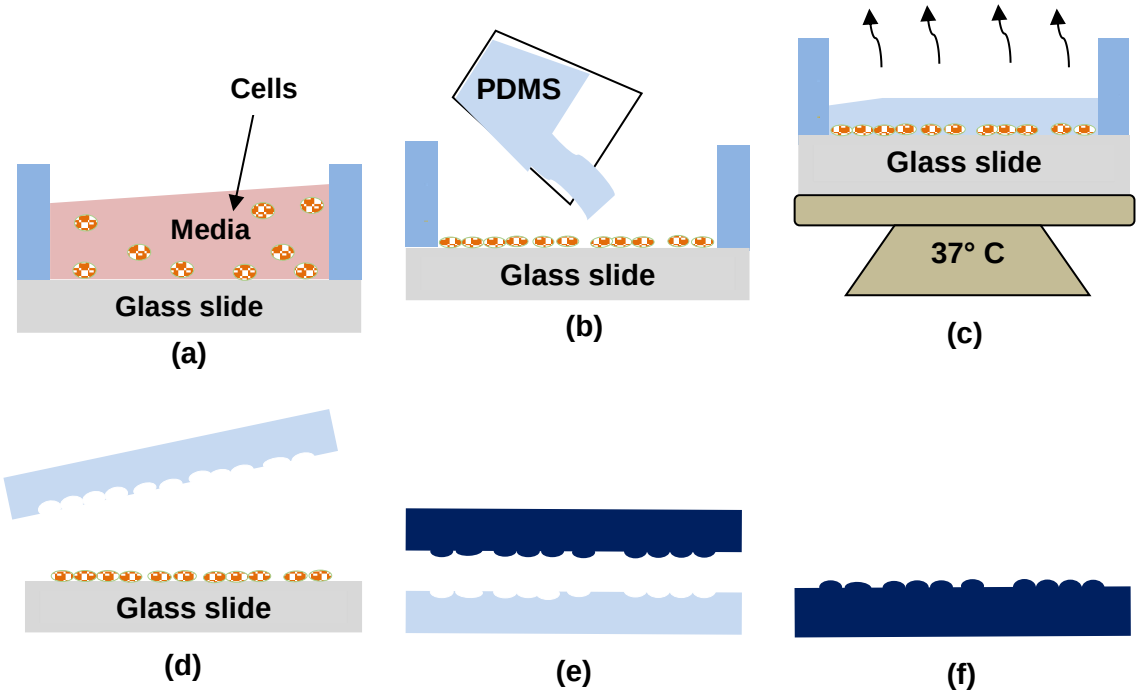

Figure 5.4: Schematic diagram of conductive bioimprint process: (a) cells are cultured on glass slide, (b) at 80% confluent, cells are fixed and liquid PDMS is dispensed onto the cells, (c) the polymer is cured, (d) the PDMS replica is peeled off carefully, (e) liquid cast the crosslinked CH mixture and follow the curing steps as described previously and (f) bioimprinted CH substrate is used as culture substrate.

5.4.3 Culture of C2C12 myoblasts on conductive micropillars and bioimprint

For cells cultured on flat and patterned CH substrates, PDMS sheet was first punched using a 15 mm cork borer, prepared in sterile conditions and then soaked in cell culture media for four hours at temperature 37 ℃ to extract the sol fraction from the network as shown in Figure 5.5. After sol fraction extraction, the medium was discarded. The cell suspension was then pipetted onto each CH substrate at a density of 5×10^4 cells/mL. The culture samples were incubated at temperature 37 ℃ for 24 and for 48 hours for cell viability and the staining process. The culture was maintained in Dulbecco's modified-Eagle's medium (Invitrogen) supplemented with 10% fetal bovine serum (FBS), 1% GlutaMAX and 1% penicillin-streptomycin at temperature 37

℃ and 5% of CO_2 in a humidified incubator. The working medium was replenished every day during the culture period for maximum cell growth.

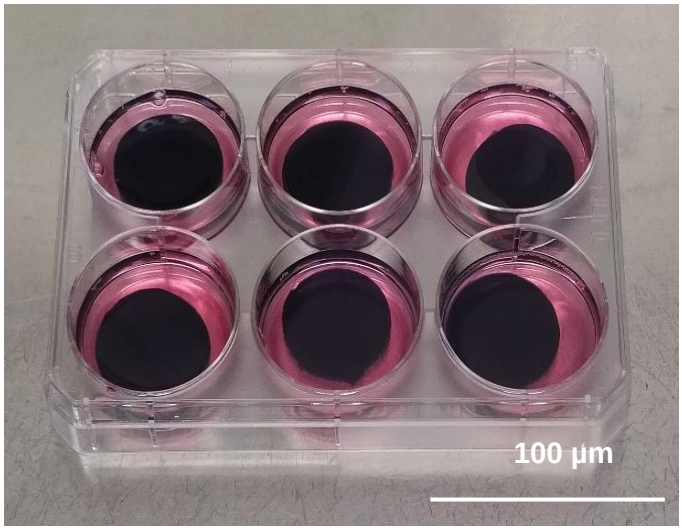

Figure 5.5: CH substrates soaking in six-well culture plates before cell seeding.

5.4.4 Cell adhesion and proliferation on crosslinked conductive micropillars and bioimprint polymeric substrate.

Crystal violet is used to stain nuclei and colonies of cells for visualisation. In this work, crystal violet assay was used to visualise the adherence of C2C12 cells onto the conductive micropillars and bioimprints. In brief, the cell culture medium was aspirated from the six-well culture plate after four and 24 hours of cell seeding to observe the cell attachment with different culture times. This is because cells that undergo cell death lose their adherence and are subsequently lost from the population of cells, reducing the amount of crystal violet staining in the culture. Then, the well was washed twice with PBS and stained with 0.2% crystal violet solution in 2.0% ethanol for 30 minutes at room temperature. After that, the excess stain was removed by washing repeatedly with tap water until the colour of the water changed blue into clear blue.

5.5 Result and discussion

In this study focused on the effects of the chemical and surface modifications on the CH films properties. The results of these analyses are presented and discussed in detail in the following sections.

5.5.1 Conductivity of the conductive hydrogel film.

Figure 5.6 shows the influence of mTg on the electrical conductivity of the different concentrations CH films. It was found that the conductivities of non-crosslinked films (red graph) has extremely low ranging from 0.8×10^{-6} to 7.9×10^{-6} Scm^{-1}. However, the conductivities of the conductive films increased about six magnitudes after the crosslinking process (blue graph). This improvement in the conductivity was due the presence of the mTg, which created a better interconnection network in the polymer matrix. Physically hydrogel are water-swelling polymer and possess poor mechanical properties. The swelling problem of the conductive hydrogel matric could lead to loss of the electrical conductive component due to the percolation circumstance. By tuning their mechanical properties using the mTg, possessed tighter internal entanglement structure which created a better interconnection network in the polymer matrix. Thus, a conductive hydrogel system could retains its electrical properties and lower its water absorption with improved mechanical properties.

This is in agreement with Zhao et al [46], where they report that the conductivity of the electrically conductive hemicellulose hydrogel (ECHH) film increased by three orders of magnitude after it was crosslinked with 10–40% aniline pentamer (AP) crosslinker. They found that there was a significant relationship between the total concentration and the proportion of the crosslinker in the hydrogel. Increasing the AP concentration resulted in a higher concentration of holes in the ECHH film, which enhanced the conductivity of the devices.

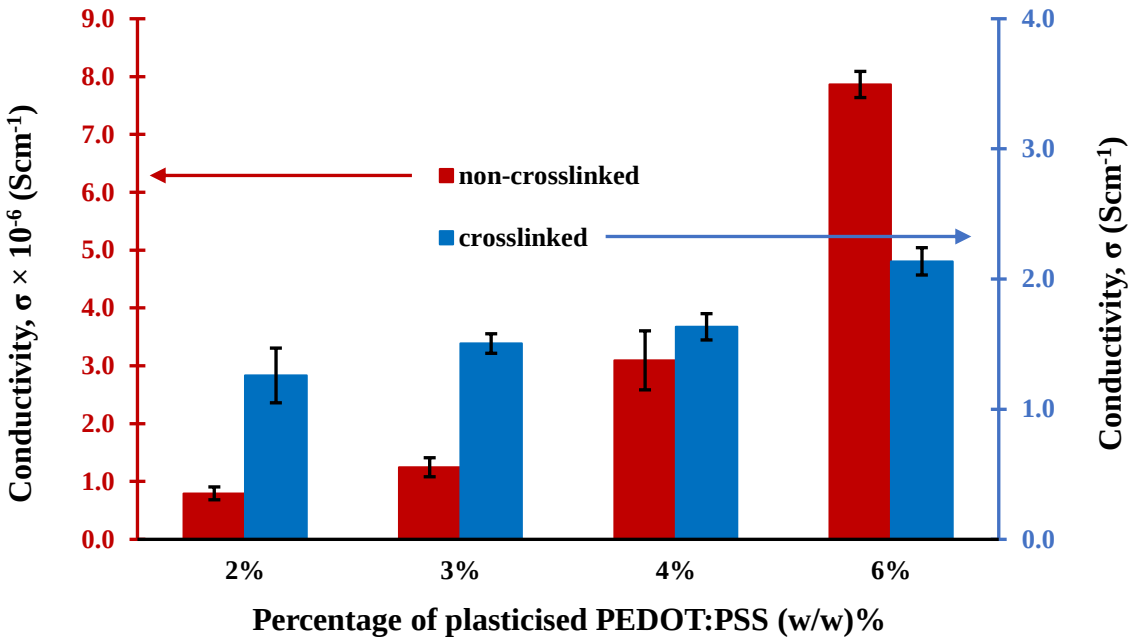

Figure 5.6: The electrical conductivity of crosslinked and non-crosslinked CH films. By using mTg to crosslink the CH films, the electrical conductivity is increased by six orders of magnitude.

5.5.2 Swelling capacity of conductive hydrogel film

Swelling behaviour is one of the important properties of the CH film when used in cell media environments. Generally, different hydrogels have network structures that exhibit different swelling behaviours. To examine the water absorption capacity, the CH films were immersed in deionised water for more than 60 minutes. Based on our findings from Figure 5.7 (a), after one hour the 4% non-crosslinked CH film was swollen to three times its original size and totally dissolved after three hours in water.

On the other hand, the crosslinked CH films exhibited less swelling behaviour and were only totally dissolved in deionised water after being soaked for 14 days as shown in Figure 5.7 (b). The significantly different swelling behaviours of these two types of hydrogel showed that the CH with a crosslinker possessed tighter internal entanglement structure and a homogeneous distribution of crosslinking centres than a non-crosslinked CH film [35], [36]. This helped produce less water uptake and less swelling.

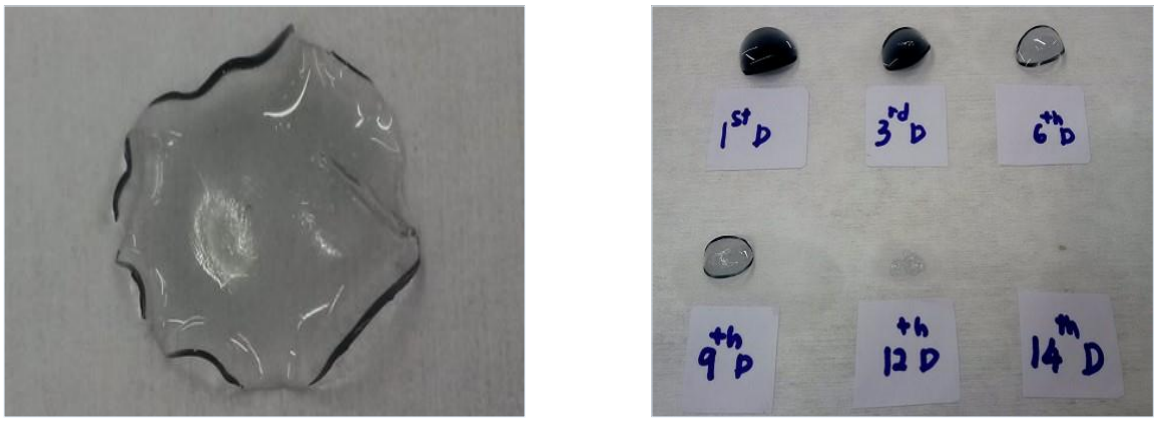

(a) (b)

Figure 5.7: The swelling behaviour of (a) non-crosslinked conductive film and (b) crosslinked conductive film. The water uptake ratio can be tailored by using the crosslinker in which the crosslinked film can survive in deionised water for more than three days and only dissolved totally after 14 days.

The swelling percentage of the 4% non-crosslinked and crosslinked CH films are shown in Figure 5.8. It can be seen that the CH without crosslinker swelled to more than 150% of its actual weight after two hours and started to dissolve completely due to the weakening of its chemical bonding. The crosslinked film, however showed higher water resistance and reached equilibrium condition after three hours in deionised water. When mTg crosslinker is added into the CH, the formation of the network in the substrate to be denser and limit diffusion which resultant in a decrease of swelling rate.

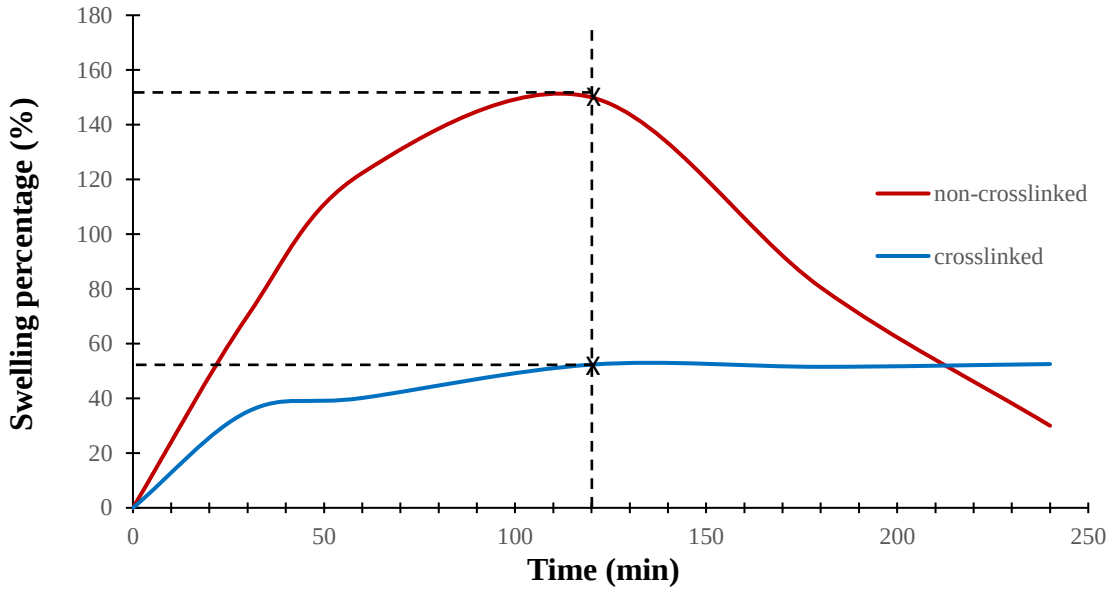

Figure 5.8: Swelling percentage of 4% (red) non-crosslinked and (blue) crosslinked conductive film. The graph shows that after the chemical crosslinking (blue curve) the swelling ratio decreased from 150% to 50% as a result of the formation of a dense network.

5.5.3 Growth of C2C12 on conductive hydrogel substrate

A key factor in developing conducting polymer-based bio-devices for applications in bone implants and tissue scaffolding is their biocompatibility. Bearing that requirement in mind, the biocompatibility of the CH has been assessed by cell adhesion and viability tests. Cell growth on glass slides and four different CH substrates was examined after 24 hours of seeding as shown in Figure 5.9.

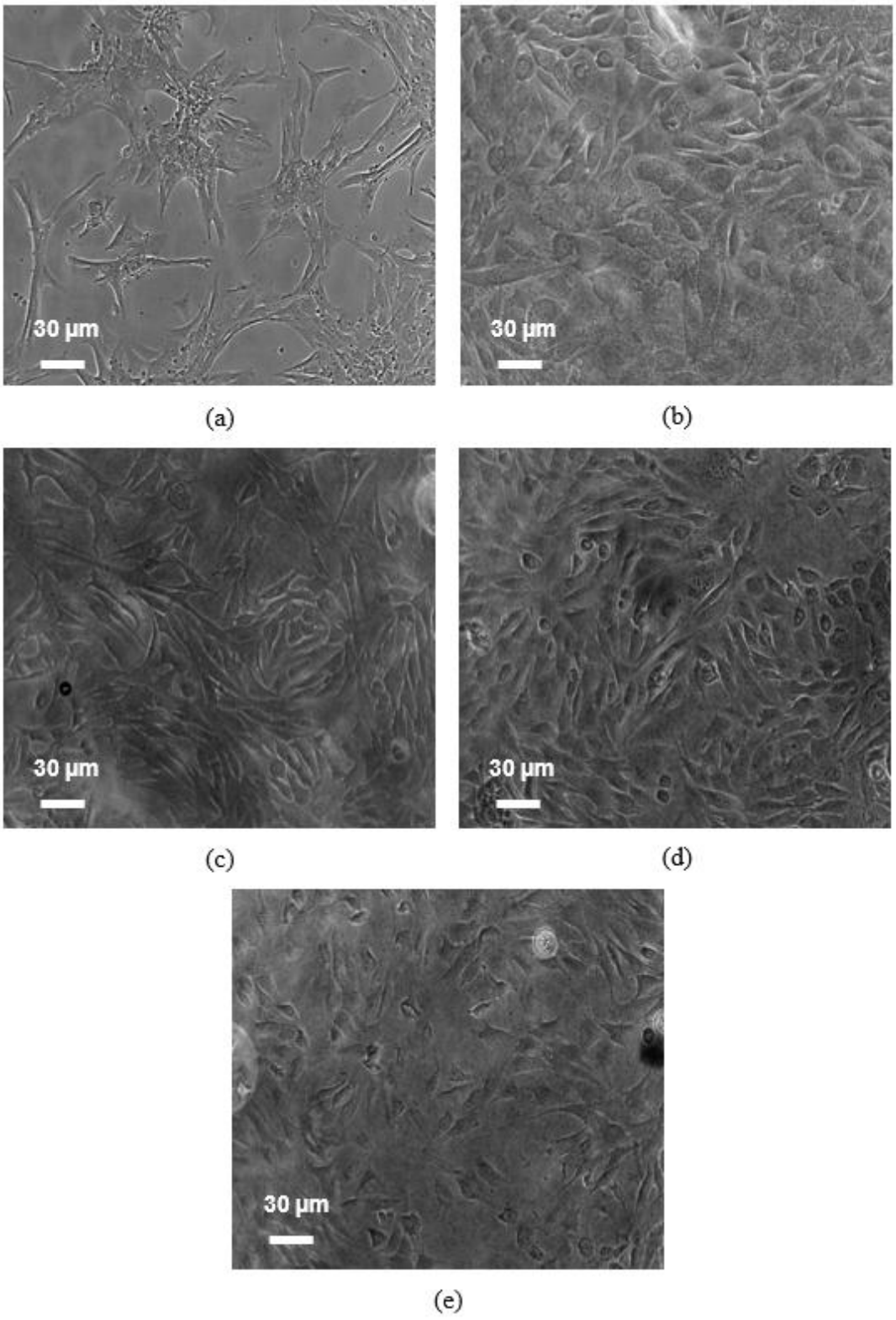

Figure 5.9: C2C12 cells seeded on (a) glass substrate (control), and different percentages of PEDOT:PSS of (b) 2% (c) 3%, (d) 4% and (e) 6%. The optical images shows that cells attached, grew and proliferated normally on all substrates.

Note that three repeated samples showed similar results and the glass slide was used as control substrate in all adhesion and viability assays. The results showed that the cells attached, grew and proliferated normally on all substrates coated with the developed CH. Cells were dissociated after 24 hours and the total numbers of cells from each growth condition were counted. The results are shown in Figure 5.10.

Figure 5.10 compares the cell viability on different culture substrates together with cell viability in a culture medium on the secondary axis. These results indicated that cells cultured on glass, and on the 3% and 4% CH substrates had the highest number of attached cells compared with other substrates. Conversely, the 6% concentration CH seeded substrate showed the lowest number of attached cells but the highest number of cells in the culture medium.

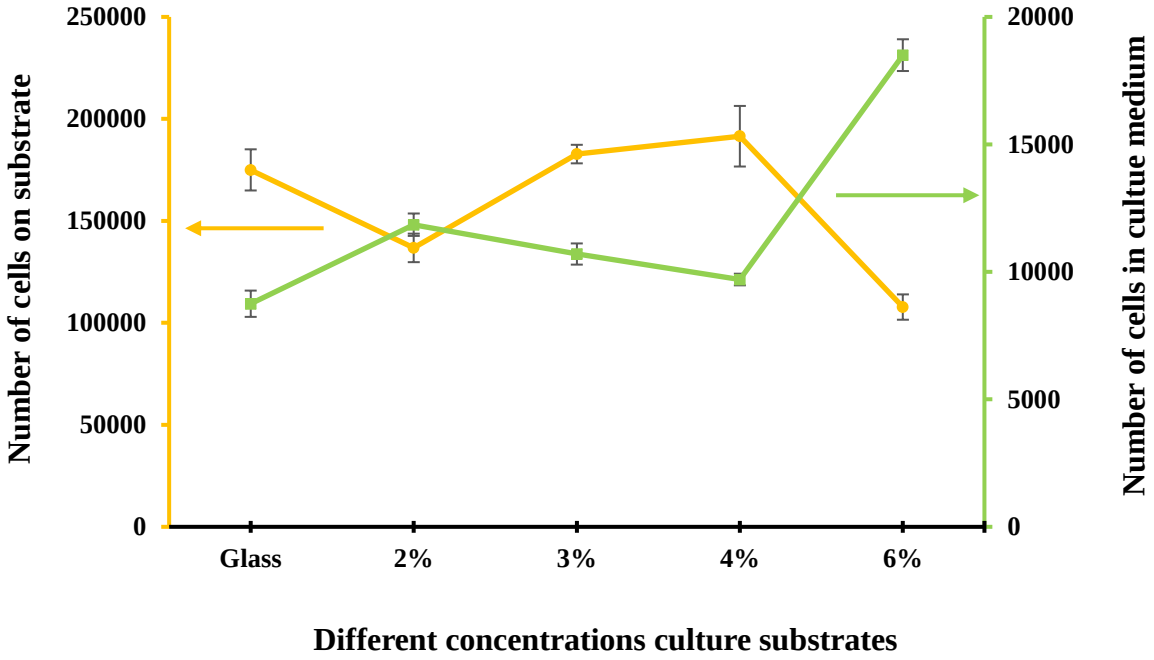

Figure 5.10: Comparison of C2C12 cell viability after 24 hours on glass substrate (control), and different concentrations of CH substrates. The data shows that the lowest number of attached cells is observed on the 6% CH substrate.

Fluorescence microscopy is one of the most sensitive and accurate technology in the cell-based method. In this work, the fluorescence staining technique has been

employed to study the cell morphology through visualising the focal adhesion within cells. Figure 5.11 showed the fluorescence staining of C2C12 cultured on four different concentrations of CH substrates after 24 hours of incubation. The bright blue spots and green represent the cell nuclei and plasma membrane respectively. Our results indicated that cells on all substrates were successfully attached, grew and proliferated. Furthermore, cells showed numerous lamellipodium and filopodium with anchorage points to the conductive substrate.

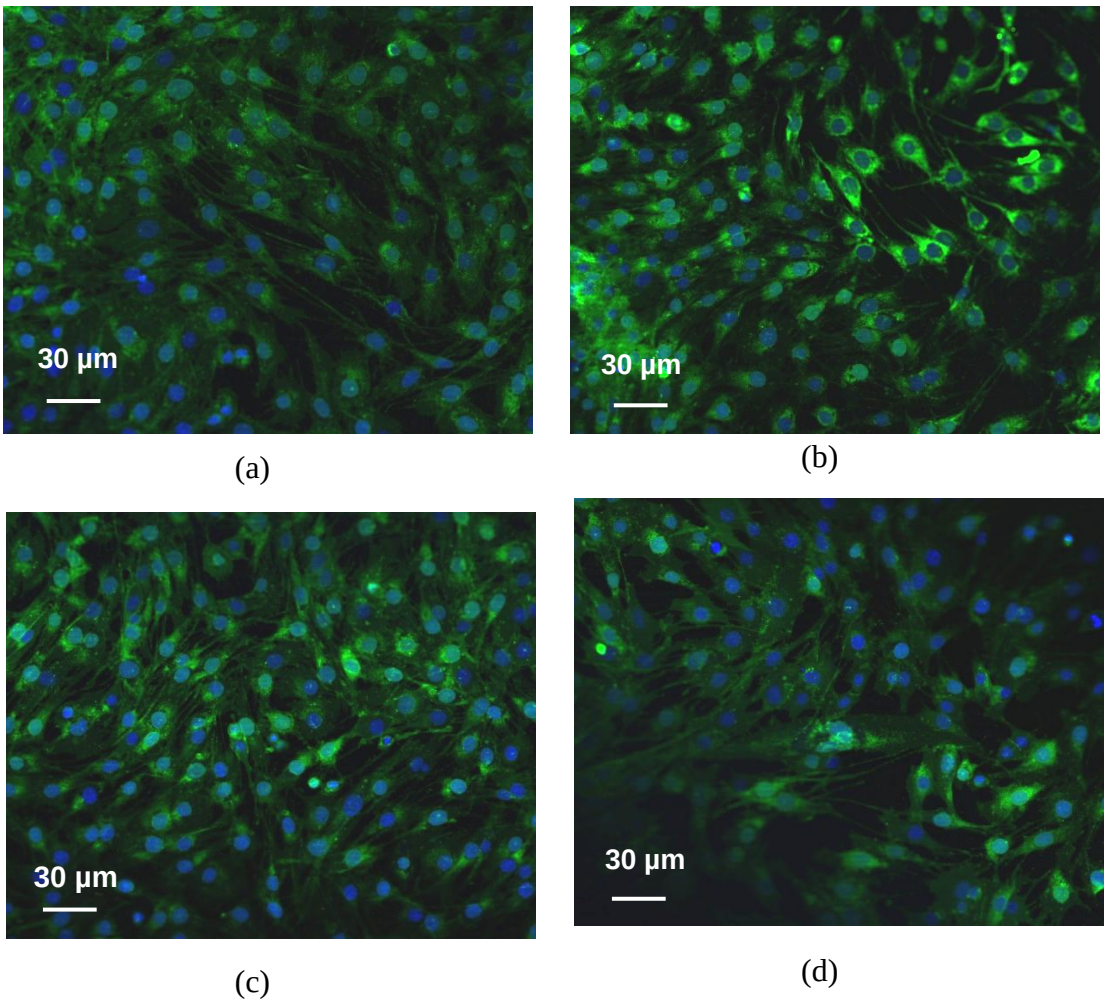

(a) (b)

(c) (d)

Figure 5.11: Merged immunofluorescent images of cell morphology of C2C12 myoblasts cultivated on conductive substrate after 24 hours with four different concentrations of PEDOT:PSS. (a) 2%, (b) 3%, (c) 4% and (d) 6%.

By counting the number of fluorescence stained cell, the adhesion of cells can be characterized. Figure 5.12 shows the densitometry analysis of C2C12 cells extracted from Figure 5.11 on different concentrations of conductive hydrogel substrates. The results revealed that the highest number of neuron grew on the 4% conductive hydrogel while lowest number of cells on 6% conductive substrate, indicating that at highest percentage of plasticised PEDOT:PSS will created toxicity to cells and this agrees with a statistic shown in Figure 5.10.

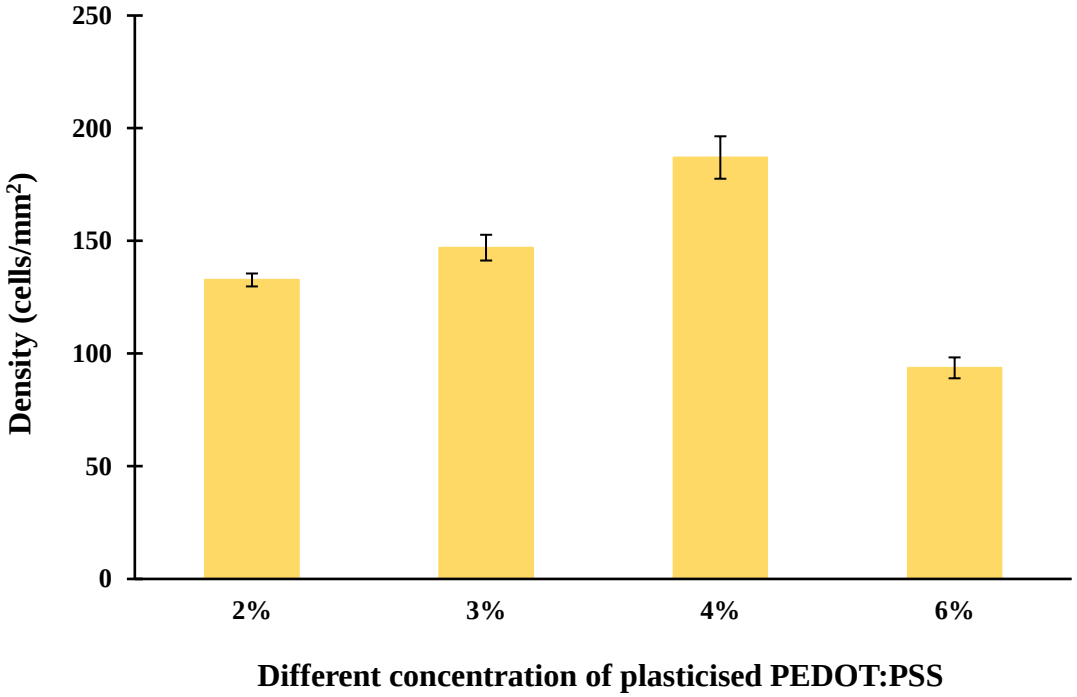

Figure 5.12: The densitometry analysis of myoblasts C2C12 cell extracted from immunofluorescent images in Figure 5.11 on different concentrations of plasticised PEDOT:PSS conductive hydrogel substrates: (a) 2%, (b) 3%, (c) 4% and (d) 6%.

5.5.4 Surface modifications

A soft lithography patterning technique was used to fabricate the micropillars and bioimprints into the CH film. Crystal violet assay was used to assess the adherence of C2C12 cells onto the conductive micropillars and bioimprints. The cell culture medium was removed from the six-well culture plate after four hours and 24 hours of cells seeding. Then, the well was washed with PBS twice and stained with 0.2% crystal

violet solution in 2.0% ethanol for 30 minutes at room temperature. After that, the excess stain was removed by washing repeatedly with tap water until the colour of the water changed blue into clear blue, and the violet-stained cells were imaged using bright-field microscopy. In this work, two different patterned substrates made of the CH: micropillars and bioimprint have been used to compare C2C12 cell behaviours under the same chemical conditions.

5.5.5 Conductive micropillars

Since topographical cues have been shown to regulate various functions of cells, the effects of substrate topography on myoblast growth and alignment using CH micropillar substrates were examined. The micropillars with dimensions of 7 µm width and 10 µm height was used.

Figure 5.13 shows the optical images of cell growth on conductive micropillars after culture for 12 hours and 24 hours. Note that 10× magnification phase-contrast microscopy was utilised to observe the cell morphology. It was found that the cell membrane body in both images was mostly localised on the top of the micropillars with their dendrites extended, reaching a length of up to 90 µm following the micropillars array. In addition, the extension of these long protrusions following the trenches give the impression the mechanism in guiding cell migration between the micropillar arrays.

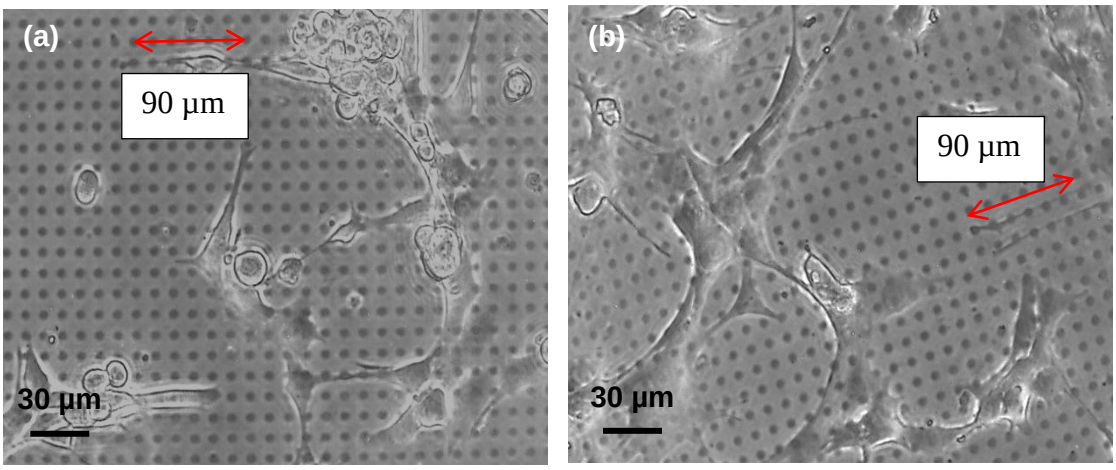

Figure 5.13: Optical photographs of C2C12 cells showing adhesion, spreading and migration on conductive micropillars at (a) 12 hours and (b) 24 hours. The red arrow showing dendrite extension.

The spreading and migration of the crystal violet stained C2C12 cells on the conductive micropillar substrate is shown in Figure 5.14 (a) and (b). These results indicated that the cells appeared to be more branched, have elongated shapes and adhered to the top of the pillar substrates. Whereas cells on the flat surface were randomly placed with the formation of large lamellipodium and short filopodium. Initially, cells behaved differently on a substrate and time by different extracellular clues including biochemistry, mechanics and topography [202]. This may be explained by the substrate topography playing an important role in influencing the cell adhesion and the contact guidance for the anchoring of cells to surfaces [203].

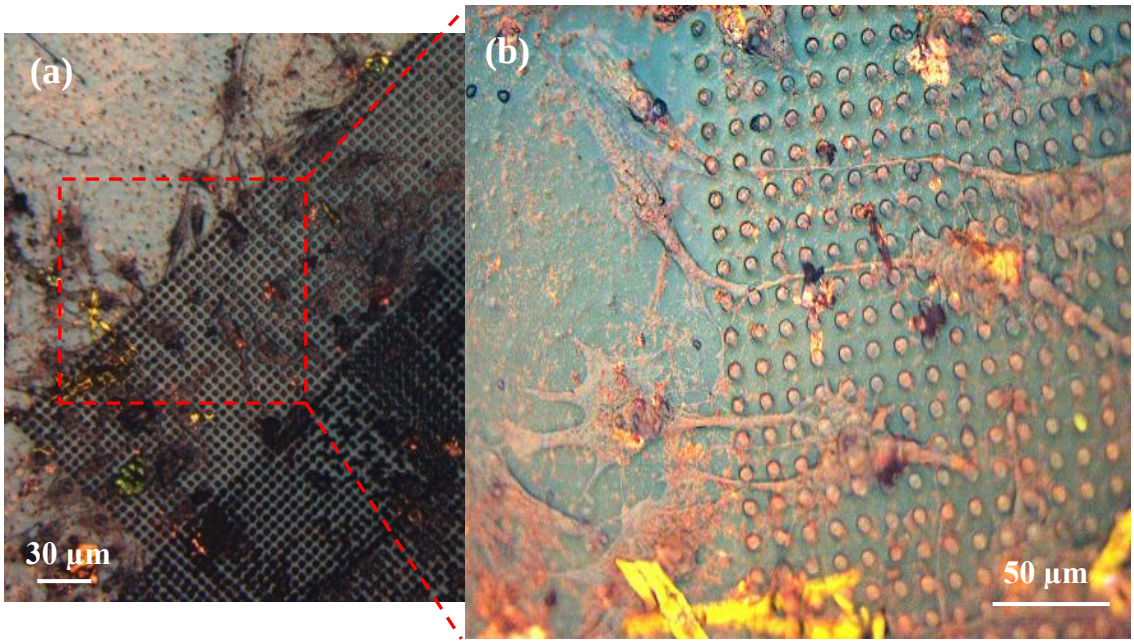

Figure 5.14: Cell adhesion on conductive micropillar substrates (a) Myoblast C2C12 cells cultured on conductive micropillars and flat areas with a scale bar of 30 µm and (b) enlarged image of stained cells grown after 24 hours with scale bar of 50 µm, showing that cells are more elongated on micropillar arrays than on flat surface substrates owing to surface topography influencing cellular behaviour.

5.5.6 Conductive bioimprint

Bioimprinted conductive substrates were successfully fabricated using the soft lithography technique outlined in Chapter 4. With its high replication fidelity of cellular footprint onto conductive substrates, it was used to investigate cells' preferential attachment behaviour on cell-like topographical features. Figure 5.15 depicts the adhesion and spreading of cells after four and 24 hours on different CH surfaces: flat surface, positive bioimprint and negative bioimprint. Negative bioimprint is an inverse replica of the original cell features, whereas a positive bioimprint is a second replication transferred from the negative bioimprint mould into another substrate resulting in surfaces that resemble cell morphology.

Culture time / Substrate	Illustrations of the replica	4 hours	24 hours
Positive Bioimprint		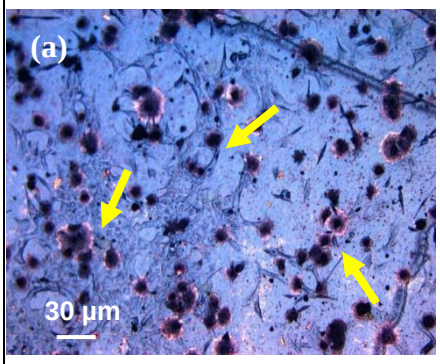	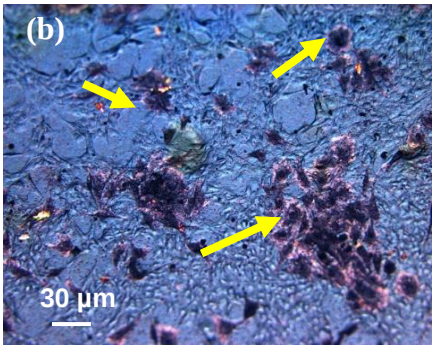
Negative Bioimprint		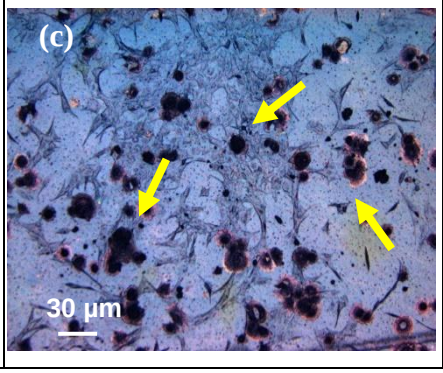	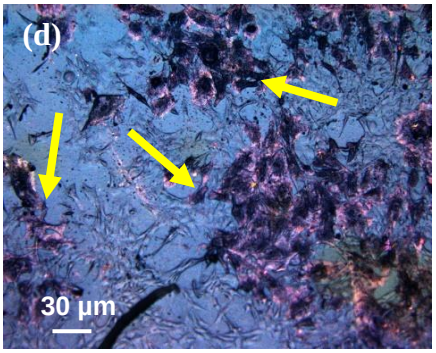

Figure 5.15: Illustration of positive and negative bioimprint and crystal violet stained C2C12 cells grown on (a) positive conductive bioimprint at four hours, (b) positive conductive bioimprint at 24 hours and (c) negative conductive bioimprint at four hours, (d) negative conductive bioimprint at 24 hours. Yellow arrows indicate bioimprint regions with cell-like features where cultured cells preferred to attach and spread compared to those on a flat surface.

From our observations in Figure 5.15, staining cells cultured on negative and positive cell-like features with crystal violet clearly showed cells preferentially adhering and spreading across the bioimprinted surfaces. As shown in Figure 5.15 (a) and (c), cells were rounded and attached more favourably on the positive and negative imprinted areas than to areas of flat surface after four hours of sedimentation. It is worth noting that after 24 hours, cells can distinguish surface patterns by growing clusters on their footprint (Figure 5.15(b) and (d)) compared to un-patterned areas. The result revealed the significant role of surface topography on cell behaviour [60], [202], [203].

5.6 Conclusions

The developed CH based on different concentrations of conducting polymer PEDOT:PSS were chemically modified and their surfaces patterned in order to investigate the influence on their electrical properties, swelling behaviour and cell response. The chemical modification was achieved by using a microbial Transglutaminase crosslinker that exhibited electrical conductivity enhancement of six orders of magnitude compared with the conductivity of non-crosslinked films. Moreover, we found that crosslinking the conducting material can reduce the water adsorption, which improves their swelling properties. Myoblast C2C12 cells cultured on these crosslinked CH substrates revealed that cells attached, grew and proliferated favourably on these films, confirming the biocompatibility of this material. Next we examined the effects on adhesion and migration of myoblasts on different well-defined patterns: micropillars and bioimprints. Under the same chemical conditions, we fabricated conductive micropillars and cell-like features to analyse the morphology of the cells and the dynamics of cell migration. Crystal violet staining experiments indicated that cells migrate with persistence, allowing their translocation from pillar to pillar and they exhibited a more elongated and branched shape than cells on a flat surface. In addition, crystal violet stained C2C12 cells grown on bioimprinted conductive substrates revealed that the cell adherence and also can distinguish surface pattern and preferentially grew on their cell-like features after four and 24 hours. This enabled us to observe for the first time how cells develop growth characteristics in response to an electro-biocompatible environment patterned with features that resemble themselves.

CHAPTER 6
Film Characterisations

This chapter investigates the physicochemical properties of the CH as a soft electrode material. This material is intended to be used as a coating for implantable devices and is based on conducting polymer PEDOT:PSS blended with hydrogel. The wettability, biocompatibility, biodegradability, physical/mechanical properties, and certain chemical analyses were examined. The wettability of various concentrations of CH films were analysed and found to be hydrophilic with contact angles between 53.24° and 67.71°, whereas the PDMS substrate was more hydrophobic with a contact angle of 113 ± 3.0°. The CH has quite similar surface energy to glass and gold, which have contact angles of 50.22 ± 1.7° and 62.29 ± 4.8°, respectively.

In the study of factors influencing the culturing of myoblast C2C12 cells, several biocompatible substrates with different surface chemistry were trialled to identify the correlation between wettability and C2C12 growth development. Results showed that the CH has good wettability and excellent hydrophilicity, which acted favourably for cell adhesion onto the substrate. Indeed, the statistical data reveal that seeded and cultured C2C12 cells grow better on CH substrate than on a glass slide, or gold and PDMS substrates, with more than 60% confluence at 24 hours and complete confluence after 48 hours. Furthermore, the *in vitro* biodegradation test on CH that was performed at temperature 37 ℃ in a culture medium showed a mass loss of 60–78%. The tensile test showed the CH exhibited excellent stress–strain properties, where the elasticity modulus decreased from 77.87 ± 1.12 MPa to 1.11 ± 0.10 MPa indicating that the CH is stretchable.

In addition, the chemical properties of synthesised CH polymers were characterised by using ultraviolet visible spectroscopy (UV-Vis), X-ray photoelectron spectroscopy (XPS), Fourier transform infrared spectroscopy (FTIR) and thermogravimetric analysis

(TGA). These results indicate that the CH polymer developed has the potential for bone coatings and tissue engineering.

6.1 Introduction

Considerable efforts have been focused on the synthesis and characterisation of the electroactive hydrogels for their use in drug delivery [34], [204], artificial skin [34], [205], wound healing [206] and as an implant coating material [34], [43] owing to their biocompatibility, biodegradability and stretchability. In this work, the physicochemical properties of CHs were investigated.

Culture platform surface properties such as wettability play an important role in influencing cellular behaviour. An understanding of the mechanisms behind these surface characteristics are central to many developments in lab-on-chip applications, medical implants and biosensor. The success in implant technology is not only dependent on the physicochemical properties but also how strongly the morphological topography of these surfaces affect cellular responses when in contact with the biomaterial. Various studies have also shown the importance of the interactions between the biomaterial surface characteristics and cell growth that can be manipulated to control the adhesion and cell spread process [73], [191]–[193].

The wetting of the material surface will influence the protein adsorption and cell adhesion. The first work on wettability was performed in 1984 by Baier *et al*. [62]. They discovered that hydrophilic surfaces triggered the adhesion and proliferation of cells on the substrate. The contact angle of a liquid drop on a solid surface, in air, is determined by 3 interfacial tensions: solid-liquid, solid-air and liquid-air. The surface wettability of the biomaterial is usually evaluated by measuring the water contact angle on the material surface. Research on determining and investigating the contact angle for various biomaterials found that reduction in contact angle will enhance wettability and thus improve the biocompatibility of the substrate [77]. Biocompatibility represents the ability of a material to be accepted by a living cell. Therefore, it is vital to choose a suitable material in such a way that the material meets the cell's

requirements by not being toxic or injurious and not causing immunological rejection. The stretchable and biodegradable characteristics of conductive substrate are very useful to develop implantable devices and wound healing. The substrate with stretchability and flexibility properties facilitate to be moulded to rough and smooth surface alike. So when the substrate already promote the cells and no longer needed, the film will gradually degrade into nontoxic component in the human body and leaving resulting tissue behind.

In the previous chapter a novel technique was demonstrated that employed a 3D imprint of a cellular footprint at high resolution into a PEDOT:PSS substrate using a soft lithography technique. In this chapter, different concentrations of CH films were prepared and characterised. Moreover, the bio-mineralisation behaviour of the synthesised conductive scaffolds was investigated in detail and evaluated by UV-Vis, XPS, FTIR and TGA. These experiments demonstrated the biocompatibility of the CH with appropriate properties, such as improved cell proliferation and adhesion, as well as enhanced mechanical properties suitable for applications in monitoring medical implants in real time and for manipulating implant–tissue reactions for medical devices.

6.2 Materials and conductive hydrogel preparation

In this chapter, the materials and synthesis of different concentrations of CH films were prepared as described in Chapters 4. The 300 Bloom gelatin powder dissolved in PBS solution and modified with different concentration of glycerol and PEDOT:PSS (0%, 2%, 3%, 4% and 6%). A 1000 U/g mTg was used as crosslinker in CH mixtures. The crosslinked mixture spontaneously solidified during incubation at 37 ℃ for five hours and left at temperature 4 ℃ for 48 hours for further film polymerisation before use.

6.3 Contact angle measurement

The water contact angle analyses of several different substrates were performed using a high-speed contact angle measurement device telescope goniometer–CAMP 2008

KSV system. Prior to contact angle measurement, the stage level has to be calibrated. Then, microscope glass, PDMS substrate and four different concentrations of CH coated on glass substrates were placed on the stage. A 5 µL drop of deionised water was dispensed on the surface of the sample and the images of the water drop were recorded by a digital camera. Once the first image was captured, the x–y translation stage was used to focus the image of the subsequent drop on the same substrate. If there is more than one drop on the substrate, only one drop is brought into view at a time. Note that five measurements were taken from each sample and the optical images were analysed using Image J software. All readings were averaged to provide an averaged contact angle.

6.4 Biocompatibility analysis

From the studies conducted on the cell growth cultured on CH described in Chapter 5, we can conclude that the films were non-cytotoxic to the myoblast C2C12 cells. The cells exhibited good adherence, growth and proliferation on all different concentrations of the hydrogel substrates. This section discusses the effect of wettability on the biocompatibility properties of the substrates. The adhesion of living cells strongly depends on the wettability of the substrate surface. The water contact angle studies give information on the wettability of the substrate surface. A small water contact angle indicates high surface free energies, resulting in a better performance in biocompatibility as well as in the adhesion properties of the material.

In this work, the oxygen plasma treated microscope glass slides were liquid cast with crosslinked CH mixtures and dried in the incubator at temperature 37 ℃ for five hours. The incubated films were placed in an enclosure held at temperature 4 ℃ for 48 hours to complete the polymerisation. The cured films were then sealed together with the 15 mm diameter circular chamber PDMS as described in detail in Chapter 5.

Meanwhile, three different films were used as a control in this experiment. These films includes a plain glass slide, PDMS cured film and sputter-coated glass with 40 nm thickness of gold. Figure 6.1 shows the different substrates sealed together with PDMS

circular chamber. All of the substrates (glass, PDMS, gold and CH films) must be sealed with the PDMS chamber. This is performed immediately after the oxygen plasma treatment which is conducted at 100 Watt for 30 seconds to form permanent bonding.

All the substrates were then sterilised using UV exposure in a laminar flux cabinet for 60 minutes. After sterilisation, the CH substrates were incubated in culture medium for four hours until they reached swelling equilibrium. Subsequently, the films were washed with sterilised PBS solution followed by cell medium to neutralise leaching of the CH film. Cells were seeded at 5×10^4 cells/mL on glass, PDMS, gold and different CH substrates and incubated as mentioned in the chapter 3. The culture medium was changed every 24 hours for optimum cell growth and adherence onto the CH film [198].

The cell were imaged and their viability measured after 24 and 48 hours of incubation. In brief, the culture medium was discarded from the culture flask and rinsed twice with PBS (pH 7.4) solution to remove any unattached cells. A 5 mL sample of 0.5% trypsin-EDTA solution was pipetted until it covered the culture surface and was then kept in the incubator at temperature 37 ℃ for 10 to 15 minutes for the detaching process. Then, the detached cells were removed into a centrifuge tube and spun at 1500 rpm for five minutes. The cell viability measurement was performed using trypan blue exclusion method as described in the Chapter 3.

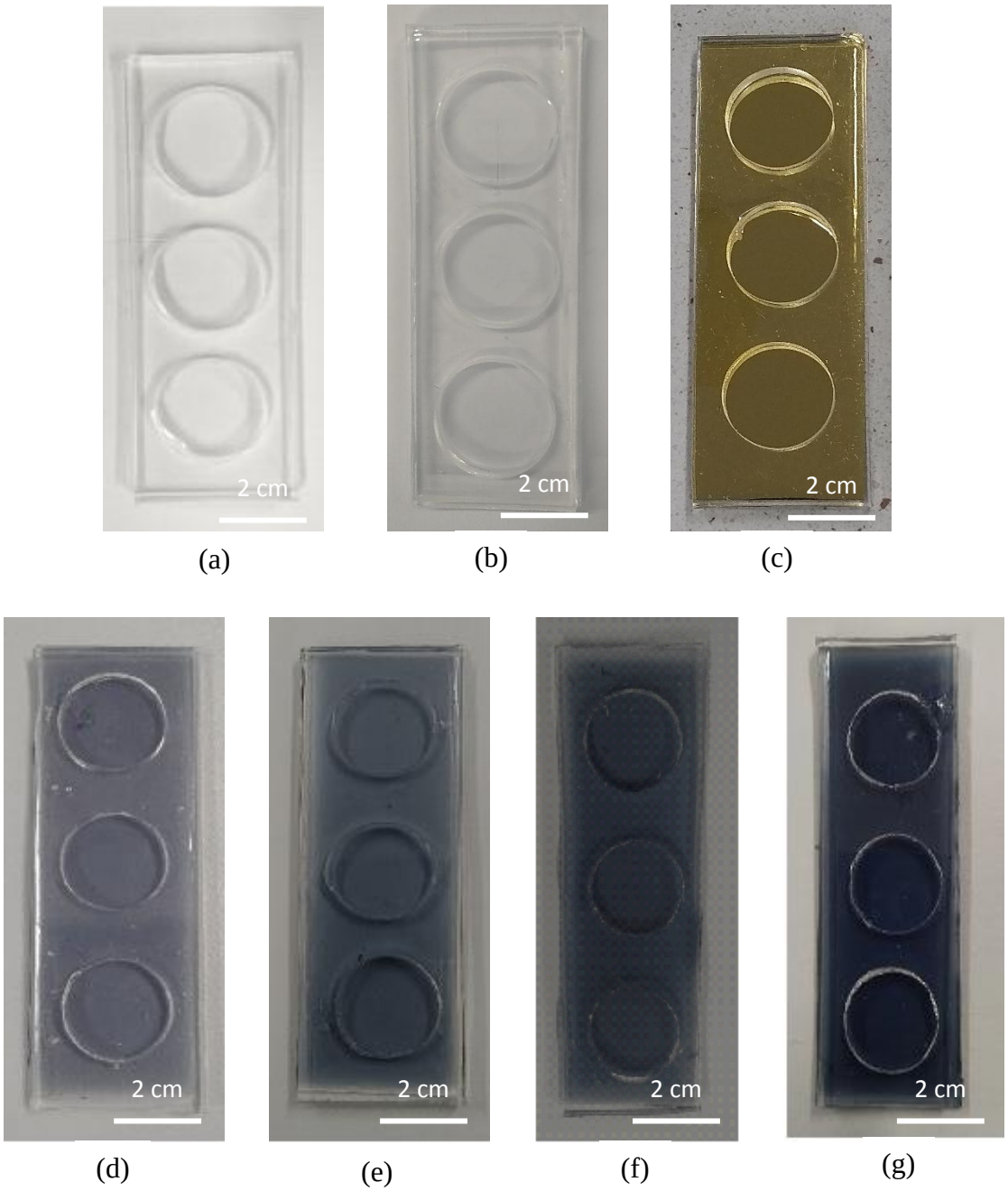

Figure 6.1: Photographs of PDMS circular chambers sealed onto different substrates for use as a cell-culture platform: (a) glass, (b) treated PDMS, (c) gold, (d) 2% CH, (e) 3% CH, (f) 4% CH and (g) 6% CH.

6.5 Biodegradability test

In vitro biodegradability of the crosslinked CH films with different concentrations of glycerol/ PEDOT:PSS were evaluated in terms of weight loss. The films were cut with

approximate weight of 2 g (W_d) each and incubated in culture medium at 37 ℃ for 15 days. At specific time intervals, the films were removed from the culture media and dried with a Kimwipes tissue before measuring their weight loss (W_L). The weight loss or degradation rate is calculated using the following equation:

$$\text{Degradation} = \frac{W_d - W_L}{W_d} \times 100 \quad (6.1)$$

Weight loss indicates the weight of material left in the sample compared to its original mass. For example, 50% weight loss means only half of the original mass of the scaffold remains; 100% degradation indicates the complete collapse of the scaffold.

6.6 Mechanical properties

The tensile modulus is used to measure the elasticity properties of CH films. The young's modulus (E), is the slope of the straight line between stress (∂)–strain (ε) curve and can be expressed using Hooke's law expresses as:

$$Young's\ Modulus, E = \partial/\varepsilon \quad (6.2)$$

Figure 6.2 is an illustration of a rectangular sample used for the elasticity analysis. Tensile tests were performed according to ASTM D882, which is the standard test method for tensile properties of thin plastic sheeting [175] due to the film thickness less than 1 mm, and the test being carried out at room temperature.

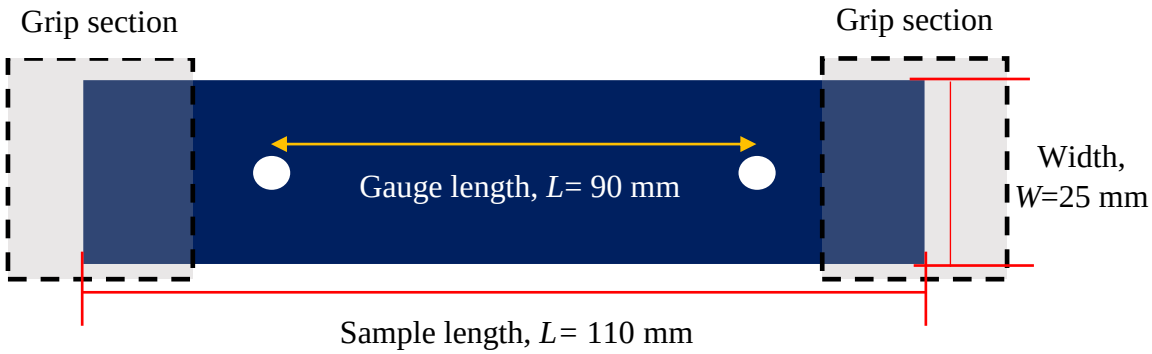

Figure 6.2: The rectangular shape of CH films with the dimensions 25 mm × 110 mm used for tensile testing experiment.

Figure 6.3 shows the procedure followed for the tensile test on conductive substrates using MTS858, a tensile machine with pneumatic pressure-controlled grips. Four samples of 2%, 3%, 4%, and 6% CH films were prepared for this test. The computer system connected to the MTS858 was set up by setting the necessary information of the material, length and width of the sample. Then, the CH film with a length of 110 mm, width 25 mm and gauge length 90 mm was fitted between the fixed and removable grips. The extensometer automatically recorded the change in gauge length during the tensile test as shown in Figure 6.3 (a). Throughout the tests, the control system was recording the load and the length of extension of the sample (Figure 6.3 (b)). During the tensile test, the grips are moved apart at a constant rate to pull and stretch the conductive film as shown in Figure 6.3 (c). Figure 6.3 (d) shows how the force applied to the sample and its displacement was continuously monitored and plotted on a stress–strain curve until sample was broken under the test. The obtained tensile results determine the tensile properties such as ultimate tensile strength, yield strength and elongation.

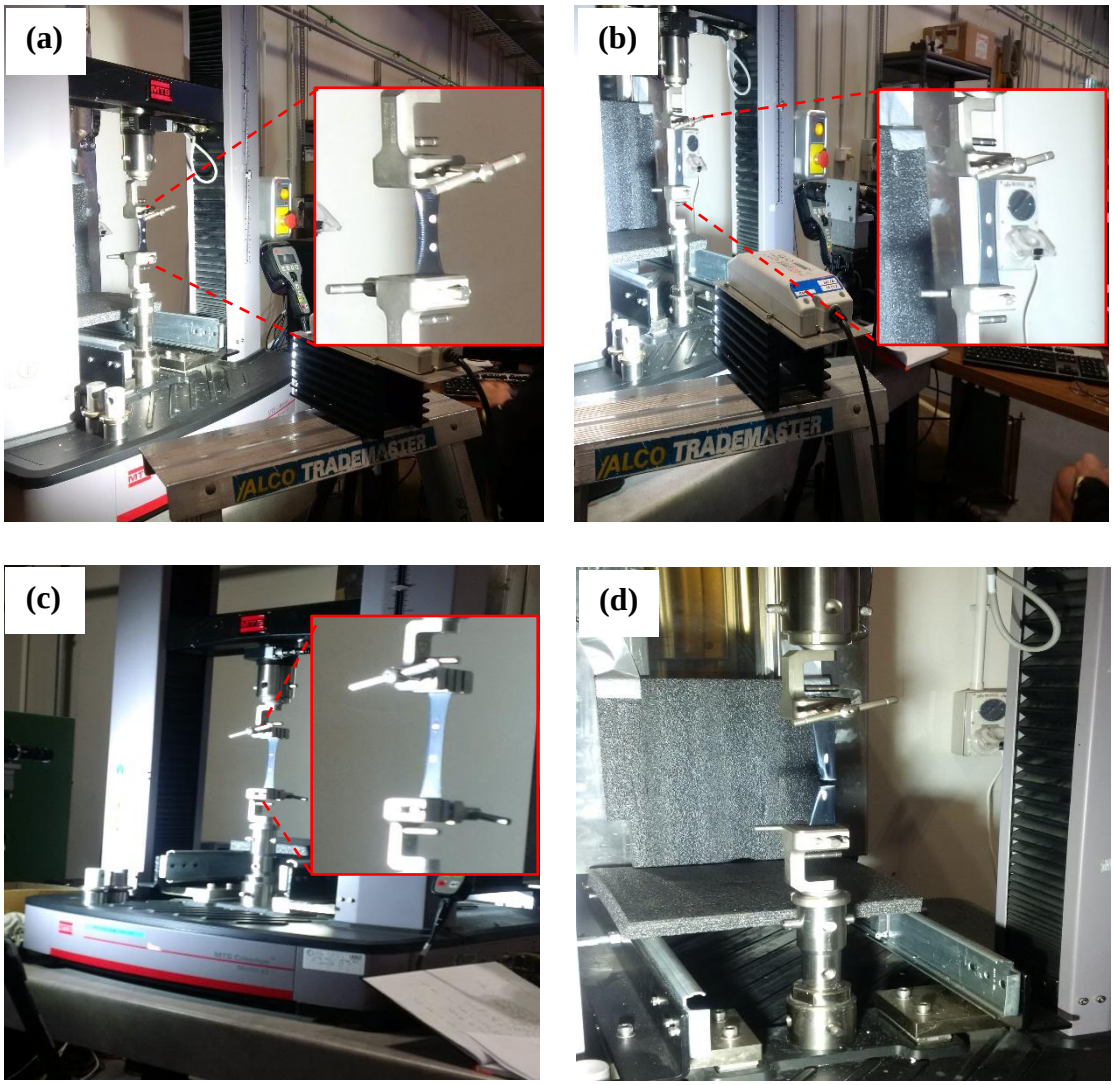

Figure 6.3: Tensile test experiment on CH films: (a) the CH film is securely held between two grips, (b) the control system recorded the load and extension of the sample, (c) the grips pulled and stretched the CH film, and (d) the CH film is continuously pulled until broken.

6.7 Film chemical characterisations

The chemical properties of the synthesised CH films were characterised by using ultraviolet–visible spectroscopy (UV-Vis) to determine the optical properties of the samples, Fourier transform infrared spectroscopy (FTIR) to analyse the chemical structure and X-ray photoelectron spectroscopy to examine the elemental composition and electronic state of the material.

6.7.1 Ultraviolet–Visible (UV-Vis) Spectroscopy

The absorptions of CH films were measured using an Agilent Cary 600i UV–Vis NIR spectrophotometer. This machine is equipped with InGaAs detection used to measure the absorption of a material ranging from ultraviolet (UV) to the near infra-red (NIR), and covering the visible part of the spectrum (Vis). A reference spectrum from an opaque mask was measured and used as a baseline. The absorbance spectra were recorded at wavelengths between 300 nm and 800 nm at room temperature. The wavelength-selected light is passed through a beam splitter that splits the light into two directions: one goes to sample and the other directly goes to a reference detector. The beam transmitted though the sample is collected by another detector. All measurements obey the Beer-Lambert law, as described in Chapter 3.

6.7.2 X-Ray Photoelectron Spectroscopy (XPS)

XPS examined the surface properties in the conductive hydrogel and valuable in the development of a new conductive biomaterial. This measurements were analysed using a Kratos Axis Ultra DLD XPS equipped with a hemispherical electron energy analyser. XPS result were used to analyse the chemistry of the CH polymer films. Spectra were recorded using monochromatic Al Kα X-rays (1486.69 eV) with the X-ray source operating at 100 Watt. The measurements were carried out in a normal emission geometry. The analysis chamber was at a pressure in the 10^{-9} torr range throughout the data collection. XPS peaks were analysed to determine the presence of conductive particles and hydrogel C, N, O, and Si using the XPS survey scan, CasaXPS (www.casaXPS.com).

6.7.3 Fourier Transform Infrared (FTIR) Spectroscopy

FTIR is an analytical technique used to identify organic, polymeric, and, in some cases, inorganic materials. The FTIR analysis method uses infrared light to scan test samples and observe chemical properties. This gives chemists a powerful tool, enabling us to

identify specific functional groups in molecules in the sample and each detection mode has its benefits.

The PEDOT:PSS, gelatin and glycerol chemical compound in CH matrix were analysed using a FTIR spectrometer ALPHA from Bruker Optics equipped with single reflection diamond-attenuated total reflectance (ATR) from Graseby Specac (Kent, U.K) and supported by OPUS Mentor software. Thin films (< 1 mm thick) were cut into (5 × 5) mm square and placed onto a sample holder for FTIR analysis, which provides the chemical bonding and functional groups of the CH films in a dry state. Transmission mode was used with 32 scans per sample in the wavenumber range between 4000 and 500 cm^{-1}. A background channel was run prior to the scans and a baseline correction was applied when the FTIR spectra were obtained.

6.7.4 Thermogram Analysis (TGA)

TGA is an analytical method suitable for monitoring physical and chemical changes of conductive hydrogel when the sample was exposed to heating. This technique determine the weight change as a function of temperature and presented in TG curves. The results from this analysis are important to provide solutions for the current problems such as drying, moisture, oxidation, etc. associated with biomedical applications of conductive biomaterials.

Thermal stability of the CH was analysed by TGA in order to measure any changes in mass as a function of temperature. This technique can analyse thermal events like decomposition and residual weight of the material. Approximately 10 mg of the dried sample was heated in platinum crucible under a nitrogen atmosphere at a heating rate of 5 ℃/minute from temperature 25 ℃ to 600 ℃ by using STA 449F1 Jupiter® (NETZSCH-Geratebau GmbH, Selb, Germany).

6.8 Results and discussion

The crosslinked CHs were synthesised with five different concentrations of PEDOT:PSS/glycerol. The resulted CP films were characterised using several

techniques. Systematic investigation methods such as water contact angle analysis, cell adhesion analysis, biodegradation, tensile strength tests, UV-Vis, XPS, FTIR and TGA were used to measure wettability, biocompatibility, biodegradability, and mechanical and certain chemical properties. The results of these analyses are presented and discussed in detail in the following sections.

6.8.1 Wettability Properties

The water contact angle analysis for four different substrates were carried out by using a telescope goniometer-CAMP 2008 KSV system. The contact angle was obtained by drawing a tangent line along the liquid–vapour interface at the point where it meets a substrate surface. For each type of substrate, five independent samples were tested.

Figure 6.4 shows the water contact angles of four different substrate surfaces; glass, PDMS, gold and different concentrations CH substrates. The average water contact angles for the 2%, 3%, 4% and 6% concentrations of CH films exhibited good water wettability of 62.5 ± 1.3°, 60.6 ± 1.7°, 66.7 ± 1.2° and 56.2 ± 3.0° respectively, whereas the glass slide and gold substrate showed hydrophilic properties with contact angles of 50.2 ± 1.7° and 62.2 ± 4.8° respectively. In contrast, the contact angle of the PDMS substrate was about 113.8 ± 3.0° and showed notable hydrophobic properties. Further examination the influence of hydrophilic and hydrophobic properties on cell growth will be discussed in the next section.

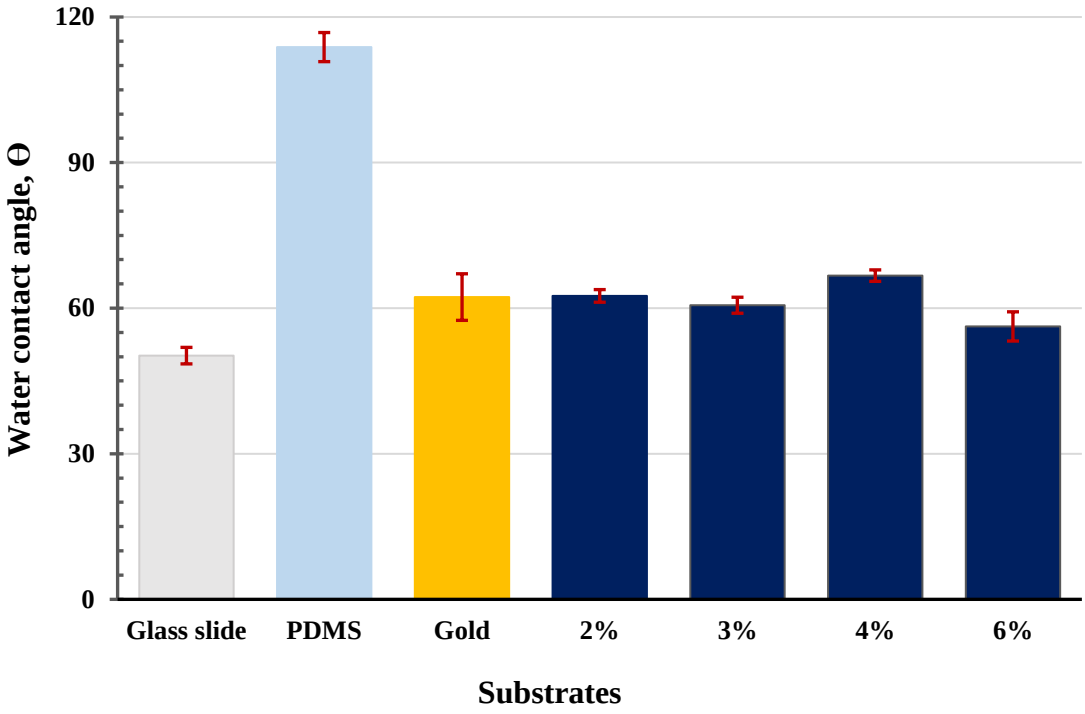

Figure 6.4: The average contact angle values for four different substrates: glass slide, PDMS substrate, gold and different concentration of CH substrates (*blue*). The graph indicates that the CH surfaces have good wettability with an average contact angle between 56.2 ± 3.0° to 66.7 ± 1.2°.

6.8.2 The effects of wettability on cell growth

This section investigates the relation between the wettability and biocompatibility of the substrates in terms of the cell adhesion process. Numerous studies have shown that the suitability of biomaterials in biological applications is generally determined by their biocompatibility. It is essential that this property, together with other properties of the materials such as toxicity, bioactivity, bio-stability and compatibility with the surrounding environment of the body such as tissues and blood, be considered in medical applications [207].

In investigating the biocompatibility, C2C12 responses such as adhesion and spreading were monitored at 24 and 48 hours of culture time on different substrates. The experiment using a cell seeding density of 5×10^4 cells/mL was repeated three times. Figure 6.5 shows cells grown on different flat substrates: glass slide, PDMS, gold and

4% concentration CH. At 24 hours, cell morphology on the 4% CH showed the extension of the membrane protrusions and well spread, whereas very few cells remained adhered on the PDMS substrate surface after 24 hrs.

However, C2C12 cells on the CH were appeared well-spread and reached confluence compared with the other substrates after 48 hours. Although PDMS is a biocompatible substrate, it is not very favourable for cell culture owing to its poor wettability. Thus, C2C12 cells started showing attachment and spreading only after 48 hours on the PDMS substrate. At 24 and 48 hours, cells cultured on the glass slide exhibited similar morphologies to those on the gold substrate. Based on the viability measurement, the CH substrate is non-cytotoxic and favourable to the living cells. The relative cell viabilities (live cells) on different substrates were quantified, as shown in Figure 6.6.

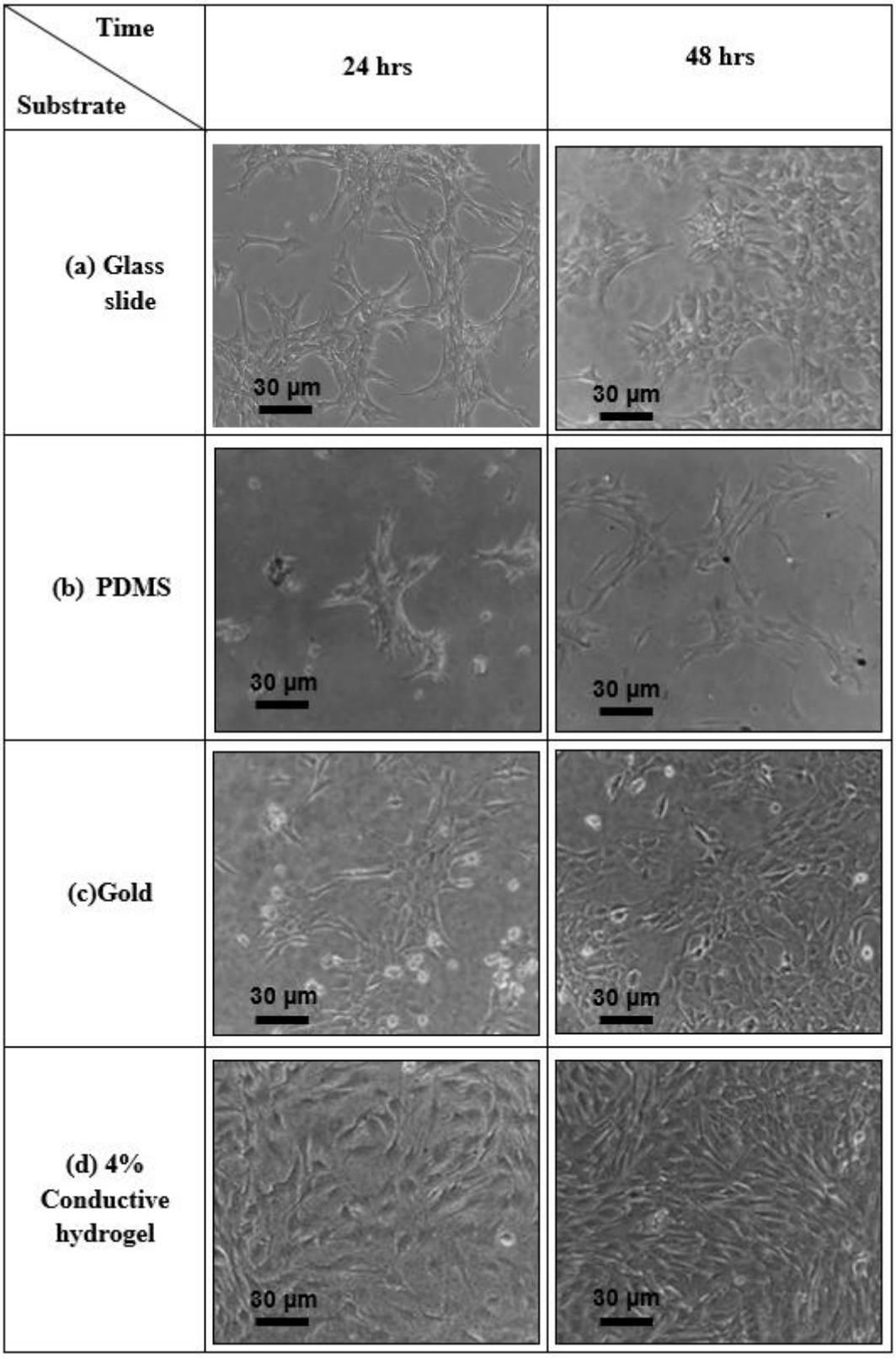

Figure 6.5: The growth of C2C12 cells at 24 and 48 hours on different substrates. The image shows cells growing on (a) glass slide (control), (b) PDMS, (c) gold and (d) 4% CH.

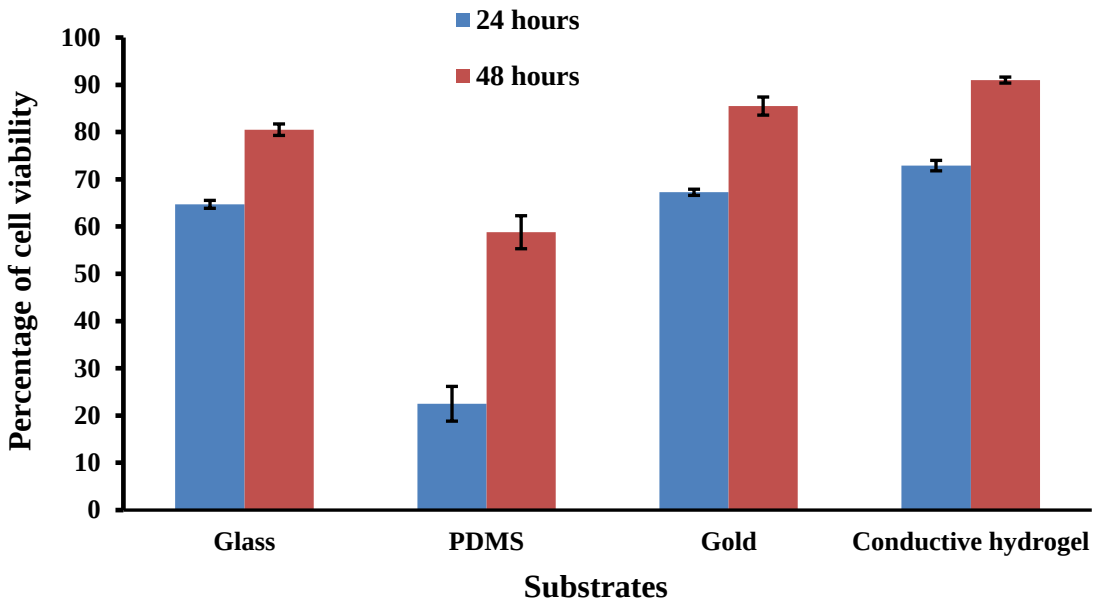

Figure 6.6: Percentage of live C2C12 cells on different substrates: glass slide, PDMS, gold and 4% CH. The data indicates that the percentages of live cells on CH film is more than 60% after 24 hours and it increased with culture time.

The number of living cells for each substrate was determined by using trypan blue and the data was exported to Excel for analysis. After 24 hours the percentage of cell growth was more than 50% on three substrates: glass slide, gold and CH. Notably, a lower percentage of cell viability was found on the PDMS substrate, which produced only about 20% at 24 hours and increased to more than 50% after 48 hours of culture time. Furthermore, at 48 hours the percentage of living cells spreading on the CH showed complete confluence (> 90%) and is higher than the glass slide and gold substrates.

6.8.3 Biodegradability test

The successful development of a conducting polymer for tissue scaffold or implantable devices requires the material to be biodegradable and biocompatible. These are important features to minimise the inflammatory reaction in a tissue that is host to the biomaterial device. In order to assess their suitability for clinical applications such as tissue scaffolds, CH films were subjected to degradation measurements in addition to

the biocompatibility tests. This degradation process involve breakage of the backbone of the polymer chains. Figure 6.7 represents the percentage of weight loss for different concentrations of crosslinked CH films in culture medium over a 15 days period. The degradation results showed that incorporation of PEDOT:PSS and glycerol highly affect the degradation behaviour of the CH film. The 0% CH film exhibited a higher percentage of degradation and completely degraded in 11 days, while the 2% and 3% CH films were degraded about 87.8% to 93% after 15 days in the culture medium. This was significantly faster than the CH films with concentration of 4% and 6%. This behaviour could be attributed to the separation of PEDOT:PSS grains from the conductive matrix at lower concentration. On other hand, the weight loss percentage of the 4% and 6% concentration films decreased slowly during the first five days of immersion in cell culture medium.

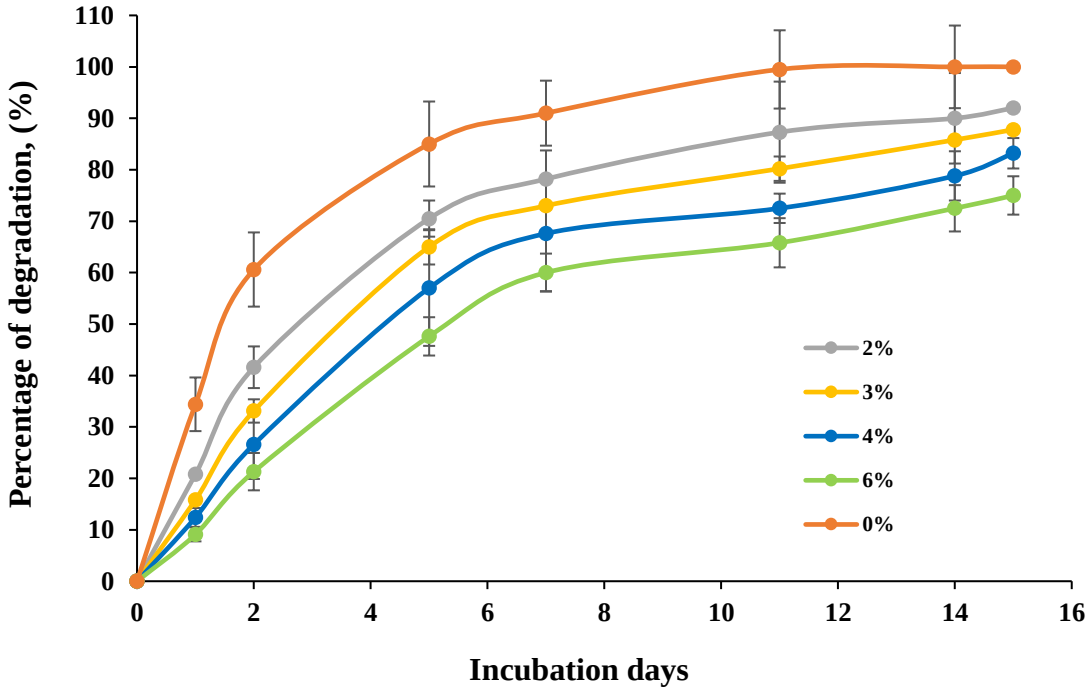

Figure 6.7: The weight loss of CH films immersed in cell culture medium. The presence of PEDOT:PSS slowed the CH degradation significantly.

Indeed, Shahini *et al.* showed that the presence of PEDOT:PSS slows or delays the degradation processes and weakened the water uptake of the conductive

nanocomposite scaffolds [36]. On the other hand, Tsukada *et al*. have reported that the presence of glycerol improved the water resistance of the PEDOT:PSS silk thread, which resulted in stability of the electrical property [208]. Therefore, the degradation test results revealed that the CH matrix is essential to provide conductive biodegradable polymer-based tissue scaffolds suitable for cell culture applications.

6.8.4 Mechanical properties

The incorporation of plasticiser glycerol in synthesised crosslinked CH matrices produces significant changes in the mechanical properties of the resulting composites. It has been reported that the PEDOT:PSS electrochemically deposited into *Bombyx mori* silk, showed a reduction in the tensile strength when compared with the pristine silk thread. Moreover, they found that the addition of glycerol in PEDOT:PSS silk thread increased the softness of the conductive silk thread [208]. The stiffness plays an important role when these materials are used as substrates for cell culture for tissue engineering applications.

The elastic modulus was calculated from the slope of the plot of stress versus strain, which is directly related to the stiffness of the material. Figure 6.8 presents the experimental tensile test measurements of the CH films. The average of Young's moduli under dry conditions of the 2%, 3%, 4%, 5% and 6% films were 77.87, 8.70, 2.78 and 1.11 MPa respectively. These results reveal that the addition of PEDOT:PSS/glycerol reduces the stiffness of the CH films, thus making the conductive material more elastic with good stretchability.

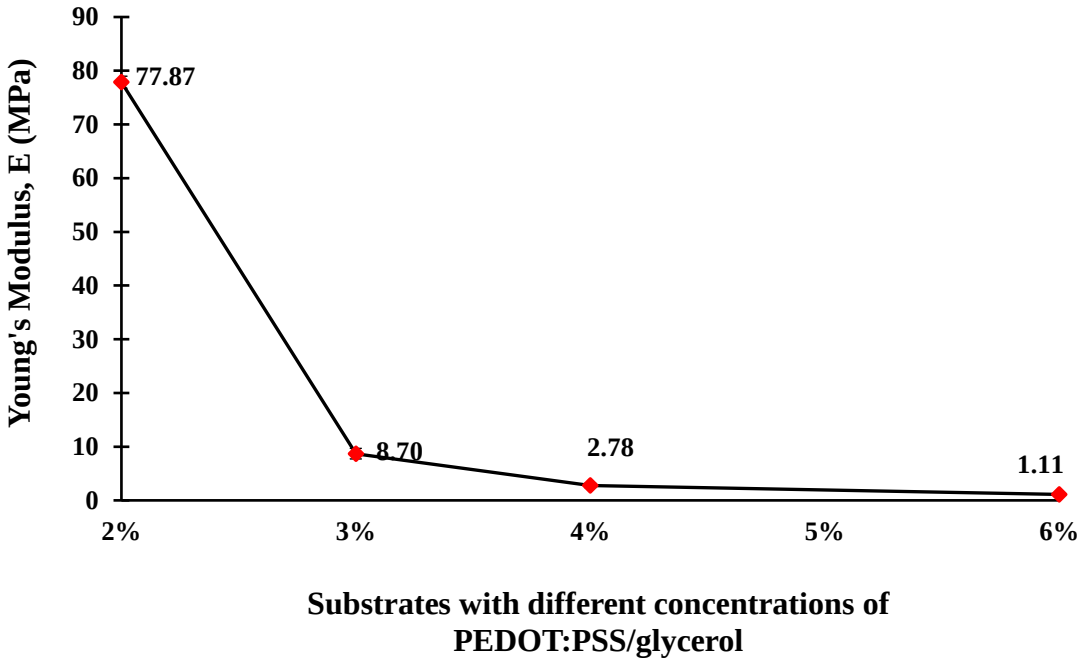

Figure 6.8: The young's moduli of the CH films at different concentrations (n=4). The data shows a significant decrease in mechanical properties of stiffness as percentage of PEDOT:PSS and glycerol increased in the hydrogel matrix.

Analysis / Substrates (PEDOT:PSS/ Glycerol)	Elastic Modulus, E MPa	Tensile Strength MPa	Toughness MPa
2%	77.86 ± 1.11	2.95 ± 0.98	18.74 ± 5.19
3%	8.69 ± 0.98	1.54 ± 0.24	3.96 ± 0.53
4%	2.78 ± 0.39	0.97 ± 0.98	1.49 ± 0.37
6%	1.11 ± 0.09	0.25 ± 0.04	0.81 ± 0.08

Table 6.1: Summary of the mechanical properties: elastic modulus, tensile strength and toughness of the CH films (n=4). All of the measured mechanical parameters decreased with increasing the percentage concentration of the PEDOT:PSS / glycerol.

As shown in Table 6.1, the films' mechanical properties: Young's modulus, tensile strength and toughness of all the CH films are strongly dependent on the PEDOT:PSS and glycerol concentrations. The average Young's moduli for the 2%, 3%, 4% and 6% CH was found to be 77.86 ± 1.11 MPa, 8.69 ± 0.98 MPa, 2.78 ± 0.39 MPa and 1.11 ± 0.09 MPa, respectively. The average tensile strength for these conductive films were 2.95 ± 0.98 MPa, 1.54 ± 0.24 MPa, 0.97 ± 0.98 MPa and 0.25 ± 0.04 MPa. The toughness of the films decreases from 18.74 ± 5.19 MPa to 0.81 ± 0.08 MPa with increasing glycerol concentration. These results provide quantitative data for designing materials for sensors and actuators that might be integrated with other biomedical devices. The biodegradation tests conducted and discussed in the previous section demonstrate that films containing PEDOT:PSS/glycerol can be optimised to meet the required mechanical and electrical properties.

6.8.5 Ultraviolet Visible (UV-Vis) Spectroscopy

The formation of PEDOT:PSS particles in the hydrogel network was identified by analyzing the UV spectrum. UV spectroscopic analysis is primarily effective in confirming the presence of conductive elements in the UV region as well as in the visible region, depending on particle size. Figure 6.9 shows the optical properties of pure hydrogel and four different concentrations of CH composites. Figure 6.9 (a) indicates that 0% film has a weak absorption spectrum and provides a transparent substrate when placed, for illustration, on top of the University of Canterbury logo printed on paper. Moreover, there are significant increases in the absorption as the concentration increases from 2% to 6% due to higher concentration of PEDOT:PSS particles entrapped in the hydrogel network. The colour of the CH films have significantly darkened with the increase in the concentration of the CP, PEDOT:PSS. The CH film colours have changed from light blue at 2% of PEDOT:PSS (Figure 6.9 (b)) to a dark grey for 3% PEDOT:PSS but still translucent as the "UC" letter (Figure 6.9 (c)) is reasonably visible. When the PEDOT:PSS concentration was increased to 4%, the film colour became dark blue (Figure 6.9 (d)) and totally opaque dark blue at 6% w/w of PEDOT:PSS (Figure 6.9 (e)). These results clearly indicate

that at 6% PEDOT:PSS a stronger absorption was exhibited, preventing any light from passing through compared with the other CH films.

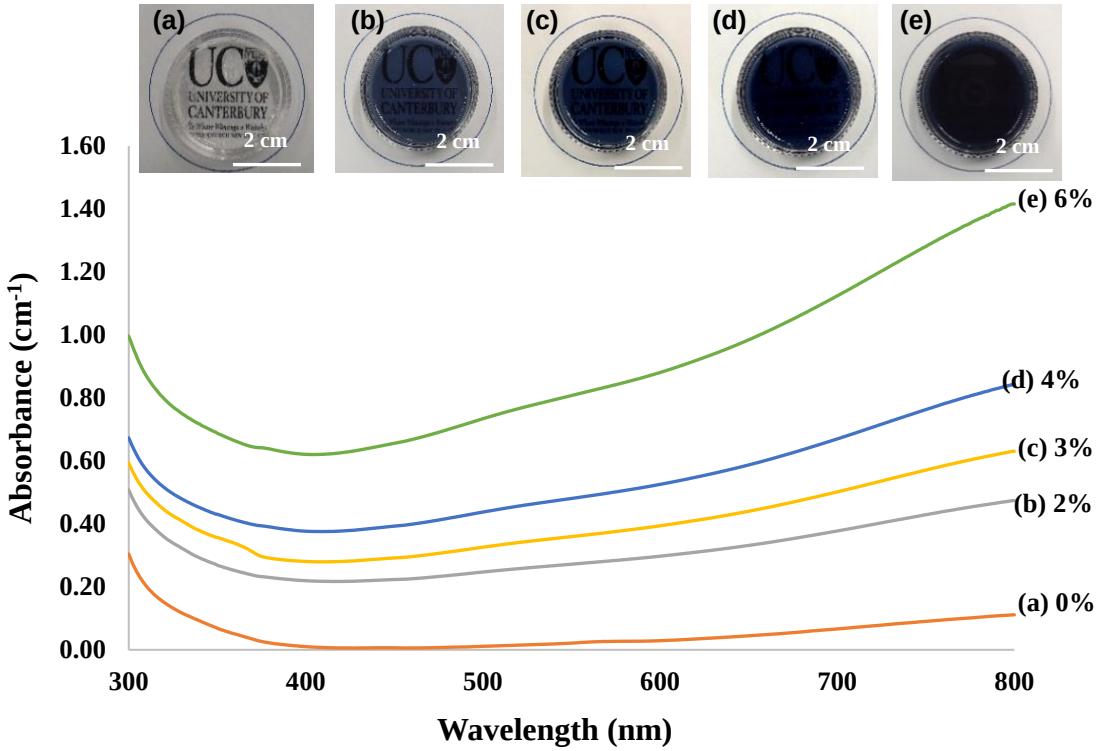

Figure 6.9: Photographic images and UV-Vis spectra of CH films with the following concentrations (a) 0%, (b) 2%, (c) 3%, (d) 4% and (e) 6% of PEDOT:PSS. Both data indicated the colours of CH films changed from transparent to translucent and finally opaque at higher concentration of CP.

6.8.6 X-Ray Photoelectron Spectroscopy (XPS)

X-ray photoelectron spectroscopy (XPS) was performed using a Kratos Axis Ultra DLD XPS to examine the changes in surface composition and surface chemistry of the pure hydrogel and four different concentrations of CH, as shown in Figure 6.10. The conductive films were characterised by Dr Colin Doyle from the University of Auckland using the experimental setup described in Chapter 3. The assignment of XPS peaks was made according to CasaXPS software (www.casaxps.com).

The main elemental components of the PEDOT:PSS were oxygen, carbon, and sulfur, which are consistent with the XPS study and confirmed that this polymer film was of the expected composition. The spectral signals of the CH films revealed the existence of nitrogen (N1s) peak around 397–400 eV that represented multiple amine groups of gelatin.

The intense photoelectron peaks at the binding energies of 530–550 eV correspond to photoelectrons emitted from oxygen at O1s core level. The carbon C1s peak is around 285 eV. The S2p peak at the binding energy of around 165–163 eV corresponds to the sulfur signal of conducting polymer PEDOT:PSS polymerised through the hydrogel [12]. The data obtained from XPS were not significantly different for any concentrations of the CH polymers [12], [209]. The XPS results helped in a better understanding of how the surface of a biomaterial substrate influences the biological environment and how to create a conductive biomaterial with biological properties [210].

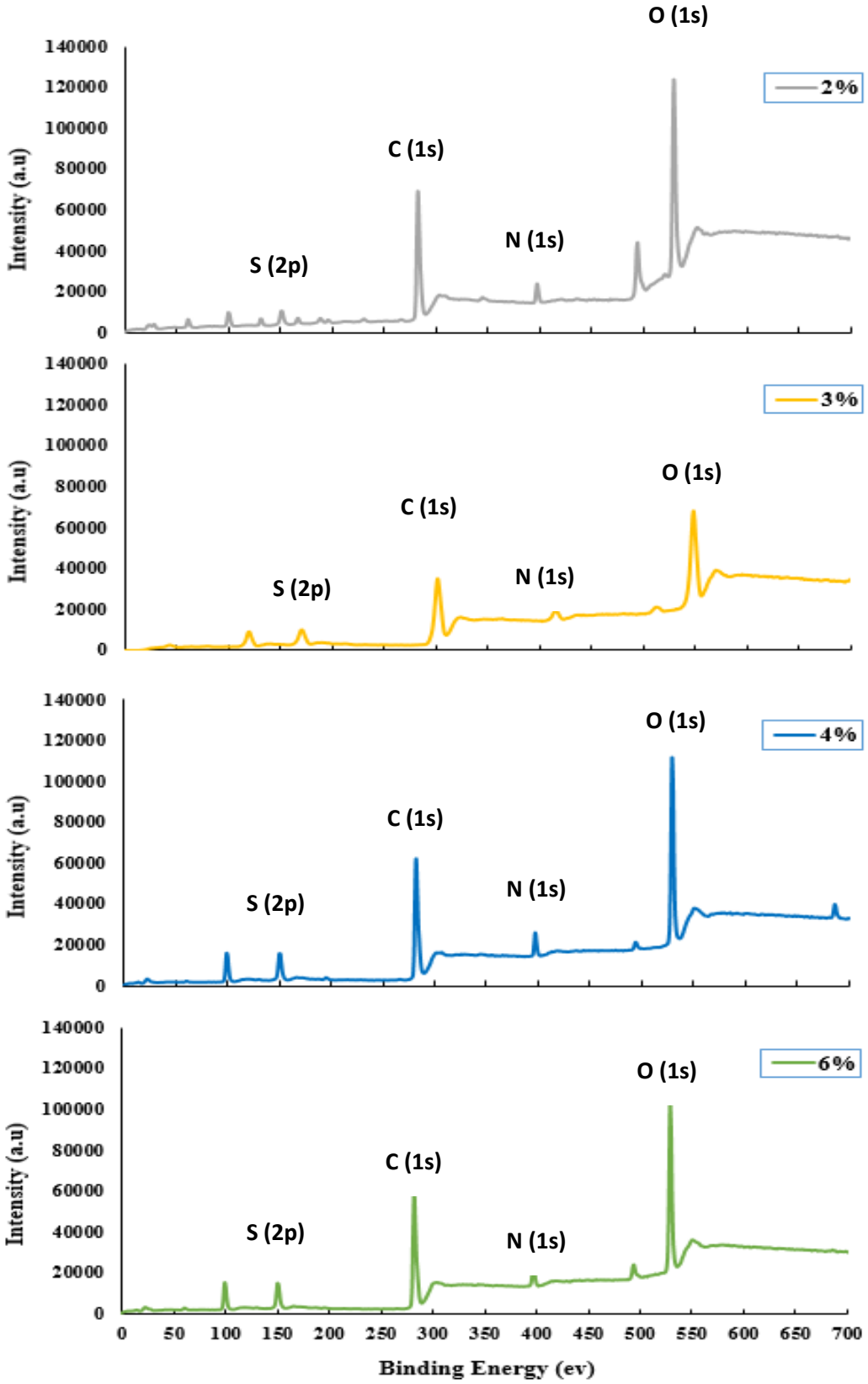

Figure 6.10: XPS spectra and sulfur peak analysis for CH films. The data shows the presence of sulfur, carbon, nitrogen and oxygen peaks in the CH matrices.

6.8.7 Fourier Transform Infrared (FTIR) Spectroscopy

Infrared spectroscopy is a useful technique in characterising the structures of materials. FTIR spectroscopy was used to assess the polymer chemical groups; PEDOT:PSS and gelatin networks. These vibrational modes are quantitatively measurable by IR spectroscopy [211]–[214]. Figure 6.11 represent the FTIR spectra relative to the PEDOT:PSS blends with gelatin solution.

The spectra of pristine gelatin showed characteristic peaks in the broad range of 3200–3500 cm^{-1} due to N–H stretching of the secondary amide. C=O stretching at 1650 cm^{-1} indicated the primary amide, whereas N=H bending resulted in peaks between 1500 cm^{-1} and 1550 cm^{-1}. In addition, aliphatic C–N bond stretching vibrations were observed at band 1075 cm^{-1}. It is suspected that the broad N–H bending and C=O stretching of gelatin implied that the carboxyl and amide group of gelatin tended to form a hydrogen bond network [215].

In the CH spectrum, the broad band in the range of 3200–3300 cm^{-1} represent the peak of the N–H bond of gelatin peak in the substrates. It was observed that the peak at 1650 cm^{-1} changes to 1625 cm^{-1} due to the incorporation of PEDOT:PSS in hydrogel [216]. The band at 1520 cm^{-1} is attributed to the C–C stretching vibration of the thiophene rings and the sulfonic acid groups of PSS [217], whereas the strong peak at 1050 cm^{-1} was ascribed to C–O stretching vibration of the ethylenedioxy group of the PEDOT material [217]. Thus, these results confirmed the successful combination of the conductive and gelatin elements in the CH.

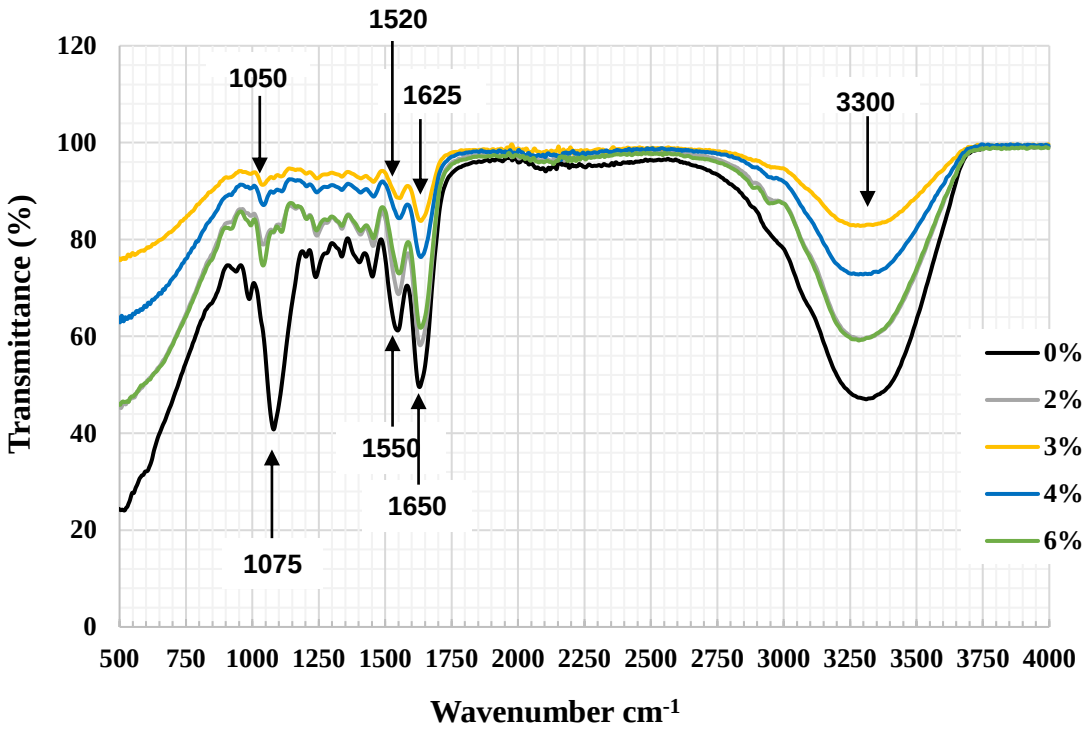

Figure 6.11: FTIR spectrum of CH. Changes in the peaks represent the formation of the CH blends with different concentrations: 0%, 2%, 3%, 4% and 6% of PEDOT:PSS.

6.8.8 Thermogravimetric Analysis (TGA)

The thermal stability of the synthesised CH was analysed with thermogravimetric analysis (TGA). Figure 6.12 presents the TGA family of curves for the 2%, 3%, 4% and 6% concentration CH films. TGA is an analytical method suitable for monitoring physical and chemical changes of conductive hydrogel when the sample was exposed to heating. This technique determine the weight change as a function of temperature and presented in TG curves. The results from this analysis are important to provide solutions for the current problems such as drying, moisture, oxidation, etc. associated with biomedical applications of conductive biomaterials. The thermal behaviour of the CH is different for each film depending on the concentration of the conducting polymer PEDOT:PSS. Overall the thermal behaviour of the CH has three distinct stages. The first stage was explained by the evaporation of any absorbed water, the second stage is attributed to the

decomposition of the film and the third stage to the elimination of the volatile products in the film.

In the first step, 20% weight loss was observed at temperature 60 ℃. This can be attributed to loss of water molecules from the polymer matrix. The second weight loss started at around temperature 150 ℃, which is the onset of chemical decomposition of the material; and the third stage, starting at temperature 250 ℃ onwards represents the collapse of the chemical structure and elimination of the backbone of the PEDOT:PSS.

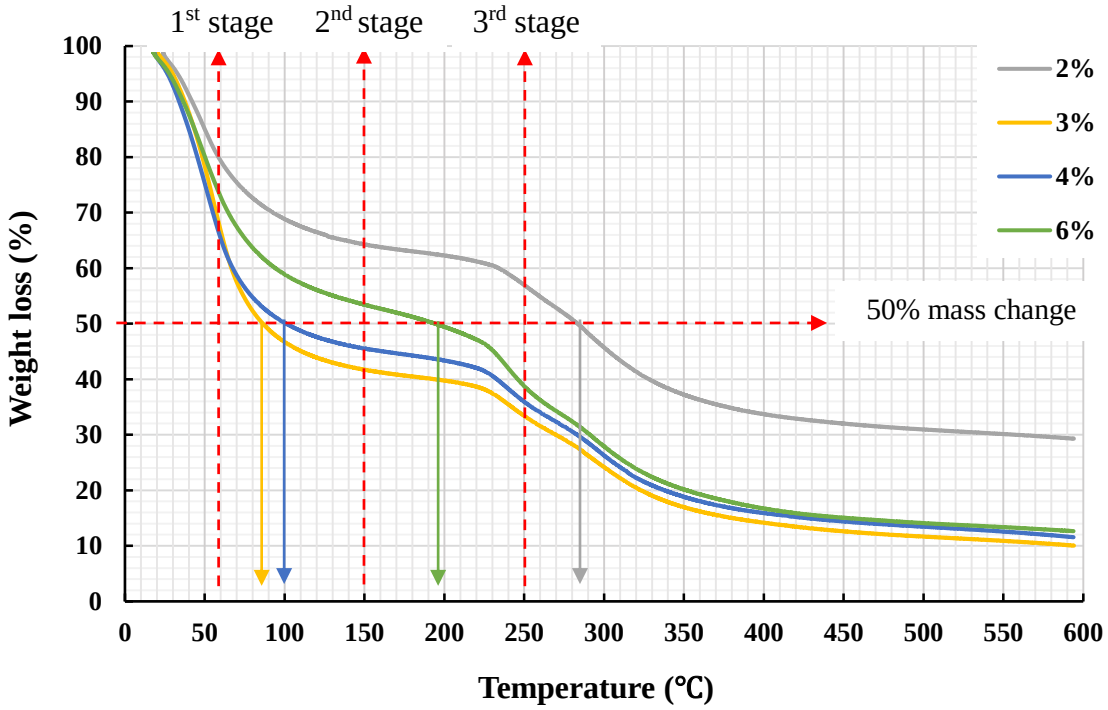

Figure 6.12: TGA curves of the different concentrations of PEDOT:PSS in hydrogel matrix, showing weight loss of the films as the temperature is increased from room temperature to 600 ℃.

Furthermore, the set point weight loss of 50% for the 2%, 3%, 4% and 6% concentrations of the CH films started at a temperature of 285 ℃, 85 ℃, 100 ℃ and 195 ℃, respectively. In addition, at a temperature higher than 320 ℃, the TGA curves level off indicating that the samples undergoes 90% weight loss.

6.9 Conclusions

Several techniques were used to characterise the conductive film, such as water wettability, biocompatibility, and biodegradation, mechanical, physical and chemical analysis. The water contact angle measurement showed that the CH contact angles were between 53.2° and 67.7° depending on the concentration of the PEDOT:PSS/glycerol in CH mixture, and the film has good wettability with excellent hydrophilicity that were favourable for cell culture growth. Seeded and cultured C2C12 cells grew better on the CH substrate than on the glass slide, PDMS and gold substrates. The developed CH films have mechanical properties that can be tuned, with the elasticity modulus changing from 77.87 ± 1.12 MPa to 1.11 ± 0.10 MPa, depending on the mixture's concentration. In addition, the chemical analysis confirmed that the expected components were present in the respective CH films. The biocompatible, soft-but-strong properties of the conductive film obtained in this work indicate that it can potentially be used as coating for medical implants, tissue engineering scaffolds and other biomedical uses.

CHAPTER 7

Cell–Substrate Impedance Sensing

This chapter describes the use of cell–substrate impedance sensing in studying myoblast C2C12 adhesion and viability in real-time measurement. Gold interdigitated electrodes (IDEs) coated with CH were employed for this study. A pair of gold IDEs with different electrode width and spacing (30 µm × 30 µm and 50 µm × 50 µm) were fabricated on a glass substrate by conventional photolithography. These biochips were used for measuring the changes in impedance due to the behaviour of cells cultured on the CH coated gold IDEs and compared with a control IDE. The measurements of impedance magnitude were performed using Agilent Precision Impedance Analyser 4294A at frequencies ranging from 100 Hz to 1 MHz.

The impedance magnitudes of the CH biochip and gold biochip (control platform) were tested with cells in culture medium DMEM. The results showed a decrease in impedance for the CH biochip compared to the control biochip from 4.27 kΩ to 3.70 kΩ for 30 µm × 30 µm and from 3.85 kΩ to 3.37 kΩ for 50 µm × 50 µm at a frequency of 100 Hz. In addition, the phase angle of the CH coated gold electrode decreased to −90° below 10 kHz, dominated by the capacitive reactance, and became close to 0° above 10 kHz, showing a tendency to more resistive behaviour at high frequency.

When C2C12 cells were cultured on the both biochips, the impedance exhibits a rapid increase starting after two hours of sedimentation. The notably large change in impedance is an indication of changes in cell adhesion and proliferation. After this, the impedance value flattened after the myoblasts reached confluency after 12 to 24 hrs. In investigating the toxin effects on the myoblast C2C12 adhesion and impedance, doxorubicin (DOX) was used as a toxicant agent. The results show that there was significant reduction in impedance magnitude after four hours of toxin treatment, which indicates that the cells start to lose their cell–substrate contact, reducing the cell

coverage area on the surface. After 12 hours, cells were shrunken and dead, clumping together and completely detached from the sensor's electrode surface.

7.1 Introduction

Electric cell–substrate impedance sensing (ECIS) is increasingly used in real-time for monitoring the changes in cellular behaviours and response to drugs *in vitro*. The idea of using electric cell–substrate impedance sensing was first reported in 1984 [155], [218], [219]. Researchers used an alternating electrical signal to observe cell growth on gold electrodes and measured changes in the impedance of the system. The development of electric cell–substrate sensing to study cellular behaviour has important applications in the fields of bioengineering and biomedicine.

In ECIS, various studies have reported the use of gold [164], [220]–[223], platinum [224], [225], aluminium [226], carbon [227] and indium tin oxide [158] as electrode materials for impedance measurements. The selection of the materials for electrode fabrication depends on the fabrication process, bioreceptors, cost, suitability of the material for the environment and the specific application. Currently, CHs have been demonstrated to be an effective material for biosensing owing to their biocompatibility, processability, good wettability, biomechanical properties and a continuous improvement in their electrical properties [228]. CH is a hybrid material, a combination of a hydrogel matrix with the electronic functionality of a CP (polypyrrole, polyaniline, etc.). Several studies have demonstrated that CHs have great potential for coating materials [42], [229], [230].

In this chapter, a novel application of electric cell–substrate impedance sensing was performed to study cellular response and toxin sensitivity in real-time using electrodes coated with CH. To achieve this, a high density of myoblasts cells were seeded on a CH substrate for 24 hours and the changes in impedance were monitored. The cell growth and viability on the CH were compared with those on the uncoated gold electrode platform. In addition, real-time impedimetric analysis of inhibitor toxin on the cell formation was carried out for 12 hours. The impedimetric properties in the

presence of the CH layer and on the gold electrodes were obtained similarly. In conclusion, the use of CH provides a simple fabrication method for devices and can successfully detect cells' impedance response. The CH can also be employed as a platform for the development of implantable biochips or for bone implants.

7.2 Materials and methods

The following materials and chemicals were used in this part of the work:
AZ 1518 photoresists (MicroChemicals GmbH), AZ 326 MIF developer (MicroChemicals GmbH,), microscope glass slide 25 mm × 75 mm (Corning, Amsterdam, Netherlands), acetone, methanol and isopropanol (Sigma Aldrich, Dorset, UK). PEDOT:PSS with 1.3 wt.% dispersion in deionised water (483095-250G, Sigma Aldrich), Type A porcine skin powder (G2500, Sigma Aldrich), phosphate-buffered saline (PBS) tablets (Sigma Aldrich), 1000U/g microbial Transglutaminase (supplied from Ajinomoto, Japan), GlutaMAX (11995-065, Gibco via Invitrogen), fetal bovine serum (Gibco via Invitrogen), penicillin-streptomycin 100x (Gibco via Invitrogen), Fungizone (Gibco via Invitrogen), Polydimethylsiloxane, (Sylgard 184, Dow Corning Corp.), ethanol and glycerol (analytical grade, from LabServ).

7.2.1 Fabrication of conductive hydrogel biochip

The CH biochip was fabricated using gold IDE on a glass substrate following conventional photolithography processes. This biochip consists of two culture chambers embedded in a gold IDE with two different electrode widths and spacing dimensions of 30 µm and 50 µm. A 40 nm-thick titanium and gold layer were sputtered on a glass substrate to form an active sensing area with dimensions of 10 mm × 10 mm for each electrode. Glass was selected as a substrate to effectively decrease the measurement noise and minimise the substrate capacitance [231].

Figure 7.1 shows the fabrication process of the gold IDE using a lift-off technique. A glass substrate was cleaned using acetone, methanol and isopropanol for three minutes in each solvent. It was then oxygen plasma treated for ten minutes at power of 100 Watt

to remove any organic substances. The substrate was spin coated with AZ 1518 negative photoresist at 3000 rpm for 30 seconds and soft-baked for two minutes at temperature 100 ℃ on a hotplate (Figure 7.1 (a)). The patterns were defined onto the photoresist layer under a UV light source of wavelength 365 nm using Karl Suss MA-6 Mask Aligner in a yellow room as shown in Figure 7.1 (b).

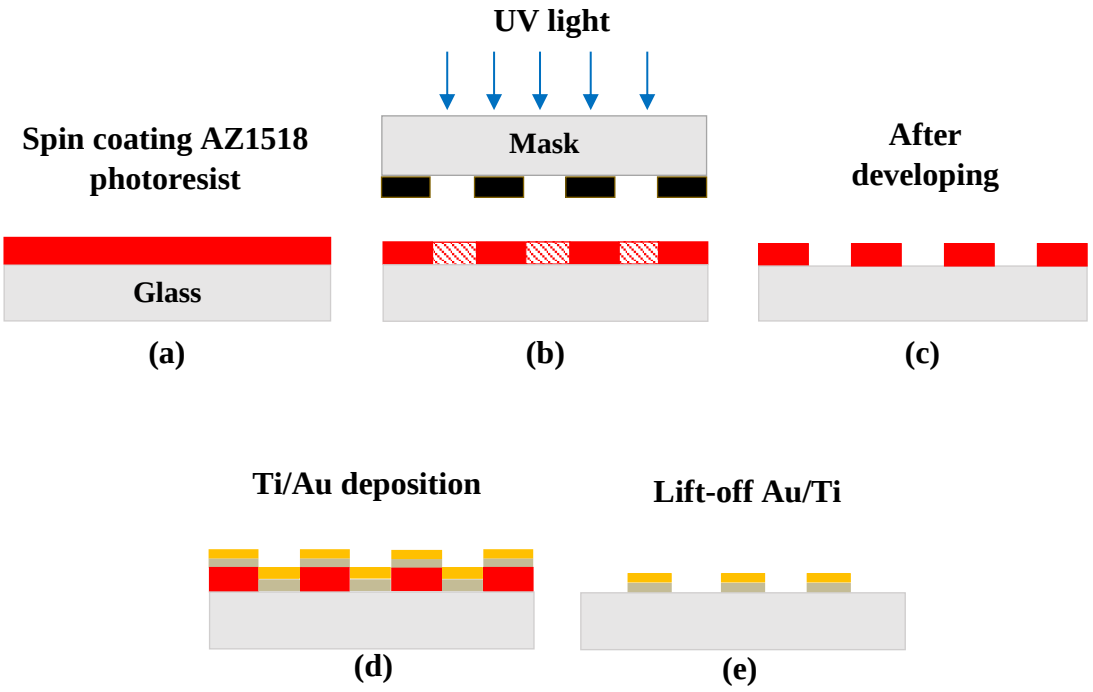

Figure 7.1: Schematic diagram of the fabrication process for the gold interdigitated electrodes on a glass substrate: (a) spin coating a glass substrate with AZ 1518 photoresist, (b) defining the patterns onto the photoresist layer under the UV light, (c) developing the photoresist patterns using AZ 326 MIF developer, (d) deposition of 40 nm Ti and Au onto a glass substrate using sputtering machine and (d) lift-off of metal strip in acetone solvent.

The exposed patterns in the photoresist layer was then developed in AZ 326 MIF developer for 60 seconds and thoroughly rinsed with deionised water (Figure 7.1 (c)). Then the patterned photoresist was soft-baked at temperature 120 ℃ for two minutes on a hot plate to harden the final resist layer so that it can withstand the harsh environment of wet etching. Figure 7.1 (d) shows the 40 nm layer of titanium that was deposited on a glass surface to increase adhesion, followed by 40 nm of gold using Edwards Auto 500 Magnetron Sputtering System. The IDE sensor pattern was lifted

off using acetone solvent in an ultrasonic bath machine for 3 minutes to strip off the metal-coated photoresist (Figure 7.1 (e)). The completed electrode structure of the gold biochip fabricated on glass substrate is shown in Figure 7.2.

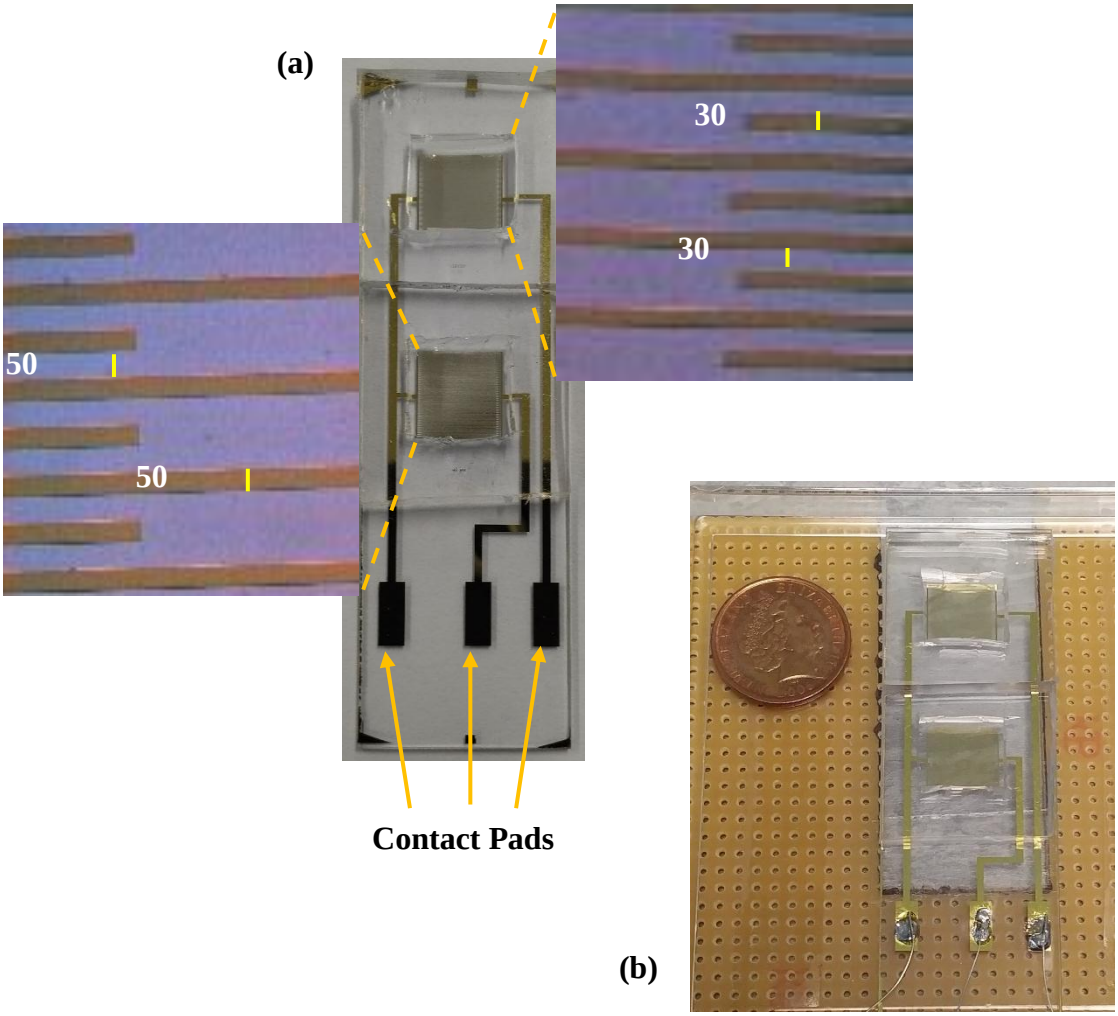

Figure 7.2: The gold biochip with connection pads on a glass substrate: (a) IDE with 30 µm × 30 µm and 50 µm × 50 µm of finger width and gap respectively, (b) the size of each sensing area as compared to the New Zealand ten cent coin.

The biochip shown in Figure 7.2 has two IDEs and was bonded with PDMS chambers. The CH mixture was prepared by mixing 12.5% w/v gelatin solution, 4% w/w of PEDOT:PSS and 4% w/w of glycerol and stirred at temperature 70 ℃until the mixtures became homogeneous. To crosslink films, 0.5 g of mTg was dissolved with 20 mL of PBS solution and mixed with the CH mixture. Subsequently, a 300 µL sample of crosslinked CH mixture was dispensed onto the pretreated gold IDE to form a controlled

thin layer of CH, because the film thickness has an influence on the sensitivity of the measurement [232].

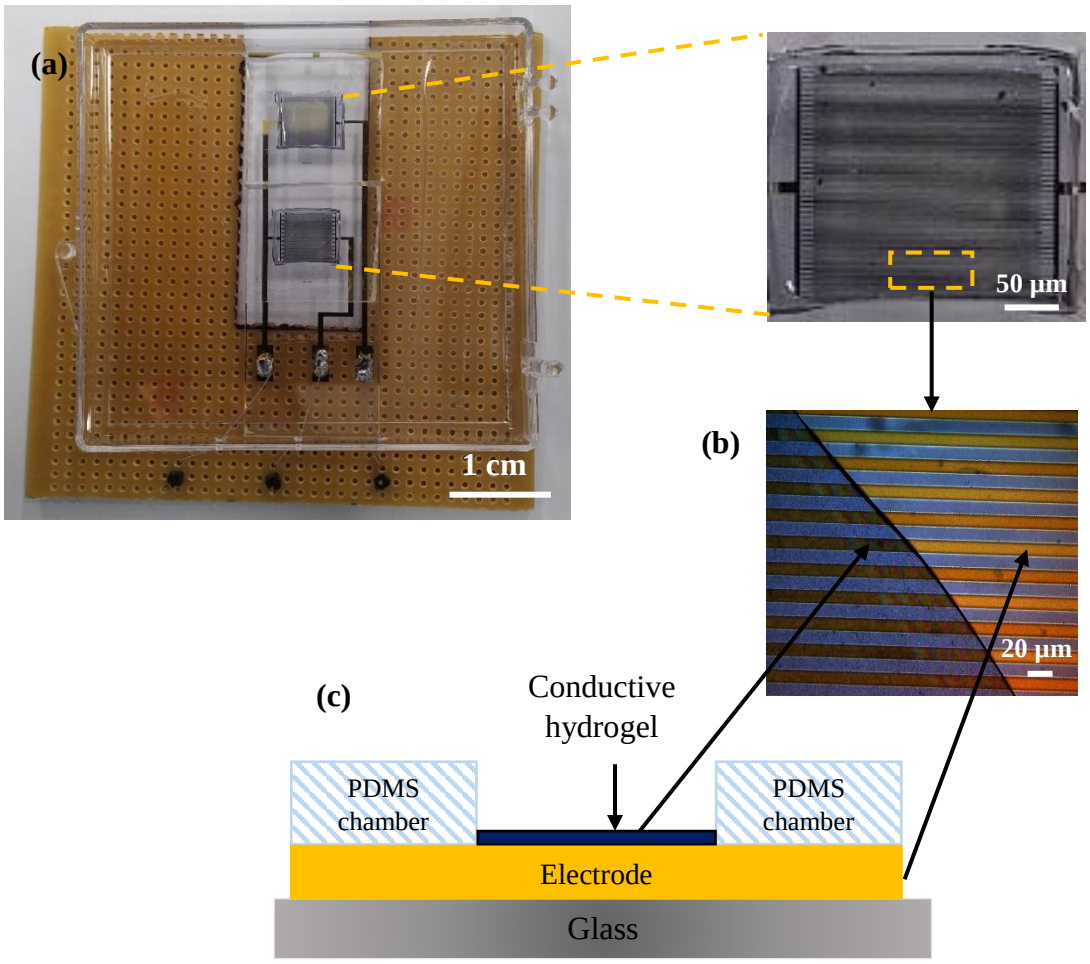

Figure 7.3: The Impedimetric system (a) Optical microscopy image of the fabricated biochip, (b) close-up image showing the difference between the CH layer and gold strips that represent the interdigitated electrodes, and (c) cross-sectional diagram of the CH biochip.

Next, the crosslinked CH layer on the IDE was placed in the incubator for one hours to form the physical and chemical crosslinks. Then, the biochip was then kept dry at temperature 4 ℃ for 48 hours to complete the polymerisation process. Upon polymerisation, the CH biochip was placed in a cell culture incubator box and contact pads were extended for connections to the impedance analyser machine, as shown in Figure 7.3 (a). The enlargement image of CH coated gold electrode is shown in Figure

7.3 (b) while Figure 7.3 (c) represent the schematic cross-sectional view of the CH biochip.

7.2.2 Bio-impedimetric measurements of the C2C12 cells

Prior to cell culture, the gold biochip (Figure 7.4 (a)) and CH biochip (Figure 7.4 (b)) were sterilised under UV irradiation in the laminar flux cabinet for 60 minutes. After sterilisation, the CH biochip was incubated at temperature 37 ℃ in a cell culture medium for one hour until it reached swelling equilibrium. Then, the CH and gold biochips were washed with sterilised PBS solution to neutralise leaching of the CH film and remove unwanted particles on gold surface.

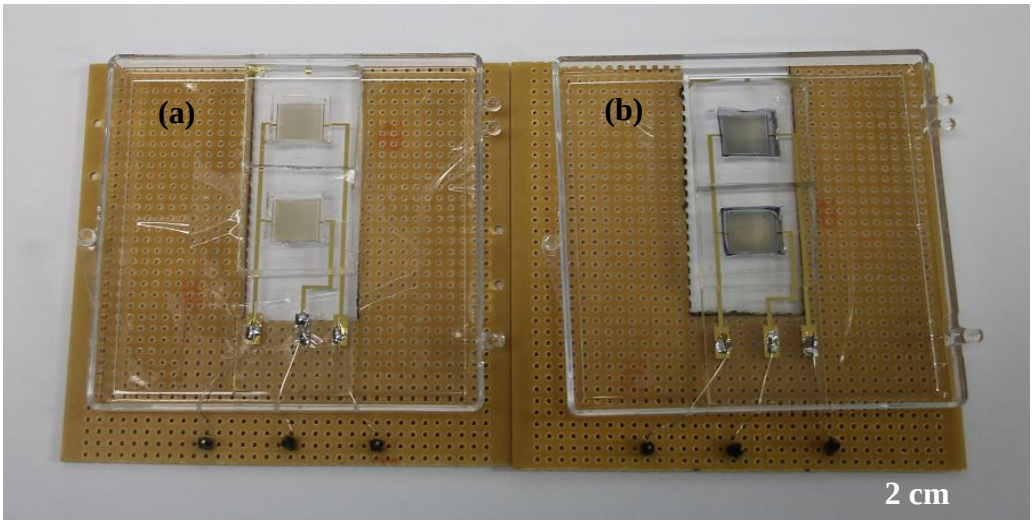

Figure 7.4: Photograph of the biochips: (a) gold and (b) CH. Both of these biochip were sealed with square chambers made from PDMS and contact pads were extended for connections to the impedance analyser machine.

The C2C12 cells were suspended in 140 µL (5×10^4 cells/mL) of culture medium and seeded in each chamber. The cell culture medium containing Dulbecco's modified Eagle's medium, 10% fetal bovine serum, 1% Fungizone and 1% penicillin-streptomycin. Then cells were incubated at temperature 37 ℃ in a 5% CO_2 humidified incubator. Figure 7.5 (a-b) shows a cross-sectional illustration and photo of the experimental setup used for electric cell–substrate sensing.

During cell culture and proliferation, impedance measurements across the parallel contact pad electrodes were performed at 0 hour, 2 hours, 12 hours and 24 hours at room temperature using an impedance analyser. The impedance was measured at frequencies ranging from 100 Hz to 1 MHz at a voltage of 40 mV_{pp} with a 0 V DC offset voltage. Impedance changes were induced by the presence of cells adhering on the electrode surface in the chamber. The change in impedance was defined by the difference between the impedance magnitude at successive measuring time points and the impedance magnitude at 0 hour. All numerical data were recorded in Excel for further analysis.

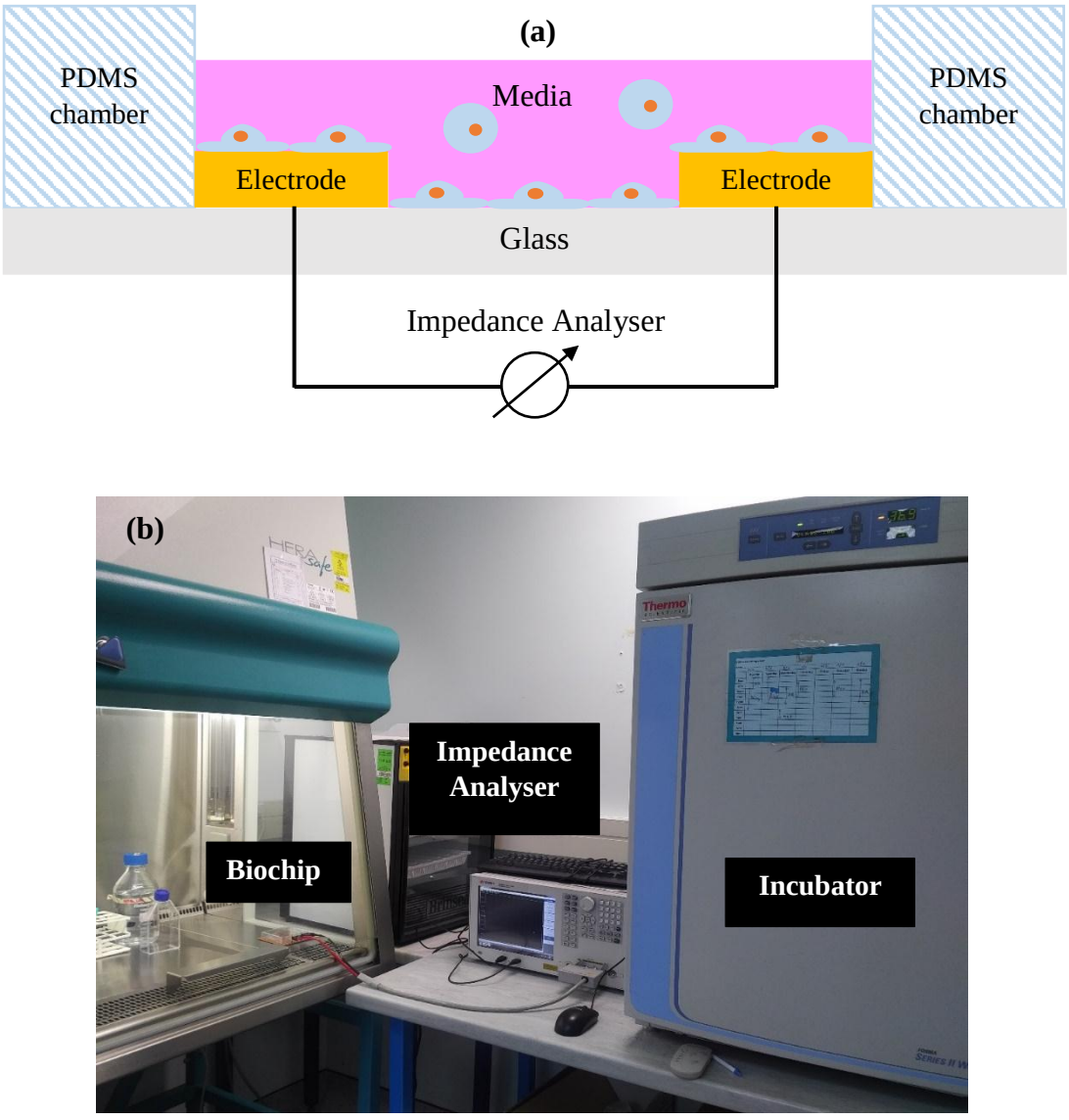

Figure 7.5: The experimental setup for impedimetric real-time monitoring of C2C12 cell interactions: (a) cross-sectional illustration, and (b) photograph of the impedance measurement in PC2 laboratory.

7.2.3 Toxin sensitivity analysis of C2C12 Cells

In order to demonstrate the sensitivity of cell impedance to drugs, the effects of the cytotoxic agents were investigated *in vitro*. In this study, the drug solution was prepared with 50 µL of DOX in 1000 µL of culture medium and dispensed onto the confluence cells in the culture chambers. DOX is a common anti-cancer drug to treat a wide range of cancer, but in this research was used to study the toxic effect on the myoblast formation [232]. The toxin-treated biochip systems were placed in the incubator at temperature 37 ℃ for 12 hours, then impedance spectra measurements of the cell–drug system were performed after 4, 8 and 12 hours at frequencies ranging from 100 Hz to 1 MHz.

7.3 Result and discussions

In this research, gold interdigitated electrodes coated with CH were used to monitor in real-time the impedance changes of C2C12 cells under different culture medium conditions. To characterise the detection sensitivity, C2C12 cells were cultured onto a thin film of CH coated on two different electrode geometries. The frequency of the impedance measurement was varied from 100 Hz to 1 MHz at 0 hour, 2 hours, 12 hours and 24 hours of culture time. The effects of cytotoxic DOX on cell adhesion after 4, 8 and 24 hours of drug exposure were measured within the same frequency range.

7.3.1 Impedimetric analysis of cell-free system

Figure 7.6 shows the impedance magnitude of gold and CH biochips with different dimensions without cells in growth medium over the frequency range from 100 Hz to 1 MHz. It was found that the impedance of the 30 µm gold biochip was 4.27 kΩ and higher than the impedance of the 50 µm gold biochip with 3.85 kΩ at a frequency of 100 Hz. The modified electrode structure was significantly lower than the bare gold electrode due to the increase in effective surface area that acted as a capacitor at low frequency. The impedance magnitude decreased from 4.27 kΩ to 3.70 kΩ for the 30 µm electrode and from 3.85 kΩ to 3.37 kΩ for the 50 µm electrode respectively. The

linear region in the curve of Figure 7.6 between 100 Hz to 10 kHz corresponds to the double layer interfacial impedance between the electrode and the DMEM medium [164], [233], while for frequencies above 10 kHz it resembles the characteristic impedance of the medium resistance [158]. Moreover, the graph shows that the impedance was increased with decrease in electrode dimension, which indicated that the size of electrode significant effect the sensitivity and signal to ratio value of the biochip [234], [235].

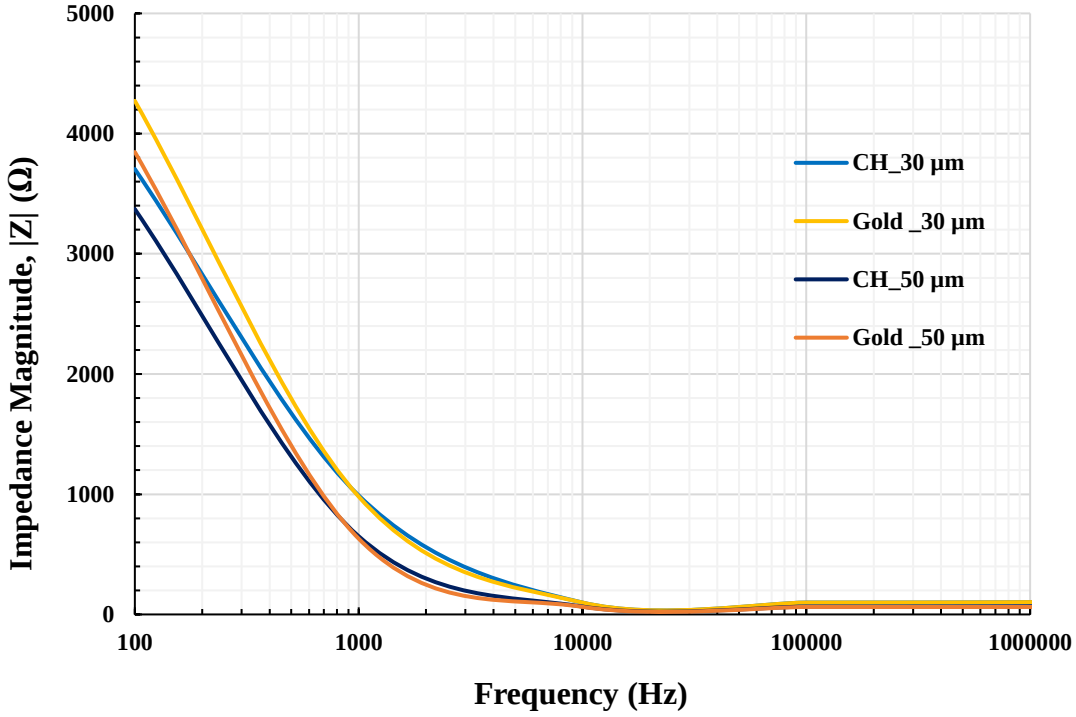

Figure 7.6: The magnitude of the impedance of gold and CH biochips measured in cell-free growth medium with different features as a function of frequency. These graphs show a linear decrease in impedance at low frequency due to the interface effect between the electrode and medium, whereas the impedance value flattened at higher frequencies.

The trend of the impedance for the CH coated electrode found in this research is similar to that reported by Abidian and co-workers [236], [237]. They found that the impedance of the modified electrode with CH was significantly lower than the bare gold electrode due to the increase in effective surface area that acted as a capacitor at

low frequency. There are numbers of reports on the characterisation of CH coated IDAs to develop highly sensitive impedimetric biochips for immobilisation of biomolecules [48], [238]–[240]. A few studies have been reported that the electro conductive hydrogels based on polypyrrole decrease limits of detection and increase sensitivity to analytes of bio transducers [238], [240].

Figure 7.7 illustrates by typical equivalent circuit of the CH coated gold electrode in cell-free growth medium, DMEM. In this work, a CH coating gold electrode system can be modelled as a resistance of growth medium (R_{MED}) series with the parallel elements of CH, capacitance (C_{CH}) and resistance (R_{CH}). Whereas, C_{CPE} is the double layer capacitance and R_1 the resistance of the gold electrode- medium interface. When the growth medium penetrate into CH, lead to increment in C_{CH} capacitance owing to water absorption and reductions in R_{CH} due to the formation of conduction path in CH matrix.

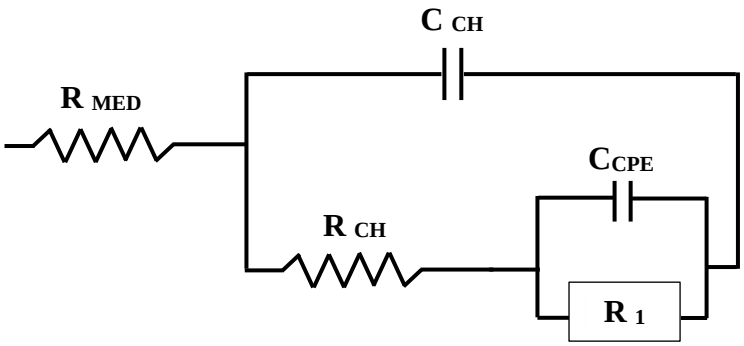

Figure 7.7: The equivalent circuit for CH coated gold electrode. C_{CPE} and R_1 represent the double layer capacitance and the resistance gold electrode-medium, while the parallel elements C_{CH} and R_{CH} represent the capacitance and resistance of CH.

Figure 7.8 shows the phase magnitude of the gold and CH biochips with different electrode dimensions. To provide a better understanding in interpreting phase behaviour, the phase spectrum can be divided into two regions. When an electrical current passes through a capacitor, the phase is shifted by −90° with respect to the capacitance region. If the current passes through a resistor, the phase angle in the resistance-dominated region is 0°. As shown in Figure 7.8 (a) and (b), the phase angle

of CH coated gold electrode for both dimensions are decreased close to −90° at below 10 kHz and towards 0° at above 10 kHz. It can be concluded that below 10 kHz the response is dominated by the capacitive reactance, and there is a tendency to more resistive behaviour above 10 kHz.

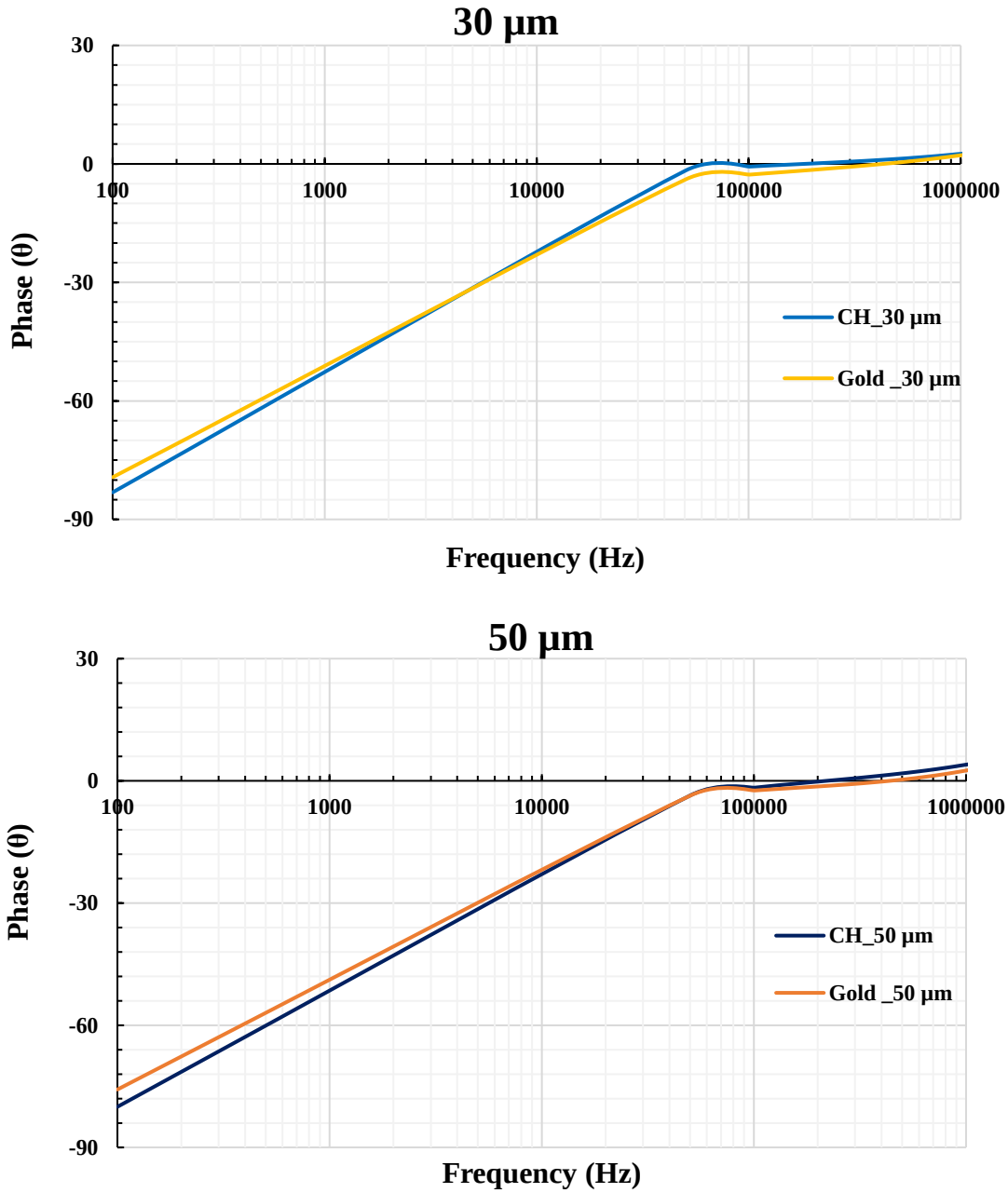

Figure 7.8: The phase magnitude of the (a) gold biochip and (b) CH biochip with two electrode dimensions, 30 × 30 µm and 50 × 50 µm as a function of frequency, showing that both dimensions of CH biochip is dominated by the capacitive behaviour below 10 kHz and by resistance behaviour above 10 kHz.

7.3.2 Visualisation and monitoring of cell adhesion on gold vs conductive hydrogel biochips

The CH impedance sensor enables the monitoring of cellular response in terms of electrical signal and has shown good biocompatibility. Figure 7.9 presents the phase contrast micrographs of the C2C12 cells showing cell attachment and proliferation on platforms made of gold electrodes and coated with CH after 0 hour, 2 hours, 12 hours and 24 hours during an ECIS experiment. In this experiment, myoblasts were seeded at densities of 50,000 cells per chamber and incubated in growth medium.

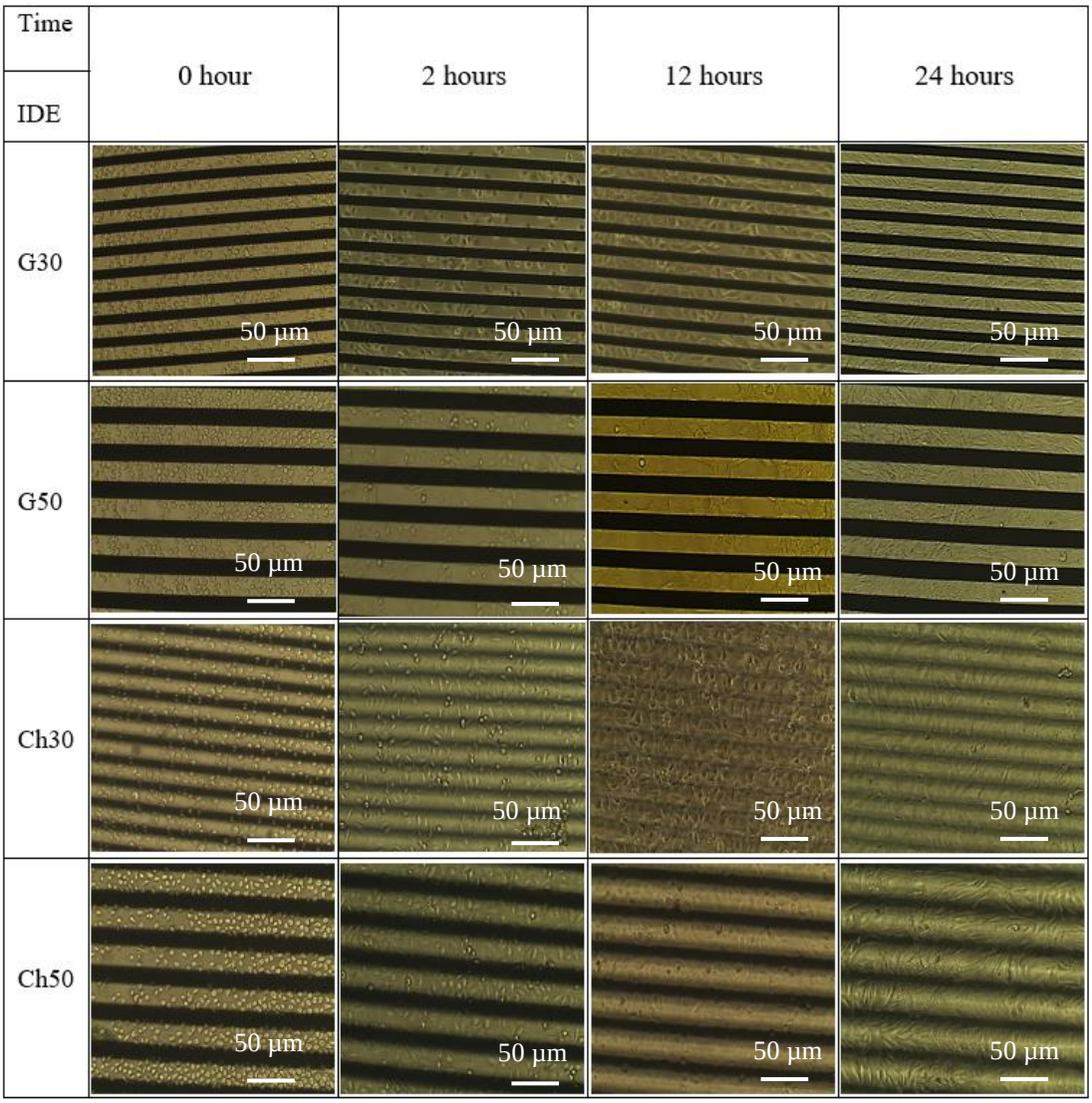

Figure 7.9: A sequence of images of C2C12 formation process at 0, 2, 12 and 24 hours on 30 µm gold IDE, 50 µm gold IDE, 30 µm CH coated IDE, and 50 µm CH coated IDE. The images show that the modified surface of gold electrodes with CH have significantly higher cell growth and reached 90% confluency after 24 hours (CH30 and CH50).

Figure 7.9, the cells show spherical morphology and did not attach on the control gold electrode surface at the start of the experiment at 0 hour. They start showing adherence and spreading on the gold electrode surface after two hours, and reach about 50% of confluency after 12 hours of cell seeding. Similarly, for the CH biochip, the cells appeared round in shape at 0 hour after cell seeding and well spread and flattened morphology with 70% of confluency after 12 hours. After 24 hours of cell sedimentation the microscopic image show that the C2C12 cells formed monolayer and 90% confluency on both types of biochip surfaces.

7.3.3 Visualisation of cell adhesion after toxin treatment

In this study, impedimetric testing of the toxicity effect on myoblasts using DOX was performed. A 200 µL sample of culture medium containing 50 µL/mL of DOX was pipetted into the culture chamber after cells had reached 90% confluency. The photograph of cell morphology and impedance measurement was conducted in real time after 4 hours, 8 hours and 12 hours during drug treatment. Figure 7.10 depicts the optical images of morphological characteristics of myoblast C2C12 apoptosis stimulated by DOX toxin at various points of time. As can be seen, DOX impairs the C2C12 cell–substrate adhesion after 4 hours of toxin treatment. The cells showed lesser degree of cell–substrate contact and weakens the cell filaments with decreased in size, but the majority of adherence cells retained a normal shape. After 12 hours of toxin addition revealed a number of effects including loss of cell–substrate contacts, shrunk, floating and dead cells clumping together were observed. All of these morphological changes suggested that the addition of DOX should lead to the expected changes in cell impedance magnitude.

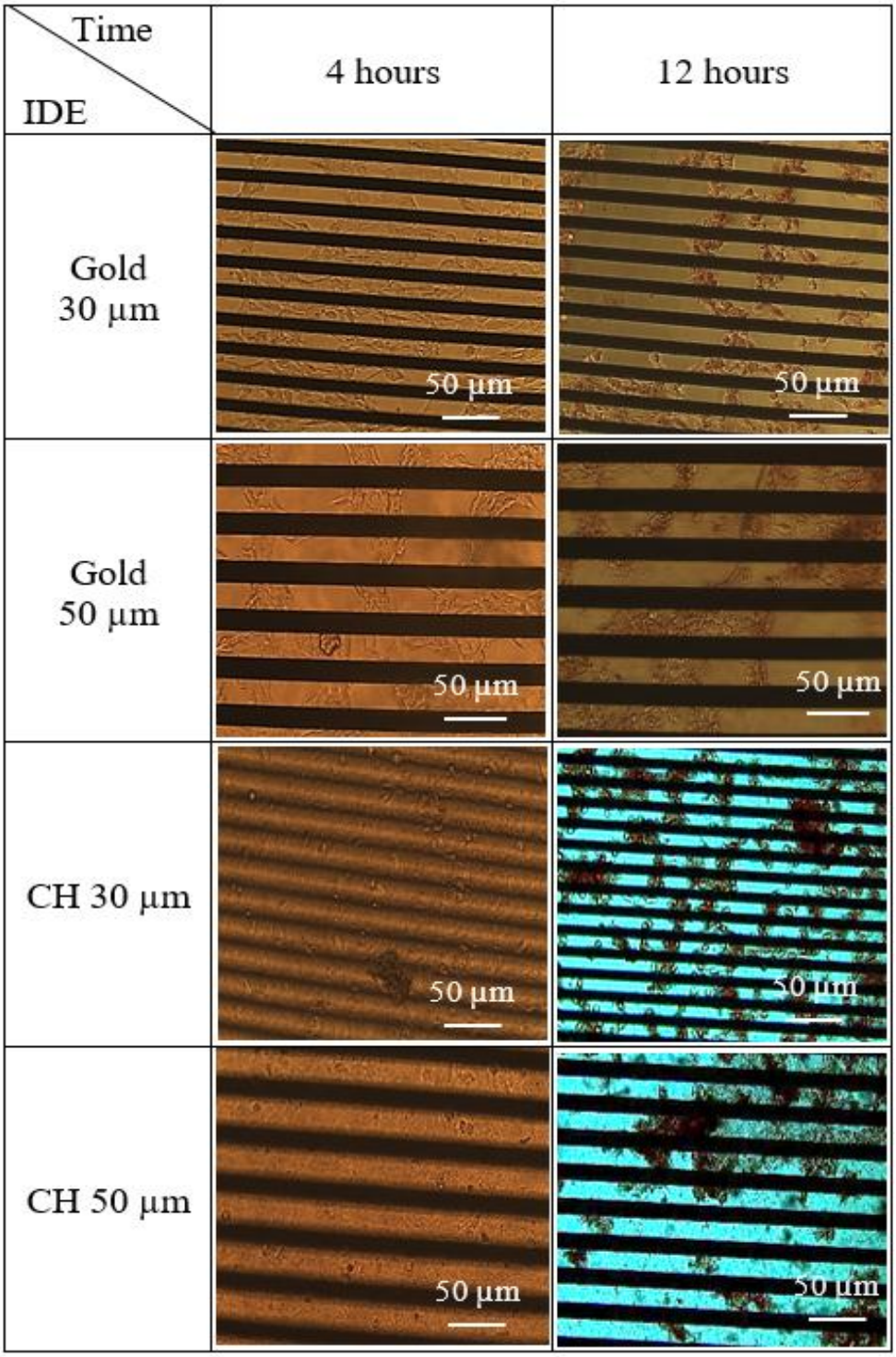

Figure 7.10: Phase contrast micrographs of C2C12 at 4 and 12 hours on 30 µm gold IDE, 50 µm gold IDE, 30 µm CH coated IDE and 50 µm CH coated IDE. Cells were exposed to DOX for the period shown.

7.3.4 Frequency optimisation for cell growth and death analysis

The impedance measurements of cells growth and apoptosis as a function of cell cultivation time on gold and CH biochips were conducted at frequencies ranging from 100 Hz to 1 MHz as shown in Figure 7.11. In preliminary stage of ECIS system, it is important to determine the optimum frequency for accurate analysis and interpretation of the data. This ideal frequency is a largest different between cell–free medium and cell–in medium system under the resistance versus frequency sweep graph [159].

The graphs in Figure 7.11 indicated that the presence of cells in the system induced the increasing of impedance magnitude across the frequencies. As cells grow over the electrode (see in Figure 7.9), they block the flow of electrical current which result an increase in impedance in the circuit [159], [241]. It can be seen that the greatest change in impedance after cells seeding occurs at the 100 Hz frequency from 3.97 kΩ to 4.27 kΩ for 30µm gold, from 3.02 kΩ to 3.85 kΩ for 50µm gold, from 3.61 kΩ to 3.99 kΩ for 30µm CH and from 3.07 kΩ to 3.30 kΩ for 50µm CH biochips. Therefore the impedance magnitude at the optimum frequency of 100 Hz was chosen for cell growth and death studies. The equivalent circuit of cells in CH system and time-impedance magnitude of C2C12 response at 100 Hz are presented in the Figure 7.12 and 7.13, respectively.

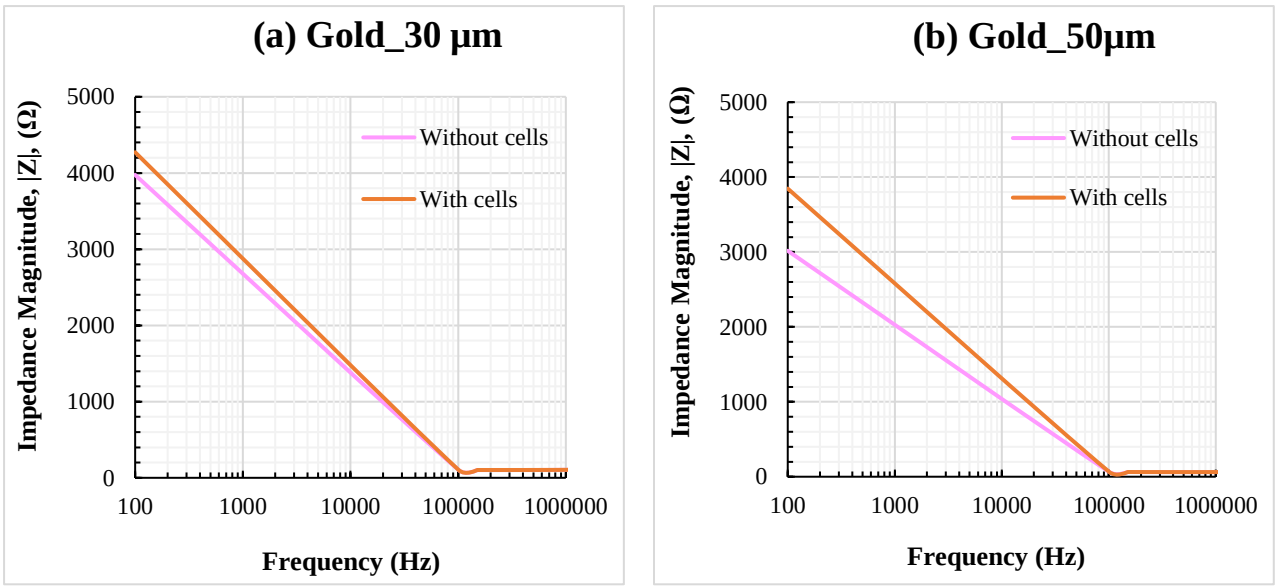

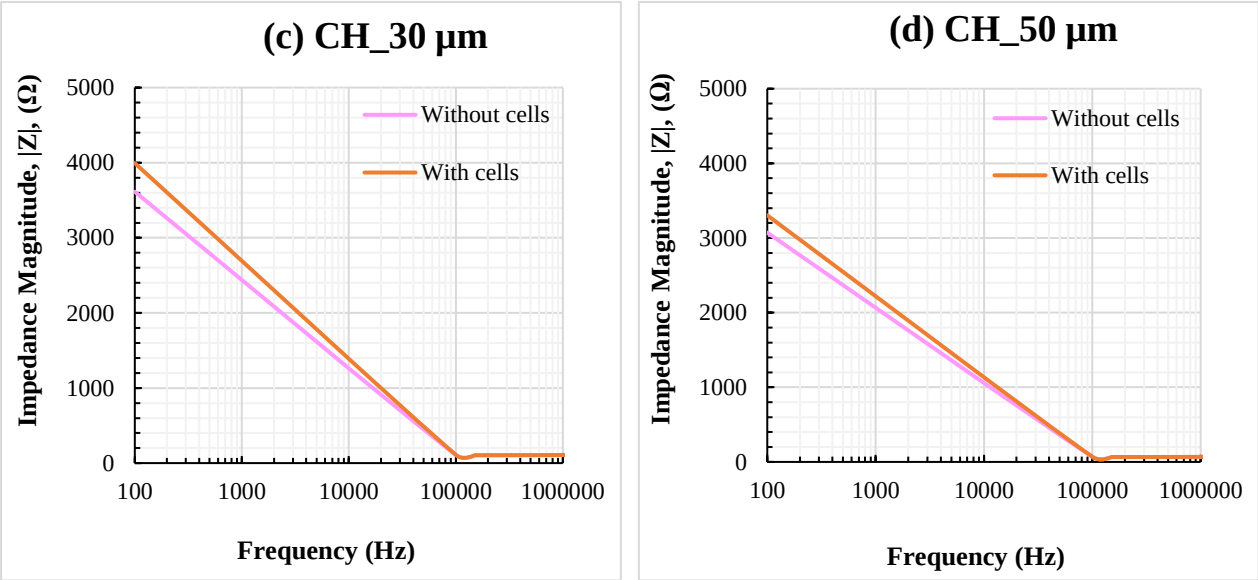

Figure 7.11: The impedance magnitude for cell growth on different dimensions of (a) gold biochip with dimensions 30 µm and (b) gold biochip with dimensions 50 µm, while (c) CH biochip with dimensions 30 µm and (d) CH biochip with dimensions 50 µm from frequency range of 100 Hz to 1 MHz. Results show that the highest changes in impedance occured at 100 Hz and this was used as the optimum frequency.

To represent the electric connection between cells intact on CH coated gold electrodes through culture medium, the equivalent circuit of Figure 7.7 must be expended and illustrated in Figure 7.12. The CH electrode–medium interface is in series with the passive electrical properties (capacitance (C_{CELL}) and resistance (R_{CELL}) are connected in parallel) of cell on electrode surface.

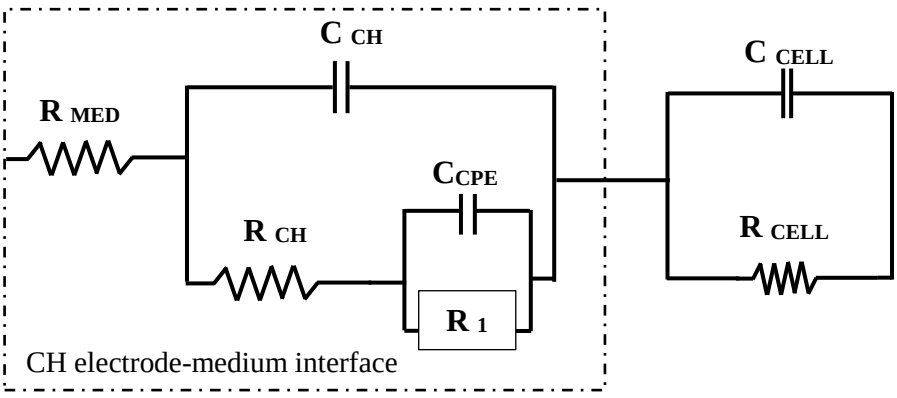

Figure 7.12: The equivalent circuit diagram for ECIS with C2C12 cells on CH coated IDE.

7.3.5 Impedimetric analysis of the C2C12 response on biochips at 100 Hz

The magnitude of the impedance changes during cell adhesion, proliferation and drug treatment at optimisation frequency of 100 Hz are plotted in Figure 7.13. In this research, the impedance analysis in terms of changes in impedance of myoblasts C2C12 response were devided into three phases: (I) cell attachment and spreading on the electrode surface, (II) cell proliferation and formation of monolayer morphology, and (III) cell shrinkage, death and detachment from the electrode surface.

Phase I in Figure 7.13 shows that the impedance magnitude on all substrates types has initially increased rapidly with time after the cell-seeding process. When the cells attach they start to restrict the current flow by spreading over the electrode and capacitance decreases in a linear fashion with the percentage of open area on the electrode. Hence, adhesion, spreading and proliferation can be quantified best, when recording capacitance at a frequency higher than 100 Hz, where the decrease in capacitance is direct proportional to the electrode coverage. Then, the magnitude of the impedance showed a very slow increase and maintained a constant value during the time period between 12 to 24 hours in phase II. These results are in agreement with that obtained in Figure 7.9 which revealed that C2C12 cells proliferate, reaching 90% confluence and form a monolayer morphology within 24 hours.

The assessment of the inflammation due to toxicity is a very important issue in developing effective and safe treatment for a variety of applications such as bone implantation, biomedical devices and artificial tissues. Impedance monitoring is a cost-effective and customised platform for screening drugs based on cellular apoptosis potentially in the development of medical implants. Impedance detection could be an effective approach for monitoring apoptosis-induced changes of cell functions in real time. The direct effects of DOX on the cultured C2C12 cells were shown in phase III where there is a notable decrease in impedance (Figure 7.13).

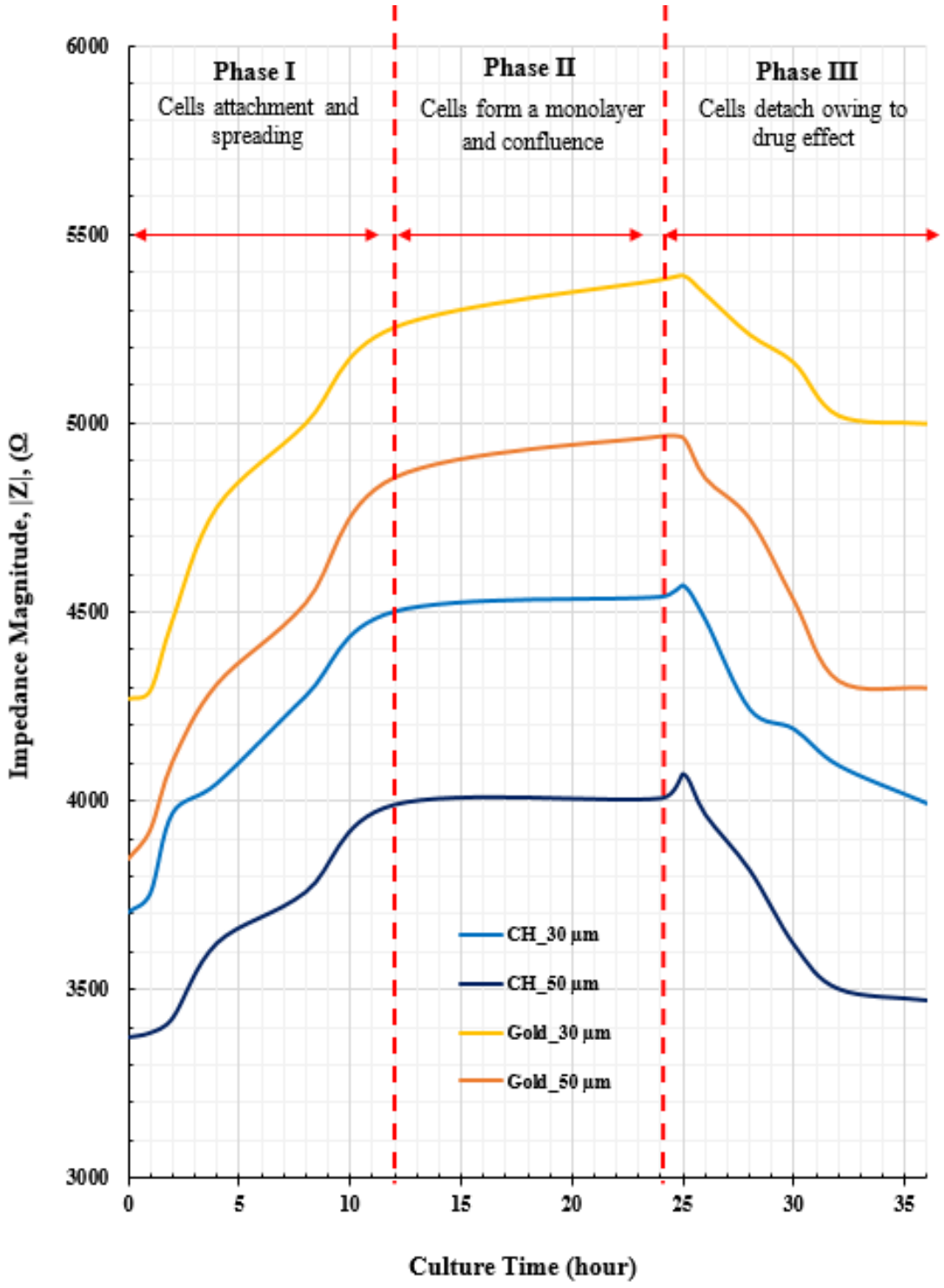

Figure 7.13: The impedance measurement of C2C12 cells monitored over 36 hours on 30 µm CH IDE, 30 µm gold IDE, 50 µm CH IDE, and 50 µm gold IDE graph. Phase I illustrates the cells' attachment and spreading on the electrode surface, causing an increase in the impedance. Phase II, in which the impedance keep increasing and reaches a constant value, correspond to the cells forming a monolayer morphology. Phase III indicates that the growth of C2C12 was inhibited by the addition of DOX.

The impedance values of the CH biochip exhibit a sharp decrease similar with gold biochip after four hours of DOX treatment. These results demonstrate that the DOX impairs C2C12 cell–substrate adhesion and increases the motility rate. After 12 hours of DOX treatement, the magnitude of the impedance reaches a steady state. This suggests that cell shinkaged, detachment and aggregation as a small cluster on the electrode is the result of the purposely introduced toxin. The trend of toxin treated established in this research is similar to that reported by Yu et al. [233]. They found that the impedance KYSE30 cancer cell in 0.01 M retinoic acid on nanoporous anodic alumina membrane was decreased with time. Overall, the data sets in Figure 7.13 show a good agreement with all optical images illustrated in Figures 7.9 and 7.10.

7.4 Conclusions

The ECIS technique has been applied to evaluate C2C12 cell attachment, spreading and apoptosis as a function of impedance. A testing platform with interdigitated electrodes was developed and was based on gold electrodes coated with CH. The developed ECIS chip was tested by detecting changes in the impedance as a function of time. Cell culture incubation and drug-induced impedance changes were conducted over a frequency range from 100 Hz to 1 MHz.

The presence of the CH layer on the gold electrodes, reduced the impedance magnitude from 4.27 kΩ to 3.70 kΩ for the 30 μm and from 3.85 kΩ to 3.37 kΩ for the 50 at a frequency of 100 Hz. This is due to the CH layer acting as a capacitor at low frequency and increasing in effective surface area. In addition, the phase angle of CH coated gold electrode decreased towards −90° below 10 kHz, which was dominated by the capacitive region, and was close to 0° above 10 kHz, showing a tendency to more resistive behaviour. The seeding of C2C12 cells on the CH electrodes exhibited a rapid increase in the real impedance signal after two to 12 hours of growth. These significant changes in impedance are correlated with the cells' adherence and the proliferation process. After this, the myoblasts formed a monolayer or reached confluency after 12 to 24 hours, resulting in an almost constant impedance value over that time period. In addition, toxicity testing was conducted to show the effects of toxin on myoblast

C2C12 adhesion and impedance. Changes in cell–electrode adherence response on both biochips were monitored for 12 hours. After four hours of exposure to toxin treatment, the results revealed a decreased in measured impedance of the CH coated electrodes with time and showed similar pattern with gold biochip. After 12 hours of DOX treatment, the impedance magnitude reached a steady state on the gold and CH coated biochips. This indicates that the cells are shrunken, possibly dead, and detached from the electrode. The results from this chapter provide a useful means for creating cell-impedance sensitive platform and using biologically active polymer coatings that can facilitate integration of the electronic active devices with a living system.

CHAPTER 8

Conclusions and Future Work

This chapter begins with a summary of the objectives that have been accomplished in this research. Then, potential future work is suggested for continuing research using the conductive bioimprint technique developed.

8.1 Conclusions

This thesis presents the development and characterisation of conductive bioimprints for cell-culture study. Conductive bioimprinting is a novel approach that combines replicating a 3D imprint of cellular morphology into a CP, named poly (3, 4-ethylenedioxythiophene): polystyrene sulfonate (PEDOT: PSS), by using a soft lithography technique. The conductive bioimprint is suitable as a cell-culture platform, enabling the monitoring of cell behaviour as a function of their conductivity.

There are four important objectives of this research identified as (a) to synthesise and optimise a CH based on PEDOT:PSS that can be utilised to replicate cell surface features at high resolution and fidelity, (b) to investigate the effects of chemical and surface modification on the electrical properties, swelling behaviour and cell growth, (c) to characterise the physicochemical properties of CH films such as wettability, biocompatibility, biodegradability, stretchability, chemical properties and (d) to demonstrate the feasibility of using electrical cell impedance sensing (ECIS) to monitor the C2C12 myoblast adherence, spreading, proliferation and motility on a CH biochip. The main challenge in the incorporation of a CP and hydrogel matrix in cell culture applications is that both of these materials are highly soluble in most common solvents and water. In spite of these difficulties with the material, this research has successfully

achieved most of the set goals. The major accomplishments of this work are described in the following paragraphs.

In this research work, a feasibility study was conducted first to employ glycerol as an additive and plasticiser in the CP to reduce the solubility and enhance the electrical properties of the PEDOT:PSS thin films. The results showed that glycerol significantly influenced film transparency, water contact angle, electrical conductivity and surface morphology of the doped PEDOT:PSS thin films. PEDOT:PSS is hydrophilic, so adding the glycerol produced a noticeable improvement in hydrophobicity, with the water contact angle increasing from 31.98° at 0% w/w to 52.94° at 4% w/w. It was found that the addition of glycerol changed the thickness and conductivity of the thin films from 90 nm to 125 nm and from 1.28 Scm^{-1} to 443 Scm^{-1} respectively. Furthermore, the 3D atomic force microscope (AFM) morphology images of plasticised PEDOT:PSS thin films showed significant changes in surface topography as the percentage of the glycerol increased in the PEDOT:PSS matrix. However, due to low viscosity and thin film thickness problems, the replication of cellular structures using plasticiser-assisted soft embossed (PASE) technique into conductive thin films has resulted in a loss of the micro- and nano-sized cellular details. To achieve the required material, a gelatin (A 300 Bloom porcine) was incorporated into the plasticised PEDOT:PSS solution to overcome those challenges. The gelatin was chosen because of its biocompatibility, biodegradability and water-solubility.

To ensure the CH mixture was able to replicate significant surface features of cells, the negative/positive replicas of the conductive and PDMS bioimprint substrates were compared with the direct cellular topography images. The AFM cross-section profiles of the mouse myoblast replicas showed that the conductive bioimprint conformed to more than 90% of the original cellular features down to micro- and nano-sized details of the PDMS master mould. Through these analyses, we validated that the fixed cells were faithfully replicated onto the conductive substrate, the process did not alter the cell morphologies and showed no distortion while the cells retained their structures.

The developed CH has promising potential as a neural electrode for biosensor applications. The chemical cross-linking process of the CH mixture results in a stable

gel structure with tuneable physicochemical properties of a conductive film. Microbial Transglutaminase (mTg) was found to crosslink with the conductive material and enhances its electrical conductivity from 10^{-6} to 1 Scm^{-1} and minimises water absorption. Moreover, the CH developed is biocompatible, as evidenced by the C2C12 cell attachment, growth and proliferation study after 24 hours of sedimentation. The CH substrate surface was further modified to become a more stimuli-responsive network for biomedical applications and implantable biomaterials devices. Since the substrate mechanics (e.g. stiffness and softness) and topography were recognised as having a strong influence on cell adhesion and cell-material interactions, conductive substrates with a flat surface, micropillars and bioimprints were used *in vitro* to investigate the cell–substrate interactions. Cell culture experiments clearly demonstrated that the C2C12 cells stained with crystal violet appeared to be more branched, have elongated shapes and adhered to the top of the micropillar substrate. In comparison with flat surfaces, the cultured cells grew randomly with the formation of large lamellipodium and short filopodium features. Indeed, cultured C2C12 cells on bioimprinted surfaces revealed that cells are very sophisticated in being able to differentiate between surface patterns and they can be guided to grow on cell-like features.

Numerous techniques were used in investigating the physicochemical properties of the CH as a soft electrode. The water contact angle is a parameter used to quantify the wettability of a CH surface. This property could also influence cell adhesion behaviour and the biocompatibility of the substrate to the living organism. The obtained water contact angles of the CH were analysed and found to promote wettability with contact angles between 53.2° and 67.7° whereas the PDMS substrate showed poor wettability with a contact angle of 113 ± 3.0°. In addition, the CP has quite similar surface energy as compared with glass and gold substrates which have a measured contact angle of 50.2° ± 1.7° and 62.2° ± 4.8°, respectively.

To identify the correlation between wettability of the conductive substrate and cells growth development, myoblast C2C12 cells were cultured on different biocompatible control substrates such as glass slides, gold and PDMS substrates. The biocompatibility analysis revealed that seeded myoblast C2C12 cells grew better on the CH substrate

than on the other substrates. The percentage of living cells on the CH exceeded 60% after 24 hours and reached 90% confluency after 48 hours.

The *in vitro* biodegradation test on the CH films was performed at temperature 37 ℃ in culture medium and showed a mass loss of 60% to 78% after culturing cells for one week. The tensile test showed the CH exhibited good stretchability, where the elastic modulus decreased from 77.87 ± 1.12 MPa for 2% to 1.11 ± 0.10 MPa for 6% films.

The Ultraviolet visible spectroscopy (UV-Vis) measurements revealed significant increments in absorption spectra and changes in the colours of the CH films from transparent to opaque as the concentrations of the CP increased.

The X-ray photoelectron spectroscopy (XPS) study confirmed the existence of conducting polymer PEDOT: PSS elements such as oxygen at the binding energy of 530–550 eV, carbon at around 285 eV and a sulfur peak at the binding energy of around 165–163 eV. In addition, a nitrogen peak at binding energy of 397–400 eV represented multiple amine groups of gelatin in the CH matrix.

Fourier transform infrared spectroscopy (FTIR) showed typical characteristics of the gelatin, glycerol and PEDOT: PSS in the conductive network. In thermogravimetric analysis (TGA) the set point weight loss of 50% for the 2%, 3%, 4% and 6% concentrations of the CH films started at temperatures of 285 ℃, 85 ℃, 100 ℃ and 195 ℃, respectively. From all chemical analyses we confirmed that the appropriate expected components were present in the respective films.

The cell-related impedance signals measured with AC electric fields were analysed as a direct reflection of cell adhesion and toxin sensitivity in real time on the CH biochips. The magnitude of the impedance of the CH biochip in a cell-free medium (DMEM) exhibits a similar pattern with the control biochip but decreased from 4.27 kΩ to 3.70 kΩ for the 30 × 30 µm biochip and from 3.85 kΩ to 3.37 kΩ for the 50 × 50 µm biochip at a frequency of 100 Hz. On the other hand, the real impedance signal of the CH electrodes when measured with C2C12 cells exhibited a rapid increase in impedance after two to 12 hours of cell growth, owing to the cells' adherence and proliferation

process. Then, when the myoblasts started to form a monolayer or reached confluency after 12 to 24 hours, the impedance value become constant. In investigating the toxin effects on the myoblast C2C12 adhesion, the doxorubicin (DOX) was used as a toxicant agent. The results show that the impedance magnitude a rapidly decreased after four hours of toxin treatment due to the weakened cell–substrate contacts and lower cell coverage on the electrode surface. After 12 hours, cells were shrunken, dead, clumping together and completely detached from the sensor's electrode surface.

The CH material with cell-like patterned surfaces that was developed offers high replication resolution, good electrical conductivity, biocompatibility, stretchability and biodegradability. Moreover, the main advantage of using cell impedance spectroscopy to examine cell behaviour in real time helps researchers in better understanding cellular events next to the implants. Possible applications of conductive bioimprint are foreseen in the field of biosensing and bio actuation in the biomedical field, for example as smart substrates for cell culturing, and enhancing bone implant healing with electrical stimuli.

8.2 Future work

This thesis has provided the synthesis and characterisation of a new technique named conductive bioimprinting based on PEDOT:PSS and has multifunctional properties for use as a cell-culture platform. However, further optimisation of the conductive bioimprint is required to enable a higher performance for implantable biochip applications. Some suggestions for future research and development are presented in sections 8.2.1 and 8.2.2.

8.2.1. Organ-on-chip

With growing interest in 3D printing and its application in organs-on-chip, in tissue engineering, drug screening and bone implants, conductive bioimprinting might offer additional important coatings with cell-like features that facilitate cell guiding and spreading. Another important area of applications that might be investigated further is

the development of conductive bioimprints as biosensors with a wireless platform for allowing medical personnel or patients to monitor and diagnose potential infection or inflammation surrounding an orthopaedic implant under the patient's skin. The radio frequency identification (RFID) technology is the best method for the physiological data transmission and electrical power of the biosensor because it can permits the operation in small size, cost effective and low applied potential. The system developed allows a device to receive a signal from the sensor, perform its primary processing and to transmit data to the target device such as computer, smartphone, tablet or any wireless telecommunications device using a Bluetooth interface.

8.2.2 Integration of conductive bioimprints with microfluidics in an ECIS System

The integration of a microfluidics system with an embedded conductive bioimprint biochip using electric cell–substrate impedance sensing (as illustrated in Figure 8.1) is also another area of interest that can be explored further. In conventional methods, microscopically, detection of indicative cellular components (e.g. DNA) and live/dead fluorescent dye staining are commonly used for assay analysis based on cell culture. Alternatively, the proposed integrated system provides a real-time and non-invasive technique that significantly helps provide a better understanding of the in *vivo* condition in some cases such as drug delivery testing on the cellular topography or monitoring cellular response in a 3D environment. The advantages of combining microfluidic flow cells with conductive bioimprints are: high detection sensitivity, small volume handling, low contamination during bacterial growth and ability to mimic the native cellular microenvironment.

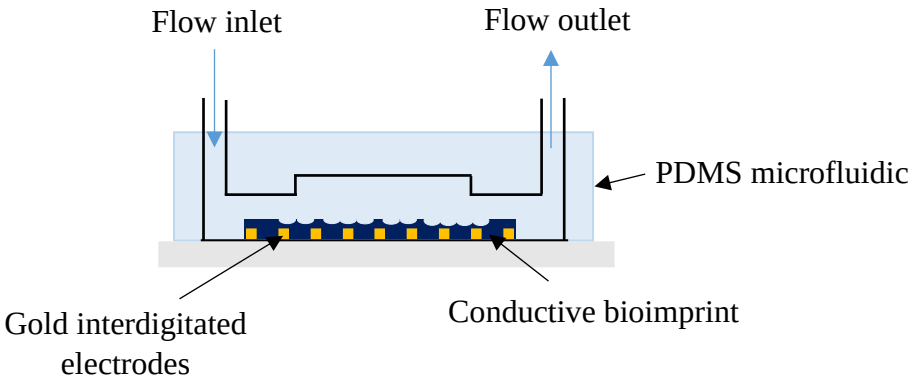

Figure 8.1: Illustration schematic of the integrated ECIS system embedded conductive bioimprint biochip with the inlet and outlet microchannel of a PDMS microfluidic chamber.

8.3 Research contribution

In this work, we present for the first time the development of conductive bioimprints with cell-like surface features based on PEDOT: PSS mixed with gelatin and glycerol using a soft lithography technique. This conductive bioimprint has been used for monitoring cell–surface interactions, growth, adhesion, spreading, morphology, and motility with respect to the electrical conductivity. The developed conductive bioimprint has shown very high replication fidelity, good electrical conductivity, biocompatibility, elasticity and biodegradability. Conductive bioimprints might be used in tissue repair and regeneration, medical implants and bioelectronics sensing.

References

[1] D. A. Puleo and A. Nanci, “Understanding and controlling the bone-implant interface.,” *Biomaterials*, vol. 20, pp. 2311–2321, 1999.

[2] K. W. Millsap, R. Bos, H. C. Van der Mei, and H. J. Busscher, “Adhesive interactions between voice prosthetic yeast and bacteria on silicone rubber in the absence and presence of saliva,” *Antonie van Leeuwenhoek, Int. J. Gen. Mol. Microbiol.*, vol. 79, pp. 337–343, 2001.

[3] R. M. Donlan and J. W. Costerton, “Biofilms: Survival Mechanisms of Clinically Relevant Microorganisms.,” *Clin.Microbiol. Rev.*, vol. 15, no. 2, pp. 167–193, 2002.

[4] K. Kulangara and K. W. Leong, “Substrate topography shapes cell function,” *Soft Matter*, vol. 5, no. 21, p. 4072, 2009.

[5] E. Martínez, E. Engel, J. A. Planell, and J. Samitier, “Effects of artificial micro- and nano-structured surfaces on cell behaviour,” *Ann. Anat.*, vol. 191, pp. 126–135, 2009.

[6] L. H. Tan, P. H. Sykes, M. M. Alkaisi, and J. J. Evans, “Cell-like features imprinted in the physical nano- and micro- topography of the environment modify the responses to anti-cancer drugs of endometrial cancer cells,” *Biofabrication*, vol. 9, no. 015017, pp. 1–10, 2017.

[7] L. H. Tan, P. H. Sykes, M. M. Alkaisi, and J. J. Evans, “The characteristics of ishikawa endometrial cancer cells are modified by substrate topography with cell-like features and the polymer surface,” *Int. J. Nanomedicine*, vol. 10, pp. 4883–4895, 2015.

[8] L. M. Murray, V. Nock, M. M. Alkaisi, J. J. M. Lee, and T. B. F. Woodfield, “Fabrication of polymeric substrates with micro- and nanoscale topography bioimprinted at progressive cell morphologies,” *J. Vac. Sci. Technol. B*, vol. 30, no. 6, p. 06F902, 2012.

[9] L. M. Murray, V. Nock, J. J. Evans, and M. M. Alkaisi, “The use of substrate materials and topography to modify growth patterns and rates of differentiation of muscle cells,” *J. Biomed. Mater. Res. - Part A*, vol. 104A, no. 7, pp. 1638–1645, 2016.

[10] D. Qin, Y. Xia, and G. M. Whitesides, “Soft lithography for micro- and nanoscale patterning.,” *Nat. Protoc.*, vol. 5, no. 3, pp. 491–502, 2010.

[11] D. B. Wolfe, J. C. Love, and G. M. Whitesides, “Nanostructures Replicated by Polymer Molding,” *Dekker Encycl. Nanosci. Nanotechnol.*, pp. 2657–2667, 2004.

[12] M. Bongo *et al.*, “PEDOT:gelatin composites mediate brain endothelial cell adhesion,” *J. Mater. Chem. B*, vol. 1, no. 31, p. 3860, 2013.

[13] A. M.-D. Wan *et al.*, “3D conducting polymer platforms for electrical control of protein conformation and cellular functions,” *J. Mater. Chem. B*, vol. 3, no. 25, pp. 5040–5048, 2015.

[14] H. Okuzaki, S. Takagi, F. Hishiki, and R. Tanigawa, “Ionic liqiud/

polyurethane/PEDOT : PSS composites for electro-active polymer actuators," *Sensors Actuators B. Chem.*, vol. 194, pp. 59–63, 2014.

[15] D. J. Lipomi, J. A. Lee, M. Vosgueritchian, B. C. Tee, J. A. Bolander, and Z. Bao, "Electronic Properties of Transparent Conductive Films of PEDOT:PSS on Stretchable Substrates," *Chem. Mater.*, vol. 24, no. 2, pp. 373–382, 2012.

[16] J. D. Madden, R. A. Cush, T. S. Kanigan, and I. W. Hunter, "Fast contracting polypyrrole actuators," *Synth. Met.*, vol. 113, no. 1–2, pp. 185–192, 2000.

[17] E. Jager, "Conducting Polymer Actuators for Medical Devices and Cell Mechanotransduction Conducting," *IEEE/ASME Int. Conf. Adv. Intell. Mechatronics*, pp. 1661–1666, 2013.

[18] E. Smela, "Conjugated Polymer Actuators for Biomedical Applications," *Adv. Mater.*, vol. 15, no. 6, pp. 481–494, Mar. 2003.

[19] D. Khodagholy *et al.*, "Highly conformable conducting polymer electrodes for in vivo recordings," *Adv. Mater.*, vol. 23, no. 36, pp. 268–272, 2011.

[20] N. K. Guimard, N. Gomez, and C. E. Schmidt, "Conducting polymers in biomedical engineering," *Prog. Polym. Sci.*, vol. 32, no. 8–9, pp. 876–921, Aug. 2007.

[21] S. Sirivisoot, R. Pareta, and T. J. Webster, "Electrically controlled drug release from nanostructured polypyrrole coated on titanium.," *Nanotechnology*, vol. 22, no. 8, p. 085101, Feb. 2011.

[22] F. Yıldırımoğlu, F. Arslan, S. Cete, and A. Yaşar, "Preparation of a polypyrrole-polyvinylsulphonate composite film biosensor for determination of cholesterol based on entrapment of cholesterol oxidase.," *Sensors (Basel).*, vol. 9, no. 8, pp. 6435–45, Jan. 2009.

[23] B. D. Malhotra, A. Chaubey, and S. P. Singh, "Prospects of conducting polymers in biosensors.," *Anal. Chim. Acta*, vol. 578, no. 1, pp. 59–74, Sep. 2006.

[24] S. M. Richardson-Burns, J. L. Hendricks, B. Foster, L. K. Povlich, D.-H. Kim, and D. C. Martin, "Polymerization of the conducting polymer poly(3,4-ethylenedioxythiophene) (PEDOT) around living neural cells.," *Biomaterials*, vol. 28, no. 8, pp. 1539–52, Mar. 2007.

[25] A. S. Karimullah, D. R. S. Cumming, M. Riehle, and N. Gadegaard, "Development of a conducting polymer cell impedance sensor," *Sensors Actuators B Chem.*, vol. 176, pp. 667–674, Jan. 2013.

[26] R. Balint, N. J. Cassidy, and S. H. Cartmell, "Conductive polymers: Towards a smart biomaterial for tissue engineering," *Acta Biomater.*, vol. 10, no. 6, pp. 2341–2353, 2014.

[27] K. Gilmore, A. J. Hodgson, B. Luan, C. J. Small, and G. G. Wallace, "Preparation of Hydrogel / Conducting Polymer Composites," *Polym. Gels Networks*, vol. 2, pp. 135–143, 1994.

[28] M. Lefebvre, Z. Qi, D. Rana, and P. G. Pickup, "Chemical Synthesis, Characterization, and Electrochemical Studies of Poly(3,4-ethylenedioxythiophene)/Poly(styrene-4-sulfonate) Composites," *Chem. Mater.*, vol. 11, no. 2, pp. 262–268, 1999.

[29] M. Nikolou and G. G. Malliaras, “Applications of poly (3,4-ethylenedioxythiophene) doped with poly(styrene sulfonic acid) transistors in chemical and biological sensors,” *Chem. Rec.*, vol. 8, no. 1, pp. 13–22, 2008.

[30] J. F. Li *et al.*, “Improving the performance of perovskite solar cells with glycerol-doped PEDOT:PSS buffer layer,” *Chinese Phys. B*, vol. 25, no. 2, 2015.

[31] R. Meier, C. Birkenstock, C. M. Palumbiny, and P. Müller-Buschbaum, “Efficiency-improved organic solar cells based on plasticizer assisted soft embossed PEDOT:PSS layers,” *Phys. Chem. Chem. Phys.*, vol. 14, no. 43, p. 15088, 2012.

[32] L. J. del Valle *et al.*, “Cellular adhesion and proliferation on poly(3,4-ethylenedioxythiophene): Benefits in the electroactivity of the conducting polymer,” *Eur. Polym. J.*, vol. 43, no. 6, pp. 2342–2349, Jun. 2007.

[33] L. Xia, Z. Wei, and M. Wan, “Conducting polymer nanostructures and their application in biosensors,” *J. Colloid Interface Sci.*, vol. 341, no. 1, pp. 1–11, Sep. 2010.

[34] D. Mawad, A. Lauto, and G. G. Wallace, “Polymeric Hydrogels as Smart Biomaterials,” pp. 19–45, 2016.

[35] M. Yazdimamaghani, M. Razavi, M. Mozafari, D. Vashaee, H. Kotturi, and L. Tayebi, “Biomineralization and biocompatibility studies of bone conductive scaffolds containing poly(3,4-ethylenedioxythiophene):poly(4-styrene sulfonate) (PEDOT:PSS),” *J. Mater. Sci. Mater. Med.*, vol. 26, no. 12, p. 274, 2015.

[36] A. Shahini *et al.*, “3D conductive nanocomposite scaffold for bone tissue engineering,” *Int. J. Nanomedicine*, vol. 9, no. 1, pp. 167–181, 2013.

[37] H. Baniasadi, A. R. S. A, and S. Mashayekhan, “International Journal of Biological Macromolecules Fabrication and characterization of conductive chitosan / gelatin-based scaffolds for nerve tissue engineering,” *Int. J. Biol. Macromol.*, vol. 74, pp. 360–366, 2015.

[38] G. Justin and A. Guiseppi-Elie, “Electroconductive Blends of Poly(HEMA-co-PEGMA-co-HMMAco-SPMA) and Poly(Py- co-PyBA): In Vitro Biocompatibility,” *J. Bioact. Compat. Polym.*, vol. 25, no. 2, pp. 121–140, 2010.

[39] S. Brahim, G. Slaughter, and A. Guiseppi-Elie, “Electrical and Electrochemical Characterization of Electroconductive PPy-p(HEMA) Composite Hydrogels,” *Proc. SPIE - Int. Soc. Opt. Eng.*, vol. 5053, no. August 2003, pp. 1–13, 2003.

[40] J. Yang, G. Choe, S. Yang, H. Jo, and J. Y. Lee, “Polypyrrole-incorporated conductive hyaluronic acid hydrogels,” *Biomater. Res.*, vol. 20, no. 1, p. 31, 2016.

[41] C. Kleber, M. Bruns, K. Lienkamp, J. Rühe, and M. Asplund, “An interpenetrating, microstructurable and covalently attached conducting polymer hydrogel for neural interfaces,” *Acta Biomater.*, vol. 58, pp. 365–375, 2017.

[42] R. A. Green *et al.*, “Conductive Hydrogels: Mechanically Robust Hybrids for Use as Biomaterials,” *Macromol. Biosci.*, vol. 12, no. 4, pp. 494–501, 2012.

[43] D. H. Kim, J. A. Wiler, D. J. Anderson, D. R. Kipke, and D. C. Martin,

"Conducting polymers on hydrogel-coated neural electrode provide sensitive neural recordings in auditory cortex," *Acta Biomater.*, vol. 6, no. 1, pp. 57–62, 2010.

[44] L. M. Lira and S. I. Córdoba De Torresi, "Conducting polymer-hydrogel composites for electrochemical release devices: Synthesis and characterization of semi-interpenetrating polyaniline- polyacrylamide networks," *Electrochem. commun.*, vol. 7, no. 7, pp. 717–723, 2005.

[45] V. Guarino, M. A. Alvarez-Perez, A. Borriello, T. Napolitano, and L. Ambrosio, "Conductive PANi/PEGDA Macroporous Hydrogels For Nerve Regeneration," *Adv. Healthc. Mater.*, vol. 2, no. 1, pp. 218–227, 2013.

[46] W. Zhao, L. Glavas, K. Odelius, U. Edlund, and A. C. Albertsson, "Facile and green approach towards electrically conductive hemicellulose hydrogels with tunable conductivity and swelling behavior," *Chem. Mater.*, vol. 26, no. 14, pp. 4265–4273, 2014.

[47] J. Huang, P. F. Miller, J. S. Wilson, A. J. De Mello, J. C. De Mello, and D. D. C. Bradley, "Investigation of the effects of doping and post-deposition treatments on the conductivity, morphology, and work function of poly(3,4-ethylenedioxythiophene)/poly(styrene sulfonate) films," *Adv. Funct. Mater.*, vol. 15, no. 2, pp. 290–296, 2005.

[48] S. Brahim and A. Guiseppi-Elie, "Electroconductive hydrogels: Electrical and electrochemical properties of polypyrrole-poly(HEMA) composites," *Electroanalysis*, vol. 17, no. 7, pp. 556–570, 2005.

[49] L. M. Murray, "Influence of substrate topography and materials on behaviour of biological cells," University of Canterbury, Christchurch, 2012.

[50] J. J. Muys *et al.*, "Cellular transfer and AFM imaging of cancer cells using Bioimprint.," *J. Nanobiotechnology*, vol. 4, no. 1, pp. 1–10, Jan. 2006.

[51] J. Muys, M. Alkaisi, and J. Evans, "Bioimprint," in *International Conference on Nanoscience and Nanotechnology*, 2006, vol. 3, no. 6, pp. 294–297.

[52] J. J. Muys, "Cellular Analysis by Atomic Force Microscopy," Univeristy of Canterbury,Christchurch, 2006.

[53] F. Samsuri, M. M. Alkaisi, J. J. Evans, K. Chitcholtan, and J. S. Mitchell, "Detection of changes in cell membrane structures using the Bioimprint technique," *Microelectron. Eng.*, vol. 88, no. 8, pp. 1871–1874, Aug. 2011.

[54] Fahmi B . Samsuri, "Single Cell analysis using Atomic Force Microscopy (AFM)," University of Canterbury, Christchurch, 2010.

[55] L. J. Guo, "Recent progress in nanoimprint technology and its applications," *J. Phys. D. Appl. Phys.*, vol. 37, no. 11, pp. R123–R141, 2004.

[56] V. Nock, L. Murray, F. Samsuri, M. M. Alkaisi, and J. J. Evans, "Microfluidic arrays for bioimprint of cancer cells," *Microelectron. Eng.*, vol. 88, pp. 1828–1831, Aug. 2011.

[57] V. Nock, "Control and Measurement of Oxygen in Microfluidic Bioreactors," University of Canterbury, Christchurch, 2009.

[58] I. Mutreja, T. B. F. Woodfield, S. Sperling, V. Nock, J. J. Evans, and M. M. Alkaisi, "Positive and negative bioimprinted polymeric substrates: new platforms for cell culture," *Biofabrication*, vol. 7, no. 2, p. 025002, 2015.

[59] A. Hashemi, I. Mutreja, M. M. Alkaisi, V. Nock, and M. Azam Ali, "Fabrication of free-standing casein devices with micro- and nanostructured regular and bioimprinted surface features," *J. Vac. Sci. Technol. B*, vol. 33, no. 6, p. 06F901, 2015.

[60] L. M. Murray, V. Nock, J. J. Evans, and M. M. Alkaisi, "Bioimprinted polymer platforms for cell culture using soft lithography," *J. Nanobiotechnology*, vol. 12, no. 60, pp. 1–9, 2014.

[61] H. G. Craighead, C. D. James, and a M. P. Turner, "Chemical and topographical patterning for direct cell attachment," *Curr. Opin. Solid State Mater. Sci.*, vol. 5, no. 2–3, pp. 177–184, 2001.

[62] K. Anselme, L. Ploux, and A. Ponche, "Cell/Material Interfaces: Influence of Surface Chemistry and Surface Topography on Cell Adhesion," *J. Adhes. Sci. Technol.*, vol. 24, pp. 831–852, 2010.

[63] A. A. Khalili and M. R. Ahmad, "A Review of cell adhesion studies for biomedical and biological applications," *Int. J. Mol. Sci.*, vol. 16, no. 8, pp. 18149–18184, 2015.

[64] B. M. Gumbiner, "Cell adhesion: The molecular basis of tissue architecture and morphogenesis," *Cell*, vol. 84, no. 3, pp. 345–357, 1996.

[65] G. Sagvolden, I. Giaever, E. O. Pettersen, and J. Feder, "Cell adhesion force microscopy," *Proc. Natl. Acad. Sci. U. S. A.*, vol. 96, no. 2, pp. 471–476, 1999.

[66] K. Anselme *et al.*, "The relative influence of the topography and chemistry of TiAl6V4 surfaces on osteoblastic cell behaviour," *Biomaterials*, vol. 21, no. 15, pp. 1567–1577, 2000.

[67] L. Wang, Y. Ding, X. Guo, and Q. Zhao, "Role and mechanism of vascular cell adhesion molecule-1 in the development of rheumatoid arthritis," *Exp. Ther. Med.*, vol. 10, no. 3, pp. 1229–1233, 2015.

[68] S. Huang and D. E. Ingber, "The structural and mechanical complexity of cell growth control," *Nat. Cell Biol.*, vol. 1, no. 5, pp. E131–E138, 1999.

[69] H. Perinpanayagam, R. Zaharias, C. Stanford, R. Brand, J. Keller, and G. Schneider, "Early cell adhesion events differ between osteoporotic and non-osteoporotic osteoblasts," *J. Orthop. Res.*, vol. 19, no. 6, pp. 993–1000, 2001.

[70] M. A. Schwartz and D. W. DeSimone, "Cell adhesion receptors in mechanotransduction," *Curr. Opin. Cell Biol.*, vol. 20, no. 5, pp. 551–556, 2008.

[71] J. E. Murphy-Ullrich, "The de-adhesive activity of matricellular proteins: Is intermediate cell adhesion an adaptive state?," *J. Clin. Invest.*, vol. 107, no. 7, pp. 785–790, 2001.

[72] M. A. Wozniak, K. Modzelewska, L. Kwong, and P. J. Keely, "Focal adhesion regulation of cell behavior," *Biochim. Biophys. Acta - Mol. Cell Res.*, vol. 1692, no. 2–3, pp. 103–119, 2004.

[73] N. J. Hallab, K. J. Bundy, K. O'Connor, R. L. Moses, and J. J. Jacobs, "Evaluation of Metallic and Polymeric Biomaterial Surface Energy and Surface Roughness Characteristics for Directed Cell Adhesion," *Tissue Eng.*, vol. 7, no. 1, pp. 55–71, 2001.

[74] A. F. V. O. N. Recum *et al.*, "Surface Roughness, Porosity, and Texture as Modifiers of Cellular Adhesion," *Tissue Eng.*, vol. 2, no. 4, pp. 241–253, 1996.

[75] R. G. Richards, "Implant Surfaces: Do they have any relevance to the surgeon?," *AO Dialogue*, vol. 07, no. 01, pp. 20–24, 2007.

[76] R. G. . Harrison, "On the Stereotropism of Embryonic Cells," vol. 34, no. 870, pp. 279–281, 1911.

[77] K. L. Menzies and L. Jones, "The impact of contact angle on the biocompatibility of biomaterials," *Optom. Vis. Sci.*, vol. 87, no. 6, pp. 387–399, 2010.

[78] S. Sirivisoot, "Biosensors as Implantable Medical Devices for Personalized Medicine," *J. Biosens. Bioelectron.*, vol. 3, no. 2, p. 6210, 2012.

[79] J. Ponmozhi, C. Frias, T. Marques, and O. Frazão, "Smart sensors/actuators for biomedical applications: Review," *Measurement*, vol. 45, no. 7, pp. 1675–1688, Aug. 2012.

[80] a Graham and M. Moo-Young, "Biosensors: recent trends.," *Biotechnol. Adv.*, vol. 3, no. 2, pp. 209–18, Jan. 1985.

[81] B. D. Malhotra, R. Singhal, A. Chaubey, S. K. Sharma, and A. Kumar, "Recent trends in biosensors," *Curr. Appl. Phys.*, vol. 5, no. 2, pp. 92–97, 2005.

[82] T. M.-H. Lee, "Over-the-Counter Biosensors: Past, Present, and Future," *Sensors*, vol. 8, no. 9, pp. 5535–5559, Sep. 2008.

[83] A. Hasan *et al.*, "Recent advances in application of biosensors in tissue engineering," *Biomed Res. Int.*, vol. 2014, pp. 1–46, 2014.

[84] D. D. Borole, U. R. Kapadi, P. P. Mahulikar, and D. G. Hundiwale, "Conducting polymers: An emerging field of biosensors," *Des. Monomers Polym.*, vol. 9, no. 1, pp. 1–11, 2006.

[85] P. Mehrotra, "Biosensors and their applications - A review," *J. Oral Biol. Craniofacial Res.*, vol. 6, no. 2, pp. 153–159, 2016.

[86] I. E. Tothill, "Biosensors developments and potential applications in the agricultural diagnosis sector," *Comput. Electron. Agric.*, vol. 30, no. 1–3, pp. 205–218, 2001.

[87] J. O. Esteves-Villanueva, H. Trzeciakiewicz, and S. Martic, "A protein-based electrochemical biosensor for detection of tau protein, a neurodegenerative disease biomarker.," *Analyst*, vol. 139, no. 11, pp. 2823–31, Jun. 2014.

[88] I. R. De Corcuera and R. P. Cavalieri, "Biosensors," *Ency*, pp. 119–123, 2003.

[89] L. C. Clark and C. Lyons, "Electrode systems for continouns monitoring in cardiovascular surgery," *Ann. New York Acad. Sci.*, vol. 102, no. 1, pp. 29–45, 1962.

[90] A. R. Inc., “Biosensors Market Outlook To 2024 : Key Product Categories,” 2017.

[91] S. Malhotra, A. Verma, N. Tyagi, and V. Kumar, “Biosensors : Principle , Types and Applications,” *Int. J. Adv. Res. Innov. Ideas Educ.*, vol. 3, no. 2, pp. 3639–3644, 2017.

[92] D. R. Thévenot, K. Toth, R. A. Durst, and G. S. Wilson, “Electrochemical biosensors: Recommended definitions and classification,” *Biosensors and Bioelectronics*, vol. 16, no. 1–2. pp. 121–131, 2001.

[93] T. Vo-Dinhn, “Biosensors and biochips,” in *BioMEMS and biomedical nanotechnology*, 2006, pp. 1–20.

[94] V. Gaudin, “Advances in biosensor development for the screening of antibiotic residues in food products of animal origin - A comprehensive review.,” *Biosens. Bioelectron.*, vol. 90, pp. 363–377, 2017.

[95] J. George G. Guilbault, Joseph G. Montalvo, “A Urea-Specific Enzyme Electrode,” *J. Am. Chem. Soc.*, vol. 91, no. 8, pp. 2164–2165, 1969.

[96] A. L. Kadilak, Y. Liu, S. Shrestha, J. R. Bernard, W. E. Mustain, and L. M. Shor, “Selective deposition of chemically-bonded gold electrodes onto PDMS microchannel side walls,” *J. Electroanal. Chem.*, vol. 727, pp. 141–147, 2014.

[97] Y. Li, H. J. Schluesener, and S. Xu, “Gold nanoparticle-based biosensors,” *Gold Bull.*, vol. 43, no. 1, pp. 29–41, 2010.

[98] S. Pandit, D. Dasgupta, N. Dewan, and P. Ahmed, “Nanotechnology based biosensors and its application,” *Pharma Innov. J. TPI*, vol. 5, no. 6, pp. 18–25, 2016.

[99] H. Fayazfar, A. Afshar, M. Dolati, and A. Dolati, “DNA impedance biosensor for detection of cancer , TP53 gene mutation , based on gold nanoparticles /aligned carbon nanotubes modified electrode,” *Anal. Chim. Acta*, vol. 836, pp. 34–44, 2014.

[100] M. Holzinger, A. Le Goff, and S. Cosnier, “Nanomaterials for biosensing applications: a review,” *Front. Chem.*, vol. 2, p. 63, 2014.

[101] C.-M. Tîlmaciu and M. C. Morris, “Carbon nanotube biosensors,” *Front. Chem.*, vol. 3, p. 59, 2015.

[102] C. B. Jacobs, M. J. Peairs, and B. J. Venton, “Review: Carbon nanotube based electrochemical sensors for biomolecules,” *Anal. Chim. Acta*, vol. 662, no. 2, pp. 105–127, 2010.

[103] S. Iijima, “Helical microtubules of graphitic carbon Sumio lijima Electron beam,” *Nature*, vol. 3, pp. 56–58, 1991.

[104] S. Iijima and T. Ichihashi, “Single-shell carbon nanotubes of 1-nm diameter,” *Nature*, vol. 363, no. 6430, pp. 603–605, 1993.

[105] J. Wang, “Carbon-Nanotube Based Electrochemical Biosensors: A Review,” *Electroanalysis*, vol. 17, no. 1, pp. 7–14, Jan. 2005.

[106] C. N. R. Rao, B. C. Satishkumar, A. Govindaraj, and M. Nath, “Nanotubes,” *ChemPhysChem*, vol. 2, no. 2, pp. 78–105, 2001.

[107] S. Sirivisoot and T. J. Webster, “Multiwalled carbon nanotubes enhance electrochemical properties of titanium to determine in situ bone formation.,” *Nanotechnology*, vol. 19, no. 29, p. 295101, Jul. 2008.

[108] A. Abarrategi *et al.*, “Multiwall carbon nanotube scaffolds for tissue engineering purposes.,” *Biomaterials*, vol. 29, no. 1, pp. 94–102, Jan. 2008.

[109] X. D. and P. C. Yuxin Liu, “Biological and chemical sensors based on graphene materials,” *UPB Sci. Bull. Ser. B Chem. Mater. Sci.*, vol. 74, no. 4, pp. 127–136, 2012.

[110] L. Wang, Q. Xiong, F. Xiao, and H. Duan, “2D nanomaterials based electrochemical biosensors for cancer diagnosis,” *Biosens. Bioelectron.*, vol. 89, pp. 136–151, 2017.

[111] M. Pumera, “Graphene in biosensing,” *Mater. Today*, vol. 14, no. 7–8, pp. 308–315, Jul. 2011.

[112] K. Arshak, V. Velusamy, O. Korostynska, K. Oliwa-Stasiak, and C. Adley, “Conducting Polymers and Their Applications to Biosensors: Emphasizing on Foodborne Pathogen Detection,” *IEEE Sens. J.*, vol. 9, no. 12, pp. 1942–1951, Dec. 2009.

[113] M. Onoda, “Culture experiments on conductive polymers,” in *Journal of Physics*, 2012, vol. 358, no. 1, p. 012004.

[114] L. Sasso, P. Vazquez, I. Vedarethinam, J. Castillo-León, J. Emnéus, and W. E. Svendsen, “Conducting polymer 3D microelectrodes,” *Sensors*, vol. 10, no. 12, pp. 10986–11000, Jan. 2010.

[115] C. Vallejo-Giraldo, A. Kelly, and M. J. P. Biggs, “Biofunctionalisation of electrically conducting polymers,” *Drug Discov. Today*, vol. 19, no. 1, pp. 88–94, 2014.

[116] M. Gerard, A. Chaubey, and B. D. Malhotra, “Application of conducting polymers to biosensors,” *Biosens. Bioelectron.*, vol. 17, no. 5, pp. 345–359, 2002.

[117] T. Ahuja, I. A. Mir, D. Kumar, and Rajesh, “Biomolecular immobilization on conducting polymers for biosensing applications.,” *Biomaterials*, vol. 28, no. 5, pp. 791–805, Mar. 2007.

[118] B. Adhikari and S. Majumdar, “Polymers in sensor applications,” *Prog. Polym. Sci.*, vol. 29, no. 7, pp. 699–766, Jul. 2004.

[119] S. Hideki, E. J. Louis, A. G. MacDiarmid, C. K. Chiang, and A. J. Heeger, “Synthesis of Electrically-Conducting organic Polymers: Halogen Derivatives of Polyacatylene, (CH)x,” *J. Chem. Soc. Chem. Commun.*, vol. 16, pp. 578–580, 1977.

[120] C. K. Chiang *et al.*, “Electrical conductivity in doped polyacetylene,” *Phys. Rev. Lett.*, vol. 39, no. 17, pp. 1098–1101, 1977.

[121] A. F. Diaz, K. K. Keiji, and G. G. Piero, “Electrochemical Polymerization of Pyrrole,” *J. Chem. Soc. Chem. Commun.*, vol. 14, pp. 635–636, 1979.

[122] A. F. Diaz and L. J. A., “ELECTROACTIVE POLYANILINE FILMS,” *J.*

Electroanal. Chem., vol. 111, pp. 111–114, 1980.

[123] W. Lövenich, "PEDOT-properties and applications," *Polym. Sci. Ser. C*, vol. 56, no. 1, pp. 135–143, Jul. 2014.

[124] S. L. Lai, M. Y. Chan, M. K. Fung, C. S. Lee, and S. T. Lee, "Concentration effect of glycerol on the conductivity of PEDOT film and the device performance," *Mater. Sci. Eng. B Solid-State Mater. Adv. Technol.*, vol. 104, no. 1–2, pp. 26–30, 2003.

[125] T.-H. Le, Y. Kim, and H. Yoon, "Electrical and Electrochemical Properties of Conducting Polymers," *Polymers (Basel).*, vol. 9, no. 4, p. 150, 2017.

[126] J. Huang, P. F. Miller, J. C. De Mello, A. J. De Mello, and D. D. C. Bradley, "Influence of thermal treatment on the conductivity and morphology of PEDOT/PSS films," *Synth. Met.*, vol. 139, no. 3, pp. 569–572, 2003.

[127] M. Lee, Y. Kim, S. Lee, J. An, and C. Im, "Improvement in power conversion efficiency by blending of poly(3,4-ethylenedioxythiophene):poly(styrenesulfonate) into poly(3-hexylthiophene):phenyl-C61-butyric acid methyl ester active layer," *Appl. Phys. Lett.*, vol. 100, no. 22, 2012.

[128] U. S. Bhansali, M. A. Khan, and H. N. Alshareef, "Electrical performance of polymer ferroelectric capacitors fabricated on plastic substrate using transparent electrodes," *Org. Electron.*, vol. 13, no. 9, pp. 1541–1545, 2012.

[129] S. Kirchmeyer and K. Reuter, "Scientific importance, properties and growing applications of poly(3,4-ethylenedioxythiophene)," *J. Mater. Chem.*, vol. 15, no. 21, pp. 2077–2088, 2005.

[130] F. Xue, Y. Su, and K. Varahramyan, "Modified PEDOT-PSS conducting polymer as S/D electrodes for device performance enhancement of P3HT TFTs," *IEEE Trans. Electron Devices*, vol. 52, no. 9, pp. 1982–1987, 2005.

[131] E. Lim, "Enhanced photovoltaic performance of P3HT:PCBM cells by modification of PEDOT:PSS layer," *Mol. Cryst. Liq. Cryst.*, vol. 585, no. 1, pp. 53–59, 2013.

[132] Y. Ding, M. a Invernale, and G. a Sotzing, "Conductivity trends of PEDOT-PSS impregnated fabric and the effect of conductivity on electrochromic textile.," *ACS Appl. Mater. Interfaces*, vol. 2, no. 6, pp. 1588–93, Jun. 2010.

[133] C. M. Palumbiny *et al.*, "Molecular reorientation and structural changes in cosolvent-treated highly conductive PEDOT:PSS electrodes for flexible indium tin oxide-free organic electronics," *J. Phys. Chem. C*, vol. 118, no. 25, pp. 13598–13606, 2014.

[134] S. Ouyang *et al.*, "Photolithographic patterning of PEDOT:PSS of highly conductive and its application in organic light emitting diodes," *J. Polym. Sci. Part B Polym. Phys.*, vol. 52, no. 18, pp. 1221–1226, 2014.

[135] J. Y. Kim, J. H. Jung, D. E. Lee, and J. Joo, "Enhancement of electrical conductivity of poly(3,4-ethylenedioxythiophene)/poly(4-styrenesulfonate) by a change of solvents," *Synth. Met.*, vol. 126, no. 2–3, pp. 311–316, 2002.

[136] G. C. Le Goff, R. L. Srinivas, W. A. Hill, and P. S. Doyle, "Hydrogel

microparticles for biosensing," *Eur. Polym. J.*, vol. 72, pp. 386–412, 2015.

[137] X. Mao, G. Chen, Z. Wang, Y. Zhang, X. Zhu, and G. Li, "Surface-immobilized and self-shaped DNA hydrogels and their application in biosensing," *Chem. Sci.*, vol. 9, no. 4, pp. 811–818, 2018.

[138] D. Buenger, F. Topuz, and J. Groll, "Hydrogels in sensing applications," *Prog. Polym. Sci.*, vol. 37, pp. 1678–1719, 2012.

[139] E. Caló and V. V. Khutoryanskiy, "Biomedical application of nanoparticles : : A review of patents and commercial products," *Eur. Polym. J.*, vol. 65, pp. 252–267, 2018.

[140] C. M. Valmikinathan, V. J. Mukhatyar, A. Jain, L. Karumbaiah, M. Dasari, and R. V. Bellamkonda, "Photocrosslinkable chitosan based hydrogels for neural tissue engineering," *Soft Matter*, vol. 8, no. 6, pp. 1964–1976, 2012.

[141] P. M. Shaibani *et al.*, "The detection of Escherichia coli (E. coli) with the pH sensitive hydrogel nanofiber-light addressable potentiometric sensor (NF-LAPS)," *Sensors Actuators, B Chem.*, vol. 226, pp. 176–183, 2016.

[142] N. S. K. Gunda, R. Chavali, and S. K. Mitra, "A hydrogel based rapid test method for detection of: Escherichia coli (E. coli) in contaminated water samples," *Analyst*, vol. 141, no. 10, pp. 2920–2929, 2016.

[143] A. Atrazhev, D. P. Manage, A. J. Stickel, H. J. Crabtree, L. M. Pilarski, and J. P. Acker, "In-Gel technology for PCR genotyping and pathogen detection," *Anal. Chem.*, vol. 82, no. 19, pp. 8079–8087, 2010.

[144] J. Y. Lee *et al.*, "Integrating sensing hydrogel microstructures into micropatterned hepatocellular cocultures," *Langmuir*, vol. 25, no. 6, pp. 3880–3886, 2009.

[145] A. L. Liu and A. J. García, "Methods for Generating Hydrogel Particles for Protein Delivery," *Ann. Biomed. Eng.*, vol. 44, no. 6, pp. 1946–1958, 2016.

[146] V. B. Knight and E. E. Serrano, "Hydrogel scaffolds promote neural gene expression and structural reorganization in human astrocyte cultures," *PeerJ*, vol. 5, p. e2829, 2017.

[147] M. E. Helgeson, S. C. Chapin, and P. S. Doyle, "Hydrogel microparticles from lithographic processes: Novel materials for fundamental and applied colloid science," *Curr. Opin. Colloid Interface Sci.*, vol. 16, no. 2, pp. 106–117, 2011.

[148] M. S. Hahn, L. J. Taite, J. J. Moon, M. C. Rowland, K. A. Ruffino, and J. L. West, "Photolithographic patterning of polyethylene glycol hydrogels," *Biomaterials*, vol. 27, no. 12, pp. 2519–2524, 2006.

[149] D. N. Kim, J. Park, and W. G. Koh, "Control of cell adhesion on poly(ethylene glycol) hydrogel surfaces using photochemical modification and micropatterning techniques," *J. Ind. Eng. Chem.*, vol. 15, no. 1, pp. 124–128, 2009.

[150] X. Wang and S. Uchiyama, "Polymers for Biosensors Construction," in *In State os the art in biosensors-general aspects. InTech*, 2013.

[151] R. M. Reano *et al.*, "Stability of functional polymers after plasticizer-assisted

imprint lithography," *J. Vac. Sci. Technol. B*, vol. 22, no. 6, pp. 3294–3299, 2004.

[152] M. Akerfeldt, M. Straat, and P. Walkenstrom, "Electrically conductive textile coating with a PEDOT-PSS dispersion and a polyurethane binder," *Text. Res. J.*, vol. 83, no. 6, pp. 618–627, Nov. 2013.

[153] J. G. Hardy *et al.*, "Conducting polymer-based multilayer films for instructive biomaterial coatings," *Futur. Sci. OA*, vol. 1, no. 4, p. fso.15.79, 2015.

[154] J. Müller, C. Thirion, and M. W. Pfaffl, "Electric cell-substrate impedance sensing (ECIS) based real-time measurement of titer dependent cytotoxicity induced by adenoviral vectors in an IPI-2I cell culture model," *Biosens. Bioelectron.*, vol. 26, no. 5, pp. 2000–2005, 2011.

[155] I. Giaever and C. R. Keese, "Micromotion of mammalian cells measured electrically.," *Proc. Natl. Acad. Sci.*, vol. 88, no. 17, pp. 7896–7900, 1991.

[156] S. A. Ozlem, "In Vitro Cytotoxicity and Cell Viability Assays: Principles, Advantages, and Disadvantages," *Genotoxicity - A Predict. Risk to Our Actual World*, pp. 1–19, 2017.

[157] F. Yang *et al.*, "Real-time, label-free monitoring of cell viability based on cell adhesion measurements with an atomic force microscope," *J. Nanobiotechnology*, vol. 15, no. 1, pp. 1–10, 2017.

[158] I. Park *et al.*, "Electrical Impedance Monitoring of C2C12 Myoblast Differentiation on an Indium Tin Oxide Electrode," *Sensors*, vol. 16, no. 12, p. 2068, 2016.

[159] R. Szulcek, H. J. Bogaard, and G. P. van Nieuw Amerongen, *Electric Cell-substrate Impedance Sensing for the Quantification of Endothelial Proliferation, Barrier Function, and Motility*, vol. 85. 2014.

[160] J. Wegener, C. R. Keese, and I. Giaever, "Electric cell-substrate impedance sensing (ECIS) as a noninvasive means to monitor the kinetics of cell spreading to artificial surfaces," *Exp. Cell Res.*, vol. 259, no. 1, pp. 158–166, 2000.

[161] Y. Koo and Y. Yun, "Effects of polydeoxyribonucleotides (PDRN) on wound healing: Electric cell-substrate impedance sensing (ECIS)," *Mater. Sci. Eng. C*, vol. 69, pp. 554–560, 2016.

[162] K. Benson, S. Cramer, and H. J. Galla, "Impedance-based cell monitoring: Barrier properties and beyond," *Fluids Barriers CNS*, vol. 10, no. 5, pp. 1–11, 2013.

[163] Y. Yun *et al.*, "Revolutionizing biodegradable metals," *Mater. Today*, vol. 12, no. 10, pp. 22–32, Oct. 2009.

[164] G. H. Lee, "Electrical impedance characterization of cell growth on IDE," *J. Nanosci. Nanotechnol.*, vol. 14, no. 11, pp. 8342–8346, 2014.

[165] R. M. Miriani, M. R. Abidian, and D. R. Kipke, "Cytotoxic analysis of the conducting polymer PEDOT using myocytes.," *Conf. Proc. ... Annu. Int. Conf. IEEE Eng. Med. Biol. Soc. IEEE Eng. Med. Biol. Soc. Annu. Conf.*, vol. 2008, pp. 1841–4, Jan. 2008.

[166] H. Chen, J. L. Muros-Cobos, and A. Amirfazli, "Contact angle measurement with a smartphone," *Rev. Sci. Instrum.*, vol. 89, no. 3, p. 035117, 2018.

[167] F. Salaün, E. Devaux, S. Bourbigot, and P. Rumeau, "Application of Contact Angle Measurement to the Manufacture of Textiles Containing Microcapsules," *Text. Res. J.*, vol. 79, no. 13, pp. 1202–1212, 2009.

[168] Y. Yuan, "Contact angle and wetting properties," in *Surface Science Techniques*, vol. 51, Berlin: Springer-Verlag Berlin Heidelberg, 2013, pp. 3–34.

[169] Y. B. Park, H. Im, M. Im, and Y. K. Choi, "Self-cleaning effect of highly water-repellent microshell structures for solar cell applications," *J. Mater. Chem.*, vol. 21, no. 3, pp. 633–636, 2011.

[170] K. Y. Law, "Definitions for Hydrophilicity, Hydrophobicity, and Superhydrophobicity: Getting the Basics Right," *J. Phys. Chem. Lett.*, pp. 686–688, 2014.

[171] T. Zhao and L. Jiang, "Colloids and Surfaces B : Biointerfaces Contact angle measurement of natural materials," *Colloids Surfaces B Biointerfaces*, vol. 161, pp. 324–330, 2018.

[172] H. Perkampus, *UV-VIS Spectroscopy and its Applications*. New York: Springer-Berlin Verlag, 1992.

[173] C. S. Doyle, C. K. Seal, and B. J. James, "Evolution of steel surface composition with heating in vacuum and in air," *Appl. Surf. Sci.*, vol. 257, no. 23, pp. 10005–10017, 2011.

[174] ASTM International, "Standard test method for tensile properties of plastics," *ASTM Int.*, vol. 08, pp. 46–58, 2003.

[175] A. -grip, "Standard Test Method for Tensile Properties of Thin Plastic Sheeting 1," 2006.

[176] J. J. Muys, M. M. Alkaisi, and J. J. Evans, "Bioimprint : Nanoscale Analysis by Replication of Cellular Topography Using Soft Lithography," *J. Biomed. Nanotechnol.*, vol. 2, no. 1, pp. 1–5, 2006.

[177] V. N. Goral, Y. Hsieh, O. N. Petzold, R. A. Faris, and P. K. Yuen, "Hot embossing of plastic microfluidic devices using poly(dimethylsiloxane) molds," in *14th International Conference on Miniaturized Systems for Chemistry and Life Sciences*, pp. 1214–1216.

[178] A. B. Faia-Torres *et al.*, "Differential regulation of osteogenic differentiation of stem cells on surface roughness gradients," *Biomaterials*, vol. 35, no. 33, pp. 9023–9032, 2014.

[179] T. Senn, J. P. Esquivel, M. Lörgen, N. Sabaté, and B. Löchel, "Replica molding for multilevel micro-/nanostructure replication," *J. Micromechanics Microengineering*, vol. 20, no. 12, p. 129804, Dec. 2010.

[180] P. Fanzio, A. Cagliani, K. G. Peterffy, and L. Sasso, "High throughput soft embossing process for micro-patterning of PEDOT thin films," *Microelectron. Eng.*, vol. 176, pp. 15–21, 2017.

[181] S. Ouyang *et al.*, "Highly Conductive PEDOT:PSS Patterning Scheme and its

Application to ITO-free Organic Light Emitting Diodes," *Highly Conduct. PEDOTPSS Patterning Scheme its Appl. to ITO-free Org. Light Emit. Diodes Shihong*, vol. 15, no. 2, pp. 1540–1543, Jun. 2005.

[182] O. P. Dimitriev, D. A. Grinko, Y. V. Noskov, N. A. Ogurtsov, and A. A. Pud, "PEDOT:PSS films-Effect of organic solvent additives and annealing on the film conductivity," *Synth. Met.*, vol. 159, no. 21–22, pp. 2237–2239, 2009.

[183] J. Gasiorowski, R. Menon, K. Hingerl, M. Dachev, and N. Serdar, "Surface morphology , optical properties and conductivity changes of by using additives," *Thin Solid Films*, vol. 536, pp. 211–215, 2013.

[184] Z. Xiong and C. Liu, "Optimization of inkjet printed PEDOT:PSS thin films through annealing processes," *Org. Electron. physics, Mater. Appl.*, vol. 13, no. 9, pp. 1532–1540, 2012.

[185] Y. Seok *et al.*, "Highly conductive and hydrated PEG-based hydrogels for the potential application of a tissue engineering scaffold," *React. Funtional Polym.*, vol. 109, pp. 15–22, 2016.

[186] S. Yang *et al.*, "Polypyrrole / Alginate Hybrid Hydrogels : Electrically Conductive and Soft Biomaterials for Human Mesenchymal Stem Cell Culture and Potential Neural Tissue Engineering Applications," *Macromol. Biosci.*, vol. 16, no. 11, pp. 1653–1661, 2016.

[187] Y. Wu *et al.*, "Fabrication of conductive gelatin methacrylate-polyaniline hydrogels," *Acta Biomater.*, vol. 33, pp. 122–130, 2016.

[188] M. Sasaki, B. C. Karikkineth, K. Nagamine, H. Kaji, K. Torimitsu, and M. Nishizawa, "Highly conductive stretchable and biocompatible electrode-hydrogel hybrids for advanced tissue engineering.," *Adv. Healthc. Mater.*, vol. 3, no. 11, pp. 1919–27, Nov. 2014.

[189] M. Thomazine, R. Carvalho, and p Sobral, "E : Food Engineering and Physical Properties Physical Properties of Gelatin Films Plasticized by Blends of Glycerol and Sorbitol Results and Discussion," vol. 70, no. 3, pp. 172–176, 2005.

[190] R. Kishi, K. Kubota, T. Miura, T. Yamaguchi, H. Okuzaki, and Y. Osada, "Mechanically tough double-network hydrogels with high electronic conductivity," *J. Mater. Chem. C*, vol. 2, no. 4, pp. 736–743, 2014.

[191] C. K. aa. Akkan *et al.*, "Surface topography and wetting modifications of PEEK for implant applications," *Lasers Med. Sci.*, vol. 29, no. 5, pp. 1633–1639, 2014.

[192] S. Patra, S. Sarkar, S. K. Bera, G. K. Paul, and R. Ghosh, "Influence of surface topography and chemical structure on wettability of electrodeposited ZnO thin films," *J. Appl. Phys.*, vol. 108, no. 8, 2010.

[193] M. Stüber *et al.*, "Surface topography, surface energy and wettability of magnetron-sputtered amorphous carbon (a-C) films and their relevance for platelet adhesion," *Adv. Eng. Mater.*, vol. 9, no. 12, pp. 1114–1122, 2007.

[194] M. Ghibaudo, L. Trichet, J. Le Digabel, A. Richert, P. Hersen, and B. Ladoux, "Substrate topography induces a crossover from 2D to 3D behavior in fibroblast migration," *Biophys. J.*, vol. 97, no. 1, pp. 357–368, 2009.

[195] C. W. Yung, L. Q. Wu, J. A. Tullman, G. F. Payne, W. E. Bentley, and T. A. Barbari, "Transglutaminase crosslinked gelatin as a tissue engineering scaffold," *J. Biomed. Mater. Res. - Part A*, vol. 83, no. 4, pp. 1039–1046, 2007.

[196] K. Kuwahara, Z. Yang, G. C. Slack, M. E. Nimni, and B. Han, "Cell delivery using an injectable and adhesive transglutaminase-gelatin gel," *Tissue Eng Part C Methods*, vol. 16, no. 4, pp. 609–618, 2010.

[197] A. L. Paguirigan and D. J. Beebe, "Protocol for the fabrication of enzymatically crosslinked gelatin microchannels for microfluidic cell culture," *Nat. Protoc.*, vol. 2, no. 7, pp. 1782–1788, 2007.

[198] J. R. Masters and G. N. Stacey, "Changing medium and passaging cell lines," *Nat. Protoc.*, vol. 2, no. 9, pp. 2276–2284, 2007.

[199] D. W. Hamilton, B. Chehroudi, and D. M. Brunette, "Comparative response of epithelial cells and osteoblasts to microfabricated tapered pit topographies in vitro and in vivo," *Biomaterials*, vol. 28, no. 14, pp. 2281–2293, 2007.

[200] L. Wang, S. K. Murthy, W. H. Fowle, G. A. Barabino, and R. L. Carrier, "Influence of micro-well biomimetic topography on intestinal epithelial Caco-2 cell phenotype," *Biomaterials*, vol. 30, no. 36, pp. 6825–6834, 2009.

[201] G. Le Saux, A. Magenau, T. Böcking, K. Gaus, and J. J. Gooding, "The relative importance of topography and RGD ligand density for endothelial cell adhesion," *PLoS One*, vol. 6, no. 7, p. e21869, 2011.

[202] J. Hu, C. Hardy, C. M. Chen, S. Yang, A. S. Voloshin, and Y. Liu, "Enhanced cell adhesion and alignment on micro-wavy patterned surfaces," *PLoS One*, vol. 9, no. 8, pp. 2–9, 2014.

[203] M. S. Lord, M. Foss, and F. Besenbacher, "Influence of nanoscale surface topography on protein adsorption and cellular response," *Nano Today*, vol. 5, no. 1, pp. 66–78, 2010.

[204] B. Guo, A. Finne-Wistrand, and A. C. Albertsson, "Degradable and electroactive hydrogels with tunable electrical conductivity and swelling behavior," *Chem. Mater.*, vol. 23, no. 5, pp. 1254–1262, 2011.

[205] B. Guo, L. Glavas, and A.-C. Albertsson, "Biodegradable and electrically conducting polymers for biomedical applications," *Prog. Polym. Sci.*, vol. 38, no. 9, pp. 1263–1286, 2013.

[206] P. Moutsatsou, K. Coopman, and S. Georgiadou, "Biocompatibility assessment of conducting PANI/chitosan nanofibers for wound healing applications," *Polymers (Basel).*, vol. 9, no. 12, 2017.

[207] Y. Wang, J. L. Robertson, W. B. Spillman, and R. O. Claus, "Effects of the Chemical Structure and the Surface Properties of Polymeric Biomaterials on Their Biocompatibility," *Pharm. Res.*, vol. 21, no. 8, pp. 1362–1373, 2004.

[208] S. Tsukada, H. Nakashima, and K. Torimitsu, "Conductive polymer combined silk fiber bundle for bioelectrical signal recording," *PLoS One*, vol. 7, no. 4, 2012.

[209] S. Khan and A. K. Narula, "Electrochemical and optical bimodal sensing of caffeic acid based on electrodes made from nanorods of AuNPs:PEDOT:PSS

and bio-hybrid chitosan:PEDOT:PSS," *New J. Chem.*, vol. 41, no. 17, pp. 8927–8939, 2017.

[210] D. G. Castner, "Biomedical surface analysis: Evolution and future directions (Review)," *Biointerphases*, vol. 12, no. 2, p. 02C301, 2017.

[211] "Infrared spectroscopy absorption table." [Online]. Available: https://chem.libretexts.org/Reference/Reference_Tables/Spectroscopic_Parameters/Infrared_Spectroscopy_Absorption_Table.

[212] "IR Spectrum Table & Chart: Sigma Aldrich." [Online]. Available: https://www.sigmaaldrich.com/technical-documents/articles/biology/ir-spectrum-table.html.

[213] P. R. Griffiths, J. A. De Haseth, and J. D. Winefordner, *Fourier Transform Infrared Spectrometry*, 2nd ed. John Wiley & Sons.

[214] C. Liu, Z. Zhang, X. Liu, X. Ni, and J. Li, "Gelatin-based hydrogels with β-cyclodextrin as a dual functional component for enhanced drug loading and controlled release," *RSC Adv.*, vol. 3, no. 47, pp. 25041–25049, 2013.

[215] N. Cebi, M. Z. Durak, O. S. Toker, O. Sagdic, and M. Arici, "An evaluation of Fourier transforms infrared spectroscopy method for the classification and discrimination of bovine, porcine and fish gelatins," *Food Chem.*, vol. 190, pp. 1109–1115, 2016.

[216] F. A. Aouada, M. R. De Moura, E. Radovanovic, E. M. Girotto, A. F. Rubira, and E. C. Muniz, "PAAm and PEDOT/PSS hydrogel as potential electroactive devices: Evaluation of surface and hydrophilic properties," *E-Polymers*, no. March 2016, pp. 1–13, 2008.

[217] D. Yoo *et al.*, "Effects of one- and two-dimensional carbon hybridization of PEDOT:PSS on the power factor of polymer thermoelectric energy conversion devices," *J. Mater. Chem. A*, vol. 3, no. 12, pp. 6526–6533, 2015.

[218] I. Giaever and C. R. Keese, "Monitoring fibroblast behavior in tissue culture with an applied electric field," *Proc. Natl. Acad. Sci. U. S. A.*, vol. 81, no. 12, pp. 3761–3764, 1984.

[219] C. R. Keese and I. Giaever, "A biosensor that monitors cell morphology with electrical fields," *IEEE Eng. Med. Biol. Mag.*, vol. 13, no. 3, pp. 402–408, 1994.

[220] H. Li and R. Bashir, "Dielectrophoretic separation and manipulation of live and heat-treated cells of Listeria on microfabricated devices with interdigitated electrodes," *Sensors Actuators B. Chem.*, vol. 86, no. 2–3, pp. 215–221, 2002.

[221] G. Slaugther, "A Gold Interdigitated Microelectrodes Fabricated on Polyhydroxybutyrate Substrate for the Determination of Urea Using Impedimetric Measurements," *IEEE Sens. J.*, vol. 12, no. 4, pp. 821–826, 2012.

[222] C. M. Lo, C. R. Keese, and I. Giaever, "Impedance analysis of MDCK cells measured by electric cell- substrate impedance sensing," *Biophys. J.*, vol. 69, no. December, pp. 2800–2807, 1995.

[223] M. Varshney, Y. Li, B. Srinivasan, and S. Tung, "A label-free, microfluidics and interdigitated array microelectrode-based impedance biosensor in combination with nanoparticles immunoseparation for detection of Escherichia coli O157:H7

in food samples," *Sensors Actuators B Chem.*, vol. 128, no. 1, pp. 99–107, Dec. 2007.

[224] R. Ehret *et al.*, "Monitoring of cellular behaviour interdigitated AG Medizinische impedance measurements on electrode structures," *Biosens. Bioelectron.*, vol. 12, pp. 29–41, 1997.

[225] S. Ahadian *et al.*, "Interdigitated array of Pt electrodes for electrical stimulation and engineering of aligned muscle tissue," *Lab Chip*, vol. 12, no. 18, p. 3491, 2012.

[226] S.-Y. Huang *et al.*, "Enhanced Sensitivity Using Microfluidic, Interdigitated Microelectrode Based Capacitance Glucose Sensor Measured at 4 MHz," *J. Electrochem. Soc.*, vol. 161, no. 5, pp. B102–B105, Apr. 2014.

[227] C. M. Daikuzono *et al.*, "Impedance spectroscopy for monosaccharides detection using responsive hydrogel modified paper-based electrodes," *Analyst*, vol. 142, no. 7, pp. 1133–1139, 2017.

[228] J. Tavakoli and Y. Tang, "Hydrogel based sensors for biomedical applications: An updated review," *Polymers (Basel).*, vol. 9, no. 8, pp. 1–25, 2017.

[229] R. T. Hassarati, W. F. Dueck, C. Tasche, P. M. Carter, L. A. Poole-Warren, and R. A. Green, "Improving cochlear implant properties through conductive hydrogel coatings," *IEEE Trans. Neural Syst. Rehabil. Eng.*, vol. 22, no. 2, pp. 411–418, 2014.

[230] N. A. Staples *et al.*, "Conductive hydrogel electrodes for delivery of long-term high frequency pulses," *Front. Neurosci.*, vol. 11, p. 748, 2018.

[231] M. H. Lee *et al.*, "A low-noise solid-state nanopore platform based on a highly insulating substrate," *Sci. Rep.*, vol. 4, pp. 1–7, 2014.

[232] K. F. Lei, B.-Y. Lin, and N.-M. Tsang, "Real-time and label-free impedimetric analysis of the formation and drug testing of tumor spheroids formed via the liquid overlay technique," *RSC Adv.*, vol. 7, no. 23, pp. 13939–13946, 2017.

[233] J. Yu, Z. Liu, M. Yang, and A. Mak, "Nanoporous membrane-based cell chip for the study of anti-cancer drug effect of retinoic acid with impedance spectroscopy," *Talanta*, vol. 80, no. 1, pp. 189–194, 2009.

[234] M. Varshney and Y. Li, "Interdigitated array microelectrodes based impedance biosensors for detection of bacterial cells.," *Biosens. Bioelectron.*, vol. 24, no. 10, pp. 2951–60, Jun. 2009.

[235] L. Yang, A. Guiseppi-Wilson, and A. Guiseppi-Elie, "Design considerations in the use of interdigitated microsensor electrode arrays (IMEs) for impedimetric characterization of biomimetic hydrogels," *Biomed. Microdevices*, vol. 13, no. 2, pp. 279–289, 2011.

[236] M. R. Abidian and D. C. Martin, "Experimental and theoretical characterization of implantable neural microelectrodes modified with conducting polymer nanotubes," *Biomaterials*, vol. 29, no. 9, pp. 1273–1283, 2008.

[237] M. R. Abidian and D. C. Martin, "Multifunctional nanobiomaterials for neural interfaces," *Adv. Funct. Mater.*, vol. 19, no. 4, pp. 573–585, 2009.

[238] C. N. Kotanen and A. Guiseppi-Elie, “Bioactive electroconductive hydrogels yield novel biotransducers for glucose,” *Macromol. Symp.*, vol. 317–318, no. 1, pp. 187–197, 2012.

[239] A. Guiseppi-Elie, “Electroconductive hydrogels: Synthesis, characterization and biomedical applications,” *Biomaterials*, vol. 31, no. 10, pp. 2701–2716, 2010.

[240] G. Justin and A. Guiseppi-Elie, “Electroconductive blends of poly(HEMA-co-PEGMA-co-HMMAco-SPMA) and poly(Py-co-PyBA): In vitro biocompatibility,” *J. Bioact. Compat. Polym.*, vol. 25, no. 2, pp. 121–140, 2010.

[241] M. Grossi and B. Ricco, “Electrical impedance spectroscopy (EIS) for biological analysis and food characterization : a review,” *J. Sensors Sens. Syst.*, vol. 6, pp. 303–325, 2017.